Uniwersytet im. Adama Mickiewicza w Poznaniu

Szkoła Doktorska Nauk Przyrodniczych

Wydział Nauk Geograficznych i Geologicznych

Martyna E. Górska

Rozprawa doktorska

Zapis wietrzenia mrozowego ziaren kwarcu w mikromorfologii i uziarnieniu – badania eksperymentalne

The record of frost weathering of quartz grains in micromorphology and grain-size composition – an experimental study

Rozprawa doktorska pod kierunkiem

Prof. dr hab. Barbary Woronko (promotorka)

Prof. dr hab. Małgorzaty Pisarskiej-Jamroży (promotorka)

Poznań, 2023

Adam Mickiewicz University in Poznań

Doctoral School of Natural Sciences

Faculty of Geographical and Geological Sciences

Martyna E. Górska

Doctoral dissertation

The record of frost weathering of quartz grains in micromorphology and grain-size composition – an experimental study

Zapis wietrzenia mrozowego ziaren kwarcu w mikromorfologii i uziarnieniu – badania eksperymentalne

Doctoral dissertation supervised by:

Prof. dr hab. Barbara Woronko (principal advisor)

Prof. dr hab. Małgorzata Pisarska-Jamroży (principal advisor)

Poznań, 2023

Spis treści / Table of contents

Załączniki / Attachments:

Publikacja nr 1 (Publication no. 1):

Górska M.E., Woronko B., Kossowski T.M., Pisarska-Jamroży M., 2022. Micro-scale frost-weathering simulation – Changes in grain-size composition and influencing factors. *Catena*, 212, 106106. https://doi.org/10.1016/j.catena.2022.106106

Publikacja nr 2 (Publication no. 2):

Górska M.E., Woronko B., 2022. Multi-stage evolution of frost-induced microtextures on the surface of quartz grains – An experimental study. *Permafrost and Periglacial Processes*, 33, 470-489. https://doi.org/10.1002/ppp.2164

Publikacja nr 3 (Publication no. 3):

Górska M.E., Woronko B., Kossowski T.M., 2023. Factors influencing the development of microtextures on cold-climate aeolian quartz grains revealed by experimental frost action. *Permafrost and Periglacial Processes*, 2023, 1-25. https://doi.org/10.1002/ppp.2179

Podziękowania

Autorka pracy pragnie podziękować:

Promotorkom,

prof. dr hab. Barbarze Woronko oraz prof. dr hab. Małgorzacie Pisarskiej-Jamroży,

które wprowadziły mnie do przepięknego mikro-świata ziaren kwarcu.

Dziękuję za inspirację, opiekę naukową, wsparcie na każdym etapie realizacji badań oraz przekazanie uniwersalnych wartości właściwych dla pracy naukowej.

dr hab. Tomaszowi M. Kossowskiemu,

za współpracę i wsparcie merytoryczne w trakcie interpretacji wyników.

mgr Bartoszowi Pieterkowi, prof. dr hab. Andrzejowi Muszyńskiemu oraz dr Łukaszowi Bujakowi,

za pomoc w poborze prób do badań.

Rodzinie i przyjaciołom,

za nieograniczone wsparcie okazywane przez cały czas mojej pracy naukowej.

Acknowledgments

The author wishes to thank:

Supervisors,

prof. dr hab. Barbara Woronko and prof. dr hab. Małgorzata Pisarska-Jamroży,

who introduced me to the beautiful micro-world of quartz grains.

Thank you for inspiration, scientific supervision, support at every stage of the research and transfer of universal values appropriate for scientific work.

dr hab. Tomasz M. Kossowski,

for cooperation and scientific support during the interpretation of the results.

mgr Bartosz Pieterek, prof. dr hab. Andrzej Muszyński and dr Łukasz Bujak,

for assistance in the collection of samples for the research.

My family and friends,

for their unlimited support throughout my research work.

LISTA PUBLIKACJI WCHODZĄCYCH W SKŁAD ROZPRAWY DOKTORSKIEJ

Niniejsza rozprawa doktorska składa się ze spójnego tematycznie zbioru **trzech recenzowanych publikacji naukowych** poprzedzonych wspólnym streszczeniem. Prace te zostały opublikowane w czasopismach posiadających współczynnik wpływu (Impact Factor, IF). Sumaryczny IF zbioru publikacji wynosi 14.891.

W skład rozprawy doktorskiej wchodzą następujące publikacje naukowe:

1. **Górska M.E.**, Woronko B., Kossowski T.M., Pisarska-Jamroży M., 2022. Micro-scale frost-weathering simulation – Changes in grain-size composition and influencing factors. *Catena*, 212, 106106.
   https://doi.org/10.1016/j.catena.2022.106106
   Q1 (Web of Science), IF_{2022} = 6.367, MEiN = 140 pkt

2. **Górska M.E.**, Woronko B., 2022. Multi-stage evolution of frost-induced microtextures on the surface of quartz grains – An experimental study. *Permafrost and Periglacial Processes*, 33, 470-489.
   https://doi.org/10.1002/ppp.2164
   Q1 (Web of Science), IF_{2021} = 4.262, MEiN = 100 pkt

3. **Górska M.E.**, Woronko B., Kossowski T.M., 2023. Factors influencing the development of microtextures on cold-climate aeolian quartz grains revealed by experimental frost action. *Permafrost and Periglacial Processes*, 2023, 1-25.
   https://doi.org/10.1002/ppp.2179
   Q1 (Web of Science), IF_{2021} = 4.262, MEiN = 100 pkt

LIST OF PUBLICATIONS INCLUDED IN THE DOCTORAL DISSERTATION

The doctoral dissertation consists of a set of **three peer-reviewed research publications** with an introductory summary section. The research papers were published in scientific journals with impact factor (IF). The total IF of the set of publications is 14.891.

The doctoral dissertation consists of the following publications:

1. **Górska M.E.**, Woronko B., Kossowski T.M., Pisarska-Jamroży M., 2022. Micro-scale frost-weathering simulation – Changes in grain-size composition and influencing factors. *Catena*, 212, 106106.
   https://doi.org/10.1016/j.catena.2022.106106
   Q1 (Web of Science), $IF_{2022} = 6.367$, 140 points on the list of scientific journals of Polish Ministry of Education and Science

2. **Górska M.E.**, Woronko B., 2022. Multi-stage evolution of frost-induced microtextures on the surface of quartz grains – An experimental study. *Permafrost and Periglacial Processes*, 33, 470-489.
   https://doi.org/10.1002/ppp.2164
   Q1 (Web of Science), $IF_{2021} = 4.262$, 100 points on the list of scientific journals of Polish Ministry of Education and Science

3. **Górska M.E.**, Woronko B., Kossowski T.M., 2023. Factors influencing the development of microtextures on cold-climate aeolian quartz grains revealed by experimental frost action. *Permafrost and Periglacial Processes*, 2023, 1-25.
   https://doi.org/10.1002/ppp.2179
   Q1 (Web of Science), $IF_{2021} = 4.262$, 100 points on the list of scientific journals of Polish Ministry of Education and Science

STRESZCZENIE ROZPRAWY DOKTORSKIEJ

**Zapis wietrzenia mrozowego ziaren kwarcu w mikromorfologii i uziarnieniu
– badania eksperymentalne**

*The record of frost weathering of quartz grains in micromorphology and grain-size
composition – experimental study*

1. <u>WPROWADZENIE</u>

Wietrzenie mrozowe, definiowane w literaturze także jako geliwacja czy wietrzenie kriogeniczne, to jeden z przykładów wietrzenia fizycznego (mechanicznego) lub zespołu procesów fizycznych, biochemicznych lub fizykochemicznych (Hall & Lautridou, 1991; French, 2017). Mimo długiej tradycji badań nad tym zjawiskiem, w dalszym ciągu uważa się, że jest to słabo poznana grupa procesów fizykochemicznych, które działają w zimnym klimacie. Wietrzenie mrozowe (fizyczne) jest procesem mechanicznej dezintegracji skał, który zachodzi na skutek cyklicznych przejść temperatury przez 0˚C (e.g. French, 2017). Warunki sprzyjające dezintegracji mrozowej skał utożsamia się z klimatem zimnym, w szczególności, ze środowiskiem peryglacjalnym (np. Hall & Lautridou, 1991; French, 2017), obejmującym głównie obszary znajdujące się na przedpolu lodowców i lądolodów, obszary wysokich szerokości geograficzne oraz wysokie partie gór. Zasięg obszaru, będącego pod wpływem procesów peryglacjalnych, jest ściśle związany z występowaniem wieloletniej zmarzliny (np. Zhang i in., 2008; French, 2017; Ballantyne, 2018; Menzies & Van der Meer, 2018) i determinowany jest regionalnymi warunkami klimatycznymi. Jednakże proces wietrzenia mrozowego zachodzi również wszędzie tam, gdzie temperatura gruntu oscyluje wokół 0°C.

Współczesne środowisko peryglacjalne zajmuje ok. 25% powierzchni lądowej Ziemi (French, 2017) i rozciąga się głównie na półkuli północnej, obejmując obszary zlokalizowane w strefie klimatu polarnego, subpolarnego, oraz wysokie góry niskich i średnich szerokości geograficznych (William & Smith, 1989; French, 2017). W przeszłości geologicznej, zasięg strefy peryglacjalnej na półkuli północnej zmieniał się w związku ze zmianami klimatu i związanym z nimi kilkukrotnym rozwojem i zanikiem lądolodów (np. Goździk, 1995; Lindner i in., 2004; Błaszkiewicz, 2011; Marks, 2011; Van Loon i in., 2014; Vandenberghe i in., 2014, 2016; Marks i in., 2019). Z tego powodu, efekty wietrzenia mrozowego są również

powszechnie rejestrowane w osadach znajdujących się poza zasięgiem współczesnej wieloletniej zmarzliny.

Historia badań nad procesami wietrzenia mrozowego, jego oddziaływania na skały i osady, oraz związanymi z nimi efektami, sięga początku XX wieku (zob. French, 2017; Matsuoka & Murton, 2008), kiedy obecność spękanych bloków piaskowców na stokach górskich Karpat została powiązana z destrukcyjną dzielnością zamrozu (np. Łoziński, 1909, 1912).

Wietrzenie mrozowe zależy od szeregu czynników operujących w środowisku naturalnym, tj.: (1) średniej rocznej temperatury powietrza (np. Halsey i in., 1995; Frauenfeld i in., 2004), (2) temperatury powierzchni skał (np. Hall, 2004), (3) dostępności wody (Hallet i in., 1991; Matsuoka, 1995), (4) ekspozycji stoku (np. Matsuoka i in., 1997; Hall, 2004), (5) warunków atmosferycznych (nasłonecznienie, zachmurzenie i wysokość opadów; Boelhouwers, 2003; McFadden i in., 2005), (6) prędkości wiatru (McKay i in., 2009), (7) pokrywy śnieżnej (Hall, 1980; Stieglitz i in., 2003; Frauenfeld i in., 2004), (8) typu skał (Hall, 1992, Matsuoka, 2001a; Rödder & Kneisel, 2012) czy też (9) wysokości n.p.m. (np. Harris i in., 2001a). Mnogość czynników decydujących o przebiegu procesu wietrzenia mrozowego, jego intensywności, zmianach w czasie, czy też efektach, a szczególnie brak informacji, jak długo dany osad podlegał temu procesowi powoduje, że trudno jest badać proces ten w warunkach naturalnych. Dlatego wiele uwagi poświęca się eksperymentom laboratoryjnym symulującym warunki peryglacjalne (np. Lautridou & Ozouf, 1982; Wright i in., 1998; Murton i in., 2000; Wright, 2000; Kaufmann, 2004). Jako pierwszy badania eksperymentalne z zakresu wietrzenia mrozowego przeprowadził w 1956 roku J. Tricart, torując drogę kolejnym badaniom, które skupiały się na przebiegu procesu wietrzenia mrozowego skał i osadów różnego typu (np. Walder & Hallet, 1986; Matsuoka, 1990). Współcześnie, badania w warunkach laboratoryjnych prowadzone są zarówno w skali makro (w skali cm - m), jak i mikro (w skali μm – cm, a nawet nm; Matsuoka, 2001b). W skali makro, wietrzenie mrozowe prowadzi do dezintegracji skał i powstawania ostrokrawędzistych bloków skalnych (Lautridou & Ozouf, 1982; Matsuoka, 2001a, b). Natomiast w skali mikro dochodzi do produkcji drobnych cząstek, w tym frakcji pyłu (Hall, 1990). Ponadto, rozpoznanie efektów wietrzenia mrozowego i czynników nim sterujących jest bardzo ważne z punktu widzenia gospodarczego w związku z mechaniczną destrukcją materiałów budowalnych wywołaną zamrozem (np. Harris i in., 2001b; Grebenets i in., 2002; Wang i in., 2004; Thomachot i in., 2005; Wei i in., 2009; Li i in., 2010; Ruedrich i in., 2011; Varlamov, 2018).

Wietrzenie mrozowe oddziałuje na skały, osady i pojedyncze ziarna poprzez: (1) wzrost objętościowy wody w trakcie zamarzania, oraz (2) wzrost soczewek lodu segregacyjnego (np. Matsuoka & Murton, 2008). Pierwszy proces, związany jest ze wzrostem objętościowym wody o 9% w trakcie zamarzania. W teorii, aby efekty tego procesu mogły się zamanifestować, osad lub skała, podlegająca wietrzeniu, musi być nasycona wodą, a front zamarzania oddziaływuje na nią równomiernie ze wszystkich stron (np. Walder & Hallet, 1985, 1986). W środowisku naturalnym warunki te spotykane są jedynie w obrębie przypowierzchniowej, kilkucentymetrowej warstwie skał / osadów, w których szczeliny / pory wypełnione są wodą, a proces zamarzania wody jest szybki (Matsuoka & Murton, 2008). W skali mikro, proces wzrostu objętościowego wody na skutek zamarzania prowadzi do mechanicznej destrukcji ziaren w wyniku wzrostu kryształów lodu w obrębie mikropęknięć i mikroszczelin lub zmiany objętości gazów / cieczy wypełniających inkluzje obecne w ziarnach w trakcie zamarzania i odmarzania (Konishchev & Rogov, 1993; Konishchev i in., 2005). Dodatkowo, obecność warstewki niezamarzniętej (higroskopijnej) wody znajdującej się na powierzchni ziaren (Konishchev & Rogov, 1993) i nacisku zamarzniętej wody błonkowej prowadzi do poszerzania istniejących już pęknięć i szczelin w ziarnach, jak również tworzenia się nowych (tzw. proces mikroszczelinowania). Tym samym dochodzi do ich destrukcji. Ten typ wietrzenia mrozowego został nazwany jako typ „F" (Woronko & Hoch, 2011).

Proces wzrostu lodu segregacyjnego odnosi się do powstawania soczewek lodu gruntowego (Walder & Hallert, 1985, 1986) na skutek sukcji wywołanej gradientem ciśnień (Williams & Smith, 1989) panującym na różnych głębokościach. Związana z działalnością zamrozu, kriosukcja wymusza migrację niezamarzniętej wody, zawartej w osadzie, w kierunku niższych wartości ciśnienia panujących wokół zamarzniętej soczewki lodu (np. Hallet i in., 1991). W wyniku tego procesu dochodzi do podnoszenia mrozowego. W środowisku naturalnym powstawaniu lodu segregacyjnego sprzyjają wolne tempo zamarzania oraz drobnoziarnisty, porowaty i nasycony wodą osad, w którym może zachodzić zjawisko kriosukcji (Anderson, 1998; Matsuoka, 2001b). Destrukcyjne efekty działalności lodu segregacyjnego zostały opisane i udokumentowane w licznych badaniach laboratoryjnych (Akagawa & Fukuda, 1991; Hallet i in., 1991; Murton i in., 2000, 2001). W skali mikro, proces ten może prowadzić do niewielkich przesunięć ziaren względem siebie i w efekcie ich destrukcji. Ten typ wietrzenia Woronko & Hoch (2011) nazwały typem „P".

1.1. Wietrzenie mrozowe ziaren kwarcu frakcji piaszczystej

W skali mikro, analizie poddawane są najczęściej ziarna kwarcu frakcji piaszczystej (np. Wright, 2000; Mahaney, 2002; Degórski & Kowalkowski, 2011; Schwamborn i in., 2012; Costa i in., 2013; Vos i in., 2014; Woronko & Pisarska-Jamroży, 2016; Kalińska-Nartiša i in., 2017; Kemnitz & Lucke, 2019). Kwarc cechuje zwiększona podatność na wietrzenie mechaniczne, co wynika z obecności defektów w ich sieci krystalicznej (Konishchev & Rogov, 1993). Tymi defektami są m.in.: inkluzje ciekłe lub gazowe, wrostki innych minerałów czy mozaikowa budowa wewnętrzna ziaren kwarcu. Dodatkowo, mechanicznej dezintegracji ziaren kwarcu sprzyja powszechna obecność spękań obserwowanych zarówno w skali całego ziarna, jak i w skali poszczególnych kryształów budujących ziarno. W konsekwencji oddziaływanie wietrzenia mrozowego na pojedyncze ziarna kwarcu prowadzi do ich mechanicznej modyfikacji pod względem wielkości, jak również mikrorzeźby. Produktami wietrzenia mrozowego ziaren kwarcu w skali mikro są: (1) ziarna frakcji pyłu, oraz (2) mikrorzeźba, którą tworzy zespół charakterystycznych dla tego procesu mikrostruktur.

(1) Produkcja ziaren frakcji pylastej na skutek wietrzenia mrozowego

Proces mechanicznej destrukcji ziaren wywołany zamrozem, prowadzący do powstania frakcji w zakresie od µm do cm, zwany jest mikrogeliwacją (Matsuoka, 2001b; zob. krytyka tego pojęcia w Hall & Thorn, 2011). Obejmuje on powstawanie i rozwój mikropęknięć oraz poszerzanie i łączenie się porów w obrębie skał / osadów (Matsuoka, 2001a). Jako pierwszy, uwagę na to zagadnienie zwrócił Vyacheslav N. Konischev (Konishchev, 1973; Kornishchev & Rogov, 1993; Konishchev i in., 2005), wskazując na mineralogiczną selektywność wietrzenia mrozowego, w wyniku której ziarna kwarcu mają skłonność do rozpadania się pod wpływem postępującego wietrzenia mrozowego na ziarna frakcji pyłu (0,01-0,05 mm). Wśród czynników wpływających na przebieg mikrogeliwacji wymienia się: (1) warunki termiczne, w tym tempo spadku temperatury (zamarzania), liczba cykli zamarzania-odmarzania, (2) dostępność wody, w tym zawartość wody w osadzie / skale i wielkość migracji wody w trakcie zamarzania osadu oraz (3) cechy osadu poddanego wietrzeniu mrozowemu, w tym podatność na odkształcenia, ich skład granulometryczny, porowatość (Matsuoka, 2001b).

Według Halla (1990) zawartość ziaren frakcji pyłu w osadzie świadczy o intensywności wietrzenia mrozowego, jakiemu ten osad podlegał. O słuszności tej hipotezy świadczy wprowadzony do literatury, *Cryogenic Weathering Index* (CWI), który wskazuje na

wzbogacenie, w stosunku do ziaren skaleni, osadu w ziarna kwarcu frakcji 0,01-0,05 mm w stosunku do frakcji 0,05-0,1 mm (Konishchev, 1998). W konsekwencji, osady znajdujące się w zasięgu wieloletniej zmarzliny i podlegające intensywnemu wietrzeniu mrozowemu, charakteryzują się wartościami CWI > 1 (Konishchev, 1999; Demitroff i in., 2007; Schwamborn i in., 2008). Na podstawie badań eksperymentalnych, symulujących 360 cykli zamarzania-odmarzania bloku kwarcowego piaskowca, Wright (2000) zaobserwowała produkcję ziaren w zakresie frakcji 2-90 µm, na które składały się: (1) ziarna powstałe przez odspojenie obwódek regeneracyjnych z ziaren kwarcu, z których zbudowany był piaskowiec, (2) całe ziarna kwarcu odspojone od wietrzejącej skały oraz (3) ziarna powstałe w wyniku pękania pojedynczych ziaren kwarcu. Wright (2000) udowodniła, że produkcja ziaren frakcji pyłu wyniosła zaledwie 0,001-0,1% oryginalnej masy bloku piaskowca, co stanowiło 28% osadu powstałego w wyniku wietrzenia mrozowego. Produkcja frakcji pylastej na skutek działalności zamrozu zachodziła wg Wright (2007) w wyniku: (1) wykorzystania spękań i szczelin obecnych w strukturze ziaren, (2) oddziaływania sił wywieranych na ziarna na skutek wzrostu kryształów lodu lub soli oraz (3) szczelinowania i odpadania fragmentów ziaren kwarcu.

(2) Modyfikacje powierzchni ziaren kwarcu na skutek wietrzenia mrozowego

Procesy oddziałujące na ziarna kwarcu frakcji piaszczystej w czasie transportu w środowiskach prądowych (np. eolicznym, fluwialnym, glacjalnym) oraz w wyniku działania procesów postdepozycyjnych zapisują się na powierzchni ziaren szeroką gamą mikrostruktur. Stąd, analiza mikrostruktur obserwowanych na powierzchni ziaren kwarcu jest powszechnie wykorzystywaną metodą w interpretacjach m.in. proweniencji osadów, charakteru środowisk sedymentacyjnych i procesów w nich działających (np. Krinsley & Doornkamp, 1973; Bull, 1981; Marshall, 1987; Mahaney, 1995, 2002; Helland & Holmes, 1997; Woronko, 2000; Mahaney i in., 2001; Van Hoesen & Orndorff, 2004; Rose & Hart, 2008; Schwamborn i in., 2008; Degórski & Kowalkowski, 2011; Krishner i in., 2011; Costa i in., 2012, 2013; Immonen i in., 2014; Vos i in., 2014; John i in., 2015; Woronko i in., 2015; Woronko, 2016; Woronko & Pisarska-Jamroży, 2016; Kalińska-Nartiša i in., 2017; Molén, 2014).

Powstawanie mikrostruktur na powierzchni ziaren kwarcu w wyniku wietrzenia mrozowego zależy od oddziaływania szeregu czynników, wśród których najważniejszymi są: (1) liczba cykli zamarzania-odmarzania, (2) tempo spadku temperatury (zamarzania), (3) typ osadu / skały, (4) cechy ziaren nabyte w czasie transportu w innych środowiskach (np.

eolicznym, fluwialnym), (5) obecność defektów w sieci krystalicznej ziaren, (6) dostępność wody oraz (7) stopień zaokrąglenia ziaren (Woronko, 2016).

Dotychczas przeprowadzone analizy powierzchni ziaren kwarcu frakcji piaszczystej pochodzących ze współczesnych i kopalnych środowisk peryglacjalnych, pozwoliły na wyróżnienie zespołu mikrostruktur wskaźnikowych dla wietrzenia mrozowego. Najważniejszymi i najczęściej występującymi są m.in. małe (<10 µm) i duże (>10 µm) przełamy muszlowe oraz struktury typu *breakage blocks* (Kowalkowski, 1988; Kowalkowski & Mycielska-Dowgiałło, 1980, 1985; Konishchev & Rogov, 1993; Konishchev i in., 2005; Schwamborn i in., 2006, 2012; Woronko, 2012; Woronko & Hoch, 2011; Woronko & Pisarska-Jamroży, 2016). Podrzędnie rejestrowane są również powierzchnie łupliwości (*fracture face*; Schwamborn i in., 2006, 2012; Woronko, 2012), struktury typu *crescentic gouges* czy złuszczone powierzchnie (*scaling surface*; Woronko, 2012; Woronko & Pisarska-Jamroży, 2016). Zidentyfikowano także oskorupienie na powierzchni ziaren kwarcu (Kowalkowski, 1988; Dietzel, 2005; Woronko, 2012; Woronko & Pisarska-Jamroży, 2016), które powiązano z produktami wietrzenia mrozowego. Schwamborn i in. (2006, 2012) opisali ziarna kwarcu z kopalnej warstwy czynnej jako kanciaste, posiadające zróżnicowany mikrorelief (ang. *high relief*) i ostre krawędzie (ang. *sharp edges*). Cechą charakterystyczną ziaren kwarcu, pochodzących ze środowiska peryglacjalnego, jest również obecność licznych ziaren pękniętych (Konishchev & Rogov, 1993; Konishchev i in., 2005; Schwamborn i in., 2006, 2012; Woronko, 2012), które mogą wskazywać na zasięg warstwy czynnej. Ponadto, badania eksperymentalne przeprowadzone przez Dietzel (2005) potwierdziły wytrącanie się substancji mineralnych na powierzchni ziaren kwarcu, na skutek powtarzających się cykli zamarzania-odmarzania.

Szczególnie istotnym problemem badawczym, w zakresie badań ziaren kwarcu poddanych procesom zamrozu, pozostaje określenie liczby cykli zamarzania-odmarzania, jakiej podlegały analizowane ziarna w przeszłości. W przypadku warunków naturalnych, czynnik ten pozostaje nieznany. W konsekwencji, analiza mikromorfologii powierzchni ziaren kwarcu rejestruje jedynie obecność lub brak mikrostruktur powstałych w efekcie wietrzenia mrozowego. Na tej podstawie trudno jest powiązać jego efekty z czasem, kiedy ziarna były poddawane wietrzeniu, a tym bardziej określeniu ile cykli zamarzania-odmarzania było potrzebnych do powstania danej mikrostruktury. Kluczowe w tym aspekcie mogą okazać się badania eksperymentalne, w których poszczególne czynniki wpływające na przebieg procesu wietrzenia są ściśle kontrolowane. **Znana liczba symulowanych cykli zamarzania-**

odmarzania pozwoli na określenie zależności pomiędzy stopniem zaawansowania procesu wietrzenia mrozowego i efektami tego procesu, manifestującymi się poprzez produkcję frakcji pylastej i powstawanie konkretnych mikrostruktur.

Pomimo szerokiej wiedzy dotyczącej procesu wietrzenia mrozowego skał zachodzącego w środowisku peryglacjalnym (np. French, 2017; Ballantyne, 2018; Menzies & Van der Meer, 2018), wietrzenie mrozowe ziaren kwarcu w skali mikro pozostaje wciąż słabo poznane. Wyróżnić można szereg zagadnień, które wymagają dalszych badań nad tym zagadnieniem: (1) przebieg wietrzenia mrozowego ziaren kwarcu w skali mikro w czasie, w tym proces ich mechanicznej destrukcji, prowadzący do powstawania mikrostruktur pochodzenia mrozowego; (2) czynniki wpływające na przebieg wietrzenia mrozowego ziaren kwarcu w skali mikro, w tym liczba cykli zamarzania-odmarzania niezbędna do zamanifestowania się efektów wietrzenia mrozowego; oraz (3) reakcja ziaren kwarcu różnej genezy na postępujący proces wietrzenia mrozowego.

Badania eksperymentalne mogą służyć doprecyzowaniu informacji o warunkach klimatycznych panujących w środowisku peryglacjalnym w przeszłości geologicznej, jak i umożliwić odtworzenie intensywności wietrzenia mrozowego oraz poznanie zależności pomiędzy procesem wietrzenia mrozowego a jego efektami w skali mikro.

2. <u>BADANIA EKSPERYMENTALNE NAD WIETRZENIEM MROZOWYM W RAMACH ROZPRAWY DOKTORSKIEJ</u>

Praca badawcza, przeprowadzona w ramach niniejszej rozprawy doktorskiej, obejmuje badania eksperymentalne w zakresie wietrzenia mrozowego w skali mikro. Obiektem badań były trzy rodzaje ziaren kwarcu frakcji piaszczystej (0,5-1,0 mm) poddane wietrzeniu mrozowemu w warunkach kontrolowanych. Przedmiot badań obejmował zagadnienie zmiany w uziarnieniu osadów oraz powstawania mikrostruktur na powierzchni ziaren kwarcu na skutek działalności zamrozu.

W rozprawie doktorskiej poruszono następujące **problemy badawcze**:

1. **Przebieg wietrzenia mrozowego ziaren kwarcu frakcji piaszczystej w skali mikro w czasie**, w tym:
   a. czynniki wpływające na proces wietrzenia,

b. reakcja ziaren kwarcu różnej genezy na wietrzenie mrozowe,

c. podatność ziaren kwarcu na modyfikacje wywołane zamrozem;

2. **Zmiany w uziarnieniu osadów na skutek wietrzenia mrozowego**, w tym:

a. czynniki wpływające na zmiany w uziarnieniu osadów oraz produkcję ziaren frakcji pylastej (liczba cykli zamarzania-odmarzania, geneza ziaren, zawartość wody, mineralizacja wody),

b. liczba cykli zamarzania-odmarzania niezbędna do dezintegracji ziaren kwarcu,

c. weryfikacja hipotezy Halla (1990) dotyczącej związku pomiędzy intensywnością wietrzenia mrozowego a udziałem frakcji pylastej w osadach poddanych wietrzeniu mrozowemu;

3. **Powstawanie mikrorzeźby pochodzenia mrozowego na powierzchni ziaren kwarcu frakcji piaszczystej**, w tym:

a. mikrostruktury charakterystyczne dla wietrzenia mrozowego,

b. rozwój mikrostruktur pochodzenia mrozowego w czasie, tj. wraz ze wzrostem liczby cykli zamarzania-odmarzania.

W rozprawie doktorskiej wyróżniono następujące **cele badawcze**:

1. Przeprowadzenie długookresowego (do 1000 cykli zamarzania-odmarzania) **eksperymentu laboratoryjnego** symulującego wietrzenie mrozowe ziaren kwarcu frakcji piaszczystej w skali mikro;

2. Rozpoznanie **efektów krótko- i długookresowego wietrzenia mrozowego** ziaren kwarcu frakcji piaszczystej, w tym:

2.1. określenie **zmian rozkładu uziarnienia** ziaren kwarcu **wywołanych zamrozem** w porównaniu z rozkładem początkowym,

2.2. określenie **wpływu zamrozu na zmiany w mikromorfologii** powierzchni ziaren kwarcu.

W celu osiągnięcia założonych celów badawczych zaplanowano następujące **zadania badawcze**:

1. **Przygotowanie eksperymentu laboratoryjnego**, w tym zaprogramowanie działania urządzenia zamrażająco-odmrażającego i ustawienie parametrów symulowanych warunków; porób próbek w terenie; przygotowanie ziaren kwarcu do eksperymentu;

2. **Przeprowadzenie eksperymentu laboratoryjnego**, w tym pobór próbek po 50, 100, 300, 700 i 1000 cyklach zamarzania-odmarzania;

3. **Analizy laboratoryjne ziaren kwarcu poddanych eksperymentalnemu wietrzeniu mrozowemu**, w tym analiza uziarnienia i analiza mikromorfologii powierzchni ziaren;

4. **Opracowania statystyczne** otrzymanych wyników analizy uziarnienia i analizy mikromorfologii powierzchni ziaren,

5. **Interpretacja wyników**.

Rozprawa doktorska składa się z trzech publikacji naukowych opublikowanych w czasopismach naukowych (zob. *Lista publikacji wchodzących w skład rozprawy doktorskiej***) i opatrzonych wspólnym streszczeniem. Pełne wersje publikacji znajdują się w załącznikach do niniejszej rozprawy doktorskiej (zob.** *Załącznik 1-3***). Wszystkie publikacje są wieloautorskie, a mój udział jest udokumentowany stosownymi oświadczeniami (zob.** *Oświadczenia autorów***). Metodologia badań przeprowadzonych w ramach niniejszej rozprawy doktorskiej została opracowana z Promotorkami pracy (prof. dr hab. Barbarą Woronko i prof. dr hab. Małgorzatą Pisarską-Jamroży). W ramach prac nad publikacjami, byłam zaangażowana w cały proces badawczy, tj. przygotowanie i przeprowadzenie eksperymentu laboratoryjnego, analiza i publikacja uzyskanych wyników.**

- W ramach pracy nad publikacją nr 1 (Górska M.E., Woronko B., Kossowski T.M., Pisarska-Jamroży M., *Micro-scale frost-weathering simulation – Changes in grain-size composition and influencing factors*), wykonałam analizę uziarnienia osadów; wspólnie ze współautorami publikacji przeprowadziłam interpretację uzyskanych wyników; uczestniczyłam w przygotowaniu pierwotnej i ostatecznej wersji manuskryptu.

- W ramach pracy nad publikacją nr 2 (Górska M.E., Woronko B., *Multi-stage evolution of frost-induced microtextures on the surface of quartz grains – An experimental study*), wykonałam analizy mikromorfologii wraz ze współautorką / promotorką (prof. dr hab. Barbarą Woronko); uczestniczyłam w przygotowaniu pierwotnej i ostatecznej wersji manuskryptu.

- W ramach pracy nad publikacją nr 3 (Górska M.E., Woronko B., Kossowski T.M., *Factors influencing the development of microtextures on cold-climate aeolian quartz grains revealed by experimental frost action*), wykonałam analizy mikromorfologii wraz ze współautorką / promotorką (prof. dr hab. Barbarą Woronko); ze współautorami publikacji

przeprowadziłam interpretację uzyskanych wyników; uczestniczyłam w przygotowaniu pierwotnej i ostatecznej wersji manuskryptu.

Do wszystkich trzech publikacji przygotowałam większość grafik (figury, tabele, załączniki), uczestniczyłam także we wszystkich etapach przygotowywania publikacji oraz w procesie odpowiedzi na recenzje, będąc autorką korespondencyjną we wszystkich publikacjach.

3. <u>MATERIAŁ BADAWCZY</u>

W eksperymencie wykorzystano trzy rodzaje kwarcu frakcji 0,5-1,0 mm. Wśród nich były to dwa rodzaje kwarcu żyłowego (Q_W, Q_K), które pochodziły z mechanicznego rozdrobnienia skał, oraz ziarna kwarcu ze środowiska eolicznego (Q_A). Kwarc żyłowy Q_W został pobrany z odsłonięcia w miejscowości Wojcieszów (Sudety Zachodnie, płd.-zach. Polska) z metamorficznych łupków serycytowo-chlorytowych (por. Kryza & Muszyński, 1992) a jego powstanie związane było z procesami hydrotermalnymi oraz lokalną aktywnością termiczną. Makroskopowo, skała ta jest biała i masywna, charakteryzuje się dużą twardością i odpornością na kruszenie. W wyniku kruszenia, rozpada się ona na wydłużone, kanciaste ziarna z tendencją do tworzenia odłamków o kształcie ostrzy lub tabliczek. Mikroskopowo, składa się z krystalicznego i zrekrystalizowanego kwarcu o ściśle przylegających do siebie kryształach subeuhedralnych. Lokalnie, badany kwarc zawiera cienkie i nieregularne zielone wrostki, prawdopodobnie o składzie epidotowo-chlorytowym (Cwojdziński & Kozdrój, 2011). Niniejszy typ kwarcu Q_W był obiektem badań w publikacjach nr 1 i 2.

Kwarc żyłowy Q_K pochodzi z odsłonięcia w miejscowości Kletno (Sudety Zachodnie, płd.-zach. Polska) z żył kwarcowych oraz kwarcowo-fluorytowych występujących w obrębie gnejsów oraz łupków mikowych. Hydrotermalne pochodzenie badanego kwarcu żyłowego związane było z migracją wysokozmineralizowanych roztworów wodnych przez regionalną strefę tektoniczną i lokalną strefą nasunięcia (Kasza, 1964; Zagożdżon & Zagrodny, 2009). Kwarc tworzy naprzemienne warstwy kwarcu mlecznego i ametystu. Makroskopowo, skała jest biała z lekkim fioletowym zabarwieniem i charakteryzuje się rozległą siecią spękań i szczelin. W wyniku kruszenia, rozpada się na prostokątne i romboedryczne kryształy. Mikroskopowo, kwarc budują głównie kryształy euhedralne, których ściany pokryte są drobnymi kryształami hematytu (Gaweł, 1947; Zieliński, 1997; Wołkowicz, 2000; Sobień & Nawrocki, 2010). Niniejszy typ kwarcu był obiektem badań w publikacji nr 1.

Ziarna kwarcu Q_A zostały pobrane z dowietrznej strony plejstoceńskiej wydmy śródlądowej w miejscowości Sławiny (Nizina Środkowomazowiecka, wsch. Polska), z głębokości ok. 3 m poniżej obecnej powierzchni wydmy, tzn. poniżej zasięgu oddziaływania współczesnych procesów mrozowych oraz wietrzenia bio-chemicznego związanych z procesami glebowymi. Rozwój form wydmowych na tym obszarze zachodził od najstarszego dryasu do wczesnego holocenu (Isarin & Renssen, 1999; Kasse, 2002; Hilgers, 2007; Zieliński i in., 2016; Moska i in., 2020, 2021), przy dominującym zachodnim kierunku wiatru (Renssen i in., 1996). Powierzchnie ziaren kwarcu Q_A charakteryzują się różnym stopniem obróbki eolicznej, od braku śladów aktywności eolicznej poprzez występujące jedynie na najbardziej wypukłych fragmentach ziaren, po ziarna w pełni zmienione przez procesy eoliczne. Na tej podstawie można przypuszczać, że procesy eoliczne były ostatnimi, które oddziaływały na powierzchnie badanych ziaren przed ich depozycją. Niniejszy typ kwarcu był obiektem badań w publikacji nr 3.

4. **METODY BADAŃ**

Fragmenty żył kwarcowych z Wojcieszowa i Kletna zostały mechanicznie rozdrobnione przy użyciu młyna skalnego (żyły kwarcowe z Wojcieszowa) oraz młotka (żyły kwarcowe z Kletna). Wszystkie próbki były przesiewane przy użyciu wytrząsarki mechanicznej w celu odseparowania ziaren frakcji grubego piasku (0,5-1 mm). Następnie próbki kwarcu żyłowego z Wojcieszowa i Kletna zostały umyte w wanience ultradźwiękowej w celu usunięcia cząsteczek powstałych w trakcie rozdrabniania osadu oraz pozbycia się ewentualnych pęknięć powstałych w czasie przygotowywania do eksperymentu. Każda próbka była analizowana pod binokularem w celu wykluczenia ziaren innych niż kwarc. Odseparowane ziarna kwarcu frakcji grubego piasku (Q_W, Q_K, Q_A) zostały podzielone na próbki o masie ok. 2 g oraz umieszczone na oddzielnych szalkach Petri'ego jako: (1) próbki suche, (2) próbki nawilżone, gdzie ziarna znajdowały się na wilgotnym sączku oraz (3) próbki mokre, gdzie ziarna były zanurzone w wodzie. Próbki podlegające wietrzeniu w warunkach nawilżonych i mokrych zostały przygotowane przy użyciu wody destylowanej, wody o niskiej i wysokiej mineralizacji. Ponadto, dla każdego rodzaju kwarcu (Q_W, Q_K, Q_A) zostały przygotowane próbki referencyjne (zawierające oryginalne ziarna kwarcu, nie poddane eksperymentalnemu wietrzeniu mrozowemu).

Symulacja wietrzenia mrozowego ziaren kwarcu frakcji piaszczystej (Q_W, Q_K, Q_A) została przeprowadzona w kontrolowanych warunkach laboratoryjnych przy użyciu komercyjnej, pionowej zamrażarki. Urządzenie zostało wyposażone w dodatkowe oprogramowanie, umożliwiające automatyczne zmiany temperatury w zakresie od -5°C do +10°C, symulujące warunki peryglacjalne. Półki, znajdujące się we wewnętrzu urządzenia, mają indywidualne systemy chłodzenia i ogrzewania, co zapewniło jednolite warunki temperaturowe i wilgotnościowe. W urządzeniu na bieżąco odprowadzane były skropliny oraz było ono automatyczne odszranianie w celu uniknięcia wewnętrznej kondensacji pary wodnej i krystalizacji kryształków lodu. Przebieg pracy urządzenia obejmował trzy powtarzające się etapy, które stanowiły jeden pełny cykl zamarzania-odmarzania, który trwał 4h. Były to: (1) faza zamarzania (2 godz.), podczas której temperatura spadała do -5°C, (2) faza stała (1 godz.), podczas której temperatura utrzymywana była na poziomie -5°C oraz (3) faza odmarzania (1 godz.), podczas której temperatura wzrastała do +10°C. Próbki kwarcu były wyjmowane z urządzenia po określonej liczbie cykli zamarzania-odmarzania i pozostawione do wyschnięcia w temperaturze pokojowej (~20°C-22°C). Zakup urządzenia zamrażająco-odmrażającego został sfinansowany ze środków Narodowego Centrum Nauki [nr projektu 2019/33/N/ST10/00021].

Na potrzeby pierwszej publikacji, próbki kwarcu Q_W, Q_K (suche, nawilżone i mokre), zostały wyjęte z urządzenia po 50, 100 i 300 cyklach zamarzania-odmarzania. Analizom laboratoryjnym i statystycznym poddano łącznie 42 próbki. Analizy laboratoryjne obejmowały analizę uziarnienia przy użyciu analizatora cząstek Malvern Morphologi G3 oraz analizę mikromorfologii powierzchni ziaren przeprowadzoną pod skaningowym mikroskopem elektronowym (SEM). Analizy statystyczne obejmowały analizę wykresów pudełkowych, test Kołmogorowa-Smirnowa, analizę składowych głównych (PCA) oraz analizę skupień.

Na potrzeby drugiej publikacji, próbki kwarcu Q_W, Q_K zostały wyjęte z urządzenia po 50, 100, 300, 700 i 1000 cyklach zamarzania-odmarzania. Obejmowały one próbki mokre przygotowane przy użyciu wody nisko i wysoko zmineralizowanej. Analizie mikromorfologii powierzchni ziaren przy użyciu skaningowego mikroskopu elektronowego (SEM) poddano łącznie 10 próbek.

Na potrzeby trzeciej publikacji, próbki kwarcu Q_A zostały wyjęte z urządzenia po 50, 100, 300, 700 i 1000 cyklach zamarzania-odmarzania. Obejmowały one próbki mokre przygotowane przy użyciu wody nisko zmineralizowanej. Analizom mikromorfologii ziaren kwarcu, nanostrukturalej i statystycznym poddano łącznie 5 próbek. Analiza mikromorfologii

powierzchni ziaren została przeprowadzona przy użyciu skaningowego mikroskopu elektronowego (SEM). Analiza nanostrukturalna została przeprowadzona przy użyciu transmisyjnego mikroskopu elektronowego (TEM). Analizy statystyczne obejmowały analizę skośności rozkładu oraz analizę detekcji obserwacji odstających (ang. *outliers*) z zastosowaniem analizy wykresów pudełkowych, filtra Hampel'a oraz Q testu Dixon'a.

Analiza mikromorfologii powierzchni ziaren wykonana została przy użyciu skaningowego mikroskopu elektronowego (SEM) typu ZEISS Sigma VP w Laboratorium Mikroskopii Elektronowej, Mikroanalizy i Dyfrakcji Rentgenowskiej (Wydział Geologii, Uniwersytet Warszawski). Wykonanie analizy zostało sfinansowane ze środków Narodowego Centrum Nauki [nr projektu 2019/33/N/ST10/00021]. Analiza nanostrukturalna została wykonana przy użyciu transmisyjnego mikroskopu elektronowego (TEM) w Helmoholtz Centre Potsdam, GFZ German Research Centre for Geosciences (Poczdam, Niemcy). Wykonanie analizy zostało sfinansowane ze środków Inicjatywa Doskonałości – Uczelnia Badawcza Uniwersytetu im. Adama Mickiewicza w Poznaniu [nr projektu 003/13/UAM/0019].

5. <u>ZARYS TREŚCI PUBLIKACJI WCHODZĄCYCH W SKŁAD ROZPRAWY DOKTORSKIEJ</u>

Wszystkie publikacje, wchodzące w skład rozprawy doktorskiej, dotyczą problemu wietrzenia mrozowego ziaren kwarcu frakcji piaszczystej w skali mikro w ujęciu eksperymentalnym.

Publikacja nr 1: Górska M.E., Woronko B., Kossowski T.M., Pisarska-Jamroży M., 2022. Micro-scale frost-weathering simulation – Changes in grain-size composition and influencing factors. *Catena*, 212, 106106.

W publikacji tej przedstawiono wpływ krótkookresowej działalności wietrzenia mrozowego (do 300 cykli zamarzania-odmarzania) na rozkład uziarnienia ziaren kwarcu żyłowego. Zmiany uziarnienia próbek poddanych wietrzeniu w stosunku do próbki referencyjnej (zawierającej oryginalne ziarna kwarcu, nie poddane eksperymentalnemu wietrzeniu mrozowemu) były analizowane po 50, 100 i 300 cyklach zamarzania-odmarzania z uwzględnieniem następujących zmiennych: rodzaju kwarcu (Q_W, Q_K), zawartości wody (próbki suche, nawilżone, mokre) oraz mineralizacji wody (woda destylowana, nisko i wysoko zmineralizowana). Różnice w rozkładzie uziarnienia, wynikające z destrukcyjnej działalności zamrozu, były obserwowane we wszystkich próbkach na każdy etapie wietrzenia (tj. po 50, 100 i 300 cyklach zamarzania-

odmarzania). Analizy statystyczne (analiza wykresów pudełkowych, test Kołmogorowa-Smirnowa, analiza składowych głównych, analiza skupień) rozkładów uziarnienia wykazały różne reakcje badanych dwóch typów ziaren kwarcu na zachodzący proces wietrzenia mrozowego, niezależnie od zawartości i mineralizacji wody. Największe zmiany w rozkładzie uziarnienia zostały odnotowane w obrębie frakcji bardzo grubego (1,0-2,0 mm) oraz grubego (0,5-1,0 mm) piasku. W przeciwieństwie do hipotezy Halla (1990), wiążącej intensywność wietrzenia mrozowego z zawartością frakcji pylastej w osadzie, produkcja ziaren frakcji pylastej (0,002-0,063 mm) stanowiła podrzędny produkt wietrzenia mrozowego. Zidentyfikowano i wykazano ponadto bardzo duży wpływ defektów pierwotnych (związanych ze strukturą wewnętrzną kwarcu; ang. *primary defects*) oraz defektów wtórnych (związanych z przygotowaniem próbki do eksperymentu; ang. *preparation defect*) ziaren kwarcu na przebieg procesu wietrzenia mrozowego. Oba nowe terminy zostały wprowadzone do literatury przez autorów publikacji. Ponadto, wykazano wpływ budowy wewnętrznej ziaren kwarcu na ich dezintegrację mechaniczną wywołaną zamrozem. Ziarna Q_W, zbudowane ze ściśle przylegających do siebie kryształów kwarcu (ang. *close contact*), ulegały dezintegracji w mniejszym stopniu, niż ziarna Q_K, które charakteryzowały się występowaniem przestrzeni porowej pomiędzy indywidualnymi kryształami kwarcu (ang. *open contact*). Świadczą o tym większe zmiany w udziale procentowym frakcji średniego, drobnego i bardzo drobnego piasku (0,063-0,5 mm) oraz pyłu (0,004-0,063 mm) w stosunku do próbek referencyjnych, odnotowane dla próbek Q_K w porównaniu z próbkami Q_W. Na podstawie zmian w uziarnieniu próbek Q_W i Q_K wywołanych działalnością zamrozu stwierdzono, że istnieje pewien przedział czasu niezbędny do zamanifestowania się efektów działalności wietrzenia mrozowego w skali mikro. Przedział ten nazwano *lag time* i wykazano jego wpływ na początkowym (do 50 cykli zamarzania-odmarzania) i bardziej zaawansowanym etapie wietrzenia (100-300 cykli zamarzania-odmarzania).

Publikacja nr 2: Górska M.E., Woronko B., 2022. Multi-stage evolution of frost-induced microtextures on the surface of quartz grains – An experimental study. *Permafrost and Periglacial Processes*, 33, 470-489.

W publikacji przedstawiono wpływ długookresowej działalności wietrzenia mrozowego na mikrorzeźbę ziaren kwarcu żyłowego (Q_W), tj. po 50, 100, 300, 700 i 1000 cyklach zamarzania-odmarzania. Badaniom poddano próbki mokre przygotowane z dodatkiem wody nisko i wysoko zmineralizowanej. Analiza mikromorfologii ziaren kwarcu frakcji piaszczystej została przeprowadzona przy użyciu skaningowego mikroskopu elektronowego (SEM) dla

próbki referencyjnej oraz po wspomnianych wyżej cyklach. Wyznaczono cztery mikrostruktury diagnostyczne dla wietrzenia mrozowego: małe i duże przełamy muszlowe (oznaczone jako cf i CF; ang. *conchoidal fractures*) oraz małe i duże *breakage blocks* (oznaczone jako bb i BB). Na podstawie zmian mikrostrukturalnych obserwowanych na powierzchni badanych ziaren kwarcu, zidentyfikowano dwa rodzaje wietrzenia mrozowego działające w skali mikro. Są to: (1) wietrzenie fizyczne, dominujące w trakcie pierwszych 300 cykli zamarzania-odmarzania, manifestujące się postępującym rozwojem mikrostruktur cf, CF, bb, BB, oraz (2) wietrzenie chemiczne, dominujące po 300 cyklach zamarzania-odmarzania i manifestujące się obecnością skorupy powstałej z wytrącania składników rozpuszczonych w wodzie w czasie zamarzania, która zaciera pierwotną mikrorzeźbę ziaren i ogranicza wietrzenie fizyczne. W ewolucji mikrorzeźby charakterystycznej dla wietrzenia mrozowego wydzielono trzy etapy: (1) etap inicjalny, w czasie którego powstaje głównie mikrostruktura CF, (2) etap rozwoju z dominacją mikrostruktur cf, oraz (3) etap zaawansowany, przejawiający się tworzeniem mikrostruktur typu bb i BB. Wykazano, że przedstawiona trzy-etapowa ewolucja mikrorzeźby, pochodzenia mrozowego może zostać przerwana przez proces „odmładzania" (ang. *refreshing*), który prowadzi do odsłonięcia świeżej, niezwietrzałej powierzchni ziaren, a tym samym proces wietrzenia zaczyna się na niej od nowa.

Publikacja nr 3: Górska M.E., Woronko B., Kossowski T.M., 2023. Factors influencing the development of microtextures on cold-climate aeolian quartz grains revealed by experimental frost action. *Permafrost and Periglacial Processes*, 2023, 1-25.

W publikacji przedstawiono efekty długookresowej działalności wietrzenia mrozowego na mikrorzeźbę ziaren kwarcu transportowanych w środowisku eolicznym (Q_A). Badaniom poddano próbki mokre przygotowane z dodatkiem wody nisko zmineralizowanej. Analiza mikrostrukturalna została przeprowadzona przy użyciu skaningowego mikroskopu elektronowego (SEM) dla próbki nie poddanej procesowi wietrzenia oraz po 50, 100, 300, 700 i 1000 cyklach zamarzania-odmarzania. Dodatkowo, wykonano analizę nanostrukturalną przy użyciu transmisyjnego mikroskopu elektronowego (TEM) dla ziaren nie poddanych procesowi wietrzenia oraz po 100 i 1000 cyklach zamarzania-odmarzania. Obserwowanymi efektami wietrzenia mrozowego były małe i duże przełamy muszlowe (oznaczone jako cf i CF; ang. *conchoidal fractures*), małe i duże *breakage blocks* (oznaczone jako bb i BB) oraz pęknięcia na powierzchni ziaren. Ze względu na kształt małych przełamów muszlowych (ang. *conchoidal fractures*) wyróżniono dwa typy tych mikrostruktur (oznaczone jako cf_I i cf_{II}). Zaobserwowano stopniowy wzrost liczby mikrostruktur pochodzenia mrozowego (cf, CF, bb, BB) na

powierzchni analizowanych ziaren kwarcu wraz z czasem trwania wietrzenia, manifestującym się liczbą cykli zamarzania-odmarzania. Liczba tych mikrostruktur była stosunkowo niewielka do 700 cykli zamarzania-odmarzania, a jej znaczny wzrost odnotowano dopiero po 1000 cyklach zamarzania-odmarzania. Na tej podstawie stwierdzono, że ziarna kwarcu pochodzenia eolicznego (Q_A), w porównaniu do ziaren kwarcu żyłowego (Q_W, Q_K), wymagają znacznie dłuższego czasu działania wietrzenia mrozowego w celu zamanifestowania się jego efektów, a więc charakteryzują się dłuższym *lag time*. Podatność ziaren eolicznych, których transport odbywał się w zimnym klimacie, na powstawanie mikrostruktur mrozowych zależy między innymi od wewnętrznych cech ziaren kwarcu, będących efektem procesów eolicznych, którym były poddawane oraz pierwotnej ich struktury. Stwierdzono, że modyfikacje struktury ziaren kwarcu na skutek procesów eolicznych prowadzą do powstania podpowierzchniowej strefy uderzeniowej (ang. *impact zone*). Miąższość tej strefy determinuje głębokość, do jakiej mogą rozwijać się mikrostruktury pochodzenia mrozowego. Drugim czynnikiem wpływającym na podatność ziaren eolicznych, pochodzących z zimnego klimatu, na powstawanie mikrostruktur mrozowych są ich pierwotne i wtórne defekty sieci krystalicznej. Wykazano także zależność pomiędzy liczbą mikrostruktur mrozowych rejestrowaną na powierzchni ziaren kwarcu pochodzenia eolicznego a kształtem samych ziaren, w szczególności ich kulistością. Stwierdzono, że ziarna charakteryzujące się niską kulistością wykazują mniejszą podatność na powstawanie mikrostruktur pochodzenia mrozowego, niż ziarna o wysokiej kulistości. Udowodniono, że w danej populacji ziaren poddawanych wietrzeniu mrozowemu, nie wszystkie ziarna reagują na zmiany temperatury w jednakowym stopniu.

6. <u>WNIOSKI</u>

Badania przeprowadzone w ramach rozprawy doktorskiej dokumentują przebieg i wyniki długookresowej symulacji eksperymentalnej wietrzenia mrozowego ziaren kwarcu frakcji piaszczystej w skali mikro. Otrzymane wyniki dają wgląd w przebieg wietrzenia mrozowego ziaren kwarcu żyłowego i eolicznego, co stanowi istotny krok ku dokładniejszym interpretacjom mikrostrukturalnym. Zaproponowana metodologia badań może stanowić punkt wyjścia dla przyszłych badań eksperymentalnych wietrzenia mrozowego ziaren kwarcu w skali mikro.

6.1. Przebieg wietrzenia mrozowego ziaren kwarcu frakcji piaszczystej w skali mikro

Badania przeprowadzone w ramach niniejszej rozprawy doktorskiej wykazały, że wietrzenie mrozowe w skali mikro jest procesem bardziej skomplikowanym, niż do tej pory sądzono. Raz zainicjowane, prowadzi do dezintegracji ziaren kwarcu i powstania charakterystycznej mikrorzeźby. Przebieg wietrzenia mrozowego w skali mikro w większej mierze zależy od czynników wewnętrznych (tj. cechy wewnętrzne ziaren kwarcu, cechy ziaren odziedziczone z poprzednich środowisk sedymentacyjnych), niż zewnętrznych (dostępność i mineralizacja wody). W konsekwencji, reakcja ziaren kwarcu różnej genezy na wietrzenie mrozowe oraz ich podatność na modyfikacje wywołane zamrozem są trudne do przewidzenia i pozostają charakterystyczne dla danego typu ziaren.

6.2. Produkcja ziaren frakcji pylastej na skutek wietrzenia mrozowego

Wietrzenie mrozowe ziaren kwarcu żyłowego (Q_W, Q_K) po 300 cyklach zamarzania-odmarzania wykazało dominujący wpływ cech wewnętrznych ziaren na przebieg ich dezintegracji mrozowej w skali mikro. Szczególną rolę pełni typ kontaktu pomiędzy poszczególnymi kryształami budującymi ziarno kwarcu oraz obecność inkluzji ciekło-gazowych lub ich pozostałości. Destrukcja mechaniczna ziaren kwarcu wywołana zamrozem wykorzystuje strefy osłabienia (ang. *weakness zones*) w obrębie ich struktury krystalicznej. Należą do nich defekty pierwotne (ang. *primary defects*) oraz wtórne (ang. *preparation / inherited defects*). Na początkowym etapie wietrzenia, tj. po 50 cyklach zamarzania-odmarzania, następuje eliminacja defektów wtórnych, która prowadzi do destrukcji ziaren frakcji bardzo grubego piasku (1-2 mm) i produkcji ziaren frakcji grubego (0,5-1 mm) i średniego (0,25-0,5 mm) piasku. Na dalszym etapie wietrzenia, tj. po 100 i 300 cyklach zamarzania-odmarzania, zostają wykorzystane defekty pierwotne, które prowadzą do produkcji ziaren frakcji bardzo grubego piasku (1-2 mm). Zagadnienie powstawania ziaren frakcji bardzo grubego (1-2 mm) i grubego (0,5-1 mm) piasku na skutek wietrzenia mrozowego nigdy wcześniej nie było omawiane w literaturze.

W wyniku eliminacji większość defektów wtórnych i pierwotnych, na bardziej zaawansowanym etapie wietrzenia, tj. po 300 cyklach zamarzania-odmarzania, dochodzi do odsłonięcia nienaruszonej, wewnętrznej części ziarna (ang. *host grain*). Od tego momentu, proces wietrzenia mrozowego ziarna jest utrudniony i większa liczba cykli zamarzania-odmarzania jest potrzebna, by doszło do jego destrukcji. Udokumentowana, w efekcie

przeprowadzonego eksperymentu, wielkość produkcji frakcji pylastej jest nieznaczna i nie odzwierciedla intensywności wietrzenia mrozowego (por. Hall, 1990).

6.3. Modyfikacje powierzchni ziaren kwarcu na skutek wietrzenia mrozowego

Długookresowa symulacja wietrzenia mrozowego, tj. po 1000 cyklach zamarzania-odmarzania, ziaren kwarcu żyłowego (Q_W) i eolicznego (Q_A) oraz analiza mikrostrukturalna powierzchni ziaren potwierdziły dominację czterech diagnostycznych dla procesu zamrozu mikrostruktur: małych (>10 µm) i dużych (<10 µm) przełamów muszlowych (oznaczone jako cf i CF) oraz małych (>10 µm) i dużych (<10 µm) mikrostruktur typu *breakage blocks* (oznaczone jako bb i BB). Poza wymienionymi wyżej mikrostrukturami odzwierciedlającymi dominację wietrzenia fizycznego, zidentyfikowano mikrostruktury pochodzenia chemicznego. Manifestują się one w formie skorupy, której obecność powoduje zatarcie pierwotnej mikrorzeźby ziaren i może zahamować proces wietrzenia fizycznego.

Z przeprowadzonych obserwacji płynie istotny wniosek dotyczący możliwości rekonstrukcji stopnia zaawansowania procesu wietrzenia mrozowego. Liczba mikrostruktur mrozowych pochodzenia mechanicznego (cf, CF, bb, BB) wskazuje na stopień rozwoju mikrorzeźby mrozowej ziaren kwarcu, ale nie świadczy ona o stopniu zaawansowania samego procesu wietrzenia mrozowego. Wynika to z faktu, że rozwój mikrorzeźby mrozowej ziaren kwarcu, w trakcie postępującego procesu wietrzenia, może zostać przerwany przez proces „odmładzania" powierzchni ziaren, który prowadzić może do odsłonięcia świeżej, niezwietrzałej powierzchni. Oddziaływanie zamrozu na powierzchnię ziaren kwarcu prowadzi do powstania cienkiej, zewnętrznej warstwy, zdefiniowanej jako warstwa wyeksponowana na zamróz (ang. *frost-exposed skin*). Jej miąższość determinuje głębokość, do jakiej wietrzenie mrozowe najprawdopodobniej penetrować będzie ziarno kwarcu, przyczyniając się do rozwoju mikrostruktur mrozowych (cf, CF, bb, BB).

Spis literatury

Akagawa S., Fukada M., 1991. Frost heave mechanism in welded tuff. Permafrost and Periglacial Processes, 2, 301-309.

Anderson R., 1998. Near-surface thermal profiles in alpine bedrock: implications for the frost weathering of rock. Arctic and Alpine Research, 30, 362-372.

Ballantyne C.K., 2018. Periglacial Geomorphology. Wiley-Blackwell, 11-22.

Błaszkiewicz M., 2011. Timing of the final disappearance of permafrost in the central European Lowland, as reconstructed from the evolution of lakes in N Poland. Geological Quaternary, 55, 361-374.

Boelhouwers J., 2003. Sensitivity and responses to climate change in the Subantarctic periglacial environment. 8th International Conference on Permafrost, Zurich, Swietzerland, 67-71.

Bull P.A., 1981. Environmental reconstruction by electron microscopy. Progress in Physical Geography, 5, 368-397.

Costa P.J.M., Andrade C., Mahaney W.C., Da Silva F.M., Freire P., Freitas M.C., Janardo C., Oliveira M.A, Silva T., Lopes, V., 2013. Aeolian microtextures in silica spheres induced in a wind tunnel experiment: Comparison with aeolian quartz. *Geomorphology*, 180, 120-129.

Costa, P.J.M., Andrade, C., Dawson A.G., Mahaney W.C., Freitas M.C., Paris R., Taborda R., 2012. Microtextural characteristics of quartz grains transported and deposited by tsunamis and storms. *Sedimentary Geology*, 275, 55-69.

Cwojdziński S., Kozdrój W., 2011. Objaśnienia do szczegółowej mapy geologicznej. Państwowy Instytut Geologiczny – Państwowy Instytut Badawczy.

Degórski M., Kowalkowski A., 2011. The use of SEM morphoscopy in researching the litho-pedogenetic environments evolution of Late Pleistocene and Holocene. Geographia Polonica, 84, 17-38.

Demitroff M., Rogov V.V., French H.M., Konishchev V.N., Streletskiy D.A., Lebedeva-Verba M.D., Alekseeva V.A., 2007. Possible evidence for episodes of Late Pleistocene cryogenic weatheing, southern New Jersey, Eastern USA. [W:] Proceedings, Volume II, Cryogenic Resources of Polar Regions, RAS, SB, Salekhard, 139-141.

Dietzel M., 2005. Impact of cyclic freezing on precipitation of silica in Me-SiO2-H2O systems and geochemical implications for cryosoils and sediments. Chemical Geology, 216, 79-88.

Frauenfeld O.W., Zhang T., Barry R.G., Gilichinsky D., 2004. Interdecadal changes in seasonal freeze and thaw depths in Russia. Journal of Geophysical Research, 109, 1-12.

French H.M., 2017. The periglacial environment. Wiley-Blackwell, 544 pp.

Gaweł A., 1947. Geological conditions of origin of blue salt, amethyst and violet fluorite. Annales Societatis Geologorum Poloniae, 17, 51-60.

Goździk J.S., 1995. Permafrost evolution and its impact on deposition conditions between 20 and 10 ka BP in Poland. Biuletyn Peryglacjalny, 34, 53-72.

Grebenets V.I., Konishchev V.N., Rogov V.V., 2002. Cryogenic destruction of construction materials in foundations of buildings erected in the permafrost zone. Soil Mechanics and Foundation Engineering, 39, 106-111.

Hall K., 1980. Freeze-thaw activity at a nivation site in northern Norway. Arctic and Alpine Research, 12, 183-194.

Hall K., 1990. Mechanical weathering rates on Signy Island, Maritime Antarctic. Permafrost and Periglacial Processes, 1, 61-67.

Hall K., 1992. Mechanical weathering on Livingstone Island, south Shetland Islands, Antarctica. [W:] Yoshida Y., Kaminuma K., Shiraishi K. (red.). Recent Progress in Antarctic Earth Science. Proceedings of the Sixth International Symposium on Antarctic Earth Sciences. Ranzan, Saitama, Japan. Terra Scientific Publishing, Tokyo, 757-762.

Hall K., 2004. Evidence for freeze-thaw events and their implications for rock weathering in northern Canada. Earth Surface Processes and Landforms, 29, 43-57.

Hall K., Lautridou J.P., 1991. Introduction - Cryogenic weathering. Permafrost and Periglacial Processes, 2, 269-270.

Hall K., Thorn C., 2011. The historical legacy of spatial scales in freeze-thaw weathering: Misinterpretation and resulting misdirection. Geomorphology, 130, 83-90.

Hallet B., Walder J.S., Stubbs C.W., 1991. Weathering by segregation ice growth in microcracks at sustained subzero temperatures: verification from an experimental study using acoustic emission. Permafrost and Periglacial Processes, 2, 283-300.

Halsey L.A., Vitt D.H., Zoltai S.C., 1995. Disequilibrium response of permafrost in boreal continental western Canada to climate change. Climatic Change, 30, 57-73.

Harris C., Davies M.C.R., Etzelmüller B., 2001b. The assessment of potential geotechnical hazards associated with mountain permafrost in a warming global climate. Permafrost and Periglacial Processes, 12, 145-156.

Harris C., Haeberli W., Vonder Mühll D., King L., 2001a. Permafrost monitoring in the high mountains of Europe: the PACE project in its global context. Permafrost and Periglacial Processes, 12, 3-11.

Helland P.E., Holmes M.A., 1997. Surface textural analysis of quartz sand grains from ODP Site 918 off the southeast coast of Greenland suggests glaciation of southern Greenland at 11 Ma. Palaeogeography, Palaeoclimatology, Palaeoecology, 135, 109-121.

Hilgers A., 2007. The chronology of late glacial and Holocene dune development in the northern central European lowland reconstructed by optically stimulated luminescence (OSL) dating. Rozprawa doktorska, University of Cologne.

Immonen N., Strand K., Huusko A., Lunkka J.P., 2014. Imprint of late Pleistocene continental processes visible in ice-rafted grains from central Arctic Ocean. Quaternary Science Reviews, 92, 133-139.

Isarin R.F., Renssen H., 1999. Reconstructing and modelling Late Weichselian climates: the Younger Dryas in Europe as a case study. Earth-Science Reviews, 48, 1-38.

John K.S.T., Passchier S., Tantillo B., Darby D., Kearns L., 2015. Microfeatures of modern sea-ice-rafted sediment and implications for paleo-sea-ice reconstructions. Annals of Glaciology, 56, 83-93.

Kalińska-Nartiša E., Woronko B., Ning W., 2017. Microtextural inheritance on quartz sand grains from Pleistocene periglacial environments of the Mazovian Lowlands, Central Poland. Permafrost and Periglacial Processes, 28, 741-756.

Kasse C., 2002. Sandy aeolian deposits and environments and their relation to climate during the Last Glacial Maximum and Late glacial in northwest and central Europe. Progress in Physical Geography: Earth and Environment, 26, 507–532.

Kasza L., 1964. Budowa geologiczna górnego dorzecza Białej Lądeckiej Geologia Sudetica, 1, 119–167.

Kaufmann J.P., 2004. Experimental identification of ice formation in small concrete pores. Cement and Concrete Research, 34, 1421-1427.

Kemnitz H., Lucke B., 2019. Quartz grain surfaces–A potential microarchive for sedimentation processes and parent material identification in soils of Jordan. Catena, 176, 209-226.

Kirshner A.E., Anderson J.B., Wellner J.S., 2011. Cenozoic glacial history of the northern Antarctic Peninsula: a micromorphological investigation of quartz sand grains. Tectonic, climatic, and cryospheric evolution of the Antarctic Peninsula, 63, 153-165.

Konishchev V.N., 1973. Frost weathering. [W:] Proceedings of the 2nd International Conference on Permafrost, 13-28 July 1973, Yakutsk, USSR. Office National Academy of Sciences, Washington, 176-181.

Konishchev V.N., 1998. Relationship between the lithology of active layer materials and mean annual ground temperature in the former USSR. Proceedings 7th International. Conference Permafrost, Yellowknife, Canada, 591-594.

Konishchev V.N., 1999. Evolution of ground temperature of Russian Arctic zone in upper Cenozoic. Earth's Cryosphere, 3, 39-47.

Konishchev V.N., Lebedeva-Verba M.P., Rogov V.V., Stalina E.E., 2005. Cryogenesis of modern and Late Pleistocene deposits Altai and periglacial region of Europa. GEOS: Moscow.

Kornishchev V.N., Rogov V.V., 1993. Investigations of cryogenic weathering in Europe and Northern Asia. Permafrost and Periglacial Processes, 4, 49-64.

Kowalkowski A., 1988. Textural features of the surface of quartz sand grains in acid and alkaline soils of the cold climate. [W:] Mycielska-Dowgiałło E. (red.). Geneza osadów i gleb w świetle badań w mikroskopie elektronowym. Wydawnictwo Uniwersytetu Warszawskiego, Warszawa, 87-99.

Kowalkowski A., Mycielska-Dowgiałło E., 1980. Soil forming processes in the tundra and arid steppe of the Khangai Mountains on the basis of quartz grain analysis with an electron microscope. Polish Journal of Soil Science XIII, 51–71.

Kowalkowski A., Mycielska-Dowgiałło E., 1985. Weathering of quartz grain in the liquefied horizon of permafrost solonchaks in the arid steppe zone, Central Mongolia. Catena 12, 179–190.

Krinsley D.H., Doornkamp J., 1973. Atlas of quartz sand surface textures. Cambridge University Press, 37 pp.

Kryza R., Muszyński A., 1992. Pre-Variscan volcanic-sedimentary succession of the central south Góry Kaczawskie, SW Poland: Outline geology. Annales Societatis Geologorum Poloniae, 62, 117–140.

Lautridou J.P., Ozouf J.C., 1982. Experimental frost shattering: fifteen years of research at the Centre de Geomorphologie du CNRS. Progress in Physical Geography, 6, 215-232.

Li G., Sheng Y., Jin H., Ma W., Qi J., Wen Z., Zhang B., Mu Y., Bi G., 2010. Development of freezing-thawing processes of foundation soils surrounding the China-Russia Crude Oil

Pipeline in the permafrost areas under a warming climate. Cold Regions Science and Technology, 64, 226-234.

Lindner L., Gozhik P., Marciniak B., Marks L., Yeloviecheva Y., 2004. Main climatic changes in the Quaternary of Poland, Belarus and Ukraine. Geological Quaternary, 48, 97-114.

Łoziński M.W., 1909. Über die mechanische Verwitterung der Sandsteine im gemassibten Klima. Académie des sciences de cracovie, Bulletin internationale, classe de science, mathématiques et naturelles, 1, 1-25.

Łoziński M.W., 1912. On the mechanical weathering of sandstones in temperate climates. [W:] Cold Climate Landforms, Evans D.J.A. (red.). Wiley, 119-134.

Mahaney W.C., 1995. Pleistocene and Holocene glacier thicknesses, transport histories and dynamics inferred from SEM microtextures on quartz particles. Boreas, 24, 293-304.

Mahaney W.C., 2002. Atlas of sand grain surface textures and applications. Oxford University Press, Oxford, 237 pp.

Mahaney W.C., Stewart A., Kalm V., 2001. Quantification of SEM microtextures useful in sedimentary environmental discrimination. Boreas, 30, 165-171.

Marks L., 2011. Quaternary Glaciations in Poland. Developments in Quaternary Sciences, 15, 299-303.

Marks L., Makos M., Szymanek M., Woronko B., Dzierżek J., Majecka A., 2019. Late Pleistocene climate of Poland in the mid-European context. Quaternary International, 504, 24-29.

Marshall J.R., 1987. Clastic Particles: Scanning Electron Microscopy and Shape Analysis of Sedimentary and Volcanic Clasts. New York, 346 pp.

Matsuoka N., 1990. The rate of bedrock weathering by frost action: field measurements and a predictive model. Earth Surface Processes and Landforms, 15, 73-90.

Matsuoka N., 1995. Rock weathering process and landform development in the Sør Rondane Mountains, Antarctica. Geomorphology, 12, 323-339.

Matsuoka N., 2001a. Direct observations of frost weathering in alpine bedrock. Earth Surface Processes and Landforms, 26, 601-614.

Matsuoka N., 2001b. Microgelivation versus Macrogelivation: towards bridging the gap between laboratory and field frost weathering. Permafrost and Periglacial Processes, 12, 299-313.

Matsuoka N., Hirakawa K., Watanabe T., Moriwaki K., 1997. Monitoring of periglacial slope processes in the Swiss Alps: the first two years of frost shattering, heave and creep. Permafrost and Periglacial Processes, 8, 155-177.

Matsuoka N., Murton J., 2008. Frost weathering: recent advances and future directions. Permafrost and Periglacial Processes, 19, 195-210.

McFadden L.D., Eppes M.C., Gillespie A.R., Hallet B., 2005. Physical weathering in arid landscapes due to diurnal variation in the direction of solar heating. Geological Society of America Bulletin, 1/2, 161-173.

McKay C., Molaro J.L., Marinova M.M., 2009. High-frequency rock temperature data from hyper-arid desert environments in the Atacama and the Antarctic Dry Valleys and implications for rock weathering. Geomorphology, 110, 182-187.

Menzies J., Van der Meer J.J.M., 2018. Past Glacial Environments. Elsevier, Amsterdam, 858 pp.

Molén M.O., 2014. A simple method to classify diamicts by scanning electron microscope from surface microtextures. Sedimentology 61, 2020–2041.

Moska P., Jary Z., Sokołowski R.J., Poręba G., Raczyk J., Krawczyk M., Skurzyński J., Zieliński P., Michczyński A., Tudyka K., Adamiec G., Piotrowska N., Pawełczyk F., Łopuch M., Szymak A., Ryzner K., 2020. Chronostratigraphy of Late Glacial aeolian activity in SW Poland – A case study from the Niemodlin Plateau. Geochronometria, 47, 124-137.

Moska P., Sokołowski R.J., Jary Z., Zieliński P., Raczyk J., Szymak A., Krawczyk M., Skurzyński J., Poręba G., Łopuch M., Tudyka K., 2021. Stratigraphy of the Late Glacial and Holocene aeolian series in different sedimentary zones related to the Last Glacial maximum in Poland. Quaternary International, 630, 65-83.

Murton J.B., Coutard J.P., Lautridou J.P., Ozouf J.C., Robinson D.A., Williams R.B.G., Guillemet G., Simmons P., 2000. Experimental design for a pilot study on bedrock weathering near the permafrost table. Earth Surface Processes and Landforms, 25, 1281-1294.

Murton J.B., Coutard J.P., Lautridou J.P., Ozouf J.C., Robinson D.A., Williams R.B.G., 2001. Physical modelling of bedrock brecciation by ice segregation in permafrost. Permafrost and Periglacial Processes, 12, 255-266.

Nicholson D.T., Nicholson F.H., 2000. Physical deterioration of sedimentary rocks subjected to experimental freeze-thaw weathering. Earth Surface Process and Landforms, 25, 1295-1307.

Renssen H., Lautenschlager M., Schuurmans C. J. E., 1996. The atmospheric winter circulation during the Younger Dryas stadial in the Atlantic/European sector: Climate Dynamics, 12, 813–824.

Rödder T., Kneisel C., 2012. Influence of snow cover and grain size on the ground thermal regime in the discontinuous permafrost zone, Swiss Alps. Geomorphology, 175-176, 176-189.

Rose K.C., Hart J.K., 2008. Subglacial comminution in the deforming bed: inferences from SEM analysis. Sedimentary Geology, 203, 87-97.

Ruedrich J., Kirchner D., Siegesmund D., 2011. Physical weathering of building stones induced by freeze-thaw action: a laboratory long-term study. Environmental Earth Sciences, 63, 1573-1586.

Schwamborn G., Förster A., Diekmann B., Schirrmeister L., Fedorov G., 2008. Mid to Late Quaternary cryogenic weathering conditions in Chukotka, northeastern Russia: inference from mineralogical and microtextural properties of the Elgygytgyn Crater Lake sediment record. Ninth International Conference On Permafrost, Institute of Northern Engineering, University of Alaska, Fairbanks, 1601-1606.

Schwamborn G., Mayer H., Fedorov G., Schirrmeister L., Hubberten H.W., 2006. Ground ice and slope sediments archiving late Quaternary paleoenvironment and paleoclimate signals at the margins of El'gygytgyn Impact Crater, NE Siberia. Quaternary Research, 66, 259-277.

Schwamborn G., Schirrmeister L., Frütsch F., Diekmann D., 2012. Quartz weathering in freeze-thaw cycles: experiment and application to the El'gygytgyn Crater Lake record for tracing Siberian permafrost history. Geografiska Annaler: Series A, Physical Geography, 94, 481-499.

Sobień K., Nawrocki J., 2010. Palaeomagnetic and petromagnetic study of uranium bearing polymetallic-fluorite mineralization in the Orlik-Kladsko crystalline complex (near Kletno, Lower Silesia, Poland). Geological Quarterly, 54, 325–336.

Stieglitz M., Déry S.J., Romanovsky V.E., Osterkamp T.E., 2003. The role of snow cover in the warming of Arctic permafrost. Geophysical Research Letters, 30, 1721.

Thomachot C., Matsuoka N., Kuchitsu N., Morii M., 2005. Frost damage of bricks composing a railway tunnel monument in Central Japan: field monitoring and laboratory simulation. Natural Hazards and Earth System Sciences, 5, 465-476.

Tricart J., 1956. Etude expérimentale du problème de la gélivation. Biuletyn Peryglacjalny, 4, 285-318.

Van Hoesen J.G., Orndorff R.L., 2004. A comparative SEM study on the micromorphology of glacial and non-glacial clasts with varying age and lithology. Canadian Journal of Earth Science, 41, 1123-1139.

Van Loon A.J., Błaszkiewicz M., Degórski M., 2014. The role of permafrost in shaping the Late Glacial relief of northern Poland. Netherlands Journal of Geosciences, 91, 223-231.

Vandenberghe J., French H.M, Gorbunov A., Marchenko S., Velichko A.A., Jin H., Cui Z., Zhang T., Wan X., 2014. The Last Permafrost Maximum (LPM) map of the Northern Hemisphere: permafrost extent and mean annual temperatures, 25-17 ka BP. Boreas, 43, 652-666.

Vandenberghe J., Woronko B., Nieuwendam A., Bateman M., 2016. Reconstruction and modelling of past permafrost and periglacial environments. Permafrost and Periglacial Processes, 27, 3-5.

Varlamov S.P., 2018. Thermal monitoring of railway subgrade in a region of ice-rich permafrost, Yakutia, Russia. Cold Regions Science and Technology, 155, 184-192.

Vos K., Vandenberghe N., Elsen J., 2014. Surface textural analysis of quartz grains by scanning electron microscopy (SEM): From sample preparation to environmental interpretation. Earth-Science Reviews, 128, 93-104.

Walder J.S., Hallet B., 1985. A theoretical model of the fracture of rock during freezing. Geological Society of America Bulletin, 96, 336-346.

Walder J.S., Hallet B., 1986. The physical basis of frost weathering: toward a more fundamental and unified perspective. Arctic and Alpine Research, 18, 27-32.

Wang G.X., Yao J.Z., Guo Z.G., Wu Q.B., Wang Y.B., 2004. Changes in permafrost ecosystem under the influences of human engineering activities and its enlightenment to railway construction. Chinese Science Bulletin, 49, 1741-1750.

Wei M., Guodong C., Qingbai W., 2009. Construction on permafrost foundations: Lessons learned from the Qinghai-Tibet railroad. Cold Regions Science and Technology, 59, 3-11.

Williams P.J., Smith M.W., 1989. The Frozen Earth. Cambridge University Press, Cambridge, 306 pp.

Wołkowicz K., 2000. O katodoluminescencji sudeckich kwarców żyłowych. Przegląd Geologiczny, 48, 625-633.

Woronko B., 2000. The influence of climatic conditions on the surface character of aeolian sand quartz grains. [W:] Dulias R., Pełka-Gościniak J. (red.). Aeolian processes in different landscape zones. Sosnowiec, 18-27.

Woronko B., 2012. Micromorphology of quartz grains as a tool in the reconstruction of periglacial environment. [W:] Churski P. (red.). Contemporary Issues in Polish Geography, 111-131.

Woronko B., 2016. Frost weathering versus glacial grinding in the micromorphology of quartz sand grains: Processes and geological implications. Sedimentary Geology, 335, 103-119.

Woronko B., Hoch M., 2011. The development of frost-weathering microstructures on sand-sized quartz grains: examples from Poland and Mongolia. Permafrost and Periglacial Processes, 22, 214-227.

Woronko B., Pisarska-Jamroży M., 2016. Micro-scale frost weathering of sand-sized quartz grains. Permafrost and Periglacial Processes, 27, 109-122.

Woronko B., Pisarska-Jamroży M., Van Loon A.J., 2015. Reconstruction of sediment provenance and transport processes from the surface textures of quartz grains from Late Pleistocene sandurs and ice-marginal valley in NW Poland. Geologos, 21, 105-115.

Wright J., Smith B., Whalley B., 1998. Mechanisms of loess-sized quartz silt production and their relative effectiveness: laboratory simulations. Geomorphology, 23, 15-34.

Wright J.S., 2000. The spalling of overgrowths during experimental freeze – thaw of quartz sandstone as mechanism of quartz silt production. Micron, 31, 631-638.

Wright J.S., 2007. An overview of the role of weathering in the production of quartz silt. Sedimentary Geology, 202, 337-351.

Zagożdżon P.P., Zagrodny K., 2009. Cyfrowe modelowanie Jaskini Niedźwiedziej w Kletnie oraz jej geologicznego otoczenia. Prace Naukowe Instytutu Górnictwa Politechniki Wrocławskiej, 128, 221–236.

Zhang T., Barry G., Knowles K., Heginbottom J.A., Brown J., 2008. Statistics and characteristics of permafrost and ground-ice distribution in the Northern Hemisphere. Polar Geography, 31, 47-68.

Zieliński P., Sokołowski R.J., Woronko B., Fedorowicz S., Jankowski M., Standzikowski K., 2016. Sandy deposition in a small dry valley in the periglacial zone of the Last Glacial Maximum: A case study from the Józefów site, SE Poland. Quaternary International, 399, 58–71.

Zieliński, G., 1997. Temperatury powstawania kwarcu i fluorytu ze złoża uranowo-polimetalicznego w Kletnie, Dolny Śląsk. Uniwersytet Warszawski, Warszawa. Praca magisterska.

SUMMARY OF THE DOCTORAL DISSRETATION

Experimental frost weathering of quartz grains – the record of changes in micromorphology and grain-size composition

Eksperymentalne wietrzenie mrozowe ziaren kwarcu
– zapis zmian w mikromorfologii i uziarnieniu

1. INTRODUCTION

Frost weathering, defined also as gelivation or cryogenic weathering, is an example of physical (mechanical) weathering or a combination of physical, biochemical or physicochemical processes (Hall & Lautridou, 1991; French, 2017). Despite the long tradition of research on this phenomenon, it is still believed that it is a poorly understood group of physicochemical processes that operate in cold climates. Frost weathering (mechanical) is a process of mechanical disintegration of rocks, which occurs as a result of cyclic transitions of temperature through 0˚C (e.g. French, 2017). Conditions conducive to frost disintegration of rocks are identified with the cold climate, in particular with the periglacial environment (e.g. Hall & Lautridou, 1991; French, 2017), which mainly covers areas located in the foreground of glaciers and ice sheets, areas of high latitude and high mountains. The extent of the area affected by periglacial processes is closely related to the presence of permafrost (e.g. Zhang et al., 2008; French, 2017; Ballantyne, 2018; Menzies & Van der Meer, 2018) and determined by regional climatic conditions. However, the process of frost weathering also occurs wherever the ground temperature oscillates around 0°C.

The present-day periglacial environment covers about 25% of the Earth's land area (French, 2017) and extends mainly in the northern hemisphere, including areas located in the polar and subpolar climate zones, as well as high mountains of low and medium latitudes (William & Smith, 1989; French , 2017). However, its maximum extent in the northern hemisphere has changed several times in the past due to multiple transgressions and regressions of the Earth's ice sheet (e.g. Goździk, 1995; Lindner et al., 2004; Błaszkiewicz, 2011; Marks, 2011; Van Loon et al., 2014; Vandenberghe et al., 2014, 2016; Marks et al., 2019). For this reason, the effects of frost weathering are also commonly recorded in sediments beyond the extent of present-day permafrost.

The history of research on frost weathering processes, its impact on rocks and sediments, and related effects dates back to the beginning of the 20th century (see French, 2017; Matsuoka & Murton, 2008), when the presence of cracked sandstone blocks on the slopes of the Carpathian Mountains was associated with destructive frost action (e.g. Łoziński, 1909, 1912).

Frost weathering depends on a number of factors operating in the natural environment, i.e.: (1) average annual air temperature (e.g. Halsey et al., 1995; Frauenfeld et al., 2004), (2) rock surface temperature (e.g. Hall, 2004), (3) water availability (Hallet et al., 1991; Matsuoka, 1995), (4) slope exposure (e.g. Matsuoka et al., 1997; Hall, 2004), (5) weather conditions (insolation, cloud cover and precipitation; Boelhouwers, 2003; McFadden et al., 2005), (6) wind speed (McKay et al., 2009), (7) snow cover (Hall, 1980; Stieglitz et al., 2003; Frauenfeld et al., 2004), (8) bedrock characteristic (e.g. Hall, 1992, Matsuoka, 2001a; Rödder & Kneisel, 2012) or (9) site altitude (e.g. Harris et al., 2001a). The multitude of factors influencing the course of the frost weathering process, its intensity, changes over time or effects, and especially the lack of information on how long a given sediment has been subjected to this process, makes it difficult to study this process in natural conditions. Therefore, much attention is paid to laboratory experiments simulating periglacial conditions (e.g. Lautridou & Ozouf, 1982; Wright et al., 1998; Murton et al., 2000; Wright, 2000; Kaufmann, 2004). The first experimental research in the field of frost weathering was carried out in 1956 by J. Tricart, paving the way for further research that focused on the process of frost weathering of rocks and sediments of various types (e.g. Walder & Hallet, 1986; Matsuoka, 1990). Nowadays, research conducted under laboratory conditions is carried out both on a macro scale (in the cm - m scale) and on a micro scale (in the μm - cm and even nm scale; Matsuoka, 2001b). On a macro scale, frost weathering leads to rock disintegration and the formation of sharp-edged, angular rock blocks (Lautridou & Ozouf, 1982; Matsuoka, 2001a, b). However, on a micro scale, it results in the production of fine particles, including silt fractions (Hall, 1990). Moreover, the recognition of the effects of frost weathering and the factors controlling it is very important from the economic point of view due to the mechanical destruction of building materials caused by frost action (e.g. Harris et al., 2001b; Grebenets et al., 2002; Wang et al., 2004; Thomachot et al., 2005; Wei et al., 2009; Li et al., 2010; Ruedrich et al., 2011; Varlamov, 2018).

Frost weathering affects rocks, sediments and individual grains by: (1) volumetric growth of water during freezing, and (2) growth of segregation ice lenses (e.g. Matsuoka & Murton, 2008). The first process is associated with a volumetric increase of water by 9% during freezing. In theory, for the effects of this process to manifest, the sediment or rock undergoing

weathering should be saturated with water, and the freezing front should affect it evenly from all sides (e.g. Walder & Hallet, 1985, 1986). In the natural environment, these conditions are found only within the near-surface, several-centimetre layer of rocks / sediments, in which cracks / pores are filled with water, and the process of water freezing is rapid (Matsuoka & Murton, 2008). On a micro scale, the process of volumetric growth of water due to freezing leads to mechanical destruction of grains as a result of ice crystal growth within microcracks and microfissures or changes in the volume of gases / liquids filling inclusions present in grains during freezing and thawing (Konishchev & Rogov, 1993; Konishchev et al., 2005). In addition, the presence of a film of unfrozen (hygroscopic) water on the surface of the grains (Konishchev & Rogov, 1993) and the pressure of frozen film water leads to the widening of existing cracks and fissures in the grains, as well as the formation of new ones (the so-called hydrofracturing process). Thus, the destruction of grains takes place. This type of frost weathering is referred as type "F" (Woronko & Hoch, 2011).

The process of segregation ice growth refers to the formation of lenses of ground ice (Walder & Hallert, 1985, 1986) as a result of suction caused by pressure gradients (Williams & Smith, 1989) prevailing at different depths. Related to the freezing activity, cryosuction forces the unfrozen water contained in the sediment to migrate toward the lower pressure values that prevail around the frozen lens of ice (e.g. Hallet et al., 1991). As a result of this process, sediment uplifting occurs. In the natural environment, the formation of segregation ice is favoured by a slow freezing rate and the presence of fine-grained, porous, and water-saturated sediment, in which cryosuction can occur (Anderson, 1998; Matsuoka, 2001b). The destructive effects of the growth of segregation ice have been described and documented in numerous laboratory studies (Akagawa & Fukuda, 1991; Hallet et al., 1991; Murton et al., 2000, 2001). On a micro scale, this process can lead to small displacements of grains relative to each other, and as a result, to their destruction. Woronko & Hoch (2011) called this type of weathering "P" type.

1.1. Frost weathering of sand-sized quartz grains

On the micro scale, analyses are most often carried out on sand-sized quartz grains (e.g. (Wright, 2000; Mahaney, 2002; Degórski & Kowalkowski, 2011; Schwamborn et al., 2012; Costa et al., 2013; Vos et al., 2014; Woronko & Pisarska-Jamroży, 2016; Kalińska-Nartiša et al., 2017; Kemnitz & Lucke, 2019). Quartz is characterized by a high susceptibility to mechanical weathering, which results from the presence of defects in its crystal lattice

(Konishchev & Rogov, 1993). These defects include liquid or gaseous inclusions, inclusions of other minerals, or mosaic internal structure of quartz grains. Moreover, the mechanical disintegration of quartz grains is favoured by the widespread presence of cracks observed both in the scale of the entire grain, and in the scale of individual crystals forming the grain. As a consequence, the impact of frost weathering on individual quartz grains leads to their mechanical modification in terms of size, as well as microrelief. The products of frost weathering of quartz grains in the micro-scale are: (1) silt-sized grains, and (2) microrelief, which consists of a set of microtextures characteristic of this process.

<u>(1) Frost-driven production of silt-sized grains</u>

The process of mechanical destruction of grains caused by freezing, leading to the formation of fractions in the range from μm to cm, is called microgelivation (Matsuoka, 2001b; see the criticism of this concept in Hall & Thorn, 2011). It involves the formation and development of micro-cracks and the widening and merging of pores within rocks/sediments (Matsuoka, 2001a). Vyacheslav N. Konischev was the first to draw attention to this issue (Konishchev, 1973; Kornishchev & Rogov, 1993; Konishchev et al., 2005), pointing to the mineralogical selectivity of frost weathering, as a result of which quartz grains tend to disintegrate into silt-sized grains (0.01-0.05 mm) under the influence of advancing frost weathering. Factors influencing the course of microgelivation include: (1) thermal conditions, including the rate of temperature decrease (freezing), the number of freeze-thaw cycles, (2) water availability, including water content in the sediment / rock and the amount of water migration during sediment freezing, and (3) characteristics of the sediment subjected to frost weathering, including susceptibility to deformation, granulometric composition, and porosity (Matsuoka, 2001b).

According to Hall (1990), the content of silt-sized grains in the sediment proves the intensity of frost weathering to which this sediment was subjected. The validity of this hypothesis is confirmed by the Cryogenic Weathering Index (CWI), which indicates the enrichment of the sediment with quartz grains of the 0.01-0.05 mm fraction in relation to the 0.05-0.1 mm fraction compared to feldspar grains of the above fractions (Konishchev, 1998). As a consequence, sediments located within the range of permafrost and subjected to intensive frost weathering are characterized by CWI values > 1 (Konishchev, 1999; Demitroff et al., 2007; Schwamborn et al., 2008). Based on experimental studies simulating 360 freeze-thaw cycles of a block of quartz sandstone, Wright (2000) observed the production of grains in the

2-90 µm fraction range, consisting of: (1) grains formed by the spalling or removal of overgrowths from the underlying grains that formed sandstone, (2) whole quartz grains detached from the weathering rock, and (3) grains formed as a result of cracking of individual quartz grains. Wright (2000) proved that the production of silt-sized grains amounted to only 0.001-0.1% of the original mass of the sandstone block, which accounted for 28% of the sediment formed as a result of frost weathering. According to Wright (2007), the production of silt-sized grains as a result of frost weathering occurred as a result of: (1) exploiting the cracks and fissures present in the grain, (2) the impact of forces exerted on the grains as a result of the growth of ice or salt crystals, and (3) fracturing and spalling of fragments of quartz grains.

(2) Frost-induced modifications of the surface of quartz grains

The processes affecting the sand-sized quartz grains during their transport in current environments (e.g. aeolian, fluvial, glacial) and as a result of post-depositional processes are recorded on the grain surface with a wide range of microtextures. Therefore, the analysis of microtextures observed on the surface of quartz grains is a commonly used method in the interpretation of, among others, the provenance of sediments, the nature of sedimentary environments and the processes operating in them (e.g. Krinsley & Doornkamp, 1973; Bull, 1981; Marshall, 1987; Mahaney, 1995, 2002; Helland & Holmes, 1997; Woronko, 2000; Mahaney et al., 2001; Van Hoesen & Orndorff, 2004; Rose & Hart, 2008; Schwamborn et al., 2008; Degórski & Kowalkowski, 2011; Krishner et al., 2011; Costa et al., 2012, 2013; Immonen et al., 2014; Vos et al., 2014; John et al. , 2015; Woronko et al., 2015; Woronko, 2016; Woronko & Pisarska-Jamroży, 2016; Kalińska-Nartiša et al., 2017; Molén, 2014).

The formation of microtextures on the surface of quartz grains as a result of frost weathering depends on the influence of a number of factors, the most important of which are: (1) number of freeze-thaw cycles, (2) rate of temperature decrease (freezing), (3) type of sediment / rock, (4) grain features formed during transport in other environments (e.g. aeolian, fluvial), (5) presence of defects in the crystal lattice of grains, (6) water availability, and (7) degree of grain roundness (Woronko, 2016).

So far, the analyses of the surface of the sand-sized quartz grains originating from present-day and ancient periglacial environments have led to distinguish a set of diagnostic microtextures for frost weathering. The most important and most common ones are: small- (<10 µm) and large-sized (>10 µm) conchoidal fractures and breakage blocks (Kowalkowski, 1988; Kowalkowski & Mycielska-Dowgiałło, 1980, 1985; Konishchev & Rogov, 1993; Konishchev

et al., 2005; Schwamborn et al., 2006, 2012; Woronko, 2012; Woronko & Hoch, 2011; Woronko & Pisarska-Jamroży, 2016). Other microtextures, such as fracture face (Schwamborn et al., 2006, 2012; Woronko, 2012), crescentic gouges or scaling surface (Woronko, 2012; Woronko & Pisarska-Jamroży, 2016) are recorded subordinately. The crust on the surface of quartz grains was also identified and associated with frost weathering products (Kowalkowski, 1988; Dietzel, 2005; Woronko, 2012; Woronko & Pisarska-Jamroży, 2016). Schwamborn et al. (2006, 2012) described quartz grains from the fossil active layer as angular, exhibiting high relief and sharp edges. A characteristic feature of quartz grains originating from the periglacial environment is also the presence of numerous cracked grains (Konishchev & Rogov, 1993; Konishchev et al., 2005; Schwamborn et al., 2006, 2012; Woronko, 2012), which may indicate the extent of the active layer. Moreover, experimental research conducted by Dietzel (2005) confirmed the precipitation of mineral substances on the surface of quartz grains as a result of repeated freeze-thaw cycles.

A particularly important scientific problem in the study of quartz grains subjected to freezing processes is the determination of the number of freeze-thaw cycles that the analysed grains underwent in the past. In the case of natural conditions, this factor remains unknown. As a consequence, analysis of the surface micromorphology of quartz grains records only the presence or absence of microtextures formed as a result of frost weathering. In the light of the above, it is difficult to link its effects with the time interval in which the grains were weathered, and therefore to determine how many freeze-thaw cycles were needed for the formation of a given microstructure. Experimental research, in which individual factors that influence the course of the weathering process are strictly controlled, may be crucial in this regard. **The known number of simulated freeze-thaw cycles will allow for the determination of the relationship between the degree of advancement of the frost weathering process and the effects of this process, manifested by the production of the silt-sized grains and the formation of specific microtextures.**

Despite extensive knowledge on the process of frost weathering of rocks that occurs in the periglacial environment (e.g. French, 2017; Ballantyne, 2018; Menzies & Van der Meer, 2018), the micro-scale frost weathering of quartz grains remains poorly understood. There are a number of issues that require further research: (1) the course of micro-scale frost weathering of quartz grains over time, including the process of their mechanical destruction, leading to the formation of frost-originated microtextures; (2) factors influencing the course of micro-scale frost weathering of quartz grains, including the number of freeze-thaw cycles necessary to

manifest the effects of frost weathering; (3) the reaction of quartz grains of various origin to the progressing process of frost weathering.

Experimental research can be employed to clarify information about the climatic conditions prevailing in the periglacial environment in the geological past, as well as to reconstruct the intensity of frost weathering and explain the relationship between the frost weathering process and its micro-scale effects.

2. EXPERIMENTAL STUDIES ON FROST WEATHERING CONDUCTED AS A PART OF THE DOCTORAL DISSERTATION

The research work carried out as part of the doctoral dissertation includes an experimental study on the micro-scale frost weathering. The object of the study included three types of sand-sized (0.5-1.0 mm) quartz grains subjected to frost weathering under controlled laboratory conditions. The subject of the research concerned the issue of changes in the grain-size composition of sediments and the formation of microtextures on the surface of quartz grains as a result of frost weathering.

For the purposes of the dissertation, the following **scientific problems** were addressed:

1. **The general course of micro-scale frost weathering of sand-sized quartz grains over time**, including:
   a. the factors influencing the process,
   b. the reaction of quartz grains of different origin to the frost weathering,
   c. the susceptibility of quartz grains to frost-induced modifications;
2. **The frost-driven production of a silt-sized fraction**, including:
   a. the factors influencing the changes in grain-size composition of sediments and production of silt-sized fraction (number of freeze-thaw cycles, origin of quartz grains, water content, water mineralization),
   b. the number of freeze-thaw cycles required for grain disintegration to occur,
   c. the verification of Hall's (1990) hypothesis on the relationship between the intensity of frost weathering and the content of silt-sized fraction in sediments subjected to frost action;

3. **The formation of frost-originated microrelief on the sand-sized quartz grains**, including:

   a. the microtextures peculiar for frost weathering,

   b. the evolution of frost-induced microtextures over time, i.e. with an increase in the number of freeze-thaw cycles.

The **main goals** of the conducted research involve:

1. A long-term (up to 1 000 freeze-thaw cycles) **experimental simulation** of the micro-scale frost weathering of sand-sized quartz grains;

2. Identification of **short- and long-term effect of frost weathering** of sand-sized quartz grains, including:

   a. Identification of **frost-induced changes in grain-size distribution** of quartz grains compared to the reference distribution,

   b. Identification of **frost-induced changes in micromorphology** of quartz grains.

The following **research tasks** were undertaken to achieve the research goals:

1. **Preparation of the experimental study**, including the development of workflow of the freeze-thaw device and setting the parameters of simulated conditions; the collection of samples in the field; the preparation of quartz grains for the experimental study;

2. **Main phase of the experimental study**, including the collection of the samples after 50, 100, 300, 700 and 1 000 freeze-thaw cycles;

3. **Analyses of quartz grains subjected to the experimental frost weathering**, including the analysis of grain-size distribution and microtextural analysis;

4. **Statistical analyses** of the obtained results of grain-size distribution and microtextural analysis,

5. **Interpretation of the results**.

    The doctoral dissertation consists of a set of three peer-reviewed research publications (see *List of publications included in the doctoral dissertation*) with an introductory summary section. The original full-text publications are provided in the attachments (see *Attachments 1-3*). All the publications are multi-authored, and my participation in each of

them is documented with relevant declarations (see *Declaration of authors*). **The research methodology employed in the study was developed together with supervisors (prof. dr hab. Barbara Woronko, prof. dr hab. Małgorzata Pisarska-Jamroży). As part of the work documented in each of the publications, I was involved in the entire research process, i.e. preparation and conduction of the experimental study, analysis, and publication of the obtained results.**

- For the purpose of the first publication (Górska M.E., Woronko B., Kossowski T.M., Pisarska-Jamroży M., *Micro-scale frost-weathering simulation – Changes in grain-size composition and influencing factors*), I conducted all the analyses of the grain-size distribution; I interpreted the obtained results with all the co-authors; I participated in the preparation of the original and final draft of manuscript.

- For the purpose of the second publications (Górska M.E., Woronko B., *Multi-stage evolution of frost-induced microtextures on the surface of quartz grains – An experimental study*), I conducted all the microtextural analyses of quartz grains along with the interpretation of the results together with co-author / supervisor (prof. dr hab. Barbara Woronko); I participated in the preparation of the original and final draft of manuscript.

- For the purpose of the third publication (Górska M.E., Woronko B., Kossowski T.M., *Factors influencing the development of microtextures on cold-climate aeolian quartz grains revealed by experimental frost action*), I conducted all the microtextural analyses of quartz grains together with co-author / supervisor (prof. dr hab. Barbara Woronko); I interpreted the obtained results with all the co-authors; I participated in the preparation of the original and final draft of manuscript.

I prepared most of the graphics (figures, tables, appendices) included in the publications. Finally, I participated in all stages of each publication process, including serving as the corresponding author and responding to reviewers.

3. <u>MATERIALS</u>

Three types of sand-sized quartz grains were subjected to the experimental simulation of frost weathering. They included two types of mechanically crushed vein quartz (Q_W, Q_K) and one type of quartz originating from the aeolian environment (Q_A). Vein quartz,

assigned as Q_W, was gathered at the Wojcieszów site (Polish Western Sudetes, SW Poland), where it forms a distinct sheet-like body within the sericite-chlorite metamorphosed claystones (cf. Kryza & Muszyński, 1992). The origin of the studied vein quartz relates to the hydrothermal processes associated with local thermal activity. Macroscopically, the rock is white and massive. It is characterised by high hardness and crushing resistance. Upon crushing, it breaks into elongated, angular grains with a tendency to form blade- or tabular-shaped pieces. Microscopically, it comprises the cross-cutting crystallized and recrystallized quartz of closely-spaced subhedral crystals. Locally, it bears thin and irregular green inclusions, probably of epidote-chlorite composition (Cwojdziński & Kozdrój, 2011). The studied vein quartz was the research object in the first and second publications included in the doctoral dissertation.

Vein quartz, assigned as Q_K, was gathered at the Kletno site (Polish Western Sudetes, SW Poland) from the quartz and quartz-fluorite vein deposits hosted within gneisses and mica schists. The hydrothermal origin of the studied vein quartz is associated with the migration of highly-mineralized water solutions through a regional tectonic zone and locally-developed thrust zone (Kasza, 1964; Zagożdżon & Zagrodny, 2009). The studied vein quartz forms alternating layers of milky quartz and amethyst. Macroscopically, the rock is white with a slight violet tint and bears extensive network of cracks and fissures. Upon crushing, it breaks into rectangular and rhombohedral crystals. Microscopically, euhedral quartz crystals predominant and fine hematite crystals are locally present on their walls (Gaweł, 1947; Zieliński, 1997; Wołkowicz, 2000; Sobień & Nawrocki, 2010). The studied vein quartz was the research object in the first publication included in the doctoral dissertation.

Aeolian quartz, assigned as Q_A, was collected from the stoss side of a Pleistocene inland dune at the Sławiny site (Middle Mazovia Lowlands, E Poland) from a depth of approx. 3m, i.e. beyond the range of present-day ground freezing and bio-chemical weathering of soils. Development of dune forms on this area continued from the Oldest Dryas to Early Holocene (Isarin & Renssen, H., 1999; Kasse, 2002; Hilgers, 2007; Zieliński et al., 2016; Moska et al., 2020, 2021) under the influence of prevailing west wind (Renssen et al., 1996). The studied quartz grains show a different degree of aeolian-induced modification of their surfaces, i.e. from non-visible aeolian-induced modifications, to modifications visible only on the most concave parts of grains, and grains with surfaces entirely imprinted by aeolian modifications. Therefore, aeolian reworking is thought to be the last process acting over the surface of studied grains prior to deposition. The studied aeolian quartz was the research object in the third publication included in the doctoral dissertation.

4. <u>METHODS</u>

The fragments of massive vein rocks gathered at the Wojcieszów and Kletno sites were mechanically crushed using a bench-top ring mill (vein rocks from Wojcieszów) and a hand hammer (vein rocks from Kletno). All samples were sieved using a mechanical shaker to separate the coarse sand fraction (0.5-1 mm). Afterwards, the samples of the vein quartz from Wojcieszów and Kletno were washed using the ultrasonic cleaner to remove the particles and eliminate the cracks formed during rock crushing. Each sample was viewed under a binocular microscope to exclude grains other than quartz from further analysis. Separated coarse sand-sized quartz grains (Q_W, Q_K and Q_A) were divided into equal samples of approx. 2 g and stacked on individual Petri dishes as: (1) dry samples, (2) moistened samples, where the grains were on filter paper soaked with water, and (3) wet samples, where the grains were immersed in water. Moistened and wet samples were prepared with distilled, low mineralized, and highly mineralized water. Moreover, the reference sample (i.e. sample consisting original grains not subjected to experimental frost weathering) was prepared for all the studied types of quartz (Q_W, Q_K, Q_A).

The experimental simulation of frost weathering of sand-sized quartz grains (Q_W, Q_K, Q_A) was conducted under controlled laboratory conditions using a commercial upright freezer. The device was equipped with special software and programmed for automated and defined temperature changes ranging from -5˚C up to +10˚C simulating the conditions of periglacial environment. The internal shelves of the device had an individual cooling and heating system, which provided the uniform temperature and humidity conditions inside the device. The device was programmed for permanent condensate drainage and automatic defrosting to avoid the internal condensation of water vapor and crystallization of ice crystals. The workflow of the device included three repeating temperature stages which constituted one complete freeze-thaw cycle. These were: (1) the freezing stage (2 hours), when the temperature decreased to -5˚C; (2) the constant stage (1 hour), when the temperature remained at -5˚C, and (3) the thawing stage (1 hour), when the temperature increased to +10˚C. The samples were collected after a specific number of freeze-thaw cycles and allowed to dry at room temperature (~20˚C-22˚C). The purchase of the freeze-thaw device used in this research was founded by the National Science Centre, Poland [grant numbers 2019/33/N/ST10/00021].

For the purpose of the first publication, the Q_W, Q_K samples (dry, moistened, and wet) were collected after 50, 100, 300 freeze-thaw cycles. A total of 42 samples were subjected to the laboratory and statistical analyses. The laboratory analyses included the grain-

size distribution and microtextural analysis conducted using the Malvern Morphologi G3 particle analyser and Scanning Electron Microscope (SEM), respectively. The statistical analyses included box plot analysis, Kolmogorov-Smirnov test, principal component analysis (PCA), and cluster analysis.

For the purpose of the second publication, the Q$_W$ samples were collected after 50, 100, 300, 700 and 1 000 freeze-thaw cycles. These included wet samples prepared with low and highly mineralized water. A total of 10 samples were collected and subjected to microtextural analysis using Scanning Electron Microscope (SEM).

For the purpose of the third publication, the Q$_A$ samples were collected after: 50, 100, 300, 700 and 1 000 freeze-thaw cycles. These included wet samples prepared with low mineralized water. A total of 5 samples were collected and subjected to microtextural, nanostructural and statistical analyses. Microtextural analysis was conducted using Scanning Electron Microscope (SEM). The nanostructural analysis of selected samples was conducted using Transmission Electron Microscope (TEM). Statistical analyses included Fisher's moments coefficient of skewness, box plot analysis, Hampel filter, Dixon's Q test.

All the microtextural analyses conducted with the employment of Scanning Electron Microscope (SEM) were carried out using ZEISS Sigma VP apparatus at the Scanning Microscope and Microanalysis Laboratory (Faculty of Geology, University of Warsaw). This work was founded by the National Science Centre, Poland [grant numbers 2019/33/N/ST10/00021]. The microstructural analysis conducted with the use of Transmission Electron Microscope (TEM) was carried out at Helmoholtz Centre Potsdam, GFZ German Research Centre for Geosciences. This work was founded by the UAM Research University – Excellence Initiative [grant numbers 003/13/UAM/0019].

5. <u>**CONTENTS OF THE PUBLICATIONS INCLUDED IN THE DOCTORAL DISSERTATION**</u>

All the publications included in the doctoral dissertation concern the issue of micro-scale frost weathering of sand-sized quartz grains in the experimental approach.

Publication no. 1: Górska M.E., Woronko B., Kossowski T.M., Pisarska-Jamroży M., 2022. Micro-scale frost-weathering simulation – Changes in grain-size composition and influencing factors. *Catena*, 212, 106106.

The publication presents the effects of short-term frost activity (up to 300 freeze-thaw cycles) on the grain-size distribution of vein-quartz grains. Changes in the grain-size composition of weathered samples in relation to reference samples (containing original quartz grains, not subjected to experimental frost weathering) were investigated after 50, 100 and 300 freeze-thaw cycles taking into account following variables: quartz origin (Q_W, Q_K), water content (dry, moistened, wet samples) and water mineralization (distilled, low and highly mineralized water). Differences in the grain-size distribution, resulting from the destructive frost action, were observed at each stage of the weathering process (i.e. after 50, 100 and 300 freeze-thaw cycles) in all the samples. Statistical analyses (Kolmogorov-Smirnov test, PCA, cluster analysis) of the grain-size distributions evidenced different reactions of both types of quartz grains to the ongoing weathering process regardless of the water content and mineralization. The greatest frost-driven changes in the grain-size distributions were attributed to the very coarse (1.0-2.0 mm) and coarse sand (0.5-1.0 mm) fractions. Contrary to the Hall's (1990) hypothesis, concerning the relationship between the intensity of frost weathering and the content of the silt fraction in the sediment, the production of the silt-sized grains (0.002-0.063 mm) constituted a minor product of the frost weathering. Moreover, it was demonstrated that primary defects (related to the internal structure of quartz) and secondary defects (related to the preparation of the sample for the experiment) of quartz grains had a great influence on the course of frost weathering. Both new terms were introduced into the literature by the authors of the publication. Moreover, the influence of the internal structure of quartz grains on their frost-induced mechanical disintegration was demonstrated. The Q_W grains, characterized by close contact between adjacent quartz crystals, disintegrated to a lesser extent than the Q_K grains, which exhibited open contact between individual quartz crystals. This was evidenced by greater changes in the percentage share of medium, fine, very fine sand (0.063-0.5 mm) and silt (0.004-0.063 mm) fractions in relation to the reference samples, recorded for the Q_K samples compared to the Q_W samples. On the basis of frost-induced changes in the grain-size compositions of the Q_W and Q_K samples, it was found that there was a certain time interval necessary for the effects of micro-scale frost weathering to appear. This interval was called *lag time*, and its influence on the initial (up to 50 freeze-thaw cycles) and more advanced stage of frost weathering (100-300 freeze-thaw cycles) was demonstrated.

Publication no. 2: Górska M.E., Woronko B., 2022. Multi-stage evolution of frost-induced microtextures on the surface of quartz grains – An experimental study. Permafrost and Periglacial Processes, 33, 4, 470-489.

The publication presents the effects of long-term frost activity on the micromorphology of vein-quartz grains (Q_W), i.e. after 50, 100, 300, 700, and 1 000 freeze-thaw cycles. Studied wet samples were subjected to weathering under low- and highly-mineralized water conditions. Microtextural analysis of sand-sized quartz grains was performed using a scanning electron microscope (SEM) for the reference sample and after the above-mentioned cycles. Four diagnostic microtextures for frost weathering were determined: small- and large-sized conchoidal fractures (labelled as cf and CF) and small- and large-sized breakage blocks (labelled as bb and BB). Based on the microtextural changes observed on the surface quartz grains, two aspects of micro-scale frost weathering were identified: (1) a physical aspect of the process, manifested during the first 300 freeze-thaw cycles by the occurrence of cf, CF, bb, BB microtextures, and (2) a chemical aspect of the process, manifested after 300 freeze-thaw cycles by the occurrence of precipitation crusts formed from the precipitation of components dissolved in water during freezing, which obliterate the grain microrelief and inhibit the process of physical weathering. The evolution of frost-induced microrelief was divided into three stages: (1) initial stage, evidenced by the predominance of the CF microtextures, (2) progress stage, evidenced by the increased development of cf, and (3) advance stage, evidenced by the dominance of bb and BB microtextures. It was further concluded that this three-stage evolution of frost-induced microrelief could be interrupted by a process of „refreshing" that led to an exposure of fresh, unweathered grain surfaces, and thus the weathering process started again.

Publication no. 3: Górska M.E., Woronko B., Kossowski T.M., 2023. Factors influencing the development of microtextures on cold-climate aeolian quartz grains revealed by experimental frost action. *Permafrost and Periglacial Processes*, 2023, 1-25.

The publication presents the effects of long-term frost activity on the microtextural characteristics of aeolian-originated grains (Q_A). Studied wet samples were subjected to weathering under low-mineralized water conditions. Scanning electron microscopic (SEM) microtextural analysis was performed for the reference sample and samples subjected to 50, 100, 300, 700, and 1 000 freeze-thaw cycles. Moreover, nanostructural analysis using transmission electron microscopic (TEM) was for the reference sample and samples after 100 and 1 000 freeze-thaw cycles. Frost weathering resulted in the formation of small- and large-sized conchoidal fractures (labelled as cf, CF, respectively), small- and large-sized breakage blocks (labelled as bb, BB, respectively) and cracks on the grain surfaces. Two types of small-sized conchoidal fractures (introduced as cf_I and cf_{II}) were recognised due to their specific shape. A gradual increase in the number of frost-originated microtextures (cf, CF, bb, BB) on

the surface of the analysed quartz grains was observed along with the duration of frost weathering manifested as the number of freeze-thaw cycles. This number was relatively small up to 700 freeze-thaw cycles, and a significant increase was noted only after 1000 freeze-thaw cycles. On this basis, it was found that quartz grains of aeolian origin (Q_A), compared to vein-quartz grains (Q_W, Q_K), required a much longer time of frost weathering in order to manifest its effects, and thus they were characterized by a longer *lag time*. The susceptibility of cold-climate aeolian-originated quartz grains to frost-induced modifications was proved to depend, among others, on the internal characteristics of grains inherited from former aeolian processes and the original structure of grains. It was concluded that aeolian-originated modification of quartz grain structure led to the development of a sub-surface *impact zone*. Its thickness clearly determined the depth to which frost-originated microtextures developed. The microstructural characteristic, i.e. primary and secondary defects in quartz crystals of the studied grains, was interpreted as a second factor influencing the susceptibility of cold-climate aeolian quartz grains to frost-induced microtextural modifications. Moreover, the relationship between the number of frost microtextures recorded on the surface of quartz grains of aeolian origin and the shape of the grains themselves, in particular their sphericity, was demonstrated. It was found that grains characterized by low sphericity showed less susceptibility to the formation of frost-induced microtextures than the grains of high sphericity. It was proved that in a given population of grains subjected to frost weathering, not all grains reacted to temperature changes to the same extent.

6. <u>CONCLUSIONS</u>

The research conducted as a part of the doctoral dissertation documents the conduction and results of a long-term experimental simulation of the micro-scale frost weathering of sand-sized quartz grains. The obtained results provide an insight into the course of frost weathering of vein-quartz and aeolian-originated quartz grains, which is an important step towards more accurate microtextural interpretations. The proposed research methodology may be a starting point for future experimental studies of micro-scale frost weathering of quartz grains.

6.1. The general course of micro-scale frost weathering of sand-sized quartz grains

The conducted research indicated that micro-scale frost weathering is a much more complex and complicated process than previously assumed. Once initiated, it leads to the disintegration of the quartz grains and the formation of a specific grain microrelief. The course of micro-scale

frost weathering seems to depend on internal (i.e. internal features of quartz grains, grain features inherited from previous sedimentary environment) rather than on external variables (water content, water mineralization). Consequently, the reaction of quartz grains of different origin to the frost weathering and their susceptibility to frost-induced modifications are unpredictable and remain peculiar for a given type of quartz grains.

6.2. The frost-driven production of silt-sized fraction

A short-term frost weathering (300 freeze-thaw cycles) of vein-quartz grains (Q_W, Q_K) indicates a significant impact of internal features of quartz grains on the course of their micro-scale frost-induced disintegration. Especially, the type of contact between adjacent quartz crystals and the presence of gas / liquid inclusions or their remnants seem to be of crucial importance. The destruction of quartz grains follows different weakness zones involved in their internal structure. These include *primary* and *preparation / inherited defects*. The elimination of *preparation / inherited defects* at the very beginning of weathering process (here up to 50 freeze-thaw cycles) results in the destruction of very coarse sand fractions (1-2 mm) and production of coarse (0.5-1 mm) and medium sand (0.25-0.5 mm) fractions. The further (here up to 300 freeze-thaw cycles) elimination of *primary defects* results in the production of very coarse sand fractions (1-2 mm). The issue of production of very coarse (1-2 mm) and coarse sand (0.5-1 mm) fractions has never been addressed or expounded before.

At a more advanced stage of the frost weathering (here up to 300 freeze-thaw cycles), most of the *preparation / inherited* and *primary* defects are eliminated and the intact *host grain* becomes exposed. At this point, frost weathering requires more freeze-thaw cycles to disturb fresh surface of grain. The production of silt-sized fractions remains insignificant and does not reflect the stage and / or intensity of weathering (cf. Hall, 1990).

6.3. The formation of frost-originated microrelief on the sand-sized quartz grains

A long-term frost weathering (up to 1 000 freeze-thaw cycles) and microtextural analysis of vein (Q_W) and aeolian (Q_A) quartz grains indicates four microtextures identified as diagnostic for the process: small- and large-sized conchoidal fractures (labelled as cf, CF, respectively), and small- and large-sized breakage blocks (labelled as bb, BB, respectively). In addition to the above-mentioned microtextures reflecting the dominance of physical aspect of frost weathering, microtextures of chemical origin were also identified. The latter includes a precipitation crust that obliterates the grain microrelief and may inhibit the process of physical weathering.

The conducted observations lead to an important conclusion regarding the possibility of reconstructing the degree of advancement of the frost weathering process. The number of mechanical microtextures observed on the surface of quartz grains indicates the stage of evolution of frost-induced microrelief, but it does not bear any information on the advancement of the weathering process itself. It stems from the fact that the evolution of frost-originated microrelief may be interrupted by the process of „refreshing" of the weathered surface that leads to exposure of the fresh, unweathered surface of the grain. Frost weathering, acting on the surface of quartz grains, leads to the formation of a thin outer layer introduced as *frost-exposed skin* (FES). Its thickness reflects the depth to which freeze front most likely penetrates the grain, leading to the formation of frost-originated microtextures (cf, CF, bb, BB).

References

Akagawa S., Fukada M., 1991. Frost heave mechanism in welded tuff. Permafrost and Periglacial Processes, 2, 301-309.

Anderson R., 1998. Near-surface thermal profiles in alpine bedrock: implications for the frost weathering of rock. Arctic and Alpine Research, 30, 362-372.

Ballantyne C.K., 2018. Periglacial Geomorphology. Wiley-Blackwell, 11-22.

Błaszkiewicz M., 2011. Timing of the final disappearance of permafrost in the central European Lowland, as reconstructed from the evolution of lakes in N Poland. Geological Quaternary, 55, 361-374.

Boelhouwers J., 2003. Sensitivity and responses to climate change in the Subantarctic periglacial environment. 8th International Conference on Permafrost, Zurich, Swietzerland, 67-71.

Bull P.A., 1981. Environmental reconstruction by electron microscopy. Progress in Physical Geography, 5, 368-397.

Costa P.J.M., Andrade C., Mahaney W.C., Da Silva F.M., Freire P., Freitas M.C., Janardo C., Oliveira M.A, Silva T., Lopes, V., 2013. Aeolian microtextures in silica spheres induced in a wind tunnel experiment: Comparison with aeolian quartz. *Geomorphology*, 180, 120-129.

Costa, P.J.M., Andrade, C., Dawson A.G., Mahaney W.C., Freitas M.C., Paris R., Taborda R., 2012. Microtextural characteristics of quartz grains transported and deposited by tsunamis and storms. *Sedimentary Geology*, 275, 55-69.

Cwojdziński S., Kozdrój W., 2011. Objaśnienia do szczegółowej mapy geologicznej. [Explanations for the Detailed Geological Map of Poland]. Polish Geological Institute - National Research Institute. [in Polish]

Degórski M., Kowalkowski A., 2011. The use of SEM morphoscopy in researching the litho-pedogenetic environments evolution of Late Pleistocene and Holocene. Geographia Polonica, 84, 17-38.

Demitroff M., Rogov V.V., French H.M., Konishchev V.N., Streletskiy D.A., Lebedeva-Verba M.D., Alekseeva V.A., 2007. Possible evidence for episodes of Late Pleistocene cryogenic weatheing, southern New Jersey, Eastern USA. [In:] Proceedings, Volume II, Cryogenic Resources of Polar Regions, RAS, SB, Salekhard, 139-141.

Dietzel M., 2005. Impact of cyclic freezing on precipitation of silica in Me-SiO2-H2O systems and geochemical implications for cryosoils and sediments. Chemical Geology, 216, 79-88.

Frauenfeld O.W., Zhang T., Barry R.G., Gilichinsky D., 2004. Interdecadal changes in seasonal freeze and thaw depths in Russia. Journal of Geophysical Research, 109, 1-12.

French H.M., 2017. The periglacial environment. Wiley-Blackwell, 544 pp.

Gaweł A., 1947. Geological conditions of origin of blue salt, amethyst and violet fluorite. Annales Societatis Geologorum Poloniae, 17, 51-60.

Goździk J.S., 1995. Permafrost evolution and its impact on deposition conditions between 20 and 10 ka BP in Poland. Biuletyn Peryglacjalny, 34, 53-72.

Grebenets V.I., Konishchev V.N., Rogov V.V., 2002. Cryogenic destruction of construction materials in foundations of buildings erected in the permafrost zone. Soil Mechanics and Foundation Engineering, 39, 106-111.

Hall K., 1980. Freeze-thaw activity at a nivation site in northern Norway. Arctic and Alpine Research, 12, 183-194.

Hall K., 1990. Mechanical weathering rates on Signy Island, Maritime Antarctic. Permafrost and Periglacial Processes, 1, 61-67.

Hall K., 1992. Mechanical weathering on Livingstone Island, south Shetland Islands, Antarctica. [In:] Yoshida Y., Kaminuma K., Shiraishi K. (eds.). Recent Progress in Antarctic Earth Science. Proceedings of the Sixth International Symposium on Antarctic Earth Sciences. Ranzan, Saitama, Japan. Terra Scientific Publishing, Tokyo, 757-762.

Hall K., 2004. Evidence for freeze-thaw events and their implications for rock weathering in northern Canada. Earth Surface Processes and Landforms, 29, 43-57.

Hall K., Lautridou J.P., 1991. Introduction - Cryogenic weathering. Permafrost and Periglacial Processes, 2, 269-270.

Hall K., Thorn C., 2011. The historical legacy of spatial scales in freeze-thaw weathering: Misinterpretation and resulting misdirection. Geomorphology, 130, 83-90.

Hallet B., Walder J.S., Stubbs C.W., 1991. Weathering by segregation ice growth in microcracks at sustained subzero temperatures: verification from an experimental study using acoustic emission. Permafrost and Periglacial Processes, 2, 283-300.

Halsey L.A., Vitt D.H., Zoltai S.C., 1995. Disequilibrium response of permafrost in boreal continental western Canada to climate change. Climatic Change, 30, 57-73.

Harris C., Davies M.C.R., Etzelmüller B., 2001b. The assessment of potential geotechnical hazards associated with mountain permafrost in a warming global climate. Permafrost and Periglacial Processes, 12, 145-156.

Harris C., Haeberli W., Vonder Mühll D., King L., 2001a. Permafrost monitoring in the high mountains of Europe: the PACE project in its global context. Permafrost and Periglacial Processes, 12, 3-11.

Helland P.E., Holmes M.A., 1997. Surface textural analysis of quartz sand grains from ODP Site 918 off the southeast coast of Greenland suggests glaciation of southern Greenland at 11 Ma. Palaeogeography, Palaeoclimatology, Palaeoecology, 135, 109-121.

Hilgers A., 2007. The chronology of late glacial and Holocene dune development in the northern central European lowland reconstructed by optically stimulated luminescence (OSL) dating. Doctoral dissertation, University of Cologne.

Immonen N., Strand K., Huusko A., Lunkka J.P., 2014. Imprint of late Pleistocene continental processes visible in ice-rafted grains from central Arctic Ocean. Quaternary Science Reviews, 92, 133-139.

Isarin R.F., Renssen H., 1999. Reconstructing and modelling Late Weichselian climates: the Younger Dryas in Europe as a case study. Earth-Science Reviews, 48, 1-38.

John K.S.T., Passchier S., Tantillo B., Darby D., Kearns L., 2015. Microfeatures of modern sea-ice-rafted sediment and implications for paleo-sea-ice reconstructions. Annals of Glaciology, 56, 83-93.

Kalińska-Nartiša E., Woronko B., Ning W., 2017. Microtextural inheritance on quartz sand grains from Pleistocene periglacial environments of the Mazovian Lowlands, Central Poland. Permafrost and Periglacial Processes, 28, 741-756.

Kasse C., 2002. Sandy aeolian deposits and environments and their relation to climate during the Last Glacial Maximum and Late glacial in northwest and central Europe. Progress in Physical Geography: Earth and Environment, 26, 507–532.

Kasza L., 1964. Budowa geologiczna górnego dorzecza Białej Lądeckiej. [Geological structure of the upper Biała Ladecka basin]. Geologia Sudetica, 1, 119–167. [in Polish with English summary]

Kaufmann J.P., 2004. Experimental identification of ice formation in small concrete pores. Cement and Concrete Research, 34, 1421-1427.

Kemnitz H., Lucke B., 2019. Quartz grain surfaces–A potential microarchive for sedimentation processes and parent material identification in soils of Jordan. Catena, 176, 209-226.

Kirshner A.E., Anderson J.B., Wellner J.S., 2011. Cenozoic glacial history of the northern Antarctic Peninsula: a micromorphological investigation of quartz sand grains. Tectonic, climatic, and cryospheric evolution of the Antarctic Peninsula, 63, 153-165.

Konishchev V.N., 1973. Frost weathering. [In:] Proceedings of the 2nd International Conference on Permafrost, 13-28 July 1973, Yakutsk, USSR. Office National Academy of Sciences, Washington, 176-181.

Konishchev V.N., 1998. Relationship between the lithology of active layer materials and mean annual ground temperature in the former USSR. Proceedings 7th International. Conference Permafrost, Yellowknife, Canada, 591-594.

Konishchev V.N., 1999. Evolution of ground temperature of Russian Arctic zone in upper Cenozoic. Earth's Cryosphere, 3, 39-47.

Konishchev V.N., Lebedeva-Verba M.P., Rogov V.V., Stalina E.E., 2005. Cryogenesis of modern and Late Pleistocene deposits Altai and periglacial region of Europa. GEOS: Moscow.

Kornishchev V.N., Rogov V.V., 1993. Investigations of cryogenic weathering in Europe and Northern Asia. Permafrost and Periglacial Processes, 4, 49-64.

Kowalkowski A., 1988. Textural features of the surface of quartz sand grains in acid and alkaline soils of the cold climate. [In:] Mycielska-Dowgiałło E. (ed.). Geneza osadów i gleb w świetle badań w mikroskopie elektronowym. University of Warsaw Press, Warsaw, 87-99.

Kowalkowski A., Mycielska-Dowgiałło E., 1980. Soil forming processes in the tundra and arid steppe of the Khangai Mountains on the basis of quartz grain analysis with an electron microscope. Polish Journal of Soil Science XIII, 51–71.

Kowalkowski A., Mycielska-Dowgiałło E., 1985. Weathering of quartz grain in the liquefied horizon of permafrost solonchaks in the arid steppe zone, Central Mongolia. Catena 12, 179–190.

Krinsley D.H., Doornkamp J., 1973. Atlas of quartz sand surface textures. Cambridge University Press, 37 pp.

Kryza R., Muszyński A., 1992. Pre-Variscan volcanic-sedimentary succession of the central south Góry Kaczawskie, SW Poland: Outline geology. Annales Societatis Geologorum Poloniae, 62, 117–140.

Lautridou J.P., Ozouf J.C., 1982. Experimental frost shattering: fifteen years of research at the Centre de Geomorphologie du CNRS. Progress in Physical Geography, 6, 215-232.

Li G., Sheng Y., Jin H., Ma W., Qi J., Wen Z., Zhang B., Mu Y., Bi G., 2010. Development of freezing-thawing processes of foundation soils surrounding the China-Russia Crude Oil Pipeline in the permafrost areas under a warming climate. Cold Regions Science and Technology, 64, 226-234.

Lindner L., Gozhik P., Marciniak B., Marks L., Yeloviecheva Y., 2004. Main climatic changes in the Quaternary of Poland, Belarus and Ukraine. Geological Quaternary, 48, 97-114.

Łoziński M.W., 1909. Über die mechanische Verwitterung der Sandsteine im gemassibten Klima. Académie des sciences de cracovie, Bulletin internationale, classe de science, mathématiques et naturelles, 1, 1-25. [in German]

Łoziński M.W., 1912. On the mechanical weathering of sandstones in temperate climates. [In:] Cold Climate Landforms, Evans D.J.A. (ed.). Wiley, 119-134.

Mahaney W.C., 1995. Pleistocene and Holocene glacier thicknesses, transport histories and dynamics inferred from SEM microtextures on quartz particles. Boreas, 24, 293-304.

Mahaney W.C., 2002. Atlas of sand grain surface textures and applications. Oxford University Press, Oxford, 237 pp.

Mahaney W.C., Stewart A., Kalm V., 2001. Quantification of SEM microtextures useful in sedimentary environmental discrimination. Boreas, 30, 165-171.

Marks L., 2011. Quaternary Glaciations in Poland. Developments in Quaternary Sciences, 15, 299-303.

Marks L., Makos M., Szymanek M., Woronko B., Dzierżek J., Majecka A., 2019. Late Pleistocene climate of Poland in the mid-European context. Quaternary International, 504, 24-29.

Marshall J.R., 1987. Clastic Particles: Scanning Electron Microscopy and Shape Analysis of Sedimentary and Volcanic Clasts. New York, 346 pp.

Matsuoka N., 1990. The rate of bedrock weathering by frost action: field measurements and a predictive model. Earth Surface Processes and Landforms, 15, 73-90.

Matsuoka N., 1995. Rock weathering process and landform development in the Sør Rondane Mountains, Antarctica. Geomorphology, 12, 323-339.

Matsuoka N., 2001a. Direct observations of frost weathering in alpine bedrock. Earth Surface Processes and Landforms, 26, 601-614.

Matsuoka N., 2001b. Microgelivation versus Macrogelivation: towards bridging the gap between laboratory and field frost weathering. Permafrost and Periglacial Processes, 12, 299-313.

Matsuoka N., Hirakawa K., Watanabe T., Moriwaki K., 1997. Monitoring of periglacial slope processes in the Swiss Alps: the first two years of frost shattering, heave and creep. Permafrost and Periglacial Processes, 8, 155-177.

Matsuoka N., Murton J., 2008. Frost weathering: recent advances and future directions. Permafrost and Periglacial Processes, 19, 195-210.

McFadden L.D., Eppes M.C., Gillespie A.R., Hallet B., 2005. Physical weathering in arid landscapes due to diurnal variation in the direction of solar heating. Geological Society of America Bulletin, 1/2, 161-173.

McKay C., Molaro J.L., Marinova M.M., 2009. High-frequency rock temperature data from hyper-arid desert environments in the Atacama and the Antarctic Dry Valleys and implications for rock weathering. Geomorphology, 110, 182-187.

Menzies J., Van der Meer J.J.M., 2018. Past Glacial Environments. Elsevier, Amsterdam, 858 pp.

Molén M.O., 2014. A simple method to classify diamicts by scanning electron microscope from surface microtextures. Sedimentology 61, 2020–2041.

Moska P., Jary Z., Sokołowski R.J., Poręba G., Raczyk J., Krawczyk M., Skurzyński J., Zieliński P., Michczyński A., Tudyka K., Adamiec G., Piotrowska N., Pawełczyk F., Łopuch M., Szymak A., Ryzner K., 2020. Chronostratigraphy of Late Glacial aeolian activity in SW Poland – A case study from the Niemodlin Plateau. Geochronometria, 47, 124-137.

Moska P., Sokołowski R.J., Jary Z., Zieliński P., Raczyk J., Szymak A., Krawczyk M., Skurzyński J., Poręba G., Łopuch M., Tudyka K., 2021. Stratigraphy of the Late Glacial and Holocene aeolian series in different sedimentary zones related to the Last Glacial maximum in Poland. Quaternary International, 630, 65-83.

Murton J.B., Coutard J.P., Lautridou J.P., Ozouf J.C., Robinson D.A., Williams R.B.G., Guillemet G., Simmons P., 2000. Experimental design for a pilot study on bedrock

weathering near the permafrost table. Earth Surface Processes and Landforms, 25, 1281-1294.

Murton J.B., Coutard J.P., Lautridou J.P., Ozouf J.C., Robinson D.A., Williams R.B.G., 2001. Physical modelling of bedrock brecciation by ice segregation in permafrost. Permafrost and Periglacial Processes, 12, 255-266.

Nicholson D.T., Nicholson F.H., 2000. Physical deterioration of sedimentary rocks subjected to experimental freeze-thaw weathering. Earth Surface Process and Landforms, 25, 1295-1307.

Renssen H., Lautenschlager M., Schuurmans C. J. E., 1996. The atmospheric winter circulation during the Younger Dryas stadial in the Atlantic/European sector: Climate Dynamics, 12, 813–824.

Rödder T., Kneisel C., 2012. Influence of snow cover and grain size on the ground thermal regime in the discontinuous permafrost zone, Swiss Alps. Geomorphology, 175-176, 176-189.

Rose K.C., Hart J.K., 2008. Subglacial comminution in the deforming bed: inferences from SEM analysis. Sedimentary Geology, 203, 87-97.

Ruedrich J., Kirchner D., Siegesmund D., 2011. Physical weathering of building stones induced by freeze-thaw action: a laboratory long-term study. Environmental Earth Sciences, 63, 1573-1586.

Schwamborn G., Förster A., Diekmann B., Schirrmeister L., Fedorov G., 2008. Mid to Late Quaternary cryogenic weathering conditions in Chukotka, northeastern Russia: inference from mineralogical and microtextural properties of the Elgygytgyn Crater Lake sediment record. Ninth International Conference On Permafrost, Institute of Northern Engineering, University of Alaska, Fairbanks, 1601-1606.

Schwamborn G., Mayer H., Fedorov G., Schirrmeister L., Hubberten H.W., 2006. Ground ice and slope sediments archiving late Quaternary paleoenvironment and paleoclimate signals at the margins of El'gygytgyn Impact Crater, NE Siberia. Quaternary Research, 66, 259-277.

Schwamborn G., Schirrmeister L., Frütsch F., Diekmann D., 2012. Quartz weathering in freeze-thaw cycles: experiment and application to the El'gygytgyn Crater Lake record for tracing Siberian permafrost history. Geografiska Annaler: Series A, Physical Geography, 94, 481-499.

Sobień K., Nawrocki J., 2010. Palaeomagnetic and petromagnetic study of uranium bearing polymetallic-fluorite mineralization in the Orlik-Kladsko crystalline complex (near Kletno, Lower Silesia, Poland). Geological Quarterly, 54, 325–336.

Stieglitz M., Déry S.J., Romanovsky V.E., Osterkamp T.E., 2003. The role of snow cover in the warming of Arctic permafrost. Geophysical Research Letters, 30, 1721.

Thomachot C., Matsuoka N., Kuchitsu N., Morii M., 2005. Frost damage of bricks composing a railway tunnel monument in Central Japan: field monitoring and laboratory simulation. Natural Hazards and Earth System Sciences, 5, 465-476.

Tricart J., 1956. Etude expérimentale du problème de la gélivation. Biuletyn Peryglacjalny, 4, 285-318.

Van Hoesen J.G., Orndorff R.L., 2004. A comparative SEM study on the micromorphology of glacial and non-glacial clasts with varying age and lithology. Canadian Journal of Earth Science, 41, 1123-1139.

Van Loon A.J., Błaszkiewicz M., Degórski M., 2014. The role of permafrost in shaping the Late Glacial relief of northern Poland. Netherlands Journal of Geosciences, 91, 223-231.

Vandenberghe J., French H.M, Gorbunov A., Marchenko S., Velichko A.A., Jin H., Cui Z., Zhang T., Wan X., 2014. The Last Permafrost Maximum (LPM) map of the Northern Hemisphere: permafrost extent and mean annual temperatures, 25-17 ka BP. Boreas, 43, 652-666.

Vandenberghe J., Woronko B., Nieuwendam A., Bateman M., 2016. Reconstruction and modelling of past permafrost and periglacial environments. Permafrost and Periglacial Processes, 27, 3-5.

Varlamov S.P., 2018. Thermal monitoring of railway subgrade in a region of ice-rich permafrost, Yakutia, Russia. Cold Regions Science and Technology, 155, 184-192.

Vos K., Vandenberghe N., Elsen J., 2014. Surface textural analysis of quartz grains by scanning electron microscopy (SEM): From sample preparation to environmental interpretation. Earth-Science Reviews, 128, 93-104.

Walder J.S., Hallet B., 1985. A theoretical model of the fracture of rock during freezing. Geological Society of America Bulletin, 96, 336-346.

Walder J.S., Hallet B., 1986. The physical basis of frost weathering: toward a more fundamental and unified perspective. Arctic and Alpine Research, 18, 27-32.

Wang G.X., Yao J.Z., Guo Z.G., Wu Q.B., Wang Y.B., 2004. Changes in permafrost ecosystem under the influences of human engineering activities and its enlightenment to railway construction. Chinese Science Bulletin, 49, 1741-1750.

Wei M., Guodong C., Qingbai W., 2009. Construction on permafrost foundations: Lessons learned from the Qinghai-Tibet railroad. Cold Regions Science and Technology, 59, 3-11.

Williams P.J., Smith M.W., 1989. The Frozen Earth. Cambridge University Press, Cambridge, 306 pp.

Wołkowicz K., 2000. O katodoluminescencji sudeckich kwarców żyłowych. [On the cathodoluminescence studies of the Sudetic vein quartz]. Przegląd Geologiczny, 48, 625-633. [in Polish with English summary]

Woronko B., 2000. The influence of climatic conditions on the surface character of aeolian sand quartz grains. [In:] Dulias R., Pełka-Gościniak J. (eds.). Aeolian processes in different landscape zones. Sosnowiec, 18-27.

Woronko B., 2012. Micromorphology of quartz grains as a tool in the reconstruction of periglacial environment. [In:] Churski P. (ed.). Contemporary Issues in Polish Geography, 111-131.

Woronko B., 2016. Frost weathering versus glacial grinding in the micromorphology of quartz sand grains: Processes and geological implications. Sedimentary Geology, 335, 103-119.

Woronko B., Hoch M., 2011. The development of frost-weathering microstructures on sand-sized quartz grains: examples from Poland and Mongolia. Permafrost and Periglacial Processes, 22, 214-227.

Woronko B., Pisarska-Jamroży M., 2016. Micro-scale frost weathering of sand-sized quartz grains. Permafrost and Periglacial Processes, 27, 109-122.

Woronko B., Pisarska-Jamroży M., Van Loon A.J., 2015. Reconstruction of sediment provenance and transport processes from the surface textures of quartz grains from Late Pleistocene sandurs and ice-marginal valley in NW Poland. Geologos, 21, 105-115.

Wright J., Smith B., Whalley B., 1998. Mechanisms of loess-sized quartz silt production and their relative effectiveness: laboratory simulations. Geomorphology, 23, 15-34.

Wright J.S., 2000. The spalling of overgrowths during experimental freeze – thaw of quartz sandstone as mechanism of quartz silt production. Micron, 31, 631-638.

Wright J.S., 2007. An overview of the role of weathering in the production of quartz silt. Sedimentary Geology, 202, 337-351.

Zagożdżon P.P., Zagrodny K., 2009. Cyfrowe modelowanie Jaskini Niedźwiedziej w Kletnie oraz jej geologicznego otoczenia. [Digital modeling of Niedzwiedzia Cave in Kletno (Lower Silesia) and its geological surroundings]. Prace Naukowe Instytutu Górnictwa Politechniki Wrocławskiej, 128, 221–236. [in Polish with English summary]

Zhang T., Barry G., Knowles K., Heginbottom J.A., Brown J., 2008. Statistics and characteristics of permafrost and ground-ice distribution in the Northern Hemisphere. Polar Geography, 31, 47-68.

Zieliński P., Sokołowski R.J., Woronko B., Fedorowicz S., Jankowski M., Standzikowski K., 2016. Sandy deposition in a small dry valley in the periglacial zone of the Last Glacial Maximum: A case study from the Józefów site, SE Poland. Quaternary International, 399, 58–71.

Zieliński, G., 1997. Temperatury powstawania kwarcu i fluorytu ze złoża uranowo-polimetalicznego w Kletnie, Dolny Śląsk. [Temperatures of quartz and fluorite formation from the uranium-polymetallic deposit in Kletno, Lower Silesia]. University of Warsaw, Warsaw, Poland. Master's thesis. [in Polish]

OŚWIADCZENIA AUTORÓW

Publikacja nr 1:

Górska M.E., Woronko B., Kossowski T.M., Pisarska-Jamroży M., 2022. Micro-scale frost-weathering simulation – Changes in grain-size composition and influencing factors. Catena, 212, 106106. https://doi.org/10.1016/j.catena.2022.106106
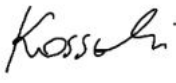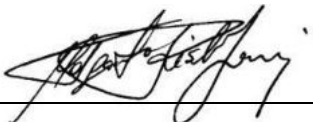
Oświadczam, że wkład Pani Martyny Górskiej w przygotowaniu powyżej publikacji wynosi 40%.

Pani Martyna Górska uczestniczyła w każdym etapie przeprowadzonej pracy eksperymentalnej, tj. przygotowania eksperymentu, przeprowadzenia eksperymentu (w tym poborze próbek po 50, 100, 300 cyklach zamarzania-odmarzania), wykonania analiz ziaren kwarcu poddanych eksperymentalnemu wietrzeniu mrozowemu (w tym przeprowadzeniu analizy rozkładu uziarnienia oraz analizy mikrostrukturalnej) oraz interpretacji wyników.

Przebieg pracy urządzenia zamrażająco-odmrażającego został opracowany przez Panią Martynę Górską, prof. dr hab. Barbarę Woronko (promotorka) i prof. dr hab. Małgorzatę Pisarską-Jamroży (promotorka).

Pani Martyna Górska przygotowała próbki do badań i wykonała wszystkie analizy rozkładu uziarnienia. Interpretacja uzyskanych wyników została przeprowadzona przez wszystkich współautorów.

Pani Martyna Górska brała udział w przygotowaniu pierwotnej wersji manuskryptu oraz przygotowała większość grafik (ryciny, tabele, załączniki) zawartych w publikacji. Pani Martyna Górska uczestniczyła we wszystkich etapach procesu publikacji wyników, w tym pełniąc funkcję autora korespondencyjnego i udzielając odpowiedzi recenzentom.

Martyna E. Górska		1.03.2023
Barbara Woronko		05.03.2023
Tomasz M. Kossowski		07.03.2023
Małgorzata Pisarska-Jamroży		06.03.2023

OŚWIADCZENIA AUTORÓW

Publikacja nr 2:

Górska M.E., Woronko B., 2022. Multi-stage evolution of frost-induced microtextures on the surface of quartz grains – An experimental study. Permafrost and Periglacial Processes, 33, 4, 470-489. https://doi.org/10.1002/ppp.2164

Oświadczam, że wkład Pani Martyny Górskiej w przygotowaniu powyżej publikacji wynosi 55%.

Pani Martyna Górska uczestniczyła w każdym etapie przeprowadzonej pracy eksperymentalnej, tj. przygotowania eksperymentu, przeprowadzenia eksperymentu (w tym poborze próbek po 50, 100, 300, 700, 1000 cyklach zamarzania-odmarzania), wykonania analiz ziaren kwarcu poddanych eksperymentalnemu wietrzeniu mrozowemu (w tym analizy mikrostrukturalnej) oraz interpretacji wyników.

Przebieg pracy urządzenia zamrażająco-odmrażającego został opracowany przez Panią Martynę Górską, prof. dr hab. Barbarę Woronko (promotorka) i prof. dr hab. Małgorzatę Pisarską-Jamroży (promotorka).

Pani Martyna Górska przygotowała próbki do badań. Analiza mikrostrukturalna oraz interpretacja uzyskanych wyników została przeprowadzona wraz ze współautorką.

Pani Martyna Górska brała udział w przygotowaniu pierwotnej wersji manuskryptu oraz przygotowała większość grafik (ryciny, tabele, załączniki) zawartych w publikacji. Pani Martyna Górska uczestniczyła we wszystkich etapach procesu publikacji wyników, w tym pełniąc funkcję autora korespondencyjnego i udzielając odpowiedzi recenzentom.

Martyna E. Górska		1.03.2023
Barbara Woronko		05.03.2023

OŚWIADCZENIA AUTORÓW

Publikacja nr 3:

Górska M.E., Woronko B., Kossowski T.M., Factors influencing the development of microtextures on cold-climate aeolian quartz grains revealed by experimental frost action. Permafrost and Periglacial Processes, 2023, 1-25. https://doi.org/10.1002/ppp.2179
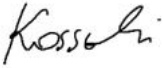
Oświadczam, że wkład Pani Martyny Górskiej w przygotowaniu powyżej publikacji wynosi 45%.

Pani Martyna Górska uczestniczyła w każdym etapie przeprowadzonej pracy eksperymentalnej, tj. przygotowania eksperymentu, przeprowadzenia eksperymentu (w tym poborze próbek po 50, 100, 300, 700, 1000 cyklach zamarzania-odmarzania), wykonania analiz ziaren kwarcu poddanych eksperymentalnemu wietrzeniu mrozowemu (w tym analizy rozkładu uziarnienia i analizy mikrostrukturalnej) oraz interpretacji wyników.

Przebieg pracy urządzenia zamrażająco-odmrażającego został opracowany przez Panią Martynę Górską, prof. dr hab. Barbarę Woronko (promotorka) i prof. dr hab. Małgorzatę Pisarską-Jamroży (promotorka).

Pani Martyna Górska przygotowała próbki do badań. Analiza mikrostrukturalna została przeprowadzona z prof. dr hab. Barbara Woronko (promotorka). Interpretacja uzyskanych wyników została przeprowadzona przez wszystkich współautorów.

Pani Martyna Górska brała udział w przygotowaniu pierwotnej wersji manuskryptu oraz przygotowała większość grafik (ryciny, tabele, załączniki) zawartych w publikacji. Pani Martyna Górska uczestniczyła we wszystkich etapach procesu publikacji wyników, w tym pełniąc funkcję autora korespondencyjnego i udzielając odpowiedzi recenzentom.

Martyna E. Górska		1.03.2023
Barbara Woronko		05.03.2023
Tomasz M. Kossowski		07.03.2023

DECLARATION OF AUTHORS

Publication no. 1:

Górska M.E., Woronko B., Kossowski T.M., Pisarska-Jamroży M., 2022. Micro-scale frost-weathering simulation – Changes in grain-size composition and influencing factors. Catena, 212, 106106. https://doi.org/10.1016/j.catena.2022.106106

I hereby declare that the contribution of Mrs. Martyna E. Górska in the preparation of the publication can be estimated at 40%.

Ms. Martyna Górska participated in each stage of the conducted experimental study, i.e. preparation of the experiment, main phase of the experiment (including the collection of the samples after 50, 100, 300 freeze-thaw cycles), analyses of quartz grains subjected to the experimental frost weathering (including the analysis of grain-size distribution and microtextural analysis) and interpretation of the results.

The workflow of the freeze-thaw device was developed by Ms. Martyna Górska, prof. dr hab. Barbara Woronko (supervisor) and prof. dr hab. Małgorzata Pisarska-Jamroży (supervisor).

Ms. Martyna Górska prepared all the samples for the experiment and conducted all the analyses of the grain-size distribution. The interpretation of the obtained results was conducted with all the co-authors.

Ms. Martyna Górska participated in the preparation of the original draft of manuscript and prepared most of the graphics (figures, tables, appendices) included in the publication. Ms. Martyna Górska participated in all the stages of each publication process, including serving as an corresponding author and responding to reviewers.

Martyna E. Górska		1.03.2023
Barbara Woronko		05.03.2023
Tomasz M. Kossowski		07.03.2023
Małgorzata Pisarska-Jamroży		06.03.2023

<div align="center">**DECLARATION OF AUTHORS**</div>

Publication no. 2:

Górska M.E., Woronko B., 2022. Multi-stage evolution of frost-induced microtextures on the surface of quartz grains – An experimental study. Permafrost and Periglacial Processes, 33, 4, 470-489. https://doi.org/10.1002/ppp.2164

I hereby declare that the contribution of Ms. Martyna E. Górska can be estimated at 55%.

Ms. Martyna Górska participated in each stage of the conducted experimental study, i.e. preparation of the experiment, main phase of the experiment (including the collection of the samples after 50, 100, 300, 700 and 1 000 freeze-thaw cycles), analyses of quartz grains subjected to the experimental frost weathering (including the microtextural analysis), and interpretation of the results.

The workflow of the freeze-thaw device was developed by Ms. Martyna Górska, prof. dr hab. Barbara Woronko (supervisor) and prof. dr hab. Małgorzata Pisarska-Jamroży (supervisor).

Ms. Martyna Górska prepared all the samples for the experiment. The microtextural analyses and interpretation of the obtained results were conducted with the co-author.

Ms. Martyna Górska participated in the preparation of the original draft of manuscript and prepared all the graphics (figures, tables, appendices) included in the publication. Ms. Martyna Górska participated in all the stages of each publication process, including serving as an corresponding author and responding to reviewers.

Martyna E. Górska		1.03.2023
Barbara Woronko		05.03.2023

DECLARATION OF AUTHORS

Publication no. 3:

Górska M.E., Woronko B., Kossowski T.M., Factors influencing the development of microtextures on cold-climate aeolian quartz grains revealed by experimental frost action. Permafrost and Periglacial Processes, 2023, 1-25. https://doi.org/10.1002/ppp.2179

I hereby declare that the contribution of Ms. Martyna E. Górska can be estimated at 45%.

Ms. Martyna Górska participated in each stage of the conducted experimental study, i.e. preparation of the experiment, main phase of the experiment (including the collection of the samples after 50, 100, 300, 700 and 1 000 freeze-thaw cycles), analyses of quartz grains subjected to the experimental frost weathering (including the grain-size analysis and microtextural analysis) and interpretation of the results.

The workflow of the freeze-thaw device was developed by Ms. Martyna Górska, prof. dr hab. Barbara Woronko (supervisor) and prof. dr hab. Małgorzata Pisarska-Jamroży (supervisor).

Ms. Martyna Górska prepared all the samples for the experiment. The microtextural analyses was conducted with prof. dr hab. Barbara Woronko (supervisor). The interpretation of the obtained results was conducted with all the co-authors.

Ms. Martyna Górska participated in the preparation of the original draft of manuscript and prepared all the graphics (figures, tables, appendices) included in the publication. Ms. Martyna Górska participated in all the stages of each publication process, including serving as an corresponding author and responding to reviewers.

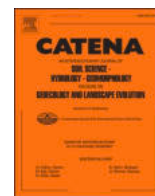| Martyna E. Górska		1.03.2023
Barbara Woronko		05.03.2023
Tomasz M. Kossowski		07.03.2023

ZAŁĄCZNIKI

ATTACHMENTS

ZAŁĄCZNIK 1

ATTACHMENT 1

Publikacja nr 1 (Publication no. 1):

Górska M.E., Woronko B., Kossowski T.M., Pisarska-Jamroży M., 2022. Micro-scale frost-weathering simulation – Changes in grain-size composition and influencing factors. *Catena*, 212, 106106. https://doi.org/10.1016/j.catena.2022.106106

Micro-scale frost-weathering simulation – Changes in grain-size composition and influencing factors

Martyna E. Górska [a,*], Barbara Woronko [b], Tomasz M. Kossowski [c], Małgorzata Pisarska-Jamroży [a]

[a] *Adam Mickiewicz University, Institute of Geology, Krygowskiego 12, 61-680 Poznań, Poland*
[b] *University of Warsaw, Faculty of Geology, Żwirki i Wigury 93, 02-089 Warsaw, Poland*
[c] *Adam Mickiewicz University, Faculty of Human Geography and Planning, Krygowskiego 10, 61-680 Poznań, Poland*

ARTICLE INFO

ABSTRACT

The experimental simulation of a micro-scale frost weathering of sand-sized (0.5–1.0 mm) quartz grains has been conducted to investigate the frost-induced changes in the grain-size distributions and factors that affect the weathering process. For the first time we present the results concerning the relationship between the course of frost weathering and the characteristics of water (content and mineralization) involved in the process. The simulation involved two types of vein quartz crushed to fresh, angular grains and arranged into dry, moistened and wet samples. Grain samples were subjected to fixed temperature oscillations (from -5 °C to $+10$ °C) under controlled laboratory conditions. Grain-size analysis were conducted after 50, 100, and 300 freeze–thaw cycles. Differences in the distributions, resulting from the production of the frost debris, were observed at each stage of the weathering process. Statistical analyses (Kolmogorov-Smirnov test, PCA, cluster analysis) demonstrated that both types of quartz grains react differently to the ongoing weathering process regardless of the moisture conditions. The production of very coarse (1.0–2.0 mm) and coarse sand (0.5–1.0 mm) fractions, resulting from the frost-induced destruction, was observed. This issue has never been addressed or expounded before. The production of fine (0.125–0.25 mm) and very fine (0.063–0.125 mm) sands was notable while the silt-sized grains (0.002–0.063 mm) constituted only a minor product of the frost weathering. Nevertheless, the combined increase in the content of these fractions may have a significant impact on the properties of the frost-affected sediments/ soils. The sample preparation (resulting in *preparation defects*) and the internal structure of quartz grains (resulting in *primary defects*) had a great influence on the initial course and manner of the frost weathering process. Other factors, such as content or mineralization of water, exerted much less influence on the frost-driven destruction during the studied weathering period.

1. Introduction

Alternating freeze and thaw cycles generate enough energy to bring about changes in the physical and mechanical properties of soils and rocks (Chamberlain and Gow, 1979; Qi et al., 2006; Ruedrich et al., 2011; Özgan et al., 2015; Liu et al., 2016; Zhou et al., 2018). This phenomenon can be observed especially in the area of permafrost thawing and active layer thickening, where the frost action is about to disturb the ever deeper structure of soils and rocks by ice segregation (Matsuoka et al., 2003; Murton et al., 2006; Bronfenbrener and Bronfenbrener, 2010; Maji and Murton, 2020). However, frost activity remains a main weathering factor in the whole periglacial environment which occupies up to 35% of the Earth's land area (e.g. Williams and Smith, 1989; French, 2017) and includes polar and sub-arctic latitudes, as well as middle-latitude and low-latitude mountain environments (e.g. Ballantyne, 2018; French, 2017).

The frost-induced destructive force has long been related to the process of volumetric expansion of the water upon freezing. However, findings from the fundamental experimental and theoretical studies (Taber, 1929; Beskow, 1935) have attributed this increased volume of frozen soil to complex heat and water-transfer processes (Bronfenbrener, 2009) that contribute to water migration and ice lenses (segregational ice) formation. A critical role in this process, commonly known as a frost heave phenomenon, is played by the susceptibility of soil to the frost

---

action (Konrad, 2005; Bronfenbrener, 2009; Bronfenbrener and Bronfenbrener, 2010; She et al., 2019). According to the classification of the International Society of Soil Mechanics and Foundation Engineering – ISSMFE (1989), soils are considered as frost-susceptible when containing: >1% of <0.002 mm grains, >3% of <0.02 mm grains and >8% of 0.074 mm grains. Their suction properties induce great negative pressures forcing the unfrozen moisture to move towards the freezing front, i.e. process known as a cryosuction. One of the most effective processes responsible for the formation of grains in mentioned fraction ranges is frost-driven mechanical destruction itself (Smith et al., 2002). It turns out that the relationship between the frost-induced destruction and amount of the silt-sized fraction (0.002–0.063 mm) creates a positive feedback, i.e. the higher content of the silt-sized fraction, the more intense frost activity, which in turn leads to a further production of this fraction. Hall (1990) was the first who associated the silt content in sediments with the frost weathering process and its intensity in a qualitative relationship. Konishchev (1998) introduced the Cryogenic Weathering Index (CWI) that expresses the role of cryogenic weathering in frozen soil formation, i.e. it indicates a relative enrichment in the quartz grains of the 0.01–0.05 mm fraction rather than of the 0.05–0.1 mm fraction. It follows that deposits that have been subjected to the frost action are characterized by CWI > 1, which argues for the intensive cryogenic weathering (Konishchev, 1999; Demitroff et al., 2007). However, the estimation of the contribution of frost activity in the production of the silt-sized fraction is impossible to be verified under the natural conditions as the grain-size distribution of the source sediments remains unknown.

Although one of the key factor influencing the course of frost weathering in the periglacial environment is water availability, a direct replication of the weathering conditions regarding water content and mineralization is beyond the bound of possibility as well. It is known that any addition of solutes (especially salts, that are commonly involved in the soil moisture) can depress the freezing point of water, and the increased solubility of carbon dioxide in low-temperature water leads to its increased concentration. Due to the restricted permeability of the permafrost-affected soils/sediments and thus restricted water circulation, the concentration of dissolved substances in surrounding water tends to increase; especially, in the case of a subsurface permafrost or talik (French, 2017). The relationship between the soil water characteristic (content, mineralization) and the intensity of frost-induced destruction has not been discussed in the literature so far. Bearing these facts in mind, it seems essential to address these issues.

So far, numerous experimental researches have been employed to examine the efficiency of cryogenic destruction and its contribution to the silt production (Lautridou and Ozouf, 1982; Woronko and Zieliński, 2006; Wright, 2000, 2007). It is widely acknowledged that micro-scale frost weathering results in fracturing or cracking of the individual grain and can develop a complex network of the weakness zones and contribute to the decay of weathering grains. However, less is, as yet, known about the grain-size changes, and thus the course and manner of the frost weathering within the wide range of sand-sized fractions (0.063–2 mm). The present study examines the frost weathering intensity of sand-sized quartz grains using a new experimental approach that incorporates different water content and mineralization into the weathering process. Although simulation of all of the factors operating in the periglacial environment is impossible in laboratory studies, the conditions assumed in this experiment intend to approximate to those experienced during the naturally-occurred microgelivation and thus replicating the process. The laboratory investigation was carried out to broaden the understanding of the micro-scale frost weathering phenomenon answering the following questions: (1) How does it affect the individual quartz grains of different internal features? (2) What grain size factions are produced during the progressive frost weathering? And what is the increase in the production of the silt-sized grains? (3) How does the water content and mineralization affect the frost-induced mechanically breakdown?

2. Material and methods

2.1. Material

Massive rocks crushed to the sand-sized grains (0.5–1.0 mm) were subjected to the frost weathering simulation. Rock samples of the vein quartz were gathered from the Polish Western Sudetes: Wojcieszów site and Kletno site. The selection of the study sites was based on the distinctive characteristics of quartz vein deposits.

Quartz from the Wojcieszów site (called as Q_W) forms a distinct sheet-like body of crystallized quartz within the sericite-chlorite metamorphosed claystones (metaclaystones; Kryza and Muszyński, 1992). These belong to the upper (epi) metamorphic zone according to Winkler (1976). The quartz vein originates from the hydrothermal processes associated with local thermal activity and magmatic intrusion. Macroscopically, the rock is white and homogeneous, formed only by crystallized and recrystallized quartz. The observations under the binoculars have revealed the presence of thin and irregular, green inclusions, probably of epidote-chlorite composition (Cwojdzinski and Kozdrój, 2011). Studied quartz is characterized by its massive structure, high hardness, and crushing resistance. The rock tended to break into elongated, angular grains with susceptibility to form blade- or tabular-shaped pieces that resemble prismatic crystals.

Quartz from the Kletno site (called as Q_K) originates from quartz and quartz-fluorite vein deposit hosted within gneisses and mica schists. Quartz occurs as a part of the quartz-fluorite-sulfide complex of a hydrothermal origin (Banas, 1965). Its formation is associated with the migration of the highly mineralized water solutions through a regional tectonic zone and locally developed thrust zone (Kasza, 1964; Zagożdżon and Zagrodny, 2009). Well-developed quartz forms alternating layers of milky quartz and amethyst. Locally observed, zonal growth of quartz reveals the presence of thin hematite crystals on the rhombohedral walls of quartz crystals (Gaweł, 1947; Zieliński, 1997; Wołkowicz, 2000; Sobień and Nawrocki, 2010). An extensive network of cracks and fissures makes these crystal aggregates easy and prone to break into rectangular and rhombohedral crystals.

Studied quartz grains (Q_W, Q_K) are characterized by a different type of an internal crystalline texture as revealed under a scanning electron microscope (SEM). Intergrown and interlocking quartz crystals can be observed in both Q_W and Q_K grains. However, these recrystallized forms consist of subhedral silica precipitation in the Q_W samples (Fig. 1A), whereas the Q_K samples (Fig. 1B) are characterized rather by the euhedral quartz crystals which remarkably predominate the grain structure. Their sizes varied from a few up to several dozen micrometers.

2.2. Sample preparation

Quartz samples (Q_W, Q_K) were mechanically crushed using the Bench Top Ring Mill and hand hammer, respectively, to obtain absolutely angular grains with fresh surfaces (cf. Wright et al., 1998). Process of the grain preparation employed here aims to reflect the high-energy crushing processes operate in the natural environment. Crushed quartz grains may therefore be regarded as representing the History-0 according to Molén (2014) and corresponding to those originating from regolith, glacial environments or tectonic zones (cf. Whalley and Krinsley, 1974; Mahaney and Andres, 1991; Hiemstra and Van der Meer, 1997; Mahaney, 2002; Rose and Hart, 2008; Vos et al., 2014). This type of grains has been commonly found in glacial mountain environments (e.g. Mahaney, 1995; Mahaney et al., 1988; Woronko, 2016).

Grain samples were sieved using a mechanical shaker to separate the designated coarse sand fraction (0.5–1.0 mm), and washed using the ultrasonic cleaner to get rid of the particles formed during rock crushing and as a result of natural processes. Prepared quartz grains were divided into equal volume samples (approx. 2 g, i.e. ~5000 grains) and stacked on the individual Petri dishes as: (1) dry samples, (2) moistened samples, where grains are on the filter paper soaked with water, (3) wet samples,
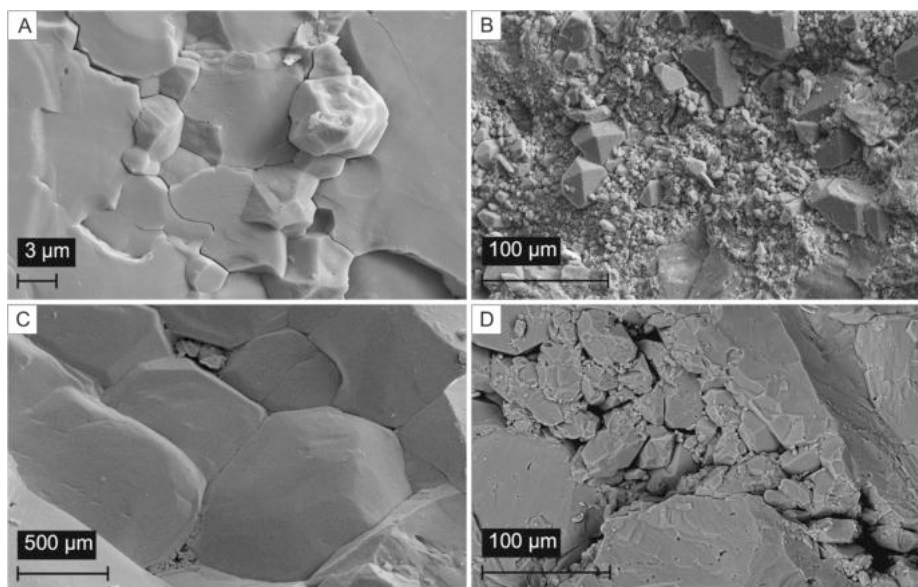
Fig. 1. SEM microphoto of a sand-sized quartz grain surface. A – Subhedral silica precipitation within Q_w grains; B – Euhedral silica precipitation within Q_K grains; C – Close contact between quartz crystals within the Q_w grains; D – Open contact between quartz crystals within the Q_K grains.

where grains are immersed in water. The moistened and wet samples were prepared with the addition of distilled, low-mineralized, and high-mineralized water. These arrangements aim to reflect the relationship between water content, water mineralization and sediments. Detailed chemistry characteristics of water are shown in Table A.1. A total of 42 samples were prepared for an experimental study. Additionally, the original sediment samples (Q_{W0}, Q_{K0} reference samples) have been analyzed before the experiment run.

2.3. Experiment design

The experimental research on the frost weathering of quartz grains was conducted under the controlled laboratory conditions. A commercial freezer has been equipped with a special software and programmed for automatic and defined temperature changes ranging from $-5\ °C$ up to $+10\ °C$ (Table 1) providing cyclic freeze–thaw processes, and thus simulating the conditions of the periglacial environment. Temperature range employed in conducted experiment corresponds to those used in previous fundamental experimental studies (e.g. Lautridou and Ozouf, 1982; Murton et al., 2000; Wright, 2000). Internal shelves of the device have an individual cooling and heating system, which ensures uniform conditions inside the device, i.e. the same temperature and humidity values would be recorded on each of the shelves. The device is programmed for permanent condensate drainage and automatic defrosting that aims to avoid the internal condensation of water vapor and crystallization of ice crystals, respectively.

Table 1
Temperature stages introduced into the freeze–thaw device workflow.

Stage	Temperature	Duration [hh:mm]	Rate of freezing [C/min]	Purpose
freezing	0 ℃	0:15	0.06	slow temperature
	−1 ℃	0:30	0.03	decrease to permit the
	−3 ℃	0:30	0.07	moisture migration
	−5 ℃	0:30	0.07	through the cracks
constant	−5 ℃	1:00		constant temperature freezing for all the water to become frozen
thawing	5 ℃	0:30		acceleration of the process of water and grains thawing
	10 ℃	0:30		
	1 ℃	0:15		

Three temperature stages have been introduced into the device workflow to set up the required climatic background: (1) the freezing stage, (2) the constant stage, and (3) the thawing stage, which constitute one complete freeze–thaw (FT) cycle that lasts four hours (Table 1).

The conducted experiment included the simulation of up to 300 FT cycles. During this time, water was replenished in the moistened and wet samples approximately every 2 days to avoid its complete evaporation. The quartz grain samples were collected after 50, 100, and 300 FT cycles. The arrangement of the samples was unchanged throughout the experiment.

2.4. Laboratory analysis

After each sampling procedure, samples were allowed to dry at the room temperature and afterwards received from the Petri dishes. The grain-size distribution was estimated for a single sample using the Malvern Morphologi G3 particle characterization system. Samples (~2 g) were quartered to fit the apparatus capacity. Quartz samples were dispersed on the microscope glass using the sample dispersion unit (SDU) with injection pressure of 4 bar and default injection time of 20 ms along with settling time of 60 s. The same standard operating procedure (SOP) and a magnification of 2.5x were employed for all samples. The obtained grain photos from each sample were reviewed to exclude from the further analysis these grains that were touch each other and therefore were measured as a single one. The circle equivalent (CE) diameter and area of the properly measured grains were used to generate the grain size distribution for each sample (Malvern Instruments Ltd., 2008). The obtained data was used to calculate the grain size parameters (Mz - mean grain size, mode, sorting, skewness, kurtosis) according to Folk and Ward's (1957) classification using Gradistat package (cf. Blott and Pye, 2001). The mean grain size was described using a modified Udden (1914) and Wentworth (1922) scale (Fig. 2A) as has been extracted from the Gradistat worksheet.

The scanning electron microscope (SEM) was employed to: (1) examine the grain shape, (2) study the microtextures of its surface and (3) determine the effects of the sample preparation on the course of frost weathering (crushing in high-energy vs low-energy stress regime). Randomly selected grains from each sample were mounted on the holders using a double-sided carbon tape. Then, samples were coated with gold. The investigation was carried out to estimate the number of cracks located on the visible surface of the grains from the reference
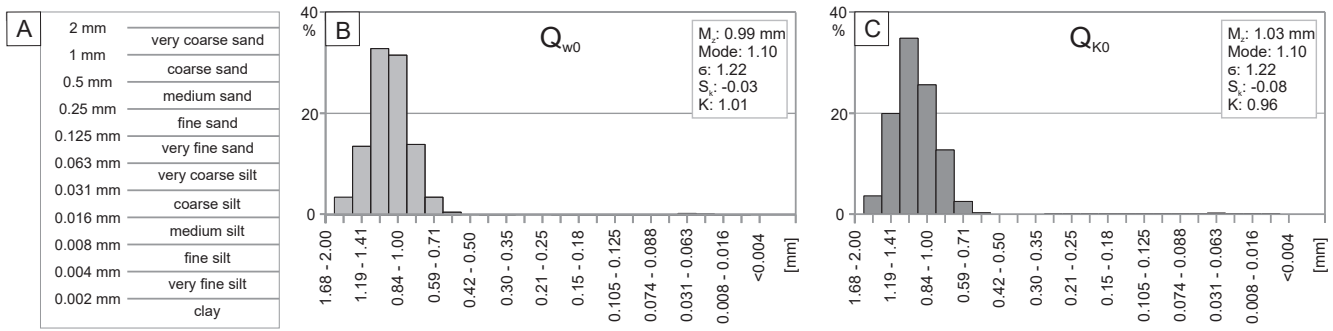
Fig. 2. Grain-size distributions of the reference samples. A – Grain-size scale modified after Udden (1914) and Wentworth (1922) adopted from the Gradistat program; B – Q_{W0} sample; C – Q_{K0} sample.

samples, and to study the frost-induced microtextural changes.

2.5. Statistical analysis

2.5.1. Kolmogorov-Smirnov test

The non-parametric Kolmogorov-Smirnov test is commonly used for the comparison of two sample distributions and applied to sedimentological research (Pereira et al., 2016; Montanher et al., 2018).

Let us assume, that X_1 and X_2 are independent random variables with two cumulative distribution functions: $F1$; $F2$. Further, let us denote $X_1 = (X_{11}, X_2, \cdots, X_{1n_1})$ and $X_2 = (X_{21}, X_{22}, \cdots, X_{2n_2})$ as two independent n_1 and n_2-element samples from populations with distributions described above.

We want to verify a null hypothesis saying that these random samples become from two populations with equal cumulative distribution functions, i.e. $H_0 : F_1(x) = F_2(x)$ for all $\times \in \mathbb{R}$. The alternative hypothesis is H_1: $F_1(x) \neq F_2(x)$ for at least one of the element $\times \in \mathbb{R}$. The Kolmogorov-Smirnov test statistic has a formula:

$$D = \sup_x \left| F_{1,n_1}(x) - F_{2,n_2}(x) \right|, \tag{1}$$

where $F_{1,n_1}(x)$, $F_{2,n_2}(x)$ are, respectively, empirical distributions of the first and the second sample.

The null hypothesis is rejected, if

$$D > \lambda_{1-\alpha}\sqrt{(n_1 + n_2)/n_1 n_2}, \tag{2}$$

where $\lambda_{1-\alpha}$ is a quantile function of Kolmogorov distribution and α is a significance level.

2.5.2. Principal component analysis

Principal component analysis (PCA) was introduced by Hotelling (1933) and is often applied to a dimensionality reduction problem. The general idea of the method is a transformation of the set p correlated variables X_i into a set m uncorrelated variables Y_j, where m ≤ p. This method reduces the multidimensional observation space to space with a fewer number of dimensions. After this transformation, new variables $Y_1, Y_2, …, Y_m$ from reduced space (called principal components) can be written as linear combinations of original variables $X_1, X_2, …, X_p$. This method was precisely described and applied in many papers and books both in statistics and geology (McCammon, 1966; Pirkle et al., 1980; Anderson, 1984; Weltje, 1997; Reid and Spencer, 2009; Shi et al., 2015; Inzoli et al., 2016; Yamashita et al., 2018; Oyedotun, 2020).

Let $X = (X_1, X_2, …, X_p)'$ will be a p-element vector of variables X_i. This vector is transformed to a vector $Y = (Y_1, Y_2, …, Y_p)'$ of new variables (principal components) by the formula:

$$Y = XA \tag{3}$$

For vectors $a_1, a_2, … a_p$ of matrix A we have $a_i' \cdot a_j = 1$ if $i = j$, or $a_i' \cdot a_j = 0$ otherwise, $i, j = 1, 2, …, p$. As a consequence of (3), we can write i-th

principal component as $Y_i = a_i X = a_{i1} X_1 + \cdots + a_{ip} X_p$. The original set of variables is transformed into a set of principal components in such a way that the first principal component has the largest variance, the second has variance less than the first and so on $var(Y_1) \geq var(Y_2) \geq \cdots \geq var(Y_p)$. The sum of principal components variance is equal to the original variables total variance, i.e. $\sum_{j=1}^{p} var(Y_j) = \sum_{i=1}^{p} var(X_i)$.

In this paper, we applied a singular value decomposition (SVD) of matrix X (Wall et al., 2003; Golub and Van Loan, 2013) for principal components extraction. This approach is necessary if we have more variables than observations, i.e. $p > n$. Using SVD we can write X = USA′, where U is a unitary n-by-n matrix with orthogonal columns being vectors of length n, S is a n-by-p matrix with singular values s_i of X, and vectors of X are centered (or standardized in the case of a correlation matrix). The covariance matrix of original variables is equal to $\Sigma = X'X/(n-1)$, and being a symmetric matrix can be written as $\Sigma = A\Lambda A'$, where Λ is a diagonal matrix of eigenvalues λ_i. Thus, we have $\Sigma = ASU'USA'/(n-1) = AS^2A'/(n-1)$ and a principal components matrix is Y = XA = US.

The number m of extracted principal components can be selected by a few different criteria. One of the most popular criteria is that theoretically confirmed by Kaiser (1960, 1974). According to it, we extract p principal components, and then we select from them only those that correspond to the eigenvalues $\lambda_i > 1$ of the original variables correlation matrix. These m ≤ p components can be interpreted using so-called *factor loadings*, i.e. correlation coefficients r_{ji} between principal component Y_j, j = 1, 2, …, m, and original variables X_i, i = 1, 2, …, p. The share of i-th principal component variance in total variance is equal to $w_i = \lambda_i/\sum_{j=1}^{p}\lambda_j$, where λ_i can be written as a function singular values s_j of X, i.e. $\lambda_j = s_j^2/(n-1)$. Principal component analysis was performed using the package stats of the R software (R Core Team, 2020).

2.5.3. Cluster analysis

Cluster analysis has a long tradition of use in sedimentological analysis (Read, 1976; Martins et al., 2016; Abdideh and Ameri, 2020). This method has a huge interest among scholars and many statistical books were devoted to its theoretical foundations (Aldenderfer and Blashfield, 1984; Everitt et al., 2011; Hennig et al., 2015; Wierzchoń and Kłopotek, 2018).

In this paper, we applied Ward's method (1963) for hierarchical cluster analysis. In this method, the objective function approach is used for the selection of the pair of clusters or observations which should be grouped at each step. Ward proposed the minimum variance as the criterion for selection, i.e. total cluster variance should be minimal. The distance between observations we defined as a squared Euclidean distance. Observations were described by scores of m principal components obtained in the previous step of the study.

The most adequate number of clusters was delivered by the silhouette method (Rousseeuw, 1987; Kaufman and Rousseeuw, 1990). For each observation so-called silhouette value is calculated. It measures,

how a given observation is similar to its cluster and compares how it is similar to other clusters. If the number of clusters c is appropriate, then observations have high values of the silhouette. It is more convenient to use a silhouette coefficient defined as freeze–thaw cycles. Valid for both Q_W and Q_K samples, the maximum value of the mean $SC = max_c \overline{s_k}$, where $\overline{s_k}$ is the mean value of silhouette for the set of all observations
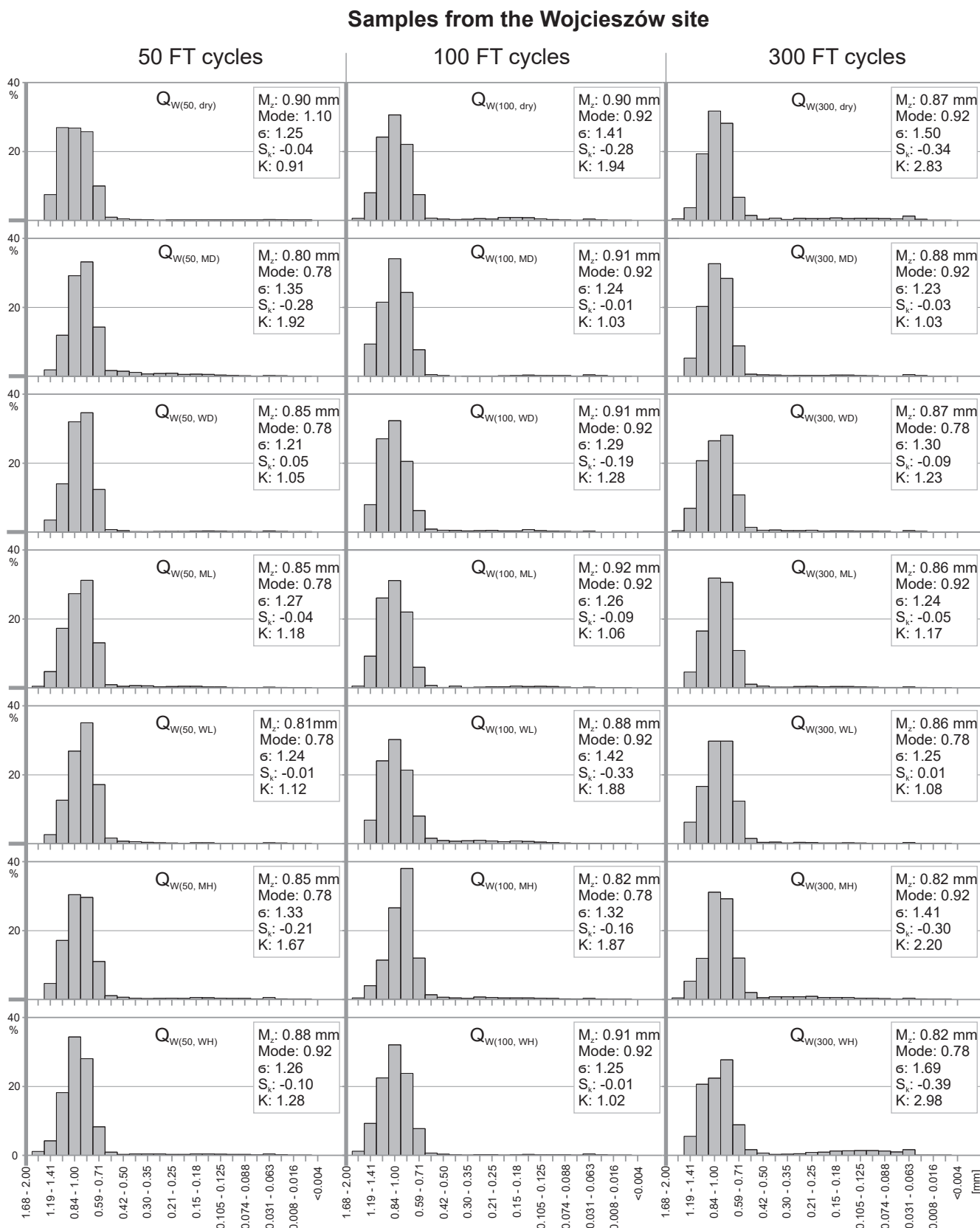

Fig. 3. Grain-size distributions of the samples subjected to the frost weathering simulation. A – Q_W samples; B – Q_K samples.

Samples from the Kletno site
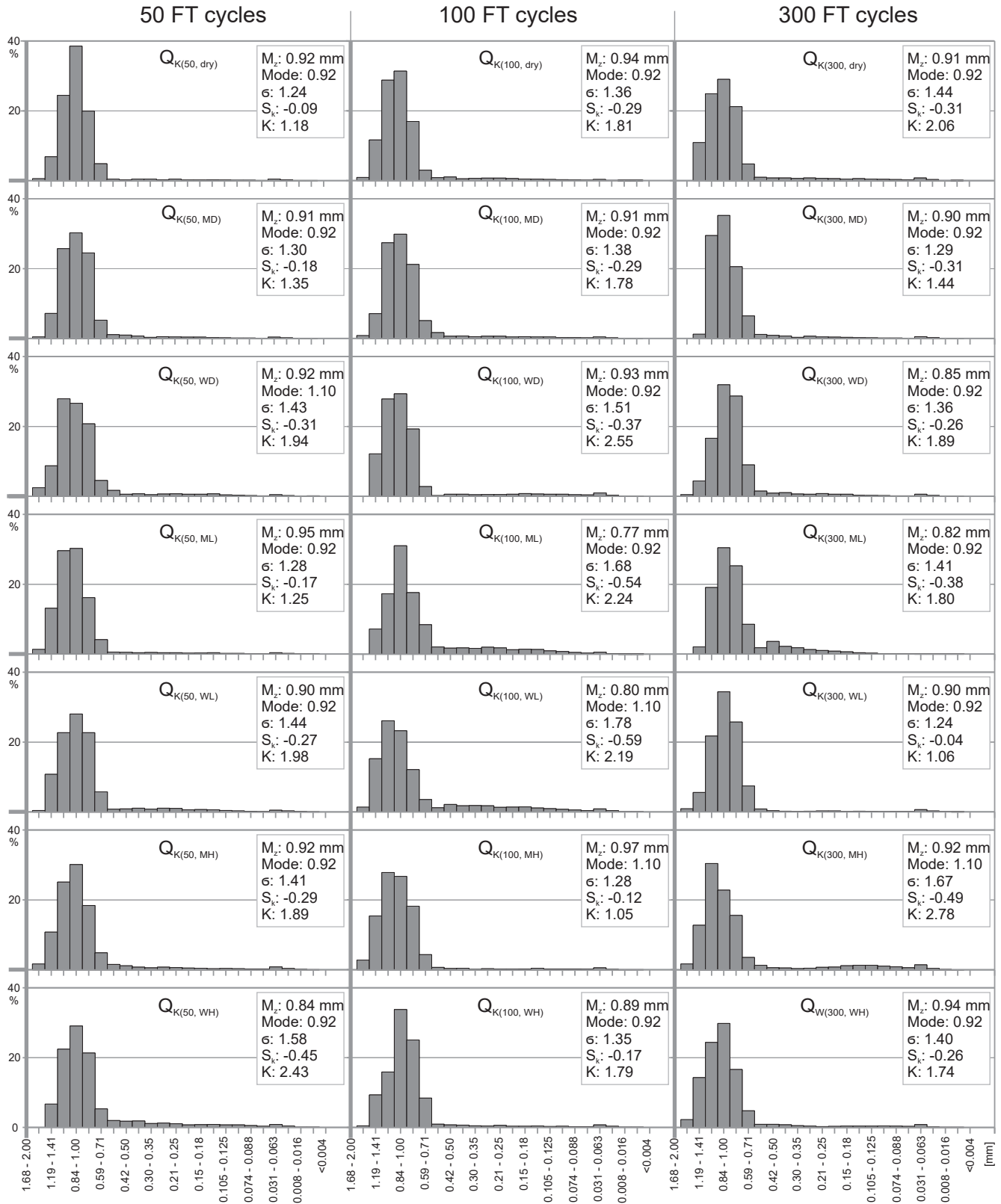
Fig. 3. (continued).

divided into *k* clusters (Kaufman and Rousseeuw, 1990). The R software was used in the cluster analysis. We applied procedures from R packages: cluster, factorextra, and NbClust to identification and visualisation of clusters.

3. Results

3.1. Grain-size distribution

As a result of the laboratory simulation of the micro-scale frost weathering, grain-size distributions were created and statistical parameters have been calculated for the reference samples (Fig. 2B, C) and samples suffered from 50, 100, 300 FT (Figs. 3, A.1, A.2, Tables 2–4).

After each stage of weathering (50, 100, 300 FT), significant differences in the grain-size distributions were observed regarding the reference samples (Fig. 2B, C). These were manifested by a decrease in the Mz values and changes in the content of individual fractions. Samples after 100 FT are particularly distinguishable from others as an increase in their Mz values in the comparison to 50 FT samples was noted. Only insignificant silt production was observed throughout the experiment (Figs. 3, A.1, A.2; Table 3). Moreover, an investigation under a SEM has revealed numerous cracks on the surface of reference samples (see Section 4.1; Table 4).

3.2. Samples distributions comparison

The results of the Kolmogorov-Smirnov test (Table 5) show the comparison of the grain-size distribution in a sample being under the experiment to the grain-size distribution in the reference sample (Fig. 2B-C, 3). If the differences between distributions are statistically significant (p-values < 0.05) then we conclude that the sample reacts on the ongoing frost weathering process. The null hypotheses on the lack of differences between the grain-size distributions of the samples under study and the grain-size distribution of the reference sample were rejected in 13 of 42 tests. The grain-size distribution was consistent with the reference sample distribution eight times in the case of the Q_K samples and five times in the case of the Q_W samples.

Four groups of samples (A–D) were identified on the base of the Kolmogorov-Smirnov test (Fig. 4). Group A consists of the Q_W and Q_K samples that significantly differ from the corresponding reference one (Q_{W0}, Q_{K0}). The group includes all of the samples subjected to 50 and 300 FT cycles with a few exceptions that are included in the group B. Group B consists of samples that differ from the Q_{W0} reference sample and do not differ from the Q_{K0} reference sample, i.e. $Q_{(50; ML)}$ – samples moistened with low-mineralized water, $Q_{(100; MH)}$, $Q_{(300; MH)}$ – moistened with high-mineralized water and $Q_{(300; WH)}$ – samples with high-mineralized water. Group C consists of samples that do not differ from the Q_{W0} reference sample and do differ from the Q_{K0} reference sample. The group includes: $Q_{(100; MD)}$ – samples moistened with distilled water, $Q_{(100; ML)}$ – moistened with low-mineralized water, and $Q_{(100; WH)}$ – samples with high-mineralized water subjected to 100 FT cycles. Group D consists of samples that do not differ from the Q_{W0} and Q_{K0} reference samples, i.e. $Q_{(100; dry)}$ – dry samples, $Q_{(100; WD)}$ – samples with distilled water, and $Q_{(100; WL)}$ – samples with low-mineralized water exposed to 100 FT cycles.

3.3. Results of principal components analysis (PCA)

PCA was performed separately for the Q_W and Q_K samples. Principal

components were extracted from a set of variables representing grain-size fractions. We excluded from the data those grain-size fractions that had a zero share in all of the samples (Table 3), i.e. 1.68–2.00, 0.002–0.004, 0.001–0.002, and < 0.001 mm. As a consequence, the number of variables (23) became slightly higher than the number of samples (22) in each site. Described in Section 2.5.2 singular value decomposition method (SVD) was employed for the extraction of principal components.

3.3.1. PCA on the Q_W samples

PCA has extracted five principal components (PC1–PC5), which explain 91.19% of the total variance. The matrix of factor loadings (Table 6) delivers information about the structure of extracted principal components. PC1 holds 41.12% of the total variance and is strongly correlated to the medium-, fine- and very fine-grained sand fractions, i.e. 0.063–0.59 mm (Table 7). PC2 has 23.59% and its factor loadings suggest that it is related to the very coarse-grained sand fractions, i.e. >1 mm. PC3 explains 13.93% of the total variance and corresponds to the silt-sized fractions, i.e. 0.004–0.063 mm. PC4 (8.08%) and PC5 (4.48%) are correlated to coarse-grained fractions (0.59–0.84 mm and 0.84–1 mm, respectively) (Tables 6 and 7).

3.3.2. PCA on the Q_K samples

PCA has extracted four principal components (PC1–PC4) that explain 88.55% of the total variance (Table 8). PC1 has 41.81% of the original variables total variance. The factor loadings matrix (Table 9) let us to interpret this principal component in terms of the coarse-, medium-, fine- and very fine-grained sand and very coarse-grained silt fractions, i.e. 0.031–0.59 mm. PC2 explains almost 15% less of total variance than PC1, i.e. for 26.06%. This principal component is highly correlated with the very coarse- and coarse-grained sand fractions, i.e. from 0.5 to 1.68 mm. PC3 shares 15.71% of total variance and relates to the fine-, medium- and coarse-grained silt fractions, i.e. 0.004–0.0031 mm. The last principal component, PC4 holds 4.97% of the total variance and does not correlate to any of the grain-size fraction (Tables 8 and 9).

3.4. Cluster analysis

Hierarchical cluster analysis has been employed to organize samples into groups of similar sedimentological characteristics, and further to examine the relationships in their reactions to the frost activity. The optimal number of clusters (k) has been determined according to the silhouette criterion.

3.4.1. Cluster analysis for the Q_W samples

According to the result of the silhouette criterion (maximum average silhouette is 0.3286), the samples are clustered into five groups (k = 5; Fig. 5A). The first group is composed mainly of the samples subjected to 50 or 300 FT cycles. It includes: $Q_{W(50; WD)}$, $Q_{W(50; ML)}$, $Q_{W(50; WL)}$, $Q_{W(50; MH)}$, $Q_{W(50; WH)}$, $Q_{W(300; dry)}$, $Q_{W(300; MD)}$, $Q_{W(300; WD)}$, $Q_{W(300; ML)}$, $Q_{W(300; WL)}$, and $Q_{W(100; MH)}$. The particle size distribution of all these samples differ significantly from the distribution of the Q_{W0} reference sample. These samples, as compared to the reference one, are characterized by a lower mode value (Fig. 3), higher standard deviation, generally lower skew values, and higher kurtosis. The second group includes: Q_{W0}, $Q_{W(50; dry)}$, $Q_{W(100; MD)}$ and $Q_{W(100; WH)}$. Only one of them ($Q_{W(50; dry)}$) has a statistically insignificant grain-size distribution as compared to the reference distribution. Samples $Q_{W(100; MD)}$ and $Q_{W(100; WH)}$ differ statistically from the Q_{W0} distribution. Samples grouped in this cluster are characterized by almost the same standard deviations values, skewness coefficients around 0, and a kurtosis close to 1 (Fig. 4). The third group includes samples that underwent 100 FT cycles, such as: $Q_{W(100; dry)}$, $Q_{W(100; WD)}$, $Q_{W(100; ML)}$. All of these samples are characterized by the equal mode values (0.92). Their probability p-values are the highest from all of the studied samples (Table 4). It is therefore a cluster of samples with the grain-size distribution most

Table 2
List of sample names according to the weathering conditions and amount of the freeze–thaw cycles. Valid for both Q_W and Q_K samples.

	50 FT	100 FT	300 FT
dry	$Q_{(50, dry)}$	$Q_{(100, dry)}$	$Q_{(300, dry)}$
moistened with distilled water	$Q_{(50, MD)}$	$Q_{(100, MD)}$	$Q_{(300, MD)}$
wet with distilled water	$Q_{(50, WD)}$	$Q_{(100, WD)}$	$Q_{(300, WD)}$
moistened with low-mineralized water	$Q_{(50, ML)}$	$Q_{(100, ML)}$	$Q_{(300, ML)}$
wet with low-mineralized water	$Q_{(50, WL)}$	$Q_{(100, WL)}$	$Q_{(300, WL)}$
moistened with high-mineralized water	$Q_{(50, MH)}$	$Q_{(100, MH)}$	$Q_{(300, MH)}$
wet with high-mineralized water	$Q_{(50, WH)}$	$Q_{(100, WH)}$	$Q_{(300, WH)}$

Table 3
Results of grain-size distribution analysis (in %) and statistical parameters. A – Q_W samples; B – Q_K samples.

	[mm/FT]	Q_{W0}	$Q_{W(dry)}$ 50	100	300	$Q_{W(MD)}$ 50	100	300	$Q_{W(WD)}$ 50	100	300	$Q_{W(ML)}$ 50	100	300	$Q_{W(WL)}$ 50	100	300	$Q_{W(MH)}$ 50	100	300	$Q_{W(WH)}$ 50	100	300
vcS	1.68–2.00	0,00	0,00	0,00	0,00	0,00	0,00	0,00	0,00	0,00	0,00	0,00	0,00	0,00	0,00	0,00	0,00	0,00	0,00	0,00	0,00	0,00	0,00
	1.41–1.68	3,49	0,00	0,62	0,51	0,00	0,00	0,00	0,00	0,00	0,44	0,47	0,58	0,00	0,00	0,00	0,00	0,00	0,48	0,46	1,12	1,19	0,00
	1.19–1.41	13,50	7,53	8,06	3,73	1,84	9,36	5,28	3,52	7,94	6,91	4,78	9,18	4,60	2,63	6,87	6,26	4,69	4,01	5,31	4,23	9,27	5,53
	1.00–1.19	32,79	26,94	24,20	19,35	11,91	21,50	20,27	14,03	27,05	20,68	17,31	26,06	16,52	12,61	24,02	16,65	17,13	11,42	12,00	18,23	22,44	20,63
cS	0.84–1.00	31,50	26,78	30,60	31,70	29,20	34,06	32,64	31,98	32,31	26,46	27,35	31,12	31,86	26,87	30,19	29,77	30,39	26,58	31,12	34,34	32,05	22,40
	0.71–0.84	13,89	25,75	22,07	28,19	33,14	24,29	28,39	34,62	20,50	28,14	31,22	22,00	30,64	35,07	21,34	29,75	29,65	38,00	29,24	28,08	23,75	27,74
	0.59–0.71	3,46	10,02	7,53	6,71	14,27	7,68	8,80	12,38	6,26	10,82	13,10	6,02	10,82	17,16	8,04	12,34	11,06	12,03	12,05	8,29	7,80	8,90
	0.50–0.59	0,53	0,96	0,70	1,45	1,67	0,48	0,63	0,72	0,91	1,40	0,95	0,72	1,10	1,67	1,58	1,52	1,14	1,39	2,05	0,94	0,71	1,67
mS	0.42–0.50	0,00	0,50	0,41	0,35	1,44	0,20	0,44	0,41	0,53	0,56	0,46	0,18	0,53	0,76	0,94	0,45	0,66	0,69	0,57	0,30	0,33	0,65
	0.35–0.42	0,03	0,28	0,32	0,67	1,12	0,00	0,37	0,14	0,47	0,63	0,68	0,56	0,20	0,59	0,72	0,48	0,41	0,51	0,82	0,40	0,19	0,30
	0.30–0.35	0,03	0,24	0,33	0,28	0,71	0,05	0,25	0,09	0,35	0,39	0,63	0,14	0,22	0,41	0,91	0,22	0,26	0,33	0,85	0,42	0,08	0,33
	0.25–0.30	0,00	0,06	0,52	0,64	0,82	0,11	0,30	0,17	0,41	0,40	0,34	0,22	0,41	0,31	1,04	0,40	0,36	0,74	0,78	0,41	0,21	0,51
fS	0.21–0.25	0,00	0,09	0,40	0,57	0,89	0,08	0,30	0,17	0,47	0,57	0,41	0,38	0,47	0,22	0,80	0,33	0,45	0,61	0,95	0,27	0,21	0,89
	0.18–0.21	0,02	0,11	0,86	0,52	0,54	0,17	0,29	0,17	0,36	0,30	0,48	0,36	0,39	0,18	0,63	0,20	0,35	0,46	0,61	0,31	0,11	0,95
	0.15–0.18	0,02	0,09	0,90	0,74	0,59	0,21	0,33	0,20	0,33	0,35	0,46	0,52	0,42	0,27	0,79	0,23	0,60	0,51	0,59	0,45	0,18	1,25
	0.125–0.15	0,04	0,07	0,79	0,57	0,57	0,33	0,33	0,27	0,72	0,33	0,30	0,44	0,39	0,26	0,70	0,26	0,56	0,49	0,60	0,40	0,27	1,35
vfS	0.105–0.125	0,05	0,03	0,51	0,61	0,33	0,25	0,24	0,19	0,40	0,29	0,28	0,47	0,31	0,19	0,49	0,20	0,45	0,42	0,45	0,33	0,14	1,42
	0.088–0.105	0,05	0,03	0,32	0,60	0,28	0,23	0,15	0,18	0,27	0,26	0,14	0,39	0,24	0,10	0,34	0,14	0,37	0,34	0,41	0,29	0,18	1,40
	0.074–0.088	0,05	0,05	0,14	0,57	0,16	0,19	0,12	0,14	0,19	0,19	0,12	0,23	0,17	0,08	0,20	0,13	0,34	0,23	0,30	0,32	0,14	1,30
	0.063–0.074	0,03	0,05	0,10	0,51	0,09	0,10	0,11	0,07	0,12	0,11	0,07	0,11	0,14	0,05	0,11	0,08	0,24	0,14	0,17	0,17	0,10	1,03
silt	0.031–0.063	0,28	0,21	0,44	1,27	0,23	0,44	0,47	0,30	0,26	0,40	0,24	0,25	0,32	0,30	0,18	0,34	0,59	0,38	0,45	0,42	0,40	1,64
	0.016–0.031	0,16	0,15	0,15	0,34	0,14	0,21	0,21	0,18	0,11	0,25	0,16	0,05	0,18	0,21	0,10	0,18	0,24	0,18	0,16	0,20	0,18	0,09
	0.008–0.016	0,06	0,04	0,03	0,09	0,04	0,04	0,06	0,05	0,03	0,08	0,05	0,01	0,05	0,05	0,03	0,06	0,06	0,06	0,05	0,06	0,05	0,01
	0.004–0.008	0,01	0,01	0,00	0,02	0,01	0,01	0,01	0,01	0,01	0,02	0,01	0,00	0,01	0,01	0,00	0,01	0,01	0,01	0,01	0,01	0,01	0,00
	0.002–0.004	0,00	0,00	0,00	0,00	0,00	0,00	0,00	0,00	0,00	0,00	0,00	0,00	0,00	0,00	0,00	0,00	0,00	0,00	0,00	0,00	0,00	0,00
clay	0.001–0.002	0,00	0,00	0,00	0,00	0,00	0,00	0,00	0,00	0,00	0,00	0,00	0,00	0,00	0,00	0,00	0,00	0,00	0,00	0,00	0,00	0,00	0,00
	<0.001	0,00	0,00	0,00	0,00	0,00	0,00	0,00	0,00	0,00	0,00	0,00	0,00	0,00	0,00	0,00	0,00	0,00	0,00	0,00	0,00	0,00	0,00
vcS	1.00–2.00	49,78	34,48	32,89	23,59	13,75	30,87	25,56	17,55	34,99	28,03	22,56	35,82	21,12	15,24	30,88	22,91	21,82	15,91	17,77	23,58	32,91	26,16
cS	0.50–1.00	49,39	63,52	60,90	68,05	78,28	66,51	70,47	79,69	59,97	66,82	72,62	59,85	74,43	80,77	61,14	73,38	72,24	78,00	74,46	71,65	64,31	60,70
mS	0.25–0.50	0,06	1,08	1,58	1,94	4,09	0,36	1,36	0,82	1,76	1,99	2,11	1,10	1,37	2,07	3,60	1,55	1,68	2,27	3,03	1,53	0,80	1,80
fS	0.125–0.25	0,08	0,37	2,94	2,40	2,60	0,80	1,24	0,81	1,88	1,55	1,65	1,71	1,66	0,94	2,92	1,02	1,96	2,07	2,75	1,43	0,76	4,45
vfS	0.063–0.125	0,18	0,16	1,07	2,29	0,86	0,77	0,62	0,58	0,99	0,86	0,61	1,20	0,86	0,42	1,14	0,55	1,39	1,13	1,32	1,11	0,57	5,15
silt	0.004–0.063	0,51	0,41	0,63	1,72	0,41	0,70	0,76	0,54	0,41	0,75	0,45	0,32	0,56	0,57	0,31	0,60	0,90	0,62	0,67	0,70	0,64	1,74
clay	<0.004	0,00	0,00	0,00	0,00	0,00	0,00	0,00	0,00	0,00	0,00	0,00	0,00	0,00	0,00	0,00	0,00	0,00	0,00	0,00	0,00	0,00	0,00
Mean		0,99	0,90	0,90	0,87	0,80	0,91	0,88	0,85	0,91	0,87	0,85	0,92	0,86	0,81	0,88	0,86	0,85	0,82	0,82	0,88	0,91	0,82
Mode		1,10	1,10	0,92	0,92	0,78	0,92	0,92	0,78	0,92	0,78	0,78	0,92	0,92	0,78	0,92	0,78	0,78	0,78	0,92	0,92	0,92	0,78
Sorting		1,22	1,25	1,41	1,50	1,35	1,24	1,23	1,21	1,29	1,30	1,27	1,26	1,24	1,24	1,42	1,25	1,33	1,32	1,41	1,26	1,25	1,69
Skewness		−0,03	−0,04	−0,28	−0,34	−0,28	−0,01	−0,03	0,05	−0,19	−0,09	−0,04	−0,09	−0,05	−0,01	−0,33	0,01	−0,21	−0,16	−0,30	−0,10	−0,01	−0,39
Kurtosis		1,01	0,91	1,94	2,83	1,92	1,03	1,03	1,05	1,28	1,23	1,18	1,06	1,17	1,12	1,88	1,08	1,67	1,87	2,20	1,28	1,02	2,98

	[mm/FT]	Q_{K0}	$Q_{K(dry)}$ 50	100	300	$Q_{K(MD)}$ 50	100	300	$Q_{K(WD)}$ 50	100	300	$Q_{K(ML)}$ 50	100	300	$Q_{K(WL)}$ 50	100	300	$Q_{K(MH)}$ 50	100	300	$Q_{K(WH)}$ 50	100	300
vcS	1.68–2.00	0,00	0,00	0,00	0,00	0,00	0,00	0,00	0,00	0,00	0,00	0,00	0,00	0,00	0,00	0,00	0,00	0,00	0,00	0,00	0,00	0,00	0,00
	1.41–1.68	3,59	0,58	0,93	0,00	0,48	0,83	0,00	2,46	0,00	0,45	1,40	0,00	0,00	0,43	1,38	0,94	1,65	2,78	1,70	0,00	0,48	2,31
	1.19–1.41	19,91	6,85	11,67	10,96	7,16	7,15	1,22	8,72	12,15	4,43	13,16	7,21	2,08	10,81	15,28	5,55	10,80	15,42	12,77	6,72	9,34	14,30
	1.00–1.19	34,76	24,44	28,75	24,91	25,77	27,39	29,48	27,92	27,84	16,66	29,61	17,28	19,10	22,69	26,09	21,71	25,12	27,82	30,42	22,46	15,85	24,36

8

Table 3 (*continued*)

	[mm/FT]	Q$_{K0}$	Q$_{K(dry)}$ 50	100	300	Q$_{K(MD)}$ 50	100	300	Q$_{K(WD)}$ 50	100	300	Q$_{K(ML)}$ 50	100	300	Q$_{K(WL)}$ 50	100	300	Q$_{K(MH)}$ 50	100	300	Q$_{K(WH)}$ 50	100	300
cS	0.84–1.00	25,57	38,56	31,35	29,06	30,28	29,91	35,27	26,67	29,34	31,95	30,27	31,01	30,45	28,03	23,26	34,37	30,13	26,74	22,78	29,05	33,80	29,79
	0.71–0.84	12,68	19,93	16,97	21,19	24,48	21,20	20,57	20,79	19,27	28,69	16,16	17,62	25,30	22,67	12,16	25,75	18,41	18,21	15,58	21,30	25,06	16,64
	0.59–0.71	2,54	4,88	2,99	4,82	5,22	5,13	6,49	4,57	2,82	9,00	4,17	8,44	8,56	5,80	3,55	7,43	4,87	4,37	3,53	5,32	8,39	4,80
	0.50–0.59	0,23	0,48	0,83	1,00	1,13	1,71	1,17	1,68	0,24	1,51	0,59	2,07	1,83	0,83	1,23	0,83	1,52	0,70	1,34	1,99	0,91	0,93
mS	0.42–0.50	0,00	0,27	1,03	0,81	0,97	0,64	0,95	0,61	0,60	0,90	0,55	1,72	3,65	0,89	2,18	0,37	1,13	0,40	0,59	1,75	0,75	0,90
	0.35–0.42	0,00	0,48	0,55	0,78	0,76	0,73	0,76	0,73	0,57	1,08	0,41	1,79	2,18	1,07	1,80	0,22	0,75	0,44	0,58	1,88	0,66	0,82
	0.30–0.35	0,00	0,47	0,65	0,66	0,37	0,55	0,35	0,48	0,48	0,66	0,48	1,65	1,84	0,80	1,87	0,16	0,57	0,14	0,33	1,12	0,48	0,51
	0.25–0.30	0,06	0,28	0,73	0,78	0,51	0,64	0,65	0,69	0,57	0,57	0,40	1,98	1,34	1,09	1,76	0,22	0,75	0,28	0,52	1,28	0,39	0,41
fS	0.21–0.25	0,05	0,49	0,71	0,66	0,49	0,69	0,49	0,73	0,56	0,77	0,41	1,81	1,05	1,01	1,37	0,26	0,61	0,18	0,72	1,06	0,61	0,31
	0.18–0.21	0,05	0,24	0,61	0,61	0,39	0,46	0,41	0,62	0,61	0,61	0,30	1,31	0,89	0,62	1,44	0,25	0,49	0,16	0,79	0,71	0,35	0,32
	0.15–0.18	0,03	0,19	0,48	0,47	0,42	0,56	0,36	0,62	0,81	0,62	0,33	1,44	0,68	0,72	1,45	0,16	0,42	0,26	1,22	0,83	0,36	0,43
	0.125–0.15	0,05	0,28	0,38	0,59	0,28	0,49	0,30	0,75	0,66	0,36	0,39	1,38	0,40	0,62	1,15	0,19	0,33	0,42	1,29	0,88	0,38	0,41
vfS	0.105–0.125	0,03	0,23	0,35	0,49	0,22	0,45	0,19	0,41	0,61	0,27	0,21	0,97	0,27	0,41	0,97	0,16	0,39	0,27	1,29	0,73	0,30	0,41
	0.088–0.105	0,04	0,18	0,26	0,40	0,15	0,29	0,17	0,36	0,57	0,19	0,21	0,76	0,15	0,33	0,76	0,11	0,29	0,24	1,07	0,71	0,31	0,50
	0.074–0.088	0,04	0,13	0,19	0,36	0,12	0,25	0,17	0,23	0,49	0,16	0,14	0,52	0,08	0,17	0,57	0,14	0,26	0,24	0,87	0,51	0,24	0,43
	0.063–0.074	0,05	0,11	0,13	0,25	0,11	0,20	0,11	0,15	0,40	0,13	0,10	0,33	0,04	0,11	0,36	0,14	0,21	0,20	0,63	0,34	0,18	0,37
silt	0.031–0.063	0,23	0,50	0,35	0,78	0,41	0,46	0,56	0,49	0,96	0,62	0,43	0,57	0,09	0,51	0,90	0,64	0,83	0,59	1,42	0,89	0,73	0,87
	0.016–0.031	0,07	0,29	0,08	0,32	0,21	0,20	0,26	0,24	0,35	0,27	0,21	0,10	0,01	0,29	0,37	0,29	0,35	0,12	0,43	0,38	0,35	0,15
	0.008–0.016	0,01	0,11	0,02	0,08	0,05	0,05	0,07	0,06	0,09	0,07	0,06	0,02	0,00	0,08	0,10	0,08	0,09	0,02	0,11	0,08	0,08	0,02
	0.004–0.008	0,00	0,04	0,00	0,02	0,01	0,01	0,01	0,01	0,02	0,01	0,01	0,00	0,00	0,02	0,02	0,02	0,02	0,00	0,02	0,01	0,02	0,00
	0.002–0.004	0,00	0,00	0,00	0,00	0,00	0,00	0,00	0,00	0,00	0,00	0,00	0,00	0,00	0,00	0,00	0,00	0,00	0,00	0,00	0,00	0,00	0,00
clay	0.001–0.002	0,00	0,00	0,00	0,00	0,00	0,00	0,00	0,00	0,00	0,00	0,00	0,00	0,00	0,00	0,00	0,00	0,00	0,00	0,00	0,00	0,00	0,00
	<0.001	0,00	0,00	0,00	0,00	0,00	0,00	0,00	0,00	0,00	0,00	0,00	0,00	0,00	0,00	0,00	0,00	0,00	0,00	0,00	0,00	0,00	0,00
vcS	1.00–2.00	58,26	31,87	41,35	35,88	33,41	35,37	30,70	39,09	40,00	21,54	44,17	24,49	21,18	33,93	42,74	28,21	37,56	46,01	44,89	29,18	25,66	40,96
cS	0.50–1.00	41,03	63,86	52,14	56,07	61,11	57,96	63,50	53,71	51,67	71,15	51,19	59,14	66,13	57,33	40,20	68,37	54,93	50,01	43,23	57,66	68,16	52,16
mS	0.25–0.50	0,06	1,49	2,97	3,02	2,61	2,56	2,72	2,52	2,22	3,22	1,84	7,15	9,02	3,86	7,61	0,97	3,20	1,26	2,01	6,03	2,28	2,64
fS	0.125–0.25	0,18	1,20	2,18	2,34	1,57	2,20	1,56	2,71	2,64	2,36	1,44	5,94	3,02	2,96	5,40	0,87	1,86	1,02	4,02	3,48	1,69	1,48
vfS	0.063–0.125	0,16	0,64	0,93	1,51	0,61	1,19	0,63	1,15	2,07	0,75	0,65	2,59	0,54	1,02	2,66	0,55	1,15	0,95	3,87	2,29	1,03	1,71
silt	0.004–0.063	0,31	0,94	0,44	1,19	0,68	0,72	0,89	0,81	1,41	0,98	0,71	0,69	0,10	0,90	1,38	1,04	1,29	0,74	1,99	1,37	1,18	1,05
clay	<0.004	0,00	0,00	0,00	0,00	0,00	0,00	0,00	0,00	0,00	0,00	0,00	0,00	0,00	0,00	0,00	0,00	0,00	0,00	0,00	0,00	0,00	0,00
Mean		1,03	0,92	0,94	0,91	0,91	0,91	0,90	0,92	0,93	0,85	0,95	0,77	0,82	0,90	0,80	0,90	0,92	0,97	0,92	0,84	0,89	0,94
Mode		1,10	0,92	0,92	0,92	0,92	0,92	0,92	1,10	0,92	0,92	0,92	0,92	0,92	0,92	1,10	0,92	0,92	1,10	1,10	0,92	0,92	0,92
Sorting		1,22	1,24	1,36	1,44	1,30	1,38	1,29	1,43	1,51	1,36	1,28	1,68	1,41	1,44	1,78	1,24	1,41	1,28	1,67	1,58	1,35	1,40
Skewness		−0,08	−0,09	−0,29	−0,31	−0,18	−0,29	−0,31	−0,31	−0,37	−0,26	−0,17	−0,54	−0,38	−0,27	−0,59	−0,04	−0,29	−0,12	−0,49	−0,45	−0,17	−0,26
Kurtosis		0,96	1,18	1,81	2,06	1,35	1,78	1,44	1,94	2,55	1,89	1,25	2,24	1,80	1,98	2,19	1,06	1,89	1,05	2,78	2,43	1,79	1,74

Table 4
Number of cracks counted on the Q_{W0} and Q_{K0} grain surfaces and selected weathered grains ($Q_{K(100,WL)}$ and $Q_{W(50,WL)}$).

Number of grain	1	2	3	4	5	6	7	8	9	10	11	12	13	14	15	16	17	18	19	20	Average
Q_{K0}	13	10	10	0	13	5	4	5	7	2	2	3	10	5	4	0	11	5	1	2	6
Q_{W0}	13	36	27	9	5	45	29	33	8	24	8	6	5	13	19	17	7	0	29	6	17
$Q_{K(100,WL)}$	1	8	3	8	7	9	10	2	1	9	0	6	1	10	9	8	3	5	5	4	5
$Q_{W(50,WL)}$	7	11	2	18	6	5	5	3	9	2	3	0	0	9	4	4	1	5	6	3	5

Table 5
Results of the Kolmogorov-Smirnov test.

Q_W Samples	D	p-value	Q_K Samples	D	p-value
$Q_{W(50, dry)}$	0.2003	0.0361	$Q_{K(50, dry)}$	0.2638	0.0019
$Q_{W(100, dry)}$	0.1780	0.0841	$Q_{K(100, dry)}$	0.1691	0.1145
$Q_{W(300, dry)}$	0.2619	0.0021	$Q_{K(300, dry)}$	0.2238	0.0133
$Q_{W(50, MD)}$	0.3833	0.0000	$Q_{K(50, MD)}$	0.2485	0.0042
$Q_{W(100, MD)}$	0.1885	0.0574	$Q_{K(100, MD)}$	0.2288	0.0106
$Q_{(300, MD)}$	0.2423	0.0056	$Q_{K(300, MD)}$	0.2756	0.0010
$Q_{W(50, WD)}$	0.3223	0.0001	$Q_{K(50, WD)}$	0.1916	0.0508
$Q_{W(100, WD)}$	0.1476	0.2241	$Q_{K(100, WD)}$	0.1826	0.0712
$Q_{W(300, WD)}$	0.2679	0.0015	$Q_{K(300, WD)}$	0.3672	0.0000
$Q_{W(50, ML)}$	0.3138	0.0001	$Q_{K(50, ML)}$	0.1409	0.2747
$Q_{W(100, ML)}$	0.1434	0.2555	$Q_{K(100, ML)}$	0.3377	0.0000
$Q_{W(300, ML)}$	0.2866	0.0005	$Q_{K(300, ML)}$	0.3708	0.0000
$Q_{W(50, WL)}$	0.3918	0.0000	$Q_{K(50, WL)}$	0.2433	0.0054
$Q_{W(100, WL)}$	0.2021	0.0336	$Q_{K(100, WL)}$	0.1834	0.0691
$Q_{W(300, WL)}$	0.2862	0.0006	$Q_{K(300, WL)}$	0.3005	0.0002
$Q_{W(50, MH)}$	0.2907	0.0004	$Q_{K(50, MH)}$	0.2070	0.0276
$Q_{W(100, MH)}$	0.3880	0.0000	$Q_{K(100, MH)}$	0.1225	0.4463
$Q_{W(300, MH)}$	0.3240	0.0001	$Q_{K(300, MH)}$	0.1616	0.1466
$Q_{W(50, WH)}$	0.2621	0.0021	$Q_{K(50, WH)}$	0.2908	0.0004
$Q_{W(100, WH)}$	0.1687	0.1160	$Q_{K(100, WH)}$	0.3260	0.0000
$Q_{W(300, WH)}$	0.3273	0.0000	$Q_{K(300, WH)}$	0.1730	0.1005

Table 6
Explained variance in the Q_W samples.

PC	Eigenvalues λ	Variance in %	Cumulative variance in %
PC1	9.4572	41.1182	41.1182
PC2	5.4268	23.5948	64.7130
PC3	3.2032	13.9268	78.6398
PC4	1.8575	8.0759	86.7157
PC5	1.0297	4.4770	91.1927

Table 7
Factor loadings in the Q_W samples.

Variables	PC1	PC2	PC3	PC4	PC5
1.41–1.68	−0.479	0.358	0.086	−0.439	0.354
1.19–1.41	−0.562	0.678	−0.205	−0.226	0.219
1.0–1.19	−0.446	0.740	−0.181	−0.260	0.173
0.84–1.0	−0.539	0.028	0.004	−0.324	−0.713
0.71–0.84	0.375	−0.726	0.257	0.450	−0.065
0.59–0.71	0.300	−0.811	−0.032	0.423	0.161
0.50–0.59	0.744	−0.427	0.022	−0.180	0.320
0.42–0.50	0.629	−0.526	−0.328	0.006	0.069
0.35–0.42	0.562	−0.535	−0.272	−0.388	0.119
0.30–0.35	0.598	−0.403	−0.431	−0.409	0.053
0.25–0.30	0.754	−0.281	−0.223	−0.446	−0.153
0.21–0.25	0.893	−0.122	−0.164	−0.297	0.014
0.18–0.21	0.868	0.240	−0.151	−0.142	−0.166
0.15–0.18	0.890	0.307	−0.013	−0.108	−0.160
0.125–0.15	0.862	0.410	−0.043	−0.029	−0.175
0.105–0.125	0.851	0.486	0.150	0.060	−0.032
0.088–0.105	0.804	0.511	0.255	0.084	0.029
0.074–0.088	0.742	0.495	0.388	0.117	0.073
0.063–0.074	0.713	0.496	0.448	0.110	0.084
0.031–0.063	0.598	0.450	0.638	0.038	0.025
0.016–0.031	−0.189	−0.398	0.816	−0.232	−0.139
0.008–0.016	−0.222	−0.480	0.745	−0.381	−0.005
0.004–0.008	−0.204	−0.454	0.719	−0.391	0.150

Fig. 4. Four groups of samples (A-D) identified on the base of the Kolmogorov-Smirnov test.

Table 8
Explained variance in the Q_K samples.

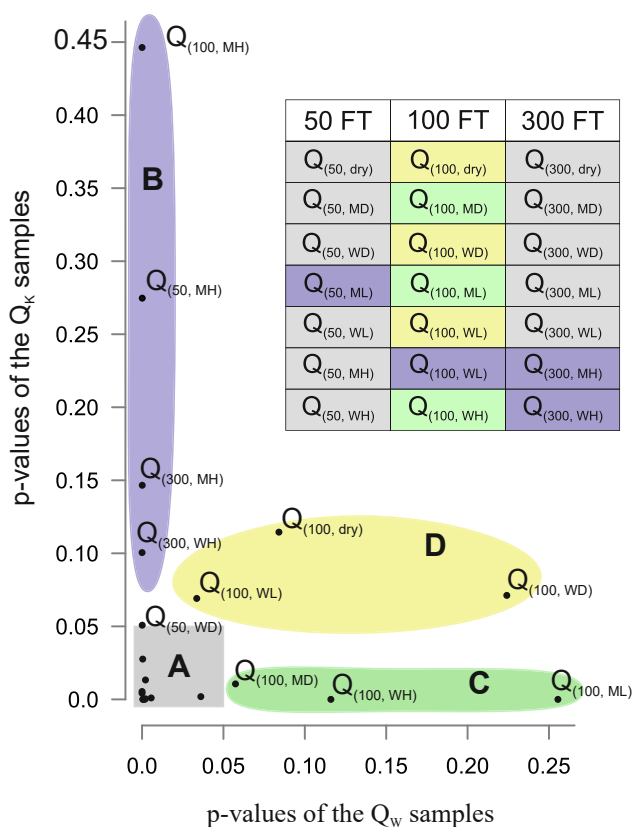| PC	Eigenvalues λ	Variance in %	Cumulative variance in %
PC1	9.6159	41.8083	41.8083
PC2	5.9934	26.0581	67.8664
PC3	3.6142	15.7139	83.5803
PC4	1.1424	4.9668	88.5470

consistent with the reference one. The fourth group includes: $Q_{W(50; MD)}$, $Q_{W(100; WL)}$ and $Q_{W(300; MH)}$. These clusters consist of the samples which grain-size distributions significantly differ from the Q_{W0} distribution. Samples grouped into the fourth cluster are characterized by kurtosis values that do not exceed 2.2, skewness coefficients raning close to −0.3, and standard deviation around 1.4. Sample $Q_{W(300; WH)}$ composes the fifth group (Fig. 5A). It shows a specific-grain size distribution (Figs. 4, A.1), characterized by the highest standard deviation (1.69) among all of the samples, the lowest skewness value (−0.39), and the highest kurtosis (2.98).

3.4.2. Cluster analysis for the Q_K samples
    The silhouette criterion (maximum average silhouette is 0.4092)

Table 9
Factor loadings in the Q_K samples.

Variables	PC1	PC2	PC3	PC4
1.41–1.68	−0.384	−0.546	0.508	−0.166
1.19–1.41	−0.121	−0.746	0.473	0.096
1.0–1.19	−0.342	−0.671	0.370	0.248
0.84–1.0	−0.386	0.542	−0.524	0.092
0.71–0.84	−0.150	0.672	−0.548	−0.299
0.59–0.71	0.150	0.796	−0.322	−0.347
0.50–0.59	0.636	0.452	0.040	−0.322
0.42–0.50	0.601	0.588	0.274	0.129
0.35–0.42	0.773	0.528	0.153	0.086
0.30–0.35	0.772	0.467	0.246	0.281
0.25–0.30	0.850	0.360	0.240	0.218
0.21–0.25	0.879	0.352	0.087	0.161
0.18–0.21	0.929	0.158	0.158	0.178
0.15–0.18	0.963	−0.079	0.105	0.031
0.125–0.15	0.922	−0.248	0.062	−0.056
0.105–0.125	0.901	−0.390	−0.017	−0.088
0.088–0.105	0.854	−0.468	−0.032	−0.150
0.074–0.088	0.780	−0.553	−0.080	−0.220
0.063–0.074	0.677	−0.620	−0.118	−0.290
0.031–0.063	0.507	−0.654	−0.430	−0.260
0.016–0.031	0.328	−0.443	−0.756	0.100
0.008–0.016	0.245	−0.373	−0.813	0.294
0.004–0.008	0.119	−0.301	−0.783	0.427

Table A1
Detailed chemistry characteristics of water used for sample preparation.

Distilled water
The sum of dissolved solids (mineralization): **0** mg/l
Low-mineralized water
The sum of dissolved solids (mineralization): **213.09** mg/l
  HCO_3^-: 121.06 mg/l
  F^-: 0.07 mg/l
  Mg^{2+}: 5.37 mg/l
  Ca^{2+}: 36.39 mg/l
  Na^{2+}: 8.29 mg/l
High-mineralized water
The sum of dissolved solids (mineralization): **1954.36** mg/l
  HCO_3^-: 1489.00 mg/l
  SO_4^{2-}: 21.80 mg/l
  Cl^-: 12.90 mg/l
  F^-: 0.16 mg/l
  Mg^{2+}: 128.30 mg/l
  Ca^{2+}: 208.00 mg/l
  Na^{2+}: 87.80 mg/l
  K^+: 6.40 mg/l

showed that the most optimal number of clusters for the Q_K samples is two (k = 2). The first one consists of all of the Q_K samples except $Q_K(_{50; WH})$, $Q_K(_{100; ML})$, $Q_K(_{100; WL})$ and $Q_K(_{300; MH})$ which belong to the second group (Fig. 5B).

This division seems not to be as clear consequence of the results from the Kolmogorow-Smirnow test as it can be observed for the Q_W samples. The second cluster consists of samples with extreme values of the moments of distribution (Fig. 5) as compared to the samples from the first group. All samples are characterized by the standard deviation ranging over 1.58, the skewness reaching −0.49, and the kurtosis of >2.19.

4. Discussion

The obtained results of laboratory and statistical analyses are the basis for drawing conclusions on how the number of FT cycles, water content, water mineralization and internal structure of quartz grains affect the micro-scale frost weathering process.

4.1. Impact of internal features of quartz grains on the course of a micro-scale frost weathering

Quartz grains that have been used in the conducted experimental study (angular with fresh surface) may reflect the grains originating from glacial regions where besides the glacial processes that affect the grains (crushing in subglacial environment under high pressures; e.g. Evans et al., 2006) the frost weathering acts as a postdepositional process and contributes to their destruction. Any modification of the grain-size composition bring about changes in the susceptibility of soil to the frost action through the changes in suction properties (e.g. Konrad, 2005; Bronfenbrener, 2009; Bronfenbrener and Bronfenbrener, 2010; She et al., 2019). Reference samples (Q_{W0}, Q_{K0}; Fig. 2B, C) are considered as non-frost susceptible due to the small content (<3%) of the very fine-grained sand and silt-sized fractions (Beskow, 1935).

The obtained results show that Q_W and Q_K react differently (Figs. 3–5, A.1, A.2; Table 3) to the ongoing freeze–thaw cycles regardless of the weathering conditions (Table A.1). It is confirmed by both the grain-size distributions and the results of statistical analyses (Table 3), including the Kolmogorov-Smirnov test (Fig. 4), PCA (Tables 6–9) and cluster analysis (Fig. 5). These results indicate that Q_K is more susceptible to the frost weathering than Q_W even though the former has been subjected to lower-energy stress regime during the preparation stage of the experiment (see Section 2.2.). It is manifested in the greater amount of the frost debris produced in a wider grain-size range. Higher production of the medium- and fine-grained sand grains (0.125–0.5 mm), and subordinately of the very fine-grained sand and silt-sized fractions (0.004–0.125 mm) are observed. This correspond to grain-size fractions which variation is explained by the PC1 and PC3 (Table 9). Whereas the Q_W samples are characterized mainly by the production of the very coarse- and coarse-grained sand fractions (0.5–1.68 mm) mainly explained by the PC2 (Table 7). It seems that such an individual grain reaction stems from the original structure of the vein quartzes. Wiman (1963) emphasized the great importance of the grain cementation as well as the degree and type of strength of their internal textures on the course and intensity of the frost weathering. Hence, any zone of weakness plays a crucial role in the frost-induced destruction. The individual crystals in the Q_W are abundant but small, usually below 10 μm, rarely reaching around 500 μm and do not form distinct seam zones (Fig. 1A). The space between the crystals is usually completely filled with recrystallized silica, exhibiting a close contact between grains (Fig. 1C). The Q_K is formed by large euhedral crystals connected by distinct zones filled with recrystallized silica (overgrowths) containing crystals of a size ranging from <10 μm to 50 μm (Fig. 1B). These recrystallized seams form an open contact between individual quartz crystals or between crystal and overgrowth (Fig. 1D).

Wright (2000) studied the influence of the frost action on quartz sandstone with grains interlocked with quartz (overgrowths) and concluded that the presence of the overgrowths is of a crucial importance in the weathering process. She suggested that the overgrowth fracture results from the stress concentration at their outer surface and may lead to their detachment or collapse through the water penetration between the overgrowth and host grain. Although here samples subjected to the frost weathering are a loose, grainy sediment, the internal structure of an individual grain formed by the crystal assemblages is noticeable. In this case stress transmission also takes place, but it occurs between adjacent crystals within a single grain.

Both Q_W and Q_K grains are characterized by a large number of inclusions of various sizes and shapes. Most of the inclusions entrapped in the Q_K crystals are fluid inclusions filled with the remnants of the crystallization solutions (Zieliński, 1997), which increase their volumes upon freezing and therefore facilitate the grain cracking. Fresh quartz grains are considered more prone to the frost weathering as compared with, e.g. unweathered feldspar, because of the presence of various inclusions in the individual crystals (Konishchev and Rogov, 1993; Konishchev, 1997, 2003; Konishchev et al., 2005; Schwamborn et al.,
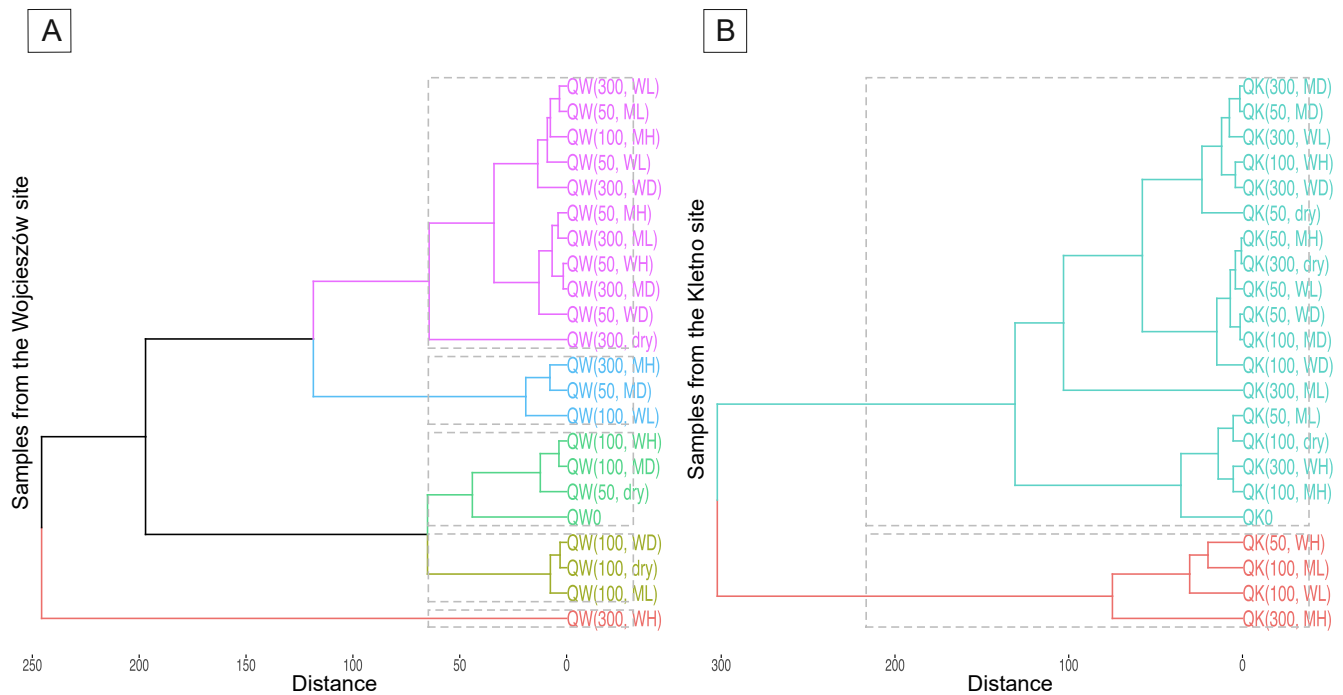
Fig. 5. Cluster dendrograms. A – Q_W samples; B – Q_K samples.

2012). It is reflected in the high values of the Cryogenic Weathering Index (CWI) estimated for the sediments that undergone a long-term frost action (Konishchev, 1997; Konishchev et al., 2005; Schwamborn et al., 2012).

4.1.1. Role of preparation/inherited defects in quartz grains destruction

The susceptibility of the studied grains to the frost weathering is also affected by the sample preparation process itself. It causes the grain surface to be artificially disturbed with numerous cracks not related to the crystallographic lattice or the weakness zones of the contact between individual crystals. This feature of surface of grains originated from the natural environment and subjected to the FT cycles has been already mentioned by Lautridou and Ozouf (1982). However, they did not study the influence of this surficial disturbance on the course of frost weathering. In the case of quartz grains originating from any natural environment, these correspond to microtextures/cracks inherited from former sedimentary environments and the dominant processes that modified the grain surface.

An investigation under a SEM has revealed the presence of fresh cracks on the analyzed surface of quartz grains. A greater number of cracks has been noted on the Q_{W0} reference sample than Q_{K0} (Table 4). We suggest therefore that these distributions should be considered as *preparation defects*. Regarding the natural quartz grains, these should be considered as *inherited defects* that have been formed before the frost-related activity as a result of non-cryogenic processes, e.g. crushing in a glacial environment, subglacial transport processes, slope processes or high-energy grain-to-grain collisions in aeolian and fluvial environment (e.g. Margolis and Kennett, 1971; Manickam and Barbaroux, 1987; Pye and Tsoar, 1990; Hiemstra and Van Der Meer, 1997; Mahaney, 1990; Altuhafi and Baudet, 2011; Altuhafi et al., 2016; Woronko, 2016). Therefore, it is assumed that the grains that have been exposed to the erosion processes under the natural conditions are similarly prepared to the frost-driven weathering as studied mechanically-crushed grains. *Preparation/inherited defects* are the first to be predisposed to the frost action as they are formed on the grain surface and penetrate the grain to the various depths (Fig. 6A, B). The elimination of the these defects may result in a production of grains of a varied size – from silt- to sand-sized ones. The former are probably associated with the Moss defect (Moss,

1966; Moss and Green, 1975) in the crystallographic lattice of the quartz crystals (Jefferson et al., 1997). It is reflected in the grain-size variance explained by the PC3 for both of the studied quartz (Tables 7 and 9) The latter are evidenced by the size of the conchoidal fractures on the Q_W and Q_K grain fractures and explained by the PC1 (Tables 7 and 9). In our study, frost-induced destruction of the *preparation defects* results probably in a reduction in the amount of the very coarse-grained sand fractions (1–2 mm) after first 50 FT cycles. It is higher in almost all of the Q_W samples than in the Q_K samples. It follows that Q_W bears more *preparation defects* which correspond to the greater number of surficial cracks (Table 4) resulting from the crushing in a high-energy disc mill. Their elimination is evidenced by the decrease in the number of surficial cracks observed on the grains suffered from 50, 100 and 300 FT cycles (Table 4). With regard to the natural conditions, it seems that, as in the case of the experiment, any cracks on the grain surfaces can be considered as areas particularly susceptible to the frost action. We consider them as a germ of the frost-induced destruction process.

4.1.2. Role of primary defects in quartz grains destruction

Besides the *preparation/inherited defects* that affect the frost-driven weathering, we suggest that all of the weakness zones associated with defects in the quartz lattice, including interlocking overgrowths and inclusions, should be considered as *primary defects* (Fig. 6C-F). These are not originated from the former sedimentary-history of grains and thus they may refer to any quartz grain, regardless of its origin (aeolian, fluvial etc.) but are related to crystallographic structure of quartz grains. In our study, their influence is particularly evidenced in the samples after 100 FT cycles. An increase in the amount of the very coarse sand fraction (1–2 mm) is observed in almost all of the Q_W and some of the Q_K samples as compared to the corresponding samples after 50 FT cycles (Figs. 3, A.1, A.2; Table 3). It is logical and widely accepted that the proportion of the coarsest-grained fractions should decrease with the increasing number of FT cycles (Wright, 2000). Therefore the obtained results have put us in a confusion. An increase in the amount of the very coarse-grained sand (1–2 mm) may be explained by the fact that their destruction has followed the surface of quartz crystals joining or occurred along the silica recrystallization zones (interlocking overgrowths). As a result, the destruction of a single elongated grain results
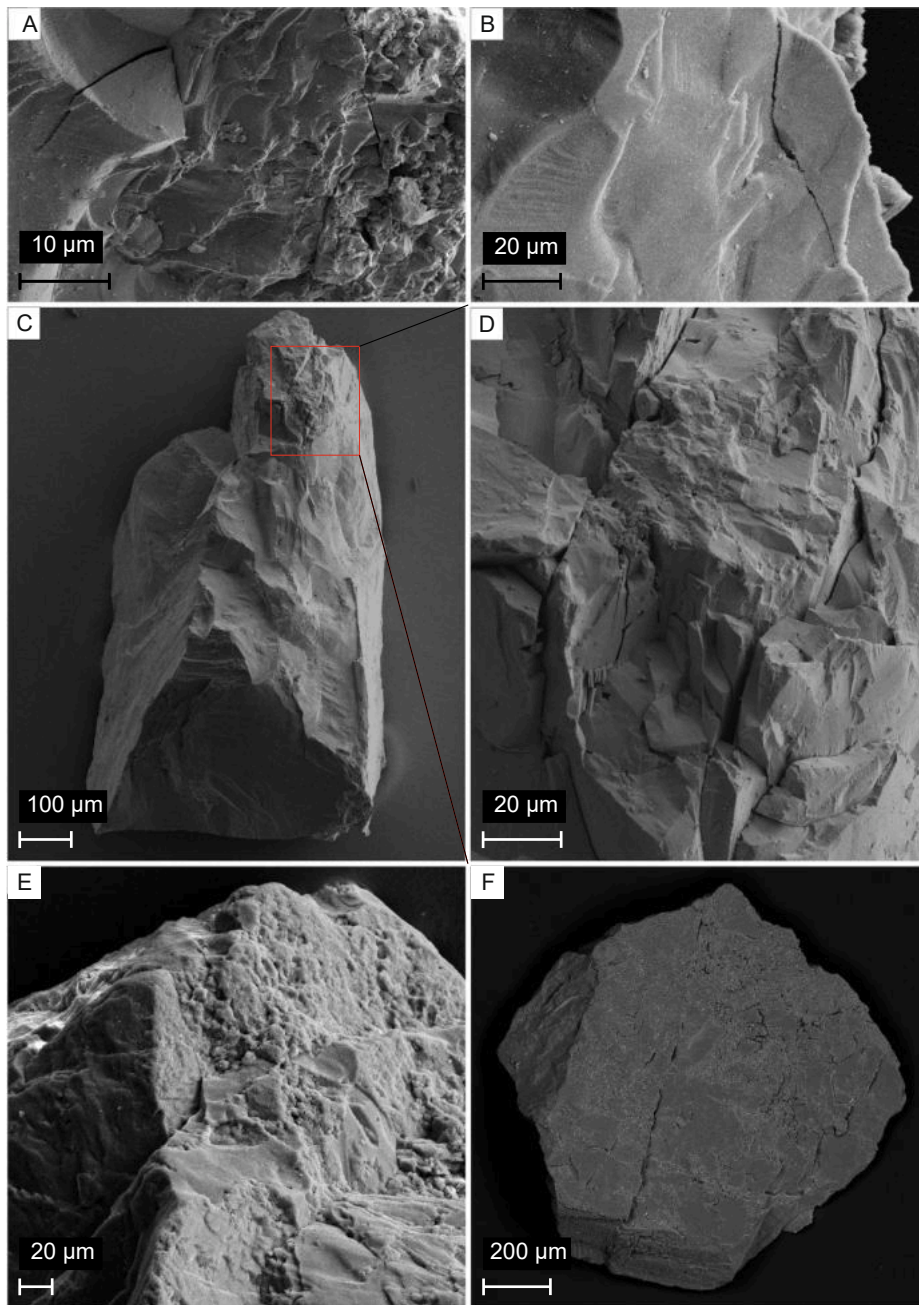
Fig. 6. Defects of the quartz grains. A – Preparation defect on the surface of the Q_{W0} grain; B – Preparation defect on the surface of the Q_{K0} grain; C – Primary defect on the edge of the Q_{W0} grain; D – Primary defects on the Q_{W0} grain, where the longitudinal-prevailed separation surfaces are noticeable; E – Primary defects on the Q_{K0} grain where the weakness zones associated with the crystal growths are visible; F – Primary defect on the Q_{K0} grain that crosses the entire grain and increases grain susceptibility to break down into two individual grains of a relatively large surface area.

in the formation of two elongated grains whose surfaces are comparative to the surface of the source one (see Section 2.4.) and therefore an increase in the amount of the very coarse-grained sand fraction (1–2 mm) is observed in both Q_K and Q_W samples (Figs. 3, A.1, A.2; Table 3). So far, all the attention has been paid to the silt fraction as a major product of the frost weathering (Lautridou and Ozouf, 1982; Hall, 1990; Wright et al., 1998; Wright, 2000; Konishchev and Rogov, 2017) and the changes within the coarse-grained sand fractions have been neglected. By contrast, in the conducted experimental study, we see that changes in the grain-size distributions are attributed mainly to the coarse-sized grain fractions. This fact strongly influences the percentage contribution of the remaining fractions in the individual sample, especially of the silt fraction which amount rarely exceeds 1% of the whole mass. As a result, only its slight increase (e.g. $Q_{W(100;\ dry)}$; $Q_{W(100;\ ML)}$; $Q_{K(100;WD)}$; $Q_{K(100;\ WL)}$) or most often a decrease is noted (e.g. $Q_{W(100;\ ML)}$; $Q_{W(100;\ WL)}$; $Q_{K(100;\ dry)}$; $Q_{K(100;MH)}$; Figs. A.1, A.2; Table 3). From the grain-size

distribution results, it was found that the weathering of the Q_K samples results in a higher production of the silt-sized fractions (0.002–0.063 mm) which indicates its greater susceptibility to the frost-driven destruction. The general content of the silt-sized fraction seems to be slightly higher than the one reported after 360 FT cycles by Wright et al. (1998) and Wright (2000). However, this difference may result from the various types of studied sediment (rock vs grains), internal (crystallographic) structure of quartz grains and/or the sample preparation process.

4.2. Impact of repeating freeze–thaw cycles on the destruction of quartz grains

An experimental design set up on 50, 100, and 300 FT cycles provides information on the course and intensity of the frost weathering of quartz grains, and their changes. The results of the Kolmogorov-Smirnov

test (Fig. 4; Table 5) clearly indicate that almost all of the Q_W and Q_K samples suffered from 50 and 300 FT cycles differ significantly from their reference sample (Q_{W0}, Q_{K0}). As it has been mentioned above, samples after 100 FT cycles deviate from the adopted concepts on frost-induced grain-size changes and their distributions do not always differ from the reference samples (Fig. 4; Table 5). The obtained data show a general decrease in the content of the very coarse-grained sand fraction (1–2 mm) in favour of an increase of coarse-grained sand fraction (0.5–1 mm). This is confirmed by the results of the PCA analysis, where PC1 explains 41% of the total variance and corresponds to the grain-size range of 0.031–0.59 mm in the Q_K samples and 0.063–0.59 mm in the Q_W samples (Tables 6–9). The values refer to the enhanced grain production in these size ranges due to the frost-induced destruction. PC2 correlates to the very coarse- and coarse sand fractions, i.e. 0.59–1.68 mm for the Q_K samples and 1.0–1.68 mm for the Q_W samples, and reflects the process of their destruction along with the production of the finer-sized grains in these size ranges. It clearly indicates that the frost weathering process is the most destructive for the coarsest-sized grain fractions (here i.e. 1–2 mm). We found that the most of the *preparation defects* are eliminated at the initial stage of the frost weathering (here up to 50 FT cycles). This is generally confirmed by a decrease of the amount of the coarse-grained sand fraction (0.5–1.0 mm) and number of cracks after 100 FT cycles (Figs. 3, A.1, A.2; Tables 3 and 4). Further, we attribute the increase of the very coarse-grained sand fractions (1–2 mm) recorded after 100 FT cycles to a successive elimination of the *primary defects* due to the ongoing weathering (see Section 4.1, Wiman, 1963).

The reappearing decrease of the content of very coarse-grained sand (1–2 mm) and a slight increase in the coarse-grained sand fraction (0.5–1 mm) are observed in most of the Q_K and Q_W samples after 300 FT cycles. On this basis, we assume that the intensity of the frost weathering is relatively high during its initial phase (here during the first 100 FT cycles) and is expressed by the production of the very coarse- (1–2 mm) and coarse-grained (0.5–1 mm) sand fractions. Then, after 100 FT cycles, the efficiency clearly decreases in these size ranges for most of the samples. This is evidenced by the differences in the percentage content of the 1–2 mm fraction achieved in the first 50 FT cycles (0 vs 50 FT cycles) which are greater than the differences in the following 200 FT cycles (100 vs 300 FT cycles). The only exceptions are $Q_{W(300;\ MH)}$ and $Q_{K(300;\ WH)}$, where the successive increase of these fractions (1–2 mm) is observed not after 100 FT cycles, but after 300 FT cycles (Figs. A.1, A.2; Table 3). This leads to the assumption that under certain conditions the initially high intensity of the frost weathering may continue over a longer period of time. We attribute it to the numerous *preparation defects*, the elimination of which has taken longer, and therefore the onset of the *primary defects* elimination has been delayed. It is difficult to estimate this number of FT cycles after which the intensity of the frost weathering begins to decline (Fig. 7). We relate it to the moment when the *host grain* (i.e. grain without any *preparation defect* and the most sensitive *primary defects*) becomes exposed due to the frost action. This is equivalent to the refreshing of the grain surface. At this point, the frost weathering of quartz grains requires more FT cycles or more favourable conditions to disturb fresh surface of grain and achieve the intensity that has been obtained during the initial stages of the process. We refer it as a *lag time*, i.e. the time or number of FT cycles that are required to re-intensify the frost weathering. It seems possible that the changes of the frost weathering intensity will exhibit the sinusoidal-like pattern. Moreover, we suggest that such a *lag time* may be also observed on the initial stage of weathering (0–50 FT), i.e. before the elimination of *preparation defects* (Fig. 7). But more research is needed to test this hypothesis.

The content of the very coarse- and coarse-grained silt fractions (0.016–0.063 mm) tends to increase slightly after 300 FT cycles as compared to the samples after 50 and 100 FT cycles (Figs. 3, A.1, A.2;
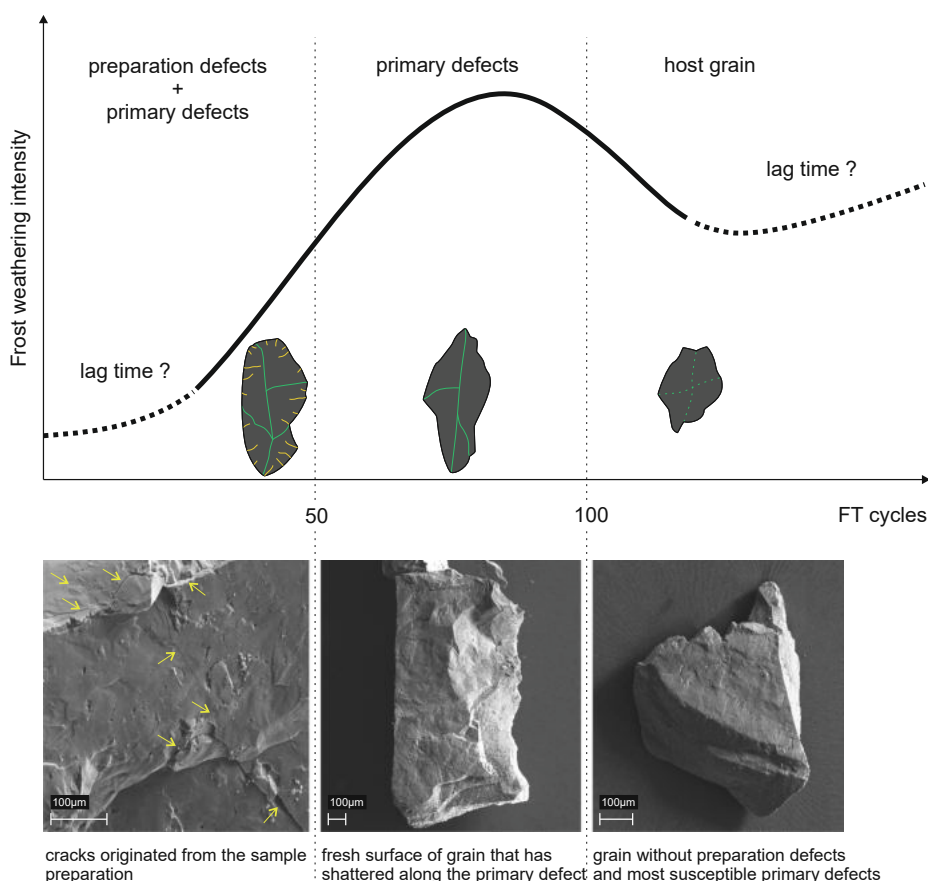

cracks originated from the sample preparation | fresh surface of grain that has shattered along the primary defect | grain without preparation defects and most susceptible primary defects

Fig. 7. Hypothetical dependences of the frost weathering intensity on the number of proceeding freeze–thaw cycles.
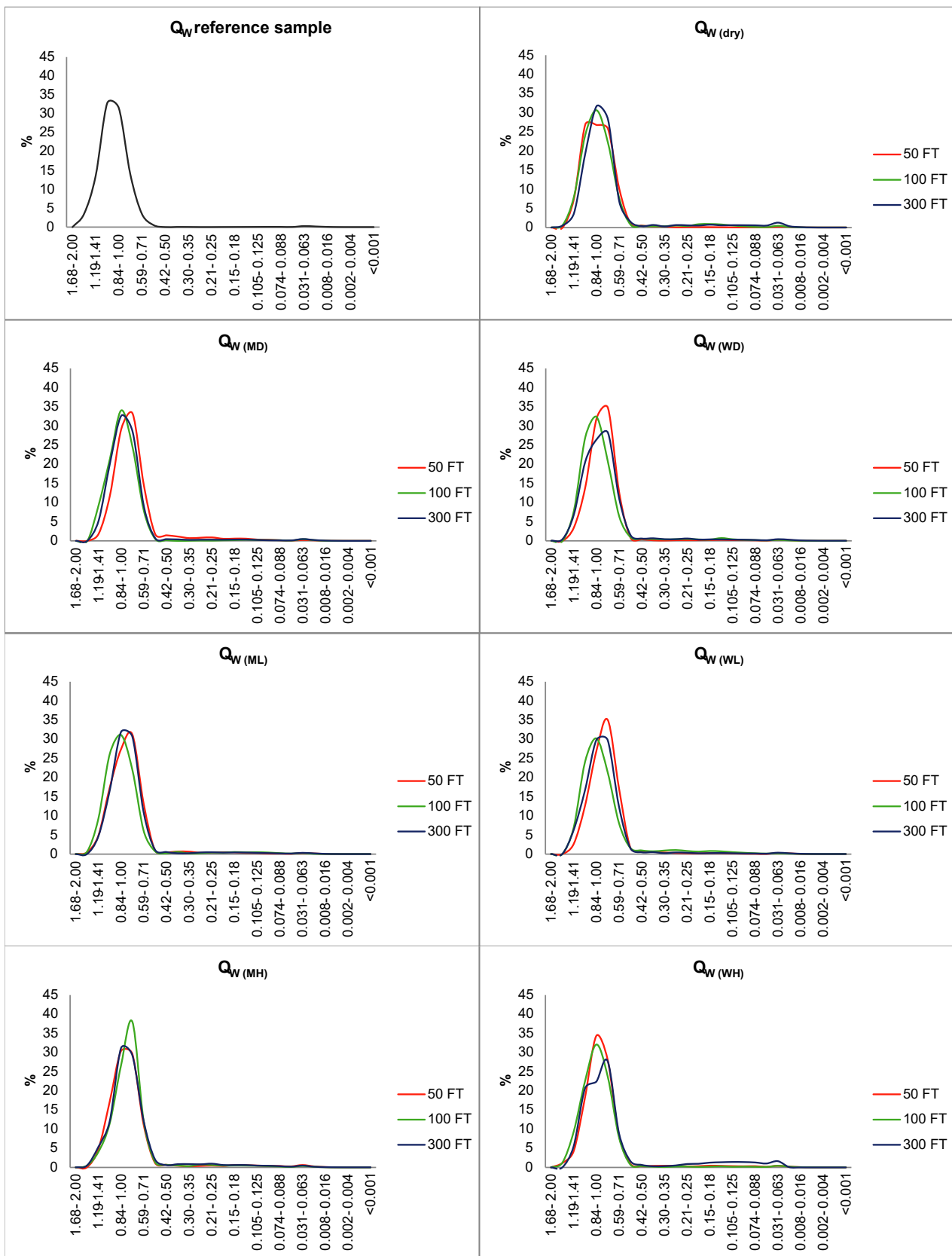
Fig. A1. Changes in the grain-size distributions in Q_W samples after the increasing number of freeze–thaw cycles.
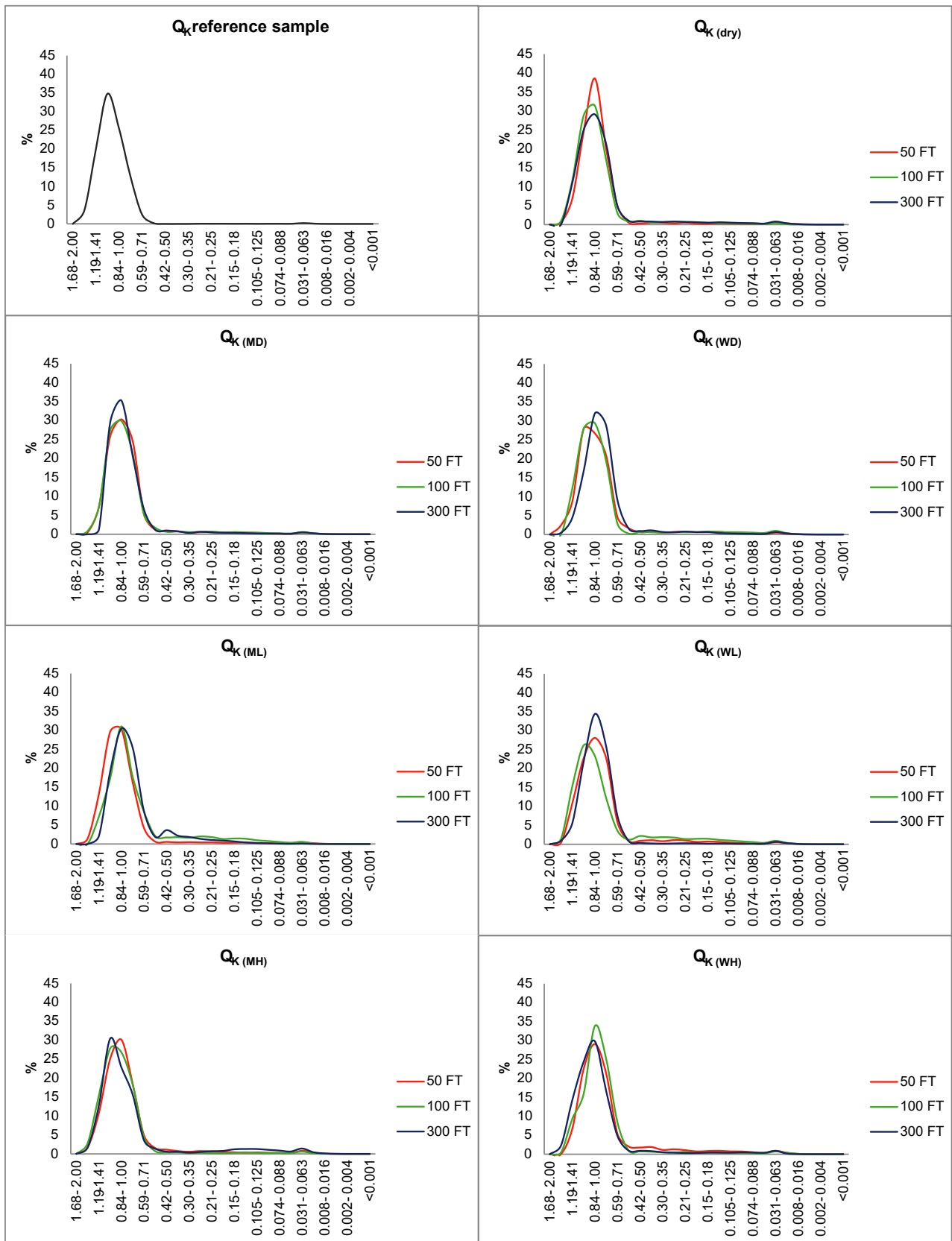
Fig. A2. Changes in the grain-size distributions in Q_K samples after the increasing number of freeze–thaw cycles.

Table 3). It is correlated with the PC3 that explains the variance within the silt-sized fractions, i.e. 0.004–0.031 mm in the Q_K samples, and 0.004–0.063 mm in the Q_W samples. This evidences the activation or intensification of the silt production due to the ongoing frost weathering. Due to the fact that the products of the frost action at this stage of weathering (after 300 FT cycles) consist of the very fine sand fractions (0.063–0.125 mm), their formation should be associated with the operation of a process other than the one that dominates after 50 and 100 FT cycles. According to Wiman (1963), this process is equated with the micro-scale frost weathering which does not depend on the structure or texture of the grain, i.e. destruction of the grains does not occur along the weakness zones but along the invisible cracks or fissures. The potential factor that contributes to the production of these fine-sized fractions seems to be the process responsible for the formation of the breakage blocks microtextures. These microtextures are formed due to the overlapping of the numerous conchoidal fractures of small (even < 10 µm) size (Woronko, 2012, 2016; Woronko and Hoch, 2011; Woronko and Pisarska-Jamroży, 2016). Micro-scale frost weathering contribute also to the production of larger-sized (40–60 µm) particles resulting from the detachment of the conchoidal fractures that have been located on the grain edges (Woronko, 2016; Woronko and Pisarska-Jamroży, 2016). The role of overgrowths should also be taken into account while considering the production of frost debris (Wright, 2000; Woronko and Hoch, 2011), especially these ones that form open contacts between the individual quartz crystals. Frost action is responsible for the detachment of the individual euhedral quartz crystals of various sizes, but mainly of the silt-sized fraction, which results in the formation of a characteristic microtexture on the quartz grain surface – *sponge structure*. In the case of the samples that contain high-mineralized water, the production of the silt-sized fraction is reinforced by the detachment of the mineral precipitations that have been formed as a result of the freezing and evaporating processes (cf. Dietzel, 2005).

The results of the PCA analysis indicate that the frost weathering process differentiates the Q_K and Q_W samples to a varying degree (Tables 6–9). The more complex interactions between the quartz grains and the frost activity are assigned to the Q_W samples (PC1-PC5) than Q_K samples (PC1-PC4). We assume that the PC4 (0.59–0.84 mm; 8.08%) and PC5 (0.84–1 mm; 4.48%), extracted from the Q_W samples, represent these grain-size fractions that have not undergone the frost-driven destruction yet. It indicates that the degree to which the frost action affects the quartz grains largely depends on an internal characteristic of the grains. Moreover, it is confirmed by the results of Kolmogorov-Smirnov test (Fig. 4) and cluster analysis (Fig. 5) which show lack of the relationship between the course of the frost weathering and changes in the grain-size distributions of samples subjected to 50, 100 and 300 FT cycles.

The results of conducted experiment may provide particular implication for studies of global warming along with periglacial environment changes, thickening of active layer of permafrost and related environmental-risk management. These clearly show that the effects of micro-scale frost weathering within a recently thawed active layer may be noticeable only after a longer period of the frost activity. Therefore, any visible frost-induced modifications of grain surface (i.e. frost-originated microtextures) should be considered relict or inherited from previous cryogenic processes. This also applies directly to any analysis of the effects of frost action withing the former permafrost layers as its thickness and lateral extent could change with the evolution of the periglacial environment.

4.3. Impact of water content on the frost weathering intensity of quartz grains

One of the key factors that determine the course and intensity of the frost weathering is the availability of water (Hall, 1991; Hallet et al., 1991; Matsuoka, 1991; Konishchev et al., 2005; Woronko and Hoch, 2011; French, 2017). However, none of the experiments to date has examined the impact of changing water content on the weathering process (e.g. Lautridou and Ozouf, 1982; Wright et al., 1998). The obtained results show that, regardless the water conditions (dry, moistened, wet samples; Table A.1), the destruction of the coarsest-sized grain fractions and the production of the silt-sized grain fractions are observed (Figs. 3, A.1, A.2; Table 3). Contrary to the expectation, it turns out that the frost weathering affecting both of the Q_W and Q_K dry samples is not inferior in terms of the silt-sized grain fraction (0.004–0.063 mm) production to the remaining moistened or wet samples (Figs. 5, A.1, A.2; Table 3). Although Wiman (1963) stated that the frost-driven production of grains does not occur in the water-free conditions.

The results of the Q_W and Q_K grain-size distribution after 50, 100, and 300 FT cycles do not show any clear relationships between the intensity of the frost weathering and the content of water (Fig. 5). However, some slight differences in the susceptibility of the Q_W and Q_K samples to the weathering under the same moisture and geochemical conditions are observed. A much higher production of the medium- and fine-grained sand fraction (0.125–0.5 mm) and slightly higher production of the very fine-grained sand and silt-sized fractions (0.004–0.125 mm) are observed in all of the Q_K samples as compared to the Q_W samples.

As the influence of water content and mineralization on the frost action is variable and it is difficult to draw general conclusions on its role, other factors affecting the weathering intensity should be considered. The lack of unambiguous relationships may indicate that at this stage of the frost weathering, the following factors are more important or as important as the content and mineralization of water: (1) the crystallographic structure of the quartz grains, (2) number of FT cycles, which in this case remains too low to cause the sample differentiation, (3) exposure of the quartz grains to the frost activity. It seems that the last factor remains particularly interesting. Dry and moistened samples are directly exposed to the frost action, while water in the wet samples may act as a protection buffer when the air temperature descends. This is related to the heat capacity of water, which determines the amount of heat needed to change the temperature of physical body by 1 °C. The higher value of heat capacity of water as compared to silica (Schärli and Rybach, 2001; Kluitenberg, 2002; Waples and Waples, 2004) leads to the delayed onset of the micro-scale frost weathering process in the wet samples. However, it seems possible that once it starts, its intensity may remain constantly high.

The frost weathering of dry and moistened samples may be much more rapid due to the grain exposure as the grain surface is directly affected by the negative temperatures. These conditions promote the thermal stress action. This phenomenon occurs when the rate of temperature changes is sufficient to cause a rock failure (Yatsu, 1988; Hall and Hall, 1991; Sumner et al., 2004). Hall (1999) associates the presence of the frost weathered sediments in cold and dry regions with the temperature changes exceeding 2 °C/min. The effects of the frost weathering under such conditions may initially be negligible, but once the effects become more substantial, further destruction of the sediments may be violent (Hall, 1999). Here, the comparable process may occur in dry and moistened samples. In the samples with the quartz grains situated on the filter paper moistened with water, the water film may appear on the filter-grain contact due to the water slippage effect. This provides moisture necessary for the frost weathering process. Moreover, any moisture present in the freeze–thaw device can be absorbed on the grain surfaces. This small amount of moisture combined with the specific grain features (see Section 4.1) can effectively contribute to the destruction of quartz grains when the temperature drops below 0 °C. It may explain the high efficiency of the frost weathering of dry and moistened samples reported in both of the Q_K and Q_W grain-size distributions.

The key role in the course of the frost weathering of wet samples is the presence of an unfrozen water film (of less than tens of nm thick) around mineral grains (Walder and Hallet, 1986; Konishchev and Rogov, 1993; Woronko and Hoch, 2011). It arises due to the reduction of

the free energy of water at the grain surface (Gilpin, 1979; Walder and Hallet, 1986). Unfrozen water film exerts an attractive force on the water in pores and disjoining pressure that separate the ice mass from the grain surface (Derjaguin and Churaev, 1978; Miller, 1978; Gilpin, 1979; Walder and Hallet, 1986).

The lack of a strict relationships between the intensity of the frost weathering and the content and mineralization of water raises a question whether there is an optimal amount of moisture at which the frost-induced destruction is most effective. Further experiments are therefore necessary to make any estimations. The obtained results show that the micro-scale frost weathering process is very complex and still poorly understood.

5. Conclusions

A laboratory experiment of a micro-scale frost weathering of the sand-sized vein-quartz grains contributes to the reconstruction of its course and determination of its intensity. The analyses of the grain-size distributions of samples suffered from 50, 100, and 300 FT cycles have led to the following conclusions:

1. The frost weathering intensity should be associated with a wider range of the grain-size fractions than it has been assumed so far.
2. The internal (crystallographic) structure of quartz grains has a great influence on the course and manner of the frost weathering process.
3. During the first stage, up to 50 FT cycles, the frost-induced destruction proceeds mainly by the elimination of the cracks and fissures created during the crushing of the samples, i.e. *preparation/inherited defects*. It results in the destruction of the very coarse-grained (1–2 mm) sand fractions and production of the coarse-(0.5–1 mm) and medium-grained (0.25–0.5 mm) sand fraction.
4. During the interval from 50 to 100 FT cycles, the weathering proceeds mainly by the elimination of the weakness zones in the crystal lattice of the quartz grains, i.e. *primary defects*. It results in the production of the very coarse-grained sand fractions (1–2 mm).
5. At a more advanced stage of the frost weathering, during the interval from 100 to 300 FT cycles, most of the *preparation/inherited defects* and *primary defects* have been already used, exposing the intact host grain. At this point, the frost weathering requires more FT cycles or to disturb fresh surface of grain. This number of FT cycles is referred as a lag time.
6. The production of the silt-sized fraction during 300 FT cycles is relatively small and does not affect the grain-size distributions. A much larger number of FT cycles is presumably required for this production to be quantitatively significant. Therefore, the most important factor determining the effects of micro-scale frost weathering is time.
7. The most effective frost weathering, expressed as grain-size changes, occurs during the first 100 FT cycles, afterwards its intensity decreases.
8. No clear influence of the moisture conditions (content and mineralization of water) on the frost weathering has been found after 300 FT cycles.
9. The presented results may be of particular interest for interpretation of paleocryoenvironment and present permafrost-related sediments.

Declaration of Competing Interest

The authors declare that they have no known competing financial interests or personal relationships that could have appeared to influence the work reported in this paper.

References

Abdideh, M., Ameri, A., 2020. Cluster Analysis of Petrophysical and Geological Parameters for Separating the Electrofacies of a Gas Carbonate Reservoir Sequence. Nat. Resour. Res. 29, 1843–1856. https://doi.org/10.1007/s11053-019-09533-1.

Aldenderfer, M., Blashfield, R., 1984. Cluster Analysis. Quantitative Applications in the Social Sciences, SAGE Publications, Inc., Thousand Oaks, California. https://doi.org/10.4135/9781412983648.

Altuhafi, F., Baudet, B.A., 2011. A hypothesis on the relative roles of crushing and abrasion in the mechanical genesis of a glacial sediment. Eng. Geol. 120, 1–9. https://doi.org/10.1016/j.enggeo.2011.03.002.

Altuhafi, F.N., Coop, M.R., Georgiannou, V.N., 2016. Effect of Particle Shape on the Mechanical Behavior of Natural Sands. J. Geotech. Geoenviron. 142, 04016071. https://doi.org/10.1061/(ASCE)GT.1943-5606.0001569.

Anderson, T.W., 1984. An Introduction to Multivariate Statistical Analysis. John Wiley & Sons, New York.

Ballantyne, C.K., 2018. Periglacial Geomorphology. Wiley-Blackwell 11–22.

Banas, M., 1965. Przejawy mineralizacji w metamorfiku Snieznika Kłodzkiego [Mineralization in the Snieznik Kłodzki Metamorphic Complex]. volume 27 of Prace Geologiczne Komisji Nauk Geologicznych PAN. Wydawnictwa Geologiczne, Warszawa. In Polish.

Beskow, G., 1935. Soil freezing and frost heaving: With special application to roads and railroads, (translated by Osterberg, J.O., 1947. Northwestern University). Swedish Geological Society, vol. 375, pp. 145.

Blott, S.J., Pye, K., 2001. Gradistat: A grain size distribution and statistics package for the analysis of unconsolidated sediments. Earth Surf. Proc. Land. 26, 1237–1248. https://doi.org/10.1002/esp.261.

Bronfenbrener, L., 2009. The modelling of the freezing process in fine-grained porous media: application to the frost heave estimation. Cold Reg. Sci. Technol. 56, 120–134. https://doi.org/10.1016/j.coldregions.2008.11.004.

Bronfenbrener, L., Bronfenbrener, R., 2010. Modeling frost heave in freezing soils. Cold Reg. Sci. Technol. 61, 43–64. https://doi.org/10.1016/j.coldregions.2009.12.007.

Chamberlain, E.J., Gow, A.J., 1979. Effect of freezing and thawing on the permeability and structure of soils. Eng. Geol. 13, 73–92. https://doi.org/10.1016/0013-7952(79)90022-X.

Cwojdzinski, S., Kozdrój, W., 2011. Objasnienia do szczegółowej mapy geologicznej Polski [Explanations for the Detailed Geological Map of Poland]. PIG-PIB. In Polish.

Demitroff, M., Rogov, V.V., French, H.M., Konishchev, V.N., Streletskiy, D.A., Lebedeva-Verba, M. D.and Alekseeva, V.A., 2007. Possible evidence for episodes of Late Pleistocene cryogenic weatheing, southern New Jersey, Eastern USA, in: Proceedings: Cryogenic Resources of Polar Regions, RAS, SB, Salekhard. pp. 139–141.

Derjaguin, B.V., Churaev, N.V., 1978. On the question of determining the concept of disjoining pressure and its role in the equilibrium and flow of thin films. J. Colloid Interf. Sci. 66, 389–398. https://doi.org/10.1016/0021-9797(78)90056-5.

Dietzel, M., 2005. Impact of cyclic freezing on precipitation of silica in Me-SiO2-H2O systems and geochemical implications for cryosoils and - sediments. Chem. Geol. 216, 79–88. https://doi.org/10.1016/j.chemgeo.2004.11.003.

Evans, D.J.A., Phillips, E.R., Hiemstra, J.F., Auton, C.A., 2006. Subglacial till: Formation, sedimentary characteristics and classification. Earth-Sci. Rev. 78, 115–176. https://doi.org/10.1016/j.earscirev.2006.04.001.

Everitt, B.S., Landau, S., Leese, M., Stahl, D., 2011. Cluster Analysis. Wiley Series in Probability and Statistics, John Wiley & Sons, Ltd. https://doi.org/10.1002/9780470977811.

Folk, R.L., Ward, W.C., 1957. Brazos River bar: a study in the significance of grain size parameters. J. Sediment. Petrol. 27, 3–26. https://doi.org/10.1306/74D70646-2B21-11D7-8648000102C1865D.

French, H.M., 2017. The Periglacial Environment, fourth ed. Wiley Blackwell.

Gaweł, A., 1947. Geological conditions of origin of blue salt, amethyst and violet fluorite. Ann. Soc. Geol. Pol. 17, 51–60.

Gilpin, R.R., 1979. A model of the 'liquid-like' layer between ice and a substrate with applications to wire regelation and particle migration. J. Colloid Interf. Sci. 68, 235–251. https://doi.org/10.1016/0021-9797(79)90277-7.

Golub, G.H., Van Loan, C.F., 2013. Matrix Computations, fourth ed. The Johns Hopkins University Press, Baltimore.

Hall, K., 1990. Mechanical weathering rates on Signy Island. Maritime Antarctic. Permafrost Periglac. 1, 61–67. https://doi.org/10.1002/ppp.3430010108.

Hall, K., 1991. Rock moisture data from the Juneau Icefield (Alaska) and its significance for mechanical weathering studies. Permafrost Periglac. 2, 321–330. https://doi.org/10.1002/ppp.3430020407.

Hall, K., 1999. The role of thermal stress fatigue in the breakdown of rock in cold regions. Geomorphology 31, 47–63. https://doi.org/10.1016/S0169-555X(99)00072-0.

Hall, K., Hall, A., 1991. Thermal gradients and rock weathering at low temperatures: Some simulation data. Permafrost Periglac. 2, 103–112. https://doi.org/10.1002/ppp.3430020205.

Hallet, B., Walder, J.S., Stubbs, C.W., 1991. Weathering by segregation ice growth in microcracks at sustained subzero temperatures: Verification from an experimental study using acoustic emissions. Permafrost Periglac. 2, 283–300. https://doi.org/10.1002/ppp.3430020404.

Hennig, C., Meila, M., Murtagh, F., Rocci, R. (Eds.), 2015. Handbook of Cluster Analysis. Chapman and Hall/CRC. https://doi.org/10.1201/b19706.

Hiemstra, J.F., Van Der Meer, J.J.M., 1997. Pore-water controlled grain fracturing as an indicator for subglacial shearing in tills. J. Glaciol. 43, 446–454. https://doi.org/10.3189/S0022143000035036.

Hotelling, H., 1933. Analysis of a complex of statistical variables into principal components. J. Educ. Psychol. 24 (417–441), 498–520. https://doi.org/10.1037/h0071325.

Inzoli, S., Giudici, M., Huisman, J.A., 2016. Estimation of sediment texture from spectral induced polarisation data using cluster and principal component analysis. Near Surf. Geophys. 14, 433–447. https://doi.org/10.3997/1873-0604.2016033.

ISSMFE, 1989. International Society of Soil Mechanics and Foundation Engineering. Work report 1985-1989, in: Proceedings of International Symposium On Frost in Geotechnical Engineering 13-15.3.1989. VTT Symposium 94, Technical Committee on Frost, TC-8, Saariselkä, Finland, pp. 15–70.

Jefferson, I.F., Jefferson, B.Q., Assallay, A.M., Rogers, C.D.F., Smalley, I.J., 1997. Crushing of Quartz Sand to Produce Silt Particles. Naturwissenschaften 84, 148–149. https://doi.org/10.1007/s001140050366.

Kaiser, H.F., 1960. The Application of Electronic Computers to Factor Analysis. Educ. Psychol. Meas. 20, 141–151. https://doi.org/10.1177/001316446002000116.

Kaiser, H.F., 1974. An index of factorial simplicity. Psychometrika 39, 31–36. https://doi.org/10.1007/BF02291575.

Kasza, L., 1964. Budowa geologiczna górnego dorzecza Białej Ladeckiej [Geological structure of the upper Biała Ladecka basin]. Geologia Sudetica 1, 119–167. In Polish with English summary.

Kaufman, L., Rousseeuw, P.J., 1990. Finding Groups in Data: An Introduction to Cluster Analysis. Wiley Series in Probability and Statistics, John Wiley & Sons, Inc. https://doi.org/10.1002/9780470316801.

Kluitenberg, G.J., 2002. Heat capacity and specific heat. In: Dane, J., Topp, G. (Eds.), Methods of Soil Analysis: Part 4 Physical Methods. Soil Science Society of America and American Society of Agronomy, Madison, Wisconsin, pp. 1201–1208.

Konishchev, V.N., 1997. A cryolithic method for estimating palaeotemperature conditions during formation of the ice complex and subaerial periglacial sediments. Earth's Cryosphere (Kryosphera Zemli) 1, 23–28.

Konishchev, V.N., 1998. Relationship between the lithology of active-layer materials and mean annual ground temperature in the former USSR. In: Lewkowicz, A., Allard, M. (Eds.), Proceedings of the 7th International Conference in Permafrost, pp. 591–594.

Konishchev, V.N., 1999. Evolution of ground temperature of Russian Arctic zone in upper Cenozoic. Earth's Cryosphere 3, 39–47.

Konishchev, V.N., 2003. A criolithogenic method for estimating paleotemperature conditions during formation of the ice complex and subaerial periglacial sediments. Earth's Cryosphere Special Issue 59–64.

Konishchev, V.N., Lebedeva-Verba, M.P., Rogov, V.V., Stalina, E.E., 2005. Cryogenesis of modern and Late Pleistocene deposits Altai and periglacial region of Europa. GEOS, Moscow.

Konishchev, V.N., Rogov, V.V., 1993. Investigations of cryogenic weathering in Europe and Northern Asia. Permafrost Periglac. 4, 49–64. https://doi.org/10.1002/ppp.3430040105.

Konishchev, V.N., Rogov, V.V., 2017. Cryogenic processes in loess. Geogr. Environ. Sustain. (GES J.) 10, 4–14. https://doi.org/10.24057/2071-9388-2017-10-2-4-14.

Konrad, J.M., 2005. Estimation of the segregation potential of fine-grained soils using the frost heave response of two reference soils. Can. Geotech. J. 42, 38–50. https://doi.org/10.1139/t04-080.

Kryza, R., Muszyński, A., 1992. Pre-Variscan volcanic-sedimentary succession of the central south Góry Kaczawskie, SW Poland: Outline geology. Ann. Soc. Geol. Pol. 62, 117–140.

Lautridou, J.P., Ozouf, J.C., 1982. Experimental frost shattering: 15 years of research at the Centre de Géomorphologie du CNRS. Prog. Phys. Geogr.: Earth Environ. 6, 215–232. https://doi.org/10.1177/030913338200600202.

Liu, J., Chang, D., Yu, Q., 2016. Influence of freeze-thaw cycles on mechanical properties of a silty sand. Eng. Geol. 210, 23–32. https://doi.org/10.1016/j.enggeo.2016.05.019.

Mahaney, W.C., 1990. Glacially-crushed quartz grains in late Quaternary deposits in the Virunga Mountains, Rwanda – indicators of wind transport from the north? Boreas 19, 81–89. https://doi.org/10.1111/j.1502-3885.1990.tb00424.x.

Mahaney, W.C., 1995. Pleistocene and Holocene glacier thicknesses, transport histories and dynamics inferred from SEM microtextures on quartz particles. Boreas 24, 293–304.

Mahaney, W.C., 2002. Atlas of Sand Grain Surface Textures and Applications. Oxford University Press, NewYork, NY, p. 237.

Mahaney, W.C., Andres, W., 1991. Glacially crushed quartz grains in loess as indicators of long-distance transport from major European ice centers during the Pleistocene. Boreas 20, 231–239.

Mahaney, W.C., Vortisch, W., Julig, P., 1988. Relative differences bewteen glacially crushed quartz transported by mountain and continental ice – some examples from North America and East Africa. Am. J. Sci. 288, 810–826.

Maji, V., Murton, J.B., 2020. Experimental observations that simulated active-layer deepening drives deeper rock fracture. Permafrost Periglac. 31, 296–310. https://doi.org/10.1002/ppp.2041.

Ltd, M.I., 2008. Morphologi G3 User Manual. Malvern Instruments Ltd., Malvern, UK.

Manickam, S., Barbaroux, L., 1987. Variations in the surface texture of suspended quartz grains in the Loire river: an SEM study. Sedimentology 34, 495–510. https://doi.org/10.1111/j.1365-3091.1987.tb00581.x.

Margolis, S.V., Kennett, J.P., 1971. Cenozoic paleoglacial history of Antarctica recorded in Subantarctic deep-sea cores. Am. J. Sci. 274, 1–36. https://doi.org/10.2475/ajs.271.1.1.

Martins, M.V.A., Pinto, A.F.S., Frontalini, F., da Fonseca, M.C.M., Terroso, D.L., Laut, L.L. M., Zaaboub, N., da Conceição Rodrigues, M.A., Rocha, F., 2016. Can benthic foraminifera be used as bioindicators of pollution in areas with a wide range of physicochemical variability? Estuar. Coast. Shelf S. 182, 211–225. https://doi.org/10.1016/j.ecss.2016.10.011.

Matsuoka, N., 1991. A model of the rate of frost shattering: application to field data from Japan, Svalbard and Antarctica. Permafrost Periglac. 2, 271–281. https://doi.org/10.1002/ppp.3430020403.

Matsuoka, N., Abe, M., Ijiri, M., 2003. Differential Frost heave and sorted patterned ground: field measurements and a laboratory experiment. Geomorphology 52, 73–85. https://doi.org/10.1016/S0169-555X(02)00249-0.

McCammon, R.B., 1966. Principal Component Analysis and its Application in Large-Scale Correlation Studies. J. Geol. 74, 721–733. https://doi.org/10.1086/627207.

Miller, R.D., 1978. Frost heaving in non-colloidal soils. In: Proceedings of the 3rd International Conference on Permafrost, pp. 708–713.

Molén, M.O., 2014. A simple method to classify diamicts by scanning electron microscope from surface microtextures. Sedimentology 61, 2020–2041. https://doi.org/10.1111/sed.12127.

Montanher, O.C., ao de Morais Novo, E.M.L., de Souza Filho, E.E., 2018. Temporal trend of the suspended sediment transport of the Amazon River (1984–2016). Hydrol. Sci. J. 63, 1901–1912. https://doi.org/10.1080/02626667.2018.1546387.

Moss, A.J., 1966. Origin, shaping and significance of quartz sand grains. J. Geol. Soc. Aust. 13, 97–136. https://doi.org/10.1080/00167616608728607.

Moss, A.J., Green, P., 1975. Sand and silt grains: Predetermination of their formation and properties by microfractures in quartz. J. Geol. Soc. Aust. 22, 485–495. https://doi.org/10.1080/00167617508728913.

Murton, J.B., Coutard, J.P., Lautridou, J.P., Ozouf, J.C., Robinson, D.A., Williams, R.B.G., Guillemet, G., Simmons, P., 2000. Experimental design for a pilot study on bedrock weathering near the permafrost table. Earth Surf. Proc. Land. 25, 1281–1294. https://doi.org/10.1002/1096-9837(200011)25:12<1281::AIDESP137>3.0.CO;2-U.

Murton, J.B., Peterson, R., Ozouf, J.C., 2006. Bedrock fracture by ice segregation in cold regions. Science 314, 1127–1129. https://doi.org/10.1126/science.1132127.

Oyedotun, T.D.T., 2020. Compositional and multivariate statistical analyses for grain-size characterisation of intertidal sedimentary facies in an estuarine environment. Geol. Ecol. Landscapes 1–7. https://doi.org/10.1080/24749508.2020.1814186.

Özgan, E., Serin, S., Ertürk, S., Vural, I., 2015. Effects of Freezing and Thawing Cycles on the Engineering Properties of Soils. Soil Mech. Found. Eng. 52, 95–99. https://doi.org/10.1007/s11204-015-9312-1.

Pereira, M.F., Albardeiro, L., Gama, C., Chichorro, M., Hofmann, M., Linnemann, U., 2016. Provenance of Holocene beach sand in the Western Iberian margin: the use of the Kolmogorov-Smirnov test for the deciphering of sediment recycling in a modern coastal system. Sedimentology 63, 1149–1167. https://doi.org/10.1111/sed.12254.

Pirkle, F.L., Campbell, K., Wecksung, G.W., 1980. Principal Components Analysis as a Tool for Interpreting Nure Aerial Radiometric Survey Data. J. Geol. 88, 57–67. https://doi.org/10.2307/30068480.

Pye, K., Tsoar, H., 1990. Aeolian Sand and Sand Dunes. Unwin Hyman, London, p. 396.

Qi, J., Vermeer, P.A., Cheng, G., 2006. A review of the influence of freezethaw cycles on soil geotechnical properties. Permafrost Periglac. 17, 245–252. https://doi.org/10.1002/ppp.559.

R Core Team, 2020. R: A Language and Environment for Statistical Computing. R Foundation for Statistical Computing, Vienna, Austria.

Read, W.A., 1976. An assessment of some quantitative methods of comparing lithological succession data, in: Marriam, D.F. (Ed.), Quantitative Techniques for the Analysis of Sediments. Pergamon, pp. 33–51. https://doi.org/10.1016/B978-0-08-020613-4.50010-0.

Reid, M.K., Spencer, K.L., 2009. Use of principal components analysis (PCA) on estuarine sediment datasets: The effect of data pre-treatment. Environ. Pollut. 157, 2275–2281. https://doi.org/10.1016/j.envpol.2009.03.033.

Rose, K.C., Hart, J.K., 2008. Subglacial comminution in the deforming bed: inferences from SEM analysis. Sed. Geol. 203, 87–97. https://doi.org/10.1016/j.sedgeo.2007.11.003.

Rousseeuw, P.J., 1987. Silhouettes: A graphical aid to the interpretation and validation of cluster analysis. J. Comput. Appl. Math. 20, 53–65. https://doi.org/10.1016/0377-0427(87)90125-7.

Ruedrich, J., Kirchner, D., Siegesmund, S., 2011. Physical weathering of building stones induced by freeze–thaw action: a laboratory long-term study. Environ. Earth Sci. 63, 1573–1586. https://doi.org/10.1007/s12665-010-0826-6.

Schärli, U., Rybach, L., 2001. Determination of specific heat capacity on rock fragments. Geothermics 30, 93–110. https://doi.org/10.1016/S0375-6505(00)00035-3.

Schwamborn, G., Schirrmeister, L., Frütsch, F., Diekmann, B., 2012. Quartz weathering in freeze–thaw cycles: experiment and application to the el`gygytgyn crater lake record for tracing siberian permafrost history. Geogr. Ann. A Phys. Geogr. 94A, 481–499. https://doi.org/10.1111/j.1468-0459.2012.00472.x.

She, W., Wei, L., Zhao, G., Yang, G., Jiang, J., Hong, J., 2019. New insights into the frost heave behavior of coarse grained soils for high-speed railway roadbed: Clustering effect of fines. Cold Reg. Sci. Technol. 167, 102863. https://doi.org/10.1016/j.coldregions.2019.102863.

Shi, Q., Niu, G., Lin, Q., Xu, T., Li, F., Duan, Y., 2015. Quantitative analysis of sedimentary rocks using laser-induced breakdown spectroscopy: comparison of

support vector regression and partial least squares regression chemometric methods. J. Anal. Atom. Spectrom. 30, 2384–2393. https://doi.org/10.1039/C5JA00255A.

Smith, B.J., Wright, J.S., Whalley, W.B., 2002. Sources of non-glacial, loesssize quartz silt and the origins of "desert loess". Earth-Sci. Rev. 59, 1–26. https://doi.org/10.1016/S0012-8252(02)00066-1.

Sobień, K., Nawrocki, J., 2010. Palaeomagnetic and petromagnetic study of uranium-bearing polymetallic-fluorite mineralization in the Orlik-Kladsko crystalline complex (near Kletno, Lower Silesia, Poland). Geol. Q. 54, 325–336.

Sumner, P.D., Nel, W., Hedding, D.W., 2004. Thermal Attributes of Rock Weathering: Zonal or Azonal? A Comparison of Rock Temperatures in Different Environments. Polar Geogr. 28, 79–92. https://doi.org/10.1080/789610119.

Taber, S., 1929. Frost Heaving. J. Geol. 37, 428–461. https://doi.org/10.1086/623637.

Udden, J.A., 1914. Mechanical composition of clastic sediments. Bull. Geol. Soc. Am. 25, 655–744. https://doi.org/10.1130/GSAB-25-655.

Vos, K., Vandenberghe, N., Elsen, J., 2014. Surface textural analysis of quartz grains by scanning electron microscopy (SEM): From sample preparation to environmental interpretation. Earth-Sci. Rev. 128, 93–104.

Walder, J.S., Hallet, B., 1986. The Physical Basis of Frost Weathering: Toward a More Fundamental and Unified Perspective. Arctic Alpine Res. 18, 27–32. https://doi.org/10.2307/1551211.

Wall, M.E., Rechsteiner, A., Rocha, L.M., 2003. Singular Value Decompo1156 sition and Principal Component Analysis. In: Berrar, D.P., Dubitzky, W., Granzow, M. (Eds.), A Practical Approach to Microarray Data Analysis. Springer, US, Boston, MA, pp. 91–109.

Waples, D.W., Waples, J.S., 2004. A Review and Evaluation of Specific Heat Capacities of Rocks, Minerals, and Subsurface Fluids. Part 2: Fluids and Porous Rocks. Nat. Resour. Res. 13, 123–130. https://doi.org/10.1023/B:NARR.0000032648.15016.49.

Ward Jr., J.H., 1963. Hierarchical Grouping to Optimize an Objective Function. J. Am. Stat. Assoc. 58, 236–244. https://doi.org/10.1080/01621459.1963.10500845.

Weltje, G.J., 1997. End-member modeling of compositional data: Numericalstatistical algorithms for solving the explicit mixing problem. Math. Geol. 29, 503–549. https://doi.org/10.1007/BF02775085.

Wentworth, C.K., 1922. A scale of grade and class terms for clastic sediments. Jour. Geol. 30, 377–392. https://doi.org/10.1086/622910.

Whalley, W.B., Krinsley, D.H., 1974. A scanning electron microscope study of surface textures of quartz grains from glacial environments. Sedimentology 21, 87–105.

Wierzchoń, S., Kłopotek, M., 2018. Modern Algorithms of Cluster Analysis. volume 34 of Studies in Big Data. Springer, Cham. https://doi.org/10.1007/978-3-319-69308-8.

Williams, P.J., Smith, M.W., 1989. The Frozen Earth. Cambridge University Press, Cambridge, p. 306.

Wiman, S., 1963. A preliminary study of experimental frost weathering. Geogr. Ann. 45, 113–121. https://doi.org/10.1080/20014422.1963.11881018.

Winkler, H.G.S., 1976. Petrogenesis of metamorphic rocks. Springer, Heidelberg.

Wołkowicz, K., 2000. O katodoluminescencji sudeckich kwarców żyłowych [On the cathodoluminescence studies of the Sudetic vein quartz (SW Poland)]. Przeglad Geologiczny 48, 625–633. In Polish with English summary.

Woronko, B., 2012. Micromorphology of quartz grains as a tool in the reconstruction of periglacial environment. Contemp. Iss. Polish Geogr. 113–131.

Woronko, B., 2016. Frost weathering versus glacial grinding in the micromorphology of quartz sand grains: Processes and geological implications. Sed. Geol. 335, 103–119. https://doi.org/10.1016/j.sedgeo.2016.01.021.

Woronko, B., Hoch, M., 2011. The Development of Frost-weathering Microstructures on Sand-sized Quartz Grains: Examples from Poland and Mongolia. Permafrost Periglac. 22, 214–227. https://doi.org/10.1002/ppp.725.

Woronko, B., Pisarska-Jamroży, M., 2016. Micro-scale frost weathering of sand-sized quartz grains. Permafr. Periglac. Process. 27, 109–122. https://doi.org/10.1002/ppp.1855.

Wright, J., Smith, B., Whalley, B., 1998. Mechanisms of loess-sized quartz silt production and their relative effectiveness: laboratory simulations. Geomorphology 23, 15–34. https://doi.org/10.1016/S0169-555X(97)00084-6.

Woronko, B., Zieliński, A., 2006. Freeze-thaw of quartz sand grains as a mechanism of quartz silt production – laboratory simulations. In: Nickling, W., Turner, S., Gillies, J., Puddister, M. (Eds.), Sixth International Conference on Aeolian Research, 24–28 July 2006. University of Guelph, Guelph, Ontario, Canada, p. 166.

Wright, J.S., 2000. The spalling of overgrowths during experimental freeze–thaw of a quartz sandstone as a mechanism of quartz silt production. Micron 31, 631–638. https://doi.org/10.1016/S0968-4328(99)00074-8.

Wright, J.S., 2007. An overview of the role of weathering in the production of quartz silt. Sed. Geol. 202, 337–351. https://doi.org/10.1016/j.sedgeo.2007.03.024.

Yamashita, S., Naruse, H., Nakajo, T., 2018. Reconstruction of sedimenttransport pathways on a modern microtidal coast by a new grain-size trend analysis method. Prog. Earth Planet. Sci. 5, 7. https://doi.org/10.1186/s40645-018-0166-9.

Yatsu, E., 1988. The Nature of Weathering: An Introduction. Sozosha, Tokyo, Japan.

Zagożdżon, P.P., Zagrodny, K., 2009. Cyfrowe modelowanie Jaskini Niedzwiedziej w Kletnie oraz jej geologicznego otoczenia [Digital modeling of Niedzwiedzia Cave in Kletno (Lower Silesia) and its geological surroundings]. Prace Naukowe Instytutu Górnictwa Politechniki Wrocławskiej 128, 221–236. In Polish.

Zhou, Z., Ma, W., Zhang, S., Mu, Y., Li, G., 2018. Effect of freeze-thaw cycles in mechanical behaviors of frozen loess. Cold Reg. Sci. Technol. 146, 9–18. https://doi.org/10.1016/j.coldregions.2017.11.011.

Zieliński, G., 1997. Temperatury powstawania kwarcu i fluorytu ze złoża uranowo-polimetalicznego w Kletnie, Dolny Śląsk [Temperatures of quartz and fluorite formation from the uranium-polymetallic deposit in Kletno, Lower Silesia]. University of Warsaw, Warsaw, Poland. Master's thesis.

ZAŁĄCZNIK 2

ATTACHMENT 2

Publikacja nr 2 (Publication no. 2):

Górska M.E., Woronko B., 2022. Multi-stage evolution of frost-induced microtextures on the surface of quartz grains – An experimental study. *Permafrost and Periglacial Processes*, 33, 470-489. https://doi.org/10.1002/ppp.2164

RESEARCH ARTICLE

WILEY

Multi-stage evolution of frost-induced microtextures on the surface of quartz grains—An experimental study

Martyna E. Górska[1] ⓘ | Barbara Woronko[2]

[1]Institute of Geology, Adam Mickiewicz University, Poznań, Poland

[2]Faculty of Geology, University of Warsaw, Warsaw, Poland

Correspondence
Martyna E. Górska, Adam Mickiewicz University, Institute of Geology, Krygowskiego 12, 61-680 Poznań, Poland.
Email: mgorska@amu.edu.pl

Abstract

Coarse sand-sized (0.5–1.0 mm) grains of vein quartz were subjected to frost-induced stress under controlled laboratory conditions. A total of 1,000 freeze–thaw (FT) cycles, simulated under different (low, high) water mineralization conditions in the temperature range from $-5°C$ up to $+10°C$, were used to test effects on collected samples. Scanning electron microscopic (SEM) microtextural analysis of grain surfaces was performed at 0 (start) and after 50, 100, 300, 700, and 1,000 FT cycles. The results indicate that variable frost-induced microtextural imprints encountered on quartz grain surfaces prior to and following analysis depend largely on the mineralization (dissolved solute content) of water involved in the weathering process. The higher the water mineralization, the greater the intensity of mechanical weathering. Two predominant outcomes in the course of these micro-scale frost weathering tests have been identified: a physical (mechanical) aspect manifested by the occurrence of conchoidal fractures and breakage block microtextures dominating up to 300 FT cycles, and a chemical aspect resulting in the occurrence of precipitation crusts and obliteration of grain microrelief. Moreover, three additional stages of microtexture development may be distinguished with the evolution of frost-induced microrelief on the surface of quartz grains: (i) initial cracks of large-sized conchoidal fractures, (ii) increasing frost cycles yielding additional small-sized conchoidal fractures, and (iii) advanced breakage blocks. Frost-induced exposure of fresh, unweathered grain surfaces leads to refreshing of the grain surface.

KEYWORDS
breakage blocks, conchoidal fractures, renewal of frost weathering, vein quartz, water mineralization

1 | INTRODUCTION

In the field, micro-scale frost weathering is thought to leave a characteristic frost-originated microtextural imprint on the surface of sand-sized quartz grains.[1,2] These diagnostic frost-originated microtextures are thought to result from both mechanical and chemical processes involved in the destruction of grains.[1,3–9] Formerly, from field examples, frost-affected grains have been identified by angular shape, high relief, sharp edges, breakage blocks, and conchoidal fractures along with frequently occurring microcracks.[1,2,5,8,9] Other microtextures, such as curved and straight grooves, scratches (striae), and chemical scaling, have been identified as a result of frost weathering as well.[3,8,10–12] In addition, the effects of frost-driven chemical weathering include precipitated mineral crust observed on the surface of weathered quartz grains.[12,13]

Interpretive difficulties regarding sediments/grains originating from the present or past periglacial environments[8,14] arise from a lack

---

of information on (i) the number of freeze–thaw (FT) cycles that studied grains have suffered, which have contributed to microtextural changes; (ii) the stage of development of a particular microtexture under study; (ii) the manner of formation and expansion of frost-induced microtextural imprints; (iv) the percentage of microtextures visible on grain surfaces originating from the frost weathering process, and how many are preserved from the environmental history (transport, deposition etc.); and (v) weathering conditions and their temporal changes (water availability, water mineralization, temperature regime). Therefore, the main issue to consider is not the type of frost-originated microtextural imprints but the time span and manner of their formation. None of the up-to-date studies have focused on the influence of water mineralization involved in frost weathering on the course of quartz mechanical destruction. Only a few studies refer to chemical by-products of frost weathering in cold climate conditions that affect weathered quartz grains[5,13,15] To elucidate these uncertainties, and to mirror field conditions, we conducted a laboratory-controlled experimental study on micro-scale frost weathering of sand-sized quartz grains. The simulation of 1,000 FT cycles aims to investigate the following issues: (i) evolution of frost-induced microtextures imprinted on the surface of fresh, mechanically crushed quartz grains with ongoing mechanical activity, (ii) susceptibility of the original quartz grain microrelief to the formation of frost-originated microtextures, (iii) impact of water mineralization (dissolved solute content) on the frost weathering of quartz grains, and (iv) temporal changes in frost weathering.

2 | MATERIALS AND METHODS

2.1 | Materials

Vein quartz samples from the Polish Western Sudetes Mountains (Wojcieszów site; 50°57′54" N, 15°55′32″ E) were used in the experiment. Studied vein quartz originated from hydrothermal processes associated with local thermal activity and magmatic intrusion of bedrock (sericite-chlorite metamorphosed claystones). It comprised cross-cutting beds of crystallized and recrystallized silica precipitation consisting mainly of subhedral quartz crystals exhibiting a close contact between adjacent crystals.

Fragments of a massive rock outcrop were mechanically crushed using bench-top ring mill and sieved to separate the designated grain-size fractions (0.5–1.0 mm). An ultrasonic cleaner was used to remove artificial fine particles from the grain surface. The grains were observed under a magnifying binocular to exclude quartz grains with visible inclusions and other mineral inhomogeneities from further analysis. Equal samples of quartz grains (approx. 2 g) were stacked on individual Petri dishes, poured over with low and highly mineralized water (called LMW and HMW, respectively; Table 1) until their complete immersion. The concentration of the dissolved solid content (especially carbonates) tends to change along with water temperature. A high mineralization of water (i.e., high dissolved solute content) is commonly reported in periglacial environments of the region,

TABLE 1 Detailed characteristic of water

Low-mineralized water (LMW)

The sum of dissolved solids (mineralization): 213.09 mg/L

HCO_3^-: 121.06 mg/L

F^-: 0.07 mg/L

Mg^{2+}: 5.37 mg/L

Ca^{2+}: 36.39 mg/L

Na^{2+}: 8.29 mg/L

High-mineralized water (HMW)

The sum of dissolved solids (mineralization): 1954.36 mg/L

HCO_3^-: 1489.00 mg/L

SO_4^{2-}: 21.80 mg/L

Cl^-: 12.90 mg/L

F^-: 0.16 mg/L

Mg^{2+}: 128.30 mg/L

Ca^{2+}: 208.00 mg/L

Na^{2+}: 87.80 mg/L

K^+: 6.40 mg/L

particularly within a layer of talik characterized by restricted circulation imposed by permafrost.[16]

2.2 | Experimental design

The frost weathering simulation was conducted under controlled laboratory conditions. A commercial upright freezer, equipped with special software and programmed for automated and defined temperature changes, was used as the experimental platform. Quartz grains were subjected to FT cycles with temperature fluctuations from −5°C up to +10°C (a temperature regime of a comparable range has been already used in previous experimental studies[17–19]). Such a temperature range would conform to high-mountain environments of various regions of the world.[16,20,21] One complete FT cycle lasts 4 h, of which 2 h is the freezing stage (temperature decrease to −5°C; decrease from 0°C to −5°C takes 1 h 45 min), 1 h is the constant stage (temperature remains at −5°C), and 1 h is the thawing stage (temperature rises up to +10°C). The duration of individual temperature values and the rate of temperature changes have been adapted to complete freezing and thawing of water (Figure 1). Fluctuations in water level were controlled macroscopically, and water was replenished approximately every 2 days to avoid its complete evaporation. The samples were collected after 50, 100, 300, 700, and 1,000 FT cycles and allowed to dry at room temperature (∼20°C–22°C).

2.3 | Laboratory analysis

The microtextures were investigated using the scanning electron microscope (SEM), ZEISS Sigma VP apparatus at the Scanning
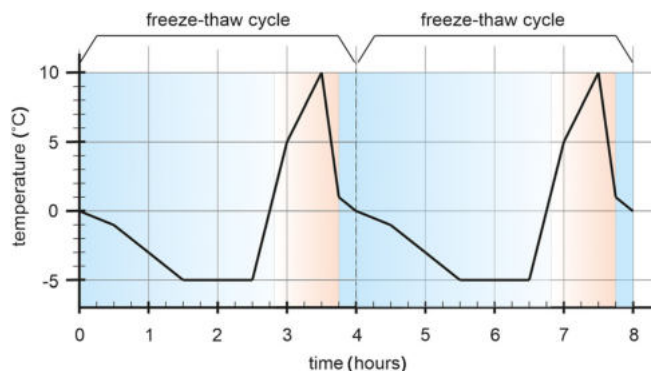
FIGURE 1 Temperature regime introduced into the freeze–thaw (FT) device workflow. Blue color—freezing stage of the FT cycle, orange color—thawing stage of the FT cycle [Colour figure can be viewed at wileyonlinelibrary.com]

Microscope and Microanalysis Laboratory (Faculty of Geology, University of Warsaw). At least 20 randomly selected sand-sized (0.5–1.0 mm) grains from each sample were mounted together on a single specimen stub and coated with gold to prevent charging. Prepared samples were placed in the SEM under vacuum. Conducted microtexture analyses followed widely used schemes.[12,22,23] Grains were observed and thoroughly examined in two steps—at low (∼100–150×) and high (∼1,000×) magnification. The type of grain edges (sharp/rounded), frequency of fractures (low/high), and microrelief diversity (low/medium/high) were determined at the low magnification. Further, the surface of each grain was thoroughly scanned at high magnification. All surficial microtextures observed on the visible side of the grain were reported (present vs. absent) and characterized. These include the remnants of the original grain microrelief of both mechanical (e.g., conchoidal fracture, breakage blocks, arc-shaped steps, linear steps, micro-steps, parallel ridges, subparallel linear fractures, sawtooth fractures, radial fractures) and chemical (e.g., dissolution surface) origin.[12,22,23]

The frequency of occurrence of the individual microtextures in a given sample (20 grains) was estimated and subdivided into the following frequency classes: (i) absent (0%), (ii) rare (1%–25%), (iii) sparse (26%–50%), (iv) common (51%–75%), (v) abundant (76%–99%), (vi) on all grains (100%). Further, those mechanical microtextures, whose frost-induced origin is indisputable, i.e., small- (<10 μm) and large-sized (>10 μm) breakage blocks and conchoidal fractures[1,3,12,13,24] (called here bb, BB, cf, CF, respectively), were carefully counted on each grain. Their sums and the average values were estimated for a given sample, and the results were analyzed statistically. The presence of chemical frost-induced imprints (i.e., surficial precipitation) was defined qualitatively. Finally, all the cracks observed on the grain surface were reported and counted.

The degree of surface coverage with a crust precipitated from the minerals dissolved in water was determined qualitatively (low/high). The elemental composition of the crust in a given area of the grain was determined using EDX (energy-dispersive X-ray spectroscopy)

analyses, and their distribution was extracted from EDX mapping (SEM, ZEISS Sigma VP apparatus).

3 | RESULTS

3.1 | Microtextural assemblages of sand-sized quartz grains

The results of the SEM investigation include a detailed microtextural description of the individual samples, including the reference group (0 FT cycles; not subjected to frost weathering called reference sample) and FT weathered samples (subjected to 50, 100, 300, 700, 1,000 FT cycles under LMW and HMW conditions; Figure 2). The frequency of frost-induced microtexture occurrence was estimated for both individual grains and the whole sample (i.e., 20 randomly selected grains; Appendix A).

3.1.1 | Reference sample microtextures

Sand-sized vein-quartz grains, comprising the prepped grains, are characterized by high or medium relief, sharp edges, fresh surfaces, and the high frequency of mechanically induced fractures (Figures 2, 3A,B). Individual grains consist of euhedral silica crystals with numerous inclusions and frequently etched surfaces (Figure 3C). Conchoidal fractures of various sizes (<10 μm, called cf; and >10 μm, called CF) predominate among the surficial microtextures. Their smooth curved surfaces are prone to exhibit numerous arc-shaped steps, linear steps, subparallel linear steps, parallel ridges, and micro steps (Figure 3D,E). Subsidiary microtextures are breakage blocks of large (>10 μm; called BB) or small size (<10 μm; called bb) that form single surficial features (Figure 2). These microtextures are found on the sharp edges of euhedral silica crystals (Figure 3F). Grain surfaces are sparsely covered with individual, small-sized, and spherically shaped adhering particles (Figure 3D). All grains are cracked (Figure 2).

3.1.2 | Mechanically induced frost-originated microtextures

All of the studied grains from the weathered samples (20 grains from each sample; 200 grains in total) are characterized by medium or high relief regardless of the number of freeze–thaw cycles and water mineralization conditions (Figure 2). Microtextural low relief is subordinately observed on the surface of grains that suffered at least 100 FT under HMW conditions (Figure 2). Moreover, all of the grains exhibit sharp edges and high frequency of mechanically induced fractures, among which CF is dominant (Figure 2). Detailed grain characteristics and surficial features of weathered grains (after 50, 100, 300, 700, and 1,000 FT) are presented on the SEM images in Figures 4(A–I), 5(A–I), 6(A–L), 7(A–I), 8(A–F).

type of microtexture / FT cycles	0	samples from LM conditions					samples from HM conditions				
		50	100	300	700	1000	50	100	300	700	1000
low relief	0%	0%	0%	0%	0%	0%	0%	1-25%	26-50%	1-25%	26-50%
medium relief	26-50%	26-50%	1-25%	26-50%	26-50%	51-75%	26-50%	1-25%	26-50%	76-99%	51-75%
high relief	51-75%	51-75%	76-99%	51-75%	51-75%	26-50%	51-75%	26-50%	1-25%	1-25%	26-50%
high frequency fractures	100%	100%	100%	100%	100%	100%	100%	100%	100%	76-99%	76-99%
low frequency fractures	0%	0%	0%	0%	0%	0%	0%	0%	0%	1-25%	1-25%
edge rounding	0%	0%	0%	0%	0%	0%	1-25%	0%	0%	1-25%	26-50%
sharp features	100%	100%	100%	100%	100%	100%	100%	100%	100%	100%	76-99%
abrasion fatigues	0%	0%	0%	0%	0%	0%	0%	0%	0%	0%	0%
abrasion feature	76-99%	100%	100%	100%	100%	100%	100%	100%	100%	100%	76-99%
fresh surface	100%	100%	100%	100%	100%	76-99%	76-99%	100%	100%	76-99%	76-99%
anastomosis	0%	0%	0%	0%	0%	0%	0%	0%	0%	0%	0%
amorphous ppt	0%	26-50%	1-25%	26-50%	76-99%	76-99%	1-25%	76-99%	76-99%	100%	100%
dissolution surface	0%	76-99%	51-75%	26-50%	26-50%	26-50%	76-99%	51-75%	1-25%	1-25%	1-25%
dulled surface	0%	0%	0%	0%	0%	0%	0%	0%	0%	0%	1-25%
caverns	0%	0%	0%	0%	0%	0%	0%	0%	0%	0%	0%
lattice shattering	0%	0%	0%	0%	0%	0%	0%	0%	0%	0%	0%
oriented etch pits	1-25%	1-25%	0%	0%	0%	0%	1-25%	0%	1-25%	1-25%	0%
solution crevasses	0%	0%	0%	0%	0%	0%	0%	0%	0%	0%	0%
solution pits	0%	0%	0%	0%	0%	0%	1-25%	0%	0%	0%	0%
arc-shaped steps	100%	100%	100%	76-99%	76-99%	76-99%	100%	76-99%	76-99%	51-75%	76-99%
breakage blocks (<10 µm)	26-50%	26-50%	1-25%	1-25%	1-25%	1-25%	26-50%	1-25%	1-25%	26-50%	1-25%
breakage blocks (>10 µm)	51-75%	100%	100%	76-99%	51-75%	51-75%	100%	100%	76-99%	76-99%	26-50%
chattermarks	0%	0%	0%	0%	0%	0%	0%	0%	1-25%	0%	0%
conchoidal fractures (<10 µm)	76-99%	26-50%	26-50%	26-50%	26-50%	26-50%	51-75%	26-50%	26-50%	51-75%	51-75%
conchoidal fractures (>10 µm)	100%	100%	100%	100%	100%	100%	100%	100%	100%	100%	76-99%
fracture faces	1-25%	26-50%	0%	1-25%	1-25%	1-25%	26-50%	1-25%	0%	0%	0%
linear steps	76-99%	76-99%	100%	76-99%	51-75%	100%	76-99%	76-99%	76-99%	76-99%	51-75%
subparallel linear fractures	51-75%	51-75%	51-75%	26-50%	1-25%	26-50%	26-50%	26-50%	26-50%	26-50%	1-25%
micro steps	51-75%	76-99%	76-99%	76-99%	76-99%	76-99%	76-99%	51-75%	76-99%	76-99%	76-99%
parallel ridges	51-75%	26-50%	51-75%	51-75%	26-50%	26-50%	51-75%	26-50%	51-75%	1-25%	1-25%
radial fractures	1-25%	1-25%	1-25%	1-25%	1-25%	1-25%	26-50%	1-25%	1-25%	0%	0%
sawtooth fractures	26-50%	1-25%	1-25%	26-50%	1-25%	1-25%	1-25%	26-50%	51-75%	0%	0%
craters	1-25%	0%	1-25%	1-25%	0%	1-25%	1-25%	1-25%	1-25%	1-25%	1-25%
crescentic gouges	0%	0%	0%	0%	0%	0%	0%	0%	0%	0%	0%
V-shaped percussion cracks	0%	0%	0%	0%	0%	0%	0%	0%	0%	0%	0%
mechanically upturned plates	0%	0%	0%	0%	0%	0%	0%	0%	0%	0%	0%
bulbous edges	0%	0%	0%	0%	0%	0%	0%	0%	0%	0%	0%
curved grooves	0%	0%	0%	0%	0%	0%	0%	0%	0%	0%	0%
deep trough	1-25%	1-25%	1-25%	1-25%	1-25%	1-25%	1-25%	1-25%	1-25%	1-25%	1-25%
straight grooves	0%	1-25%	1-25%	0%	0%	0%	1-25%	0%	1-25%	1-25%	0%
scaling	0%	0%	0%	0%	1-25%	26-50%	0%	0%	1-25%	51-75%	1-25%
adhering particles	100%	100%	100%	100%	100%	100%	100%	100%	100%	100%	100%
cracks	100%	76-99%	76-99%	76-99%	51-75%	51-75%	100%	76-99%	76-99%	51-75%	51-75%
euhedral silica precipitation	100%	100%	100%	76-99%	76-99%	51-75%	100%	76-99%	76-99%	76-99%	51-75%
inclusions	100%	100%	100%	100%	76-99%	76-99%	100%	100%	100%	76-99%	76-99%

Legend: ⊙ 100% ● 76-99% ◕ 51-75% ◐ 26-50% ◔ 1-25% ⊗ 0%

FIGURE 2 Microtextural characteristics of quartz grains from individual samples under experimental study. Comparison between reference sample (0 FT) and weathered samples (50, 100, 300, 700, 1,000 FT) indicates differences in microtextural imprints induced by frost weathering, especially in the grain relief, type of grain edges (sharp/rounded), frequency of mechanical fractures, and frost-induced microtextures (CF, CF, BB, BB) between samples weathered under low mineralized water (LMW) and high mineralized water (HMW) conditions. The abbreviations used (CF, CF, BB, BB) refer to small- (<10 µm) and large-sized conchoidal fractures (>10 µm), small- (<10 µm) and large-sized breakage blocks (>10 µm), respectively
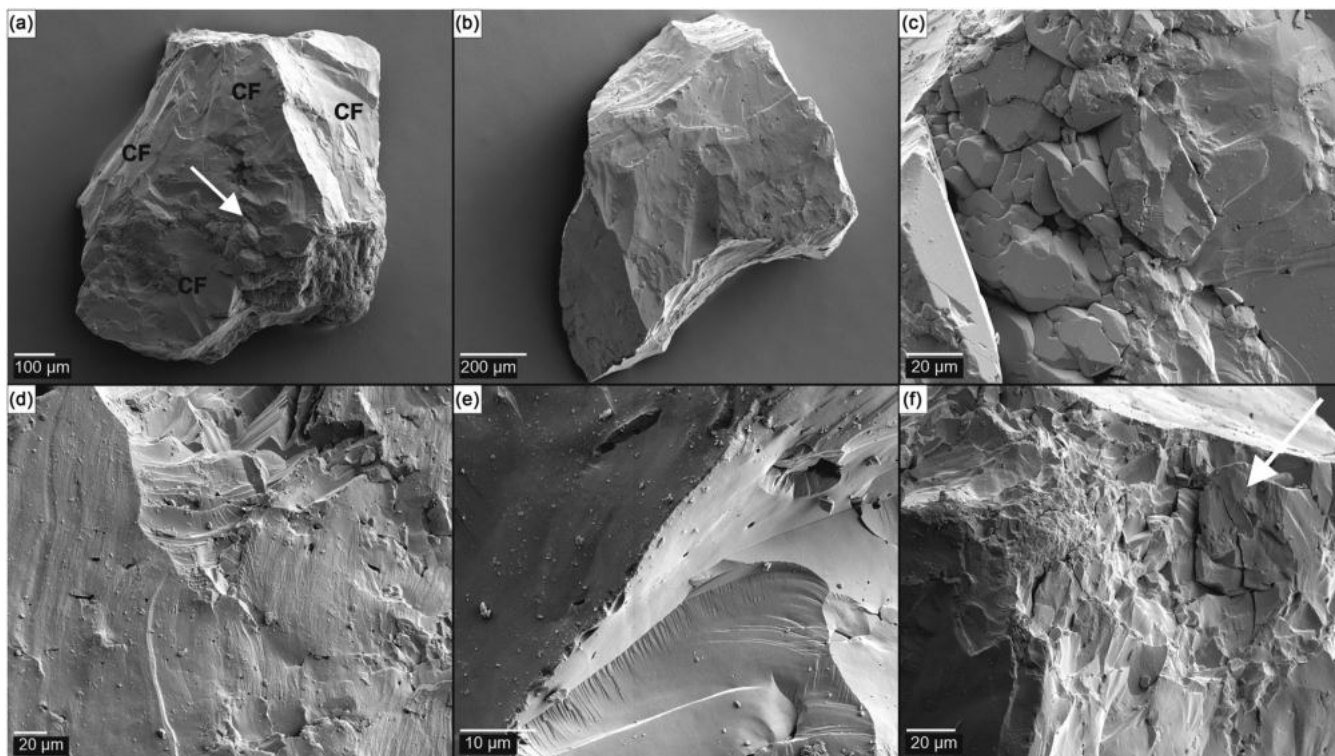
FIGURE 3 Scanning electron microscopic (SEM) image of a reference sample (0 freeze–thaw [FT]). (A), Quartz grain exhibiting high relief, sharp edges, high frequency of mechanical microtextures (e.g., CF) and euhedral silica precipitation (arrow); B, quartz grain exhibiting medium relief with sharp edges and fresh CF; C, euhedral silica precipitation; D, arc-shaped and linear steps on CF, and adhering particles; E, linear steps and CF on the sharp edges of CF; F, BB microtexture (arrow). The abbreviations used (CF, CF, BB) refer to small- (<10 μm) and large-sized conchoidal fractures (>10 μm), and large-sized breakage blocks (>10 μm), respectively

The effects of frost activity are manifested mainly by two types of microtextures: BB and CF (Figures 4A–F, 5A–F, 6A–I, 7A–D, 8A–D). Other results, but quantitatively less common frost-induced microtextures, include bb and cf (Appendix A). All frost-originated microtextures regardless of their size are fresh (bearing no evidence of amorphous precipitation) and sharp-shaped (e.g., Figures 6J, 7E,F, 8E,F) which distinguishes them from the grain surface and from similar microtextures created as a result of sample preparation (Figure 3).

Both BB and CF are detected on all of the studied quartz grains (Figure 2). Differences in the number of these microtextures are considerable for both LMW and HMW samples; however, it is particularly evident in HMW samples (Appendix A). A significant production of BB and CF is observed up to 300 FT, after which it clearly declines reaching minimum values after or up to 1,000 FT (Appendix A; Figure 9). The count of BB and CF at 1,000 FT on individual grains varies, from a single occurrence to a dozen or so, and it changes with the number of cycles. For example, the number of BB microtextures reaches its maximum on grains from the LMW sample group subjected to 50 FT and HMW samples subjected to 300 FT, while CF is the most common on the LMW and HMW grains after 300 FT (Appendix A; Figures 9–11).

The CF microtextures vary in size from >10 μm (Figures 4E,F, 5B, E, 7E, 8D) to >100 μm when covering the entire surface of the grain

(Figures 5F, 6G, 7C,D, 8B,C). Observed BBs take many different forms—from just a few overlapping conchoidal fractures (Figures 5A, B, 6J) to forms that cover larger grain surfaces (Figures 4C, 6D, 7A,B, 8A) and extensive breakage block complexes formed by the joining of several smaller forms and extending over a relatively large area of individual grain surfaces (Figures 4A–D, 5C, 6B,C). They are commonly accompanied by small cracks (Figure 6C). BB and CF occupy sharp edges, micro-steps, and micro-texturally differentiated areas of CF.

Almost all of the grains weathered under LMW and all of the grains from HMW are cracked (Figures 4G,H, 5G). However, the number of surficial cracks generally declines with the number of FT cycles (Appendix A). On grains subjected to 700 and 1,000 FT, cracks are commonly obliterated and covered by precipitation crusts (Figures 7G, 8F).

3.1.3 | Chemically originated frost-induced microtextures

The degree of precipitation coverage on grain surfaces varies both quantitatively (Figure 12A–L) and qualitatively (Figure 13A–C). Crust growth and adsorption tends to increase with progressive frost action operating under variable water mineralization conditions. It is
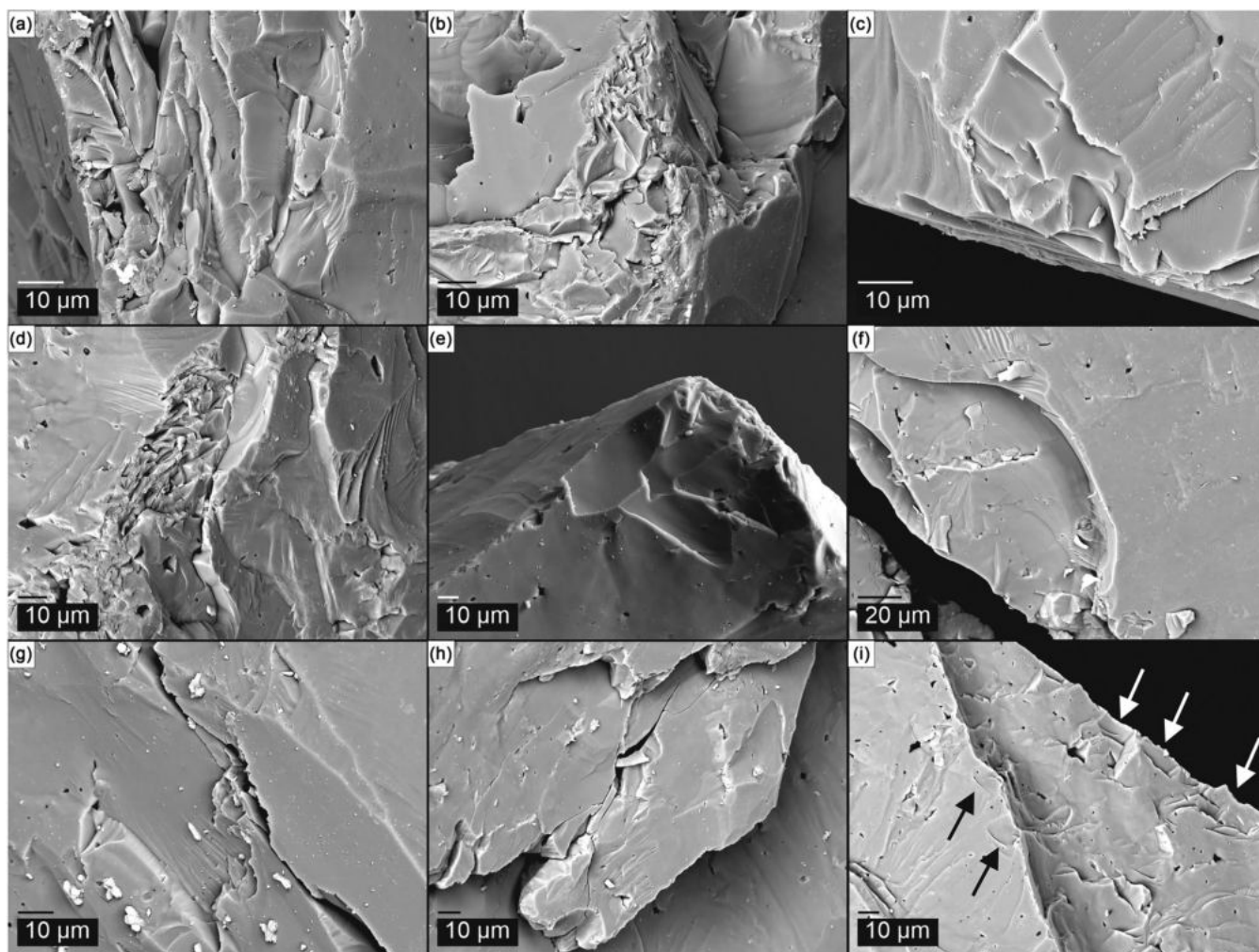
FIGURE 4   Scanning electron microscopic (SEM) images of quartz grains from a sample after 50 freeze–thaw (FT) cycles. (A, B), BB microtextures on the sharp edges of grain (high mineralized water [HMW] conditions); (C, D), BB microtextures on the sharp edges of grain (low mineralized water [LMW] conditions); ℇ, fresh CF microtextures on the sharp edges of grain (HMW conditions); (F), CF microtextures on the sharp edges of grain (LMW conditions); (G), CF microtextures on the micro-step (HMW conditions); (H), surficial cracks on the grain (HMW conditions); (I), CF microtextures on the micro-step (black arrows) and sharp edges (white arrows) of grain (LMW conditions). The abbreviations used (CF, CF, BB) refer to small- (<10 μm) and large-sized conchoidal fractures (>10 μm), and large-sized breakage blocks (>10 μm), respectively

manifested by the presence of amorphous precipitation and crystalline forms that produce a precipitation crust of significant thickness. However, grains weathered under HMW conditions bear more extensive precipitation coverage at every stage of weathering, i.e., after 50, 100, 300, 700, and 1,000 FT, as compared with LMW conditions.

At the initial stage of weathering, i.e., after 50 FT, precipitation crusts are sparse and negligible as grain surfaces are generally fresh and not different from the surface of grains from reference sample (Figures 3, 12A,B). Surfaces of HMW grains are covered by single spatial crystalline forms (Figure 12B). After 100 FT under both water mineralization conditions, crust development includes dispersed mineral aggregates, a few micrometers in size, and with irregular shapes (Figure 12C,D). In addition, HMW grains bear crystalline forms that vary, from single to more compound patterns,

consisting of numerous small clusters covering the surface with a discontinuous amorphous crust (Figure 12D). Such small clusters appear on the LMW grains after 300 FT (Figure 12E) and become more complex on the HMW grains (Figure 12F). The surface of LMW grains becomes extensively covered with amorphous precipitation after 700 FT (Figure 12G). Similar effects are observed on the surface of HMW grains; however, these are more advanced, with larger crystalline forms and more extensive precipitation crust (Figure 12H). Spatial crystalline forms are arranged into more extensive aggregates contributing to the rounding of protruding grain fragments. After 1,000 FT, the degree of crust growth of LMW grains resembles that of the HMW grains after 300 FT (Figure 12I,K). The surface of HMW grains becomes almost entirely covered with thick precipitation crusts after 1,000 FT. Observed crystalline forms are arranged into large clusters that almost entirely
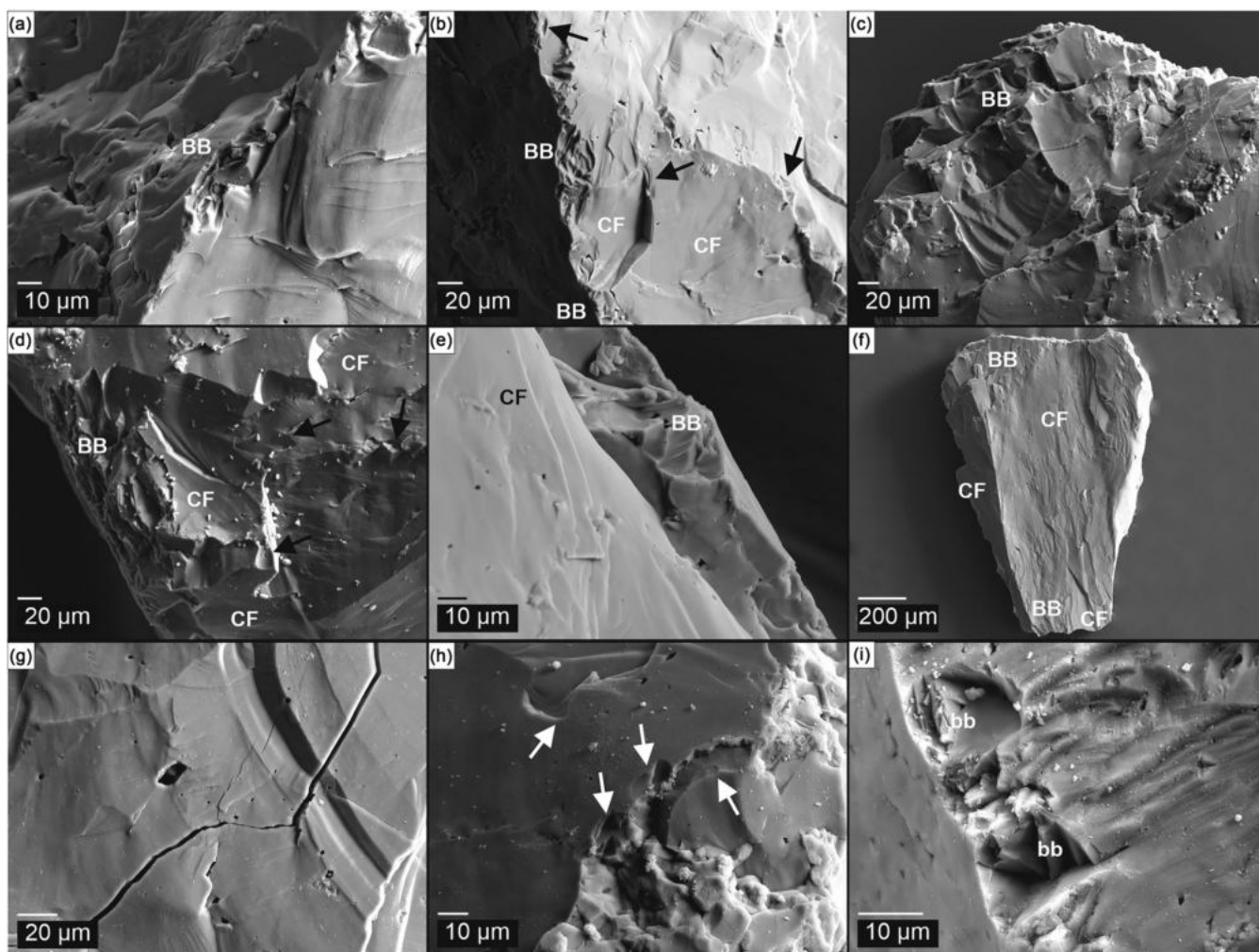
FIGURE 5 Scanning electron microscopic (SEM) images of quartz grains from a sample after 100 freeze–thaw (FT) cycles. (A), BB microtexture on the sharp edges of grain (low mineralized water [LMW] conditions); (B), BB, CF, and CF (arrows) microtextures (LMW conditions); (C), BB microtexture on the sharp edges of grain (high mineralized water [HMW] conditions); (D), BB, CF, and CF (arrows) microtextures (HMW conditions); ∈, CF and overlapping CF (BB) microtextures of a different stage of development (LMW conditions); (F), medium relief of grain (LMW conditions) with BB and CF microtextures; (G), surficial cracks on grain (LMW conditions); (H), CF microtextures on the microstep (arrows) (LMW conditions); (I), Bb microtexture (LMW conditions). The abbreviations used (CF, CF, BB, BB) refer to small- (<10 µm) and large-sized conchoidal fractures (>10 µm), small- (<10 µm) and large-sized breakage blocks (>10 µm), respectively

obliterate the original microrelief of grains (Figure 12J,L). Described crystalline forms, i.e., amorphous crust and spatial crystalline forms, occur generally in micro-depressions (e.g., next to micro-steps) and on the most convex parts of the grains (Figure 12H,J,L).

It is common that different degrees of obliteration of microtextures on grain surfaces are characteristic of individual grains in both the LMW and HMW samples, especially after 700 FT (Figure 7E,F) and 1,000 FT (Figure 8E,F). Therefore, the surface of an individual grain bears precipitation crusts of varying extent and thickness. Crust presence on studied quartz grains replaces surface microrelief and brings about a scaling process that contributes to the exposure of fresh surfaces (Figure 7H). Fragments of exposed fresh, unweathered surfaces are needed for the detachment of spatial crystalline forms, which results in a local discontinuity of the crust (Figure 7F,G). Thick

amorphous precipitation crusts are commonly cracked (Figure 8F). Results of EDX analyses indicate that spatial crystalline forms involve Ca and Na elements, whereas the amorphous crust contains only Mg (Figure 13A–C).

4 | DISCUSSION

Data obtained from this experimental study show microtextural changes on quartz grain surfaces induced by progressive frost action (50, 100, 300, 700, 1,000 FT). Micro-scale frost weathering from 0 to 1,000 FT proves important in resurfacing quartz grains, with surfaces undergoing microtextural changes recognizable on SEM images.
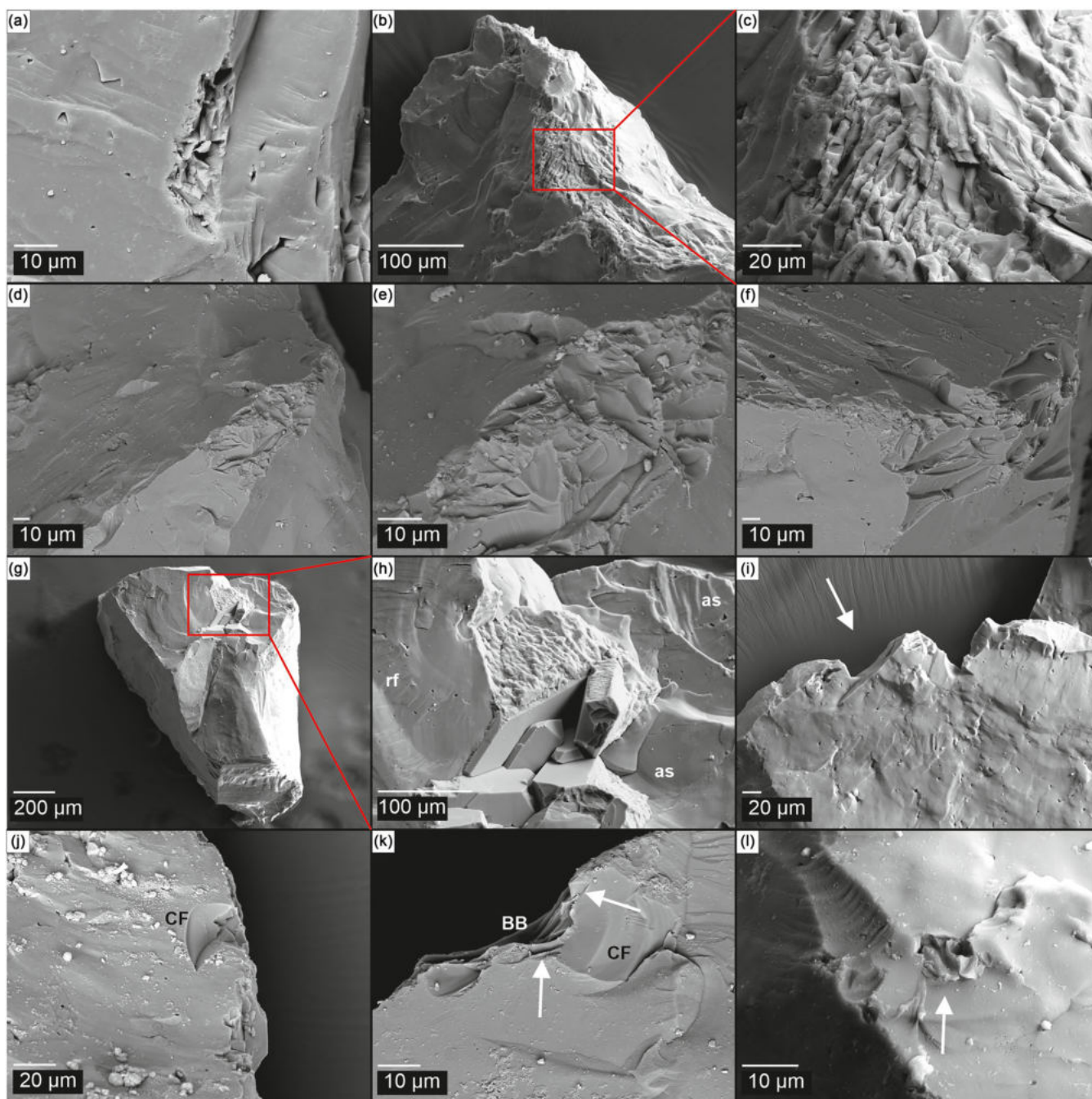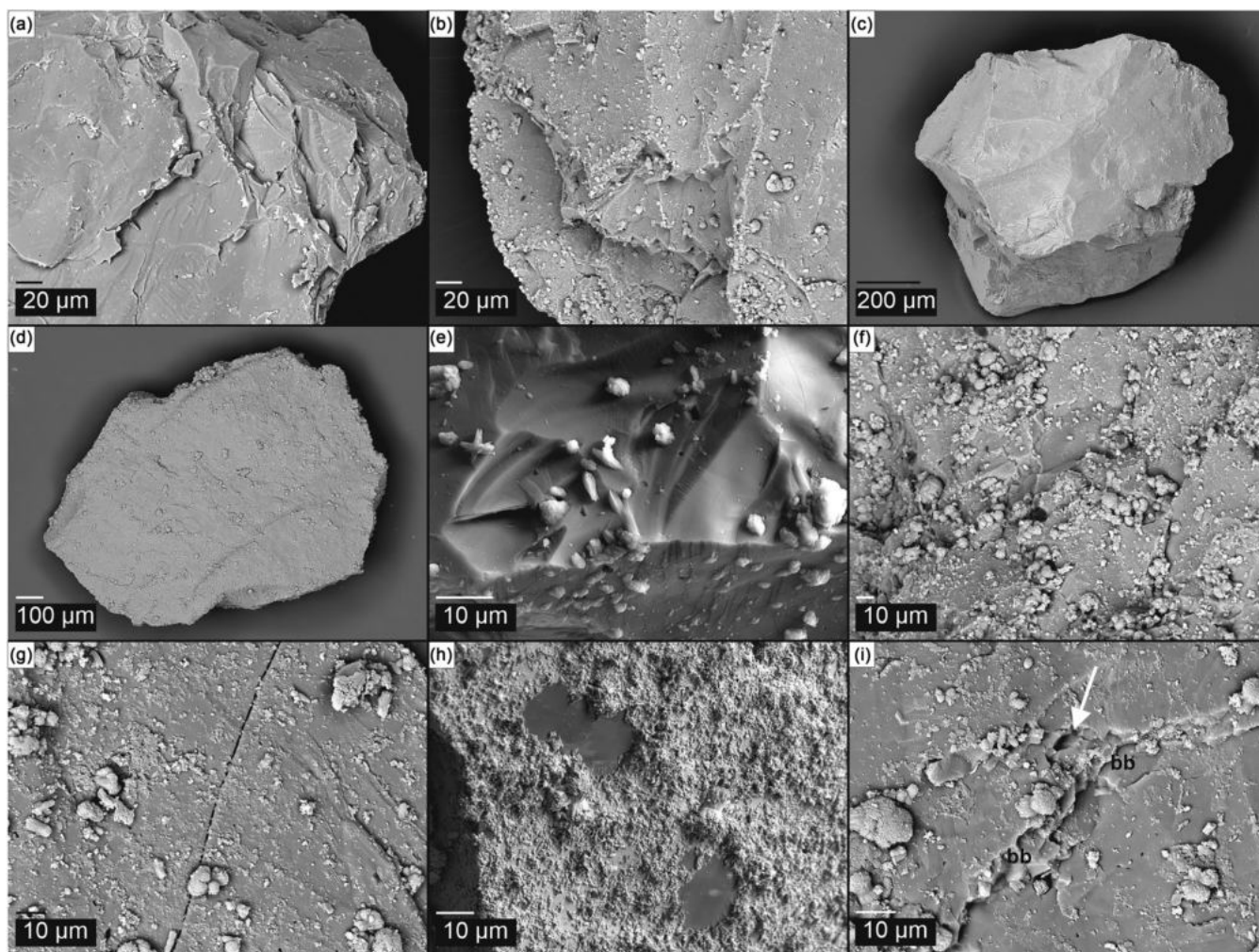
FIGURE 6 Scanning electron microscopic (SEM) images of quartz grains from a sample after 300 freeze–thaw (FT) cycles. (A), BB microtexture on the sharp edges of grain (low mineralized water [LMW] conditions); (B), extensive BB microtexture on the sharp edges of grain (LMW conditions); (C), BB microtexture at a high magnification; (D–F), extensive BB microtexture on the sharp edges of grain (HMW conditions); (G), high relief of grain with CF and sharp edges (LMW conditions); (H), fragment of grain with euhedral silica precipitation, radial fracture (rf), arc-shaped steps (as) (LMW conditions); (I), fragment of grain with CF and sawtooth fractures (arrow; HMW conditions); (J), fresh CF and BB microtextures on the sharp edge of grain (HMW conditions). Thin layer of precipitation crust on the grain surface is visible; (K), fresh CF, CF, and BB microtextures (HMW conditions). Thin layer of precipitation crust on the grain surface is visible; (L), Bb microtexture (arrow) on the grain (HMW conditions) covered with a thin layer of precipitation crust. The abbreviations used (CF, CF, BB, BB) refer to small- (<10 μm) and large-sized conchoidal fractures (>10 μm), small- (<10 μm) and large-sized breakage blocks (>10 μm), respectively [Colour figure can be viewed at wileyonlinelibrary.com]

FIGURE 7 Scanning electron microscopic (SEM) images of quartz grains from a sample after 700 freeze–thaw (FT) cycles. (A), Linear steps and BB microtextures (low mineralized water [LMW] conditions). A thin layer of precipitation crust on the grain surface is visible; (B), BB and CF microtextures (high mineralized water [HMW] conditions). A precipitation crust on the grain surface is visible; (C), fresh surface of grain with high relief and CF (LMW conditions); (D), medium relief of grain with CF microtextures. The surface of grain is obliterated with precipitated crust (HMW conditions); (E), fresh CF and CF with single precipitation forms (LMW conditions); (F), fresh CF on the surface of grain obliterated with precipitated crust (HMW conditions); (G), surficial crack on the surface of grain obliterated with precipitated crust (HMW conditions); (H), fragment of grain surface intensively covered with precipitation crust exhibiting a small area of fresh surface as an effect of scaling (HMW conditions) (I), CF (arrow) and bb microtextures on the surface covered with precipitation crust (HMW conditions). The abbreviations used (CF, CF, BB, BB) refer to small- (<10 μm) and large-sized conchoidal fractures (>10 μm), small- (<10 μm) and large-sized breakage blocks (>10 μm), respectively

4.1 | Evolution of frost-originated mechanical microtextures on the surface of quartz grains

Among the wide range of mechanically induced microtextures found on quartz grain surfaces, four were selected on the basis of frequency of occurrence as diagnostic for frost weathering. These are: cf, CF, bb, and BB as has already been emphasized by other researchers.[1–3,5,10–12] The results of this experiment show the formation of individual microtextures, their evolution, and role in the process of quartz grain weathering, with frost action progressing over time, i.e., from 0 to 1,000 FT. Here we show that frost weathering proceeds differently during its initial phase up to 300 FT

(Figure 11A–C), where the mechanical destruction of grains dominates, and its more advanced phase—from 300 up to 1,000 FT, where chemical activity dominates (Figures 9, 11D,E). This is the first time this phenomenon has been observed and described under controlled laboratory conditions.

The complexity of frost-originated microtextures and their location on grain surfaces indicate that there is a certain order to the evolution of frost-originated microrelief. The process starts with grain cracking along with the development of CF microtextures. Ongoing frost action forces CF modification and contributes to the formation of new frost-originated imprints. We have distinguished three stages (1–3) in the evolution of frost-induced microrelief.
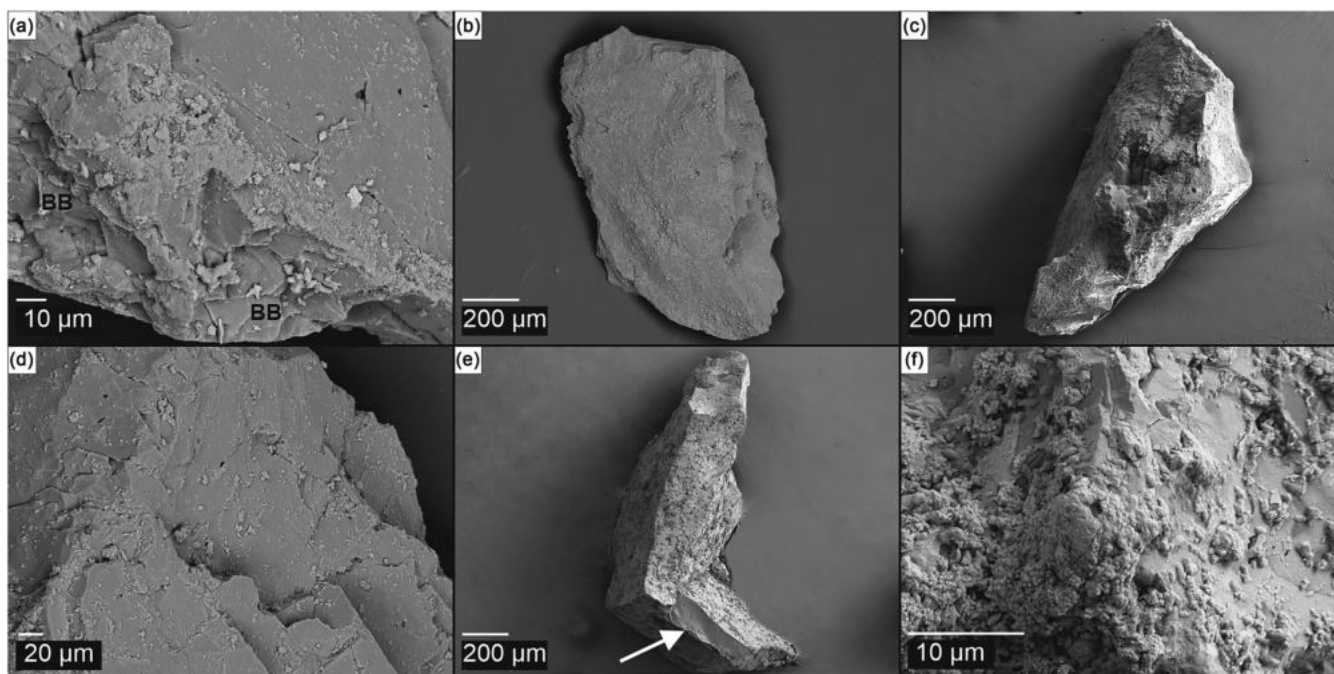
FIGURE 8 Scanning electron microscopic (SEM) images of quartz grain from a sample after 1,000 freeze–thaw (FT) cycles. (A), BB and crack (low mineralized water [LMW] conditions). A thin layer of precipitation crust on the grain surface is visible; (B), medium relief of grain with a precipitation crust on the surface. CF microtextures are visible (LMW conditions); (C), high relief and CF microtextures of grain covered with precipitation crust (high mineralized water [HMW] conditions); (D), CF microtextures on the surface of grain covered with a thin layer of precipitation crust (LMW conditions); (E), high relief of grain whose surface is covered by precipitation crust with fresh CF on the corner (arrow) (HMW condition); (F), thick layer of precipitation crust and obliterated surficial crack (HMW conditions). The abbreviations used (CF, BB) refer to large-sized conchoidal fractures (>10 μm) and large-sized breakage blocks (>10 μm), respectively
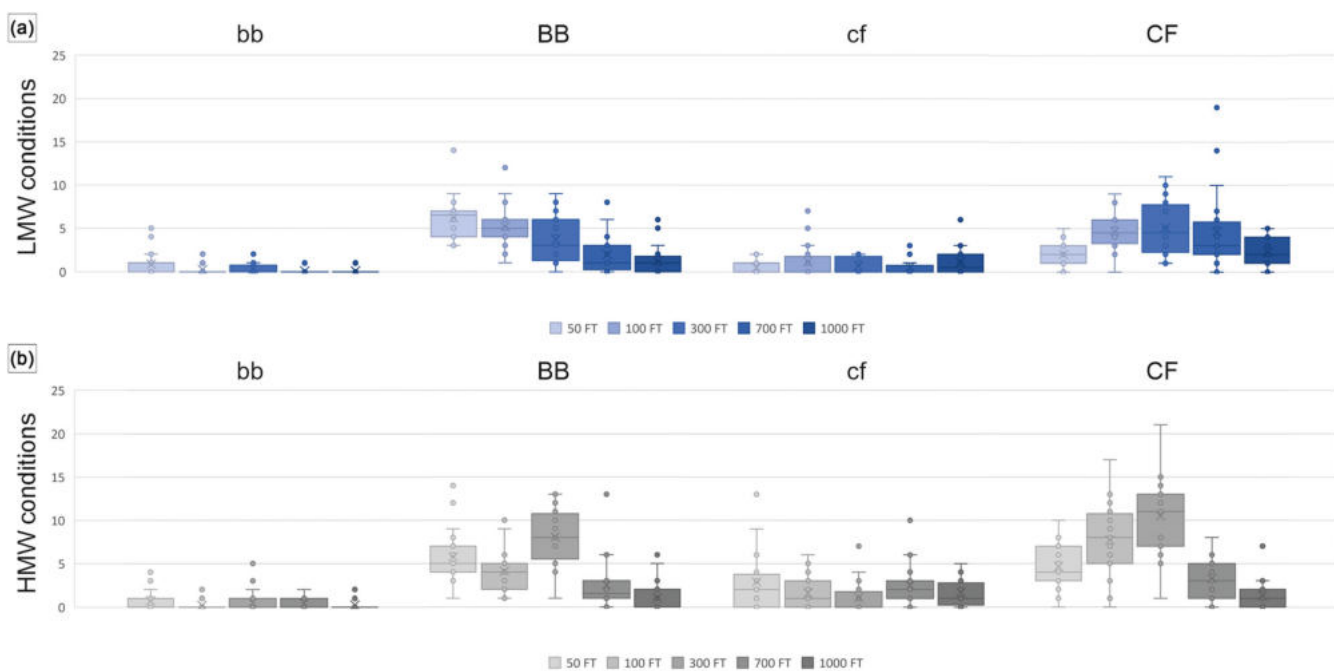
FIGURE 9 Box plot graphs of the relationship between the number of individual microtextures (BB, BB, CF, CF) and the number of FT cycles. (A), Samples weathered at low mineralized water (LMW) conditions; (B), samples weathered at high mineralized water (HMW) conditions. The abbreviations used (CF, CF, BB, BB) refer to small- (<10 μm) and large-sized conchoidal fractures (>10 μm), small- (<10 μm) and large-sized breakage blocks (>10 μm), respectively [Colour figure can be viewed at wileyonlinelibrary.com]
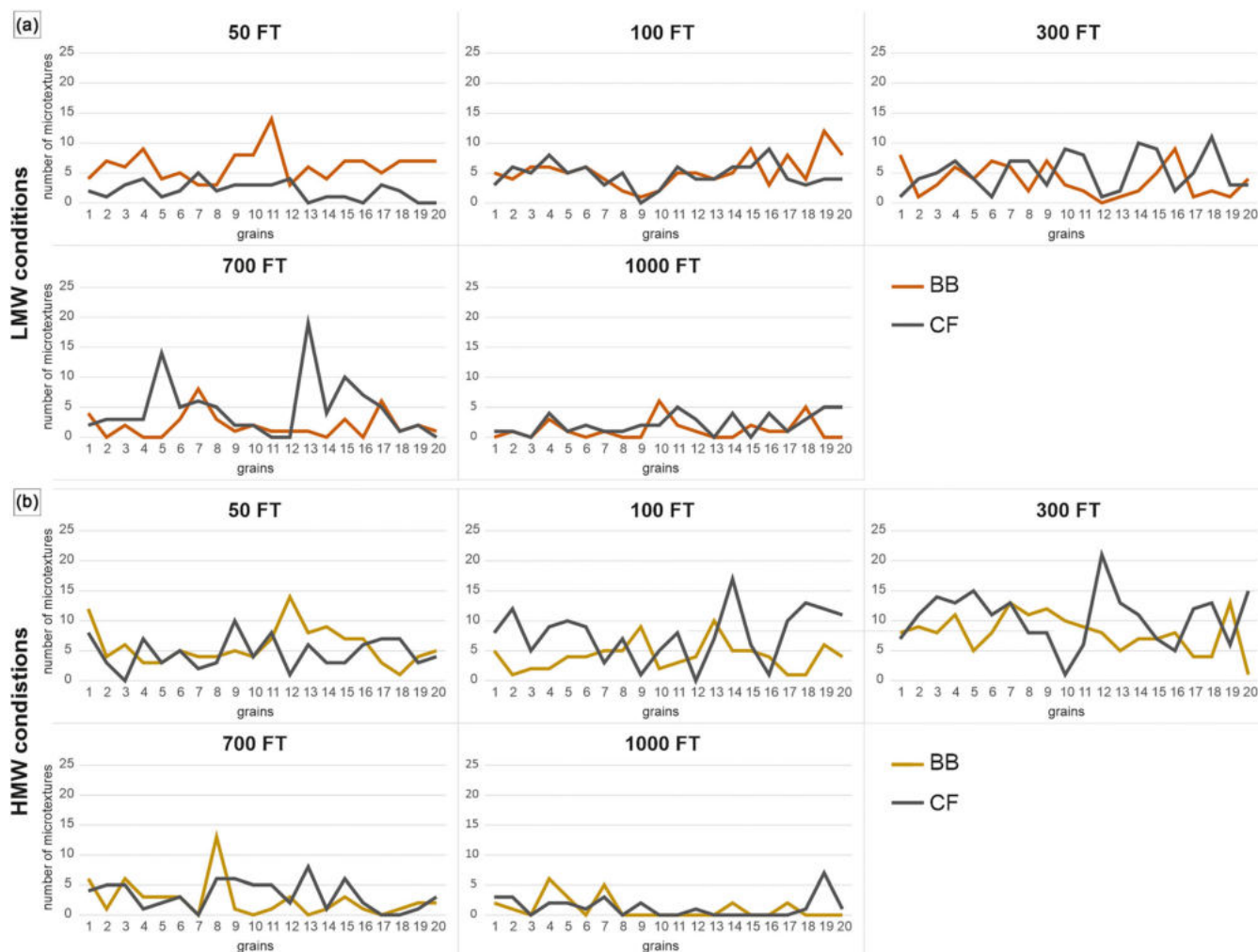
FIGURE 10 Relationship between the number of BB and CF microtextures observed on the individual grain from each sample. (A), Samples weathered at low mineralized water (LMW) conditions; (B), samples weathered at high mineralized water (HMW) conditions. The abbreviations used (CF, BB) refer to large-sized conchoidal fractures (>10 μm) and large-sized breakage blocks (>10 μm), respectively [Colour figure can be viewed at wileyonlinelibrary.com]

Stage 1—initial. Morphologically the simplest surficial microtextures resulting from frost weathering are CF. Their formation on the surface of quartz grains is crystallographically favored,[25,26] but may also depend on grain structure, including the presence of preparation (inherited)/primary defects.[27] We find that this process is reinforced by the presence of euhedral crystals with interlocking overgrowths that contribute to water penetration into the grain through free spaces between crystals (Figure 3C). Moreover, numerous inclusions, especially liquid ones (Figures 3D, 4I, 5G), can also contribute effectively to their formation.[1,3,10–12,28] As samples exposed to frost action are effectively loose grains immersed in water, we associate formation of CF to a hydrofracturing process.[12,16,29,30] The variable number of CFs noted throughout the simulation (after 50–1,000 FT; Appendix A; Figures 2, 9, 10) indicates that their formation occurs continuously.

Frost-originated CFs are characterized by sharp edges and fracture surfaces that are generally smooth and fresh and not covered with additional microtextures (Figures 4E, 5E, 6J, 7E). The only

exception to this are micro-steps imprinted sporadically on the surface of conchoidal fractures. These diagnostic features differ from the CF induced by mechanical crushing during sample preparation before the experimental run. All of the CF observed on the surface of the reference samples bear arc-shaped steps as well as parallel ridges, subparallel linear fractures, linear steps, and radial fractures (Figures 2, 3D,E). Their development is closely related to the high-energy crushing process of multiple FT cycles (10^3). Similar CFs have already been reported on quartz grains from the glacial environment.[2,22,31,32]

Stage 2—progress. Sharp edges of CFs, and micro-steps observed on their surfaces, dominate on the convex parts of grains, areas particularly predisposed to respond to stress induced by FT (Figures 4G,J, 5H, 6K, 7I). At this stage of weathering, these are single microtextures of which sizes do not exceed ~20 μm, or the height of grain microsteps (up to dozen or so μm). Regardless of the lateral dimensions, their vertical dimensions (cf depression depth) are usually very similar. Although it is difficult to measure the depression depth of concave
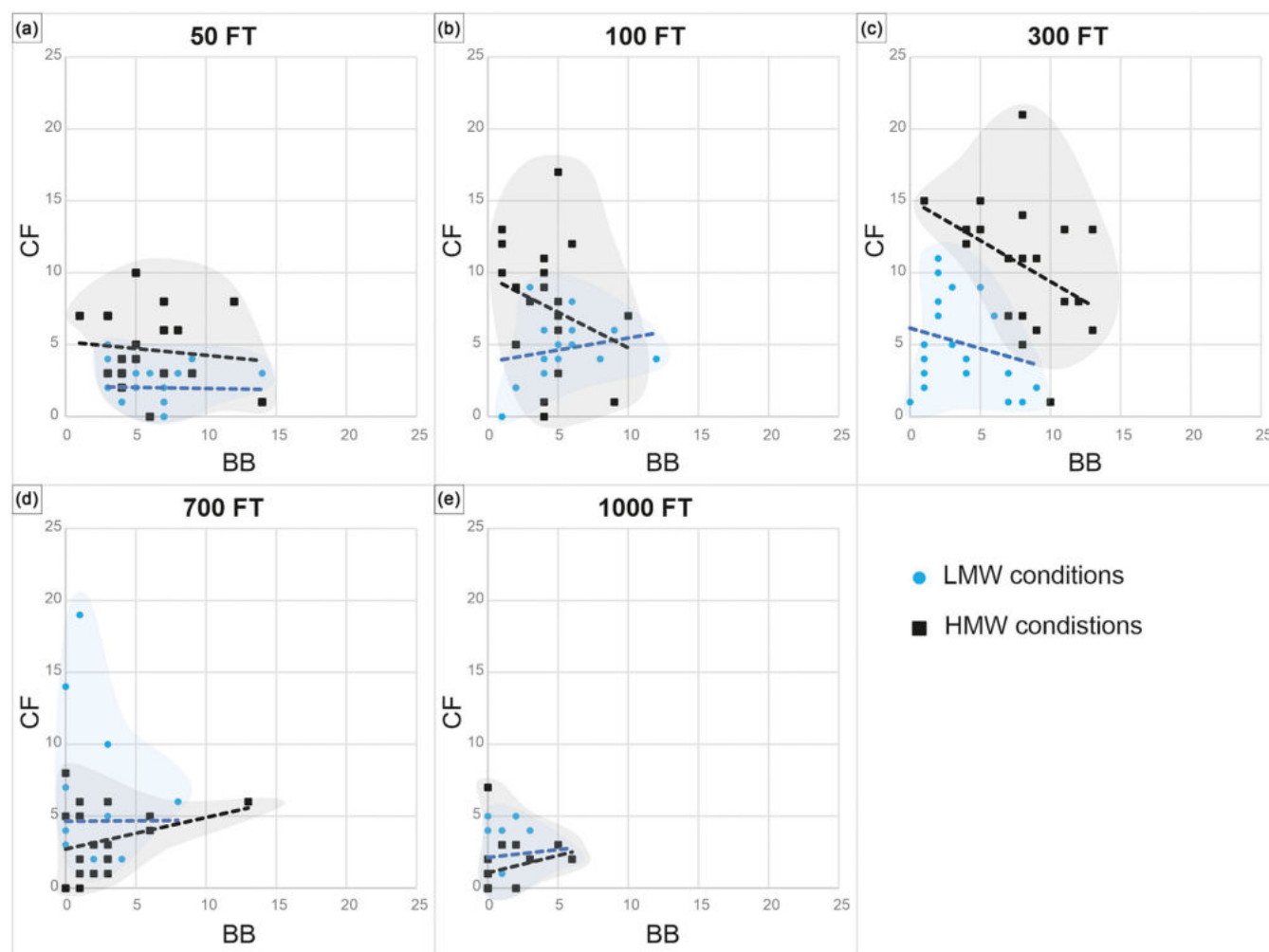
FIGURE 11 Relationship between the number of CF and BB microtextures. (A), Samples after 50 freeze–thaw (FT) cycles; (B), samples after 100 FT; (C), samples after 300 FT; (D), samples after 700 FT; (E), samples after 1,000 FT. The abbreviations used (CF, BB) refer to large-sized conchoidal fractures (>10 μm) and large-sized breakage blocks (>10 μm), respectively [Colour figure can be viewed at wileyonlinelibrary.com]

microtextures on grain surfaces, in the case of cf microtextures, it is estimated at a few micrometers. We consider that their formation may be related to the fact that the outer part of the grain is exposed to the greatest stress and modification due to frequent temperature oscillations across 0°C. The front of freezing water exerts pressure on the unfrozen hygroscopic water surrounding the grain which in turn freezes the combined mass exerting pressure on the grain surface contributing to microcracking/hydrofracturing. This pressure may be as great as several thousand $kg \cdot cm^{-2}$.[33] We recommend identifying this thin outer layer of a quartz grain structure as the *frost-exposed skin* (FES). Its thickness is difficult to determine, but taking into account the (vertical) dimensions of cf, we think that it should not exceed 10–15 μm (Figure 14).

Stage 3—advanced. The most complex microtextures among the frost-originated ones are various sized breakage blocks. We relate their development to the more advanced stage of frost-induced surface modification. These microtextures take different forms—from the small ones (bb; <10 μm) that result from the overlapping of several cfs (Figures 5I, 6L, 7I) up to extensive complexes (BB; >10 μm) that result

from the overlapping of numerous cfs or joining of several bbs (Figures 4A–D, 5A–D, 6A–F, 7A,B). Both bb and BB reveal sharp edges and smooth, fresh surfaces. They are always accompanied by cracks of various sizes (Figure 6C) which clearly indicate that development continues throughout the weathering process. BB and bb are found to be the most complex frost-originated microtextures, and the most microtexturally diversified parts of the grain surface. They are usually found on sharp grain edges and on the convex parts of grains (e.g., micro-cliffs)[3,12] accompanied by euhedral silica participation or, less often, inclusions. Neither BB nor bb was observed on the smooth or concave surfaces of CF, which seem to be non-susceptible to frost weathering (i.e., resistant to the formation of frost-originated microtextures). These microtextures seem to be relatively shallow but nevertheless occupy extensive areas of the grain surface. It can therefore be assumed that the development of these microtextures proceeds laterally along the grain edges with relatively little penetration into the inner parts of grains. We conclude that, similar to cf, the depth of grain penetration by BB and bb is controlled by the FES thickness (Figure 14). However, the areas of bb and BB development are
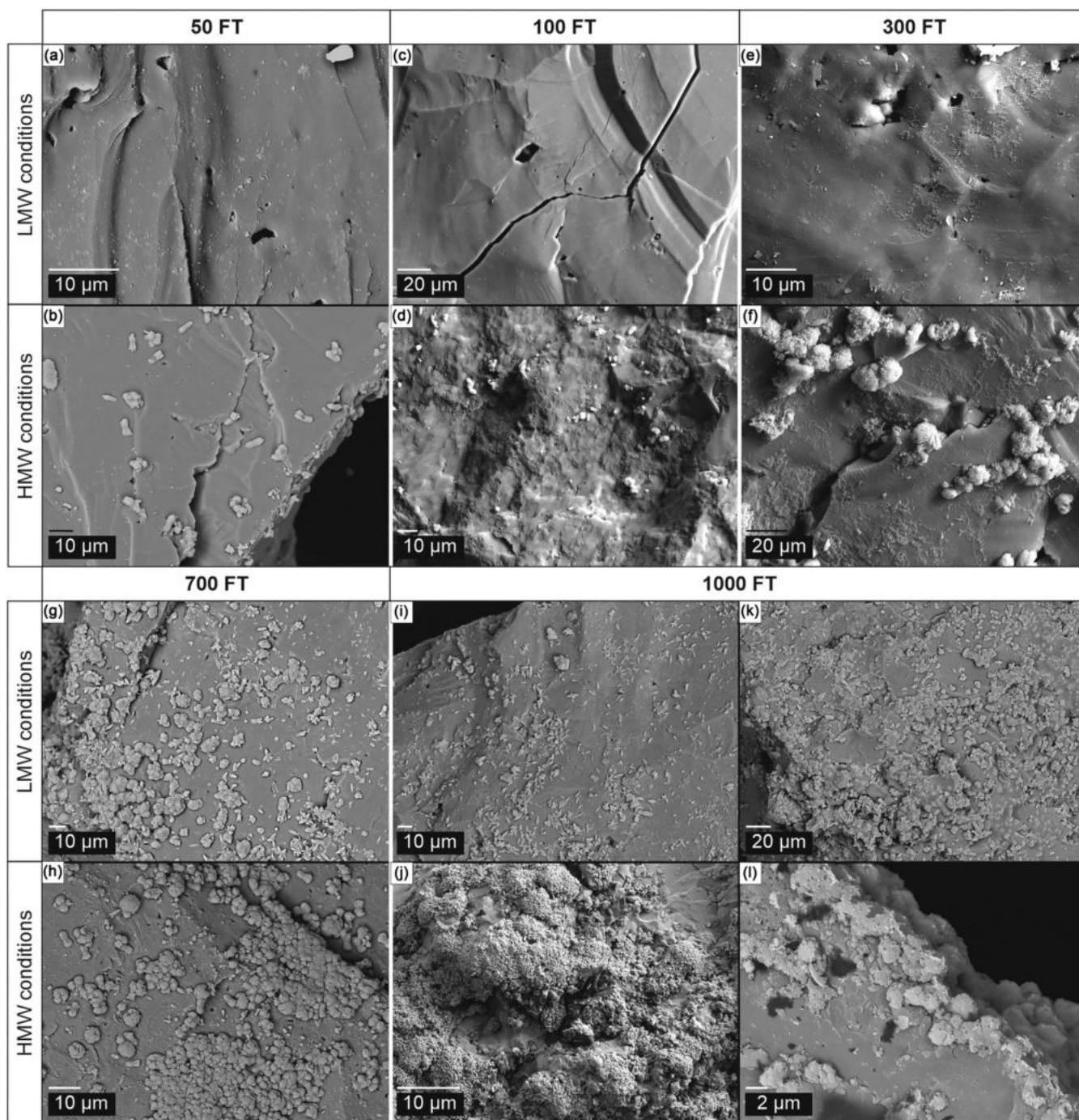
FIGURE 12 Different stages of development of precipitation crust on the surface of grains subjected to frost weathering. (A), Sparse precipitation crust after 50 FT (low mineralized water [LMW] conditions); (B), single crystalline forms after 50 FT (high mineralized water [HMW] conditions); (C), sparse precipitation crust and fresh crack after 100 FT (LMW conditions); (D), single crystalline forms and locally developed precipitation crust after 100 FT (HMW conditions); (E), single crystalline forms and locally developed precipitation cover after 300 FT (LMW conditions); (F), complex crystalline forms and precipitation crust after 300 FT (HMW conditions); (G), crystalline forms after 700 FT (LMW conditions); (H), well-developed precipitation crust after 700 F (HMW conditions); (I), different stages of development of crystalline forms after 1,000 FT (LMW conditions); (J), extensive precipitation crust after 1,000 FT (HMW conditions); (K), extensive precipitation crust after 1,000 FT (LMW conditions); (L), extensive precipitation crust on the sharp edges of grain after 1,000 FT (HMW conditions)

probably restricted to the surficial weakness zones resulting from the destructive activity of frost weathering (e.g., hydrofracturing) and/or association with grain microrelief (e.g., micro-steps) or grain defects (e.g., inclusions, euhedral silica precipitation, interlocking overgrowth). Data obtained from this experimental study indicate that the size and the complexity of the breakage block microtextures change along with
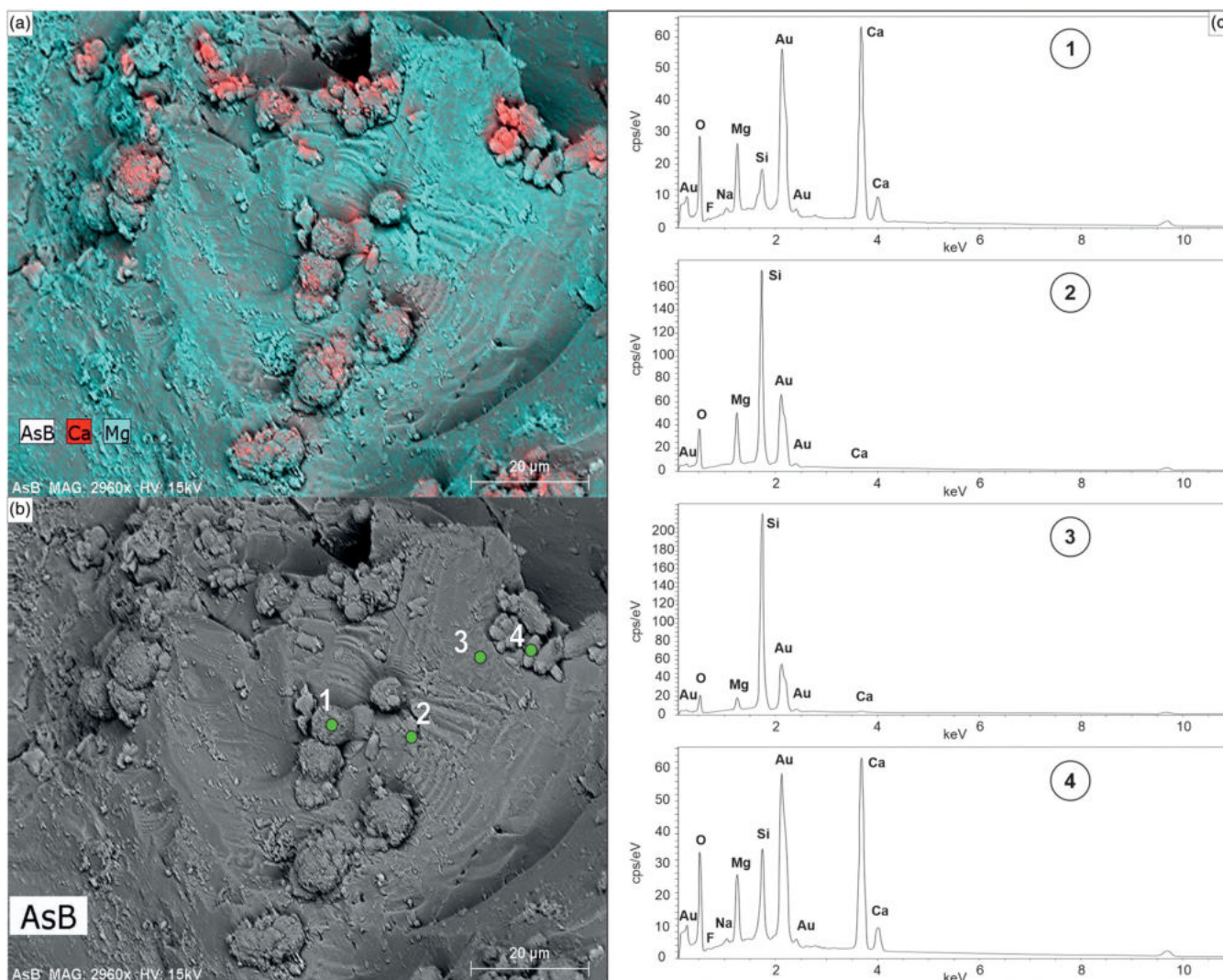
FIGURE 13 The results of the energy-dispersive X-ray spectroscopy (EDX) analyses for different forms of precipitated crust on the surface of the quartz grains. (A), EDX mapping; (B), localization of analyzed points (1–4); (C), chemical composition of precipitation forms at four analyzed points (1–4) [Colour figure can be viewed at wileyonlinelibrary.com]

the progressive frost weathering (number of FT cycles). Small-sized ones are commonly found on the grain surface after 50 FT, while their share clearly decreases on the surface of grains after 300 FT, where more extensive and complex forms dominate (Figure 2).

4.2 | Impact of water mineralization on micro-scale frost weathering

An increase in degree of grain surface coverage by precipitated solutes (i.e., surface crust development) is observed with the progression of the ongoing weathering process (50–1,000 FT; Figure 12). It results from continued cyclic freeze/thaw of mineralized water that contributes to a precipitation of the dissolved ions.[15] The intensity of the crust accretion varies depending on the mineralization of water (LMW, HMW)—the higher the water mineralization, the greater the

intensity of crust development. Up to 300 FT, crust development is relatively slow, manifested by a precipitation of a thin, Mg-rich amorphous crust that covers the surface of both LMW and HMW grains only locally. Single spatial crystalline forms of carbonates can be found rarely (Figure 12A–F). An abrupt increase in surface crust is noted after 300 FT, especially in the case of the HMW samples. It is formed by both amorphous and crystalline forms of precipitated minerals (Figure 12G–L). The precipitated crust covers a large area of grain surfaces, leveling off, and seemingly, forcing obliteration of surficial microtextures. This is evidenced by a decrease in the number of frost-originated features (Figure 9). Kowalkowski[5] emphasized that the importance of surficial microfeatures originating from a chemical decomposition (i.e., crust growth) increases in the case of grains weathered in alkaline environments under cold climatic conditions. Successive additions of freshwater to samples, compensated by evaporation loss, resulted in a gradual increase in the concentration of
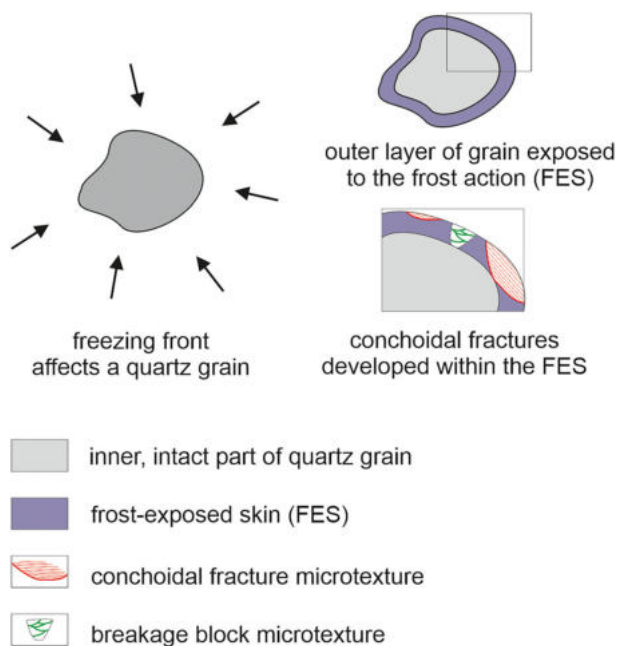
FIGURE 14 Theoretical scheme of the frost-exposed skin (FES) as an effect of multicycle freeze thaw [Colour figure can be viewed at wileyonlinelibrary.com]

dissolved components. In consequence, a decrease in the number of frost-originated microtextures (Figure 9) implies that the solution became saturated, along with increased grain porosity, probably after 300–700 FT in the case of HMW and LMW samples, respectively (Figure 12). An abrupt increase in the rate of surficial crust development noted throughout the experiment may also have occurred in the natural environment in areas of poorly developed drainage. For example, within the active layer of permafrost where processes of water evaporation (during thawing) and freezing prevail contributing to a precipitation of dissolved substances.[5] Moreover, the concentration of dissolved substances in permafrost-surrounding water tends to increase due to the restricted permeability of permafrost-affected sediments and thus limited water circulation.[16] This is evidenced by a common occurrence of encrusted grains within cold climate environments.[5,8,24] This process of surface crust development may be enhanced by the sorption properties of clay minerals (e.g., smectites) involved in the precipitation process.

A significant transition in grain surface change during frost weathering is observed after 700 FT (Figure 11). From this point, a chemical aspect of weathering prevails over a mechanical one contributing to a decline in the number of mechanically induced surficial microtextures (Figure 9). When the precipitation crust (amorphous or crystalline forms of precipitated minerals) becomes thick enough, it usually cracks followed by a scaling process. Consequently, a fresh, unweathered surface of quartz grains reveals (Figure 7H) the extent of scaling. This may be attributed to a relatively high porosity of the precipitation crust that contributes to its effective penetration by the frost front.[5,8]

4.3 | Advancement of frost weathering vs refreshing of the weathered surface

It is widely assumed that with a more advanced stage of frost weathering, the greater number of frost-originated microtextures is imprinted on the surface of quartz grains.[3,8] However, the obtained results in this study clearly indicate that this relationship is not that simple as the individual samples contain grains that bear frost-induced microtextures attributed to different stages of frost-originated micro-relief evolution (stages 1–3; see Section 4.1.).

One of the most common microtextures on the surface of quartz grains affected by frost weathering in the periglacial environment is CF.[1,3,5,9–12] Frost contributes to a destruction of quartz grains by detachment of part or most of the grain after the application of mechanically induced stress, either by sample preparation here, or by FT in field settings. This results in the modification of grain size, and the addition of morphological and microrelief attributes by continual FT. It therefore seems that the number of frost-originated CF microtextures is crucial in determining the intensity of micro-scale frost weathering.

Lab microtexture analysis of grain surfaces reveals a specific relationship between a number of individual microtextures (i.e., bb, BB, cf, CF). It is particularly clear for the BB and CF correlation (Figure 10). A high number of BBs are recognized on grain surfaces observed together with a low number of CFs, and vice versa. Assuming that a predominance of CF microtextures indicates the initial stage of weathering (stage 1) and prevailing BBs indicate the advancement of weathering (stage 3), it may be concluded that formation of CF microtextures contributes to a renewal of frost-originated microrelief. The weathered surface of quartz grains that bear cf/bb/BB microtextures becomes refreshed; that is, cracking and detachment cause the fragments of fresh, unweathered surfaces to be exposed and the grain to lack some/most of the mechanical frost-originated microtextures (crack → CF → cf → bb → BB; Figure 15). Therefore, several grain populations can be distinguished in each weathered sample regardless of the stage of weathering (50–1,000 FT). These are (i) mature grains—characterized by a relatively high number of BBs and low number of CFs; frost action has affected their surfaces without refreshment (e.g., LMW samples: grain nos. 2, 19, 20 after 50 FT; grain nos. 19, 20 after 100 FT; grain nos. 1, 6, 16 after 300 FT; and HMW samples: grain nos. 3, 12 after 50 FT; grain no. 9 after 100 FT; grain nos. 10, 19 after 300 FT; grain no. 8 after 700 FT; Figure 10); (ii) immature grains—bearing a relatively high number of CFs and low number of BBs; their surface is refreshed once or several times during the weathering process (e.g., LMW samples: grain no. 16 after 100 FT; grain nos. 8, 10, 11, 14, 15, 18 after 300 FT; grain nos. 5, 13, 15 after 700 FT; grain no. 20 after 1,000 FT; and HMW samples: grain no. 9 after 50 FT; grain nos. 2, 5, 14, 17, 18 after 100 FT; grain nos. 5, 12, 17, 18, 20 after 300 FT; grain no. 13 after 700 FT; grain no. 19 after 1,000 FT; Figure 10); (iii) other grains with a moderate number of CF and BB microtextures; both the initial (CF) and advanced (BB) products of the frost weathering can be observed on the surface of these grains (e.g., LMW samples: grain nos. 8, 12 after
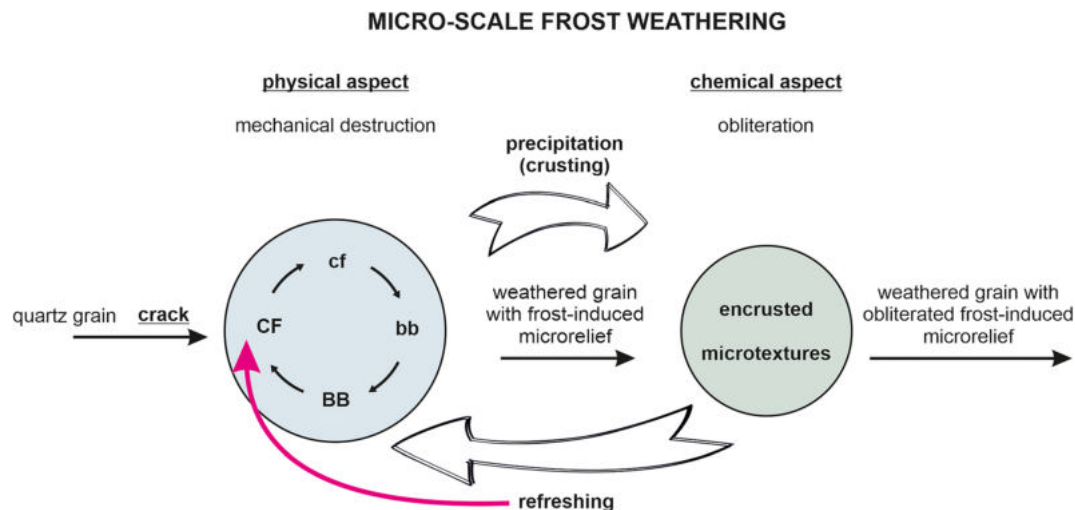
MICRO-SCALE FROST WEATHERING

FIGURE 15 Range of micro-scale frost weathering and the relationship between physical and chemical aspects of process [Colour figure can be viewed at wileyonlinelibrary.com]

50 FT; grain nos. 5, 6, 7, 10, 13, 18 after 100 FT; grain nos. 5, 7, 20 after 300 FT; grain nos. 10, 17, 18, 19 after 700 FT; grain nos. 5, 7, 17 after 1,000 FT; and HMW samples: grain nos. 2, 5, 10, 16 after 50 FT; grain nos. 7, 8 after 100 FT; grain nos. 1, 7, 15 after 300 FT; grain nos. 3, 6 after 700 FT; grain nos. 5, 6 after 1,000 FT; Figure 10).

Besides the decrease in the number of surficial microtextures, this renewal of the frost-originated microrelief is also evidenced by changes in the dominant grain microrelief, which shifts from predominantly medium/high to low surfaces dominating as the weathering process progresses (Figure 2). A discrete modification of grain shape changes from angular to sub-angular during the weathering process stemming from surficial encrustation, which is especially enhanced on grain edges (Figures 8F, 12J, L). This encrustation may be associated with the formation of CF and other frost-originated microtextures (cf, bb, BB) found on the most convex grain surfaces, which may create enough friction for moving water to loosen ions resulting in enhanced precipitation on the sharp edges of grains. However, more research is needed to confirm this hypothesis. The effects of refreshing of grain surfaces (equated with the *renewal of frost weathering*) become particularly visible as the crust-enhanced process proceeds. This is especially evident on the LMW and HMW grains after 1,000 and 700 FT, respectively (Figures 9, 12G–L). Furthermore, a varying degree of encrustation of the surface of a single grain (Figure 8E) and on the surface of grains originating from a single sample (Figure 9) indicates the refreshing of the surface as well.

Frost-induced refreshment of quartz grain surfaces may occur many times at each stage of the frost weathering process. The cycle of development of frost-originated microrelief (crack → CF → cf → bb → BB) is thus repeated (Figure 15). Therefore, care must be taken when interpreting the surficial effects of frost weathering on grains that have suffered an unknown number of FT cycles.

The presence of cracked grains that bear CF microtextures may be considered a record of surface refreshing processes that occur under periglacial conditions. A significant increase in their number as compared to underlying sediments is observed in the fossil to active-layer deposits originating over time intervals. This is especially the case at the bottommost part of active-layer deposits.[3,12]

5 | CONCLUSIONS

The results of this experimental simulation of micro-scale frost weathering of sand-sized quartz grains subjected from 0 up to 1,000 FT under two water mineralization levels (dissolved solute concentrations—LMW, HMW) indicate that:

1. Two predominant outcomes in the course of micro-scale frost weathering can be identified: a physical aspect of the process, manifested by the occurrence of cf, CF, bb, BB microtextures dominating up to 300 FT cycles; afterwards, a chemical aspect results where occurrence of precipitation crusts and obliteration of grain microrelief prevail.

2. Under these laboratory conditions, four mechanical microtextures can be identified as diagnostic for the frost weathering process: cf, CF, bb, BB.

3. Three stages in the evolution of frost-induced microrelief can be distinguished: (i) initial stage—when the development of CF predominates, (ii) progress stage—with the increased development of cf, and (iii) advance stage—with the dominance of bb and BB growth.

4. The evolution of frost-induced microrelief may be influenced and interrupted by a process of refreshing a weathered surface. In consequence, a grain with a smaller number of frost-originated microtextures is subjected to further weathering and the process of frost weathering is thus renewed.

5. The microtextural record of frost weathering is written into the surface of quartz grains subjected to weathering under the same

conditions (temperature regime, water availability, mineralization), conditions that may be different in nature.

6. Frost weathering of the quartz grains immersed in HMW is more effective than those immersed in LMW.

7. Assuming the stages of FT repeat in nature with quartz grains having undergone FT cycles in the active layer of permafrost-affected or seasonally frost-affected soils, scientists in the cold region might be expected to follow up with tests of grains under HMW and LMW conditions to determine if the requisite microtexture assemblages can be observed in other environmental conditions and landscapes.

ACKNOWLEDGEMENTS

DATA AVAILABILITY STATEMENT

The data that support the findings of this study are available from the corresponding author upon reasonable request.

ORCID

Martyna E. Górska 🔟 https://orcid.org/0000-0002-8460-2812

REFERENCES

1. Schwamborn G, Schirrmeister L, Frütsch F, Diekmann B. Quartz weathering in freeze–thaw cycles: experiment and application to the el'gygytgyn crater lake record for tracing siberian permafrost history. *Geogr Ann*. 2012;94(4):481-499. doi:10.1111/j.1468-0459.2012.00472.x

2. Woronko B. Frost weathering versus glacial grinding in the micromorphology of quartz sand grains: processes and geological implications. *Sediment Geol*. 2016;335:103-119. doi:10.1016/j.sedgeo.2016.01.021

3. Woronko B, Pisarska-Jamroży M. Micro-scale frost weathering of sand-sized quartz grains: micro-scale frost weathering of quartz grains. *Permafrost Periglac*. 2016;27(1):109-122. doi:10.1002/ppp.1855

4. Konishchev VN. *Formation of dispersed rocks in the cryolithosphere*. Novosibirsk: Nauka; 1981 197 pp.

5. Kowalkowski A. Holocene rusty and rusty brown soils in the tundra and taiga of middle Sveden. *Soil Sci Annu*. 1988;XLIX:29-44.

6. Konishchev VN, Rogov VV. *Methods of Cryolithic investigations*. Izdatel'stvo Moskovskogo Gosudarstvennogo Universiteta; 1994 [in Russian].

7. Degórski M, Kowalkowski A. The use of SEM morphoscopy in researching the litho-pedogenetic environments evolution of Late Pleistocene and Holocene. *Geographia Polonica*. 2011;84:1-38. doi:10.7163/GPol.2011.S1.3

8. Woronko B, Hoch M. The development of frost-weathering microstructures on sand-sized quartz grains: examples from Poland and Mongolia: development of frost-weathering microstructures on sand quartz grains. *Permafrost Periglac*. 2011;22(3):214-227. doi:10.1002/ppp.725

9. Schwamborn G, Mayer H, Fedorov G, Schirrmeister L, Hubberten H. Ground ice and slope sediments archiving late Quaternary paleoenvironment and paleoclimate signals at the margins of El'gygytgyn impact crater, NE Siberia. *Quatern Res*. 2006;66(2):259-277. doi:10.1016/j.yqres.2006.06.007

10. Konishchev VN, Rogov VV. Investigations of cryogenic weathering in Europe and northern Asia. *Permafrost Periglac*. 1993;4(1):49-64. doi:10.1002/ppp.3430040105

11. Konishchev VN, Lebedeva-Verba MP, Rogov VV, Stalina EE. *Cryogenesis of modern and Late Pleistocene deposits Altai and periglacial region of Europa*. Moscow: GEOS; 2005.

12. Woronko B. Micromorphology of quartz grains as a tool in the reconstruction of periglacial environment.In:Churski P. ed., *Contemp Issues Polish Geogr*. 2012:111-131.

13. Dietzel M. Impact of cyclic freezing on precipitation of silica in me–SiO2–H2O systems and geochemical implications for cryosoils and -sediments. *Chem Geol*. 2005;216(1-2):79-88. doi:10.1016/j.chemgeo.2004.11.003

14. Schwamborn G, Meyer H, Schirrmeister L, Fedorov G. Past freeze and thaw cycling in the margin of the El'gygytgyn crater deduced from a 141 m long permafrost record. *Clim Past*. 2014;10(3):1109-1123. doi:10.5194/cp-10-1109-2014

15. Dietzel M. Dissolution of silicates and the stability of polysilicic acid. *Geochim Cosmochim Acta*. 2000;64(19):3275-3281. doi:10.1016/S0016-7037(00)00426-9

16. French H. *The periglacial environmnet*. Wiley-Blackwell, 544 pp.; 2017. doi:10.1002/9781119132820.

17. Lautridou JP, Ozouf JC. Experimental frost shattering: 15 years of research at the Centre de Géomorphologie du CNRS. *Prog Phys Geog*. 1982;6(2):215-232. doi:10.1177/030913338200600202

18. Murton JB, Coutard JP, Lautridou JP, et al. Experimental design for a pilot study on bedrock weathering near the permafrost table. *Earth Surf Process Landf*. 2000;25(12):1281-1294. doi:10.1002/1096-9837(200011)25:12%3C1281::AID-ESP137%3E3.0.CO;2-U

19. Wright JS. The spalling of overgrowths during experimental freeze–thaw of a quartz sandstone as a mechanism of quartz silt production. *Micron*. 2000;31(6):631-638. doi:10.1016/S0968-4328(99)00074-8

20. Mahaney WC, Rutter NW. Amino acid D/L ratio distributions in two late quaternary soils in the Afroalpine zone of Mount Kenya, East Africa. *Catena*. 1989;16(3):205-214. doi:10.1016/0341-8162(89)90008-8

21. Mahaney WC. Late Quaternary rock glaciers, Mount Kenya, Kenya. *J Glaciol*. 1980;25(93):492-497. doi:10.1017/S0022143000015331

22. Mahaney WC. *Atlas of sand grain surface textures and applications*. Oxford University Press; 2002 237 pp.

23. Helland PE, Holmes MA. Surface textural analysis of quartz sand Grains from ODP site 918 off the southeast coast of Greenland suggests glaciation of southern Greenland at 11 ma. *Palaeogeogr Palaeoecol*. 1997;135(1-4):109-121. doi:10.1016/S0031-0182(97)00025-4

24. Kowalkowski A, Kocoń J. Microtextures of cryopedogenic weathering in soils of the mountain tundra of middle Sweden. *Soil Sci Annu*. 1998;XLIX:53-59.

25. Moss AJ. Origin, shaping and significance of quartz sand grains. *J Geol Soc Aust*. 1966;13(1):97-136. doi:10.1080/00167616608728607

26. Moss AJ, Green P. Sand and silt grains: predetermination of their formation and properties by microfractures in quartz. *J Geol Soc Aust*. 1975;22(4):485-495. doi:10.1080/00167617508728913

27. Górska ME, Woronko B, Kossowski TM, Pisarska-Jamroży M. Microscale frost-weathering simulation – changes in grain-size composition and influencing factors. *Catena*. 2022;212(106106):-1-20. doi:10.1016/j.catena.2022.106106

28. Konishchev VN. A cryolithic method for estimating palaeotemperature conditions during formation of the ice complex and subaerial periglacial sediments. *Earth's Cryoshere* Special Issue. 2003:59-64.

29. Matsuoka N, Murton J. Frost weathering: recent advances and future directions. *Permafrost Periglac*. 2008;19(2):195-210. doi:10.1002/ppp.620

30. Walder J, Hallet B. A theoretical model of the fracture of rock during freezing. *Geol Soc am Bull*. 1985;96(3):336-346. doi:10.1130/0016-7606(1985)96%3C336:ATMOTF%3E2.0.CO;2

31. Mahaney WC. Pleistocene and Holocene glacier thicknesses, transport histories and dynamics inferred from SEM microtextures on quartz particles. *Boreas*. 1995;24(4):293-304. doi:10.1111/j.1502-3885.1995.tb00781.x

32. Vos K, Vandenberghe N, Elsen J. Surface textural analysis of quartz grains by scanning electron microscopy (SEM): from sample preparation to environmental interpretation. *Earth Sci Rev*. 2014;128:93-104. doi:10.1016/j.earscirev.2013.10.013

33. Davidson GP, Nye JF. A photoelastic study of ice pressure in rock cracks. *Cold Reg Sci Technol*. 1985;11(2):141-153. doi:10.1016/0165-232X(85)90013-8

APPENDIX A

Number of surficial microtextures found on the surface of individual grain. A—Samples weathered at LMW conditions; B—Samples weathered at HMW conditions

A	Number of grain	1	2	3	4	5	6	7	8	9	10	11	12	13	14	15	16	17	18	19	20	Sum	Average
LMW conditions																							
50 FT	BB < 10	0	0	1	4	1	2	0	0	0	1	2	0	5	0	0	0	0	1	0	0	17	1
	BB > 10	4	7	6	9	4	5	3	3	8	8	14	3	6	4	7	7	5	7	7	7	124	6
	CF < 10	1	2	0	1	0	2	0	0	0	2	1	0	1	0	0	0	0	0	0	0	10	1
	CF > 10	2	1	3	4	1	2	5	2	3	3	3	4	0	1	1	0	3	2	0	0	40	2
	cracks	7	11	2	18	6	5	5	3	9	2	20	0	0	9	4	4	1	5	6	3	120	6
100 FT	BB < 10	0	0	1	0	0	0	0	0	0	0	0	0	0	0	1	0	2	1	0	0	5	0
	BB > 10	5	4	6	6	5	6	4	2	1	2	5	5	4	5	9	3	8	4	12	8	104	5
	CF < 10	0	0	1	1	0	0	0	0	0	0	5	2	0	3	3	7	1	0	0	0	23	1
	CF > 10	3	6	5	8	5	6	3	5	0	2	6	4	4	6	6	9	4	3	4	4	93	5
	cracks	1	3	3	0	7	6	4	3	0	2	2	2	1	1	4	3	0	1	6	3	52	3
300 FT	BB < 10	0	1	1	0	0	0	1	0	2	1	0	0	0	0	0	0	0	0	0	0	6	0
	BB > 10	8	1	3	6	4	7	6	2	7	3	2	0	1	2	5	9	1	2	1	4	74	4
	CF < 10	2	1	0	2	0	0	0	1	0	0	1	2	0	0	2	0	2	0	1	0	14	1
	CF > 10	1	4	5	7	4	1	7	7	3	9	8	1	2	10	9	2	5	11	3	3	102	5
	cracks	7	1	2	5	3	5	7	2	1	2	1	2	3	0	1	9	1	3	5	0	60	3
700 FT	BB < 10	0	0	1	0	0	0	1	0	0	0	0	0	0	0	0	0	0	0	0	0	2	0
	BB > 10	4	0	2	0	0	3	8	3	1	2	1	1	1	0	3	0	6	1	2	1	39	2
	CF < 10	0	0	1	0	0	0	0	0	0	0	2	3	0	0	0	2	3	0	0	0	11	1
	CF > 10	2	3	3	3	14	5	6	5	2	2	0	0	19	4	10	7	5	1	2	0	93	5
	cracks	4	0	6	0	2	2	2	6	1	2	0	1	0	0	3	0	2	0	3	0	34	2
1,000 FT	BB < 10	0	1	0	0	0	1	0	0	0	0	0	0	0	0	0	0	0	0	0	0	2	0
	BB > 10	0	1	0	3	1	0	1	1	0	6	2	1	0	0	2	1	1	5	0	0	24	1
	CF < 10	0	2	3	1	0	6	1	0	0	0	3	2	2	0	0	1	0	1	0	0	22	1
	CF > 10	1	1	0	4	1	2	1	1	2	2	5	3	0	4	0	4	1	3	5	5	45	2
	cracks	2	2	1	4	2	1	3	0	0	5	3	0	3	2	0	6	0	2	6	3	45	2

B	number of grain	1	2	3	4	5	6	7	8	9	10	11	12	13	14	15	16	17	18	19	20	sum	average
HMW conditions	50 FT																						
	BB < 10	1	4	2	0	1	1	0	1	0	0	1	0	3	0	0	0	0	0	0	0	14	1
	BB > 10	12	4	6	3	3	5	4	4	5	4	7	14	8	9	7	7	3	1	4	5	115	6
	CF < 10	6	4	9	2	2	3	1	0	6	0	3	1	0	13	3	0	0	0	3	1	57	3
	CF > 10	8	3	0	7	3	5	2	3	10	4	8	1	6	3	3	6	7	7	3	4	93	5
	cracks	27	2	14	4	5	7	8	9	16	13	10	25	3	5	7	6	8	7	3	3	182	9
	100 FT																						
	BB < 10	0	0	0	0	0	0	0	0	0	0	0	0	0	1	1	0	0	0	2	0	4	0
	BB > 10	5	1	2	2	4	4	5	5	9	2	3	4	10	5	5	4	1	1	6	4	82	4
	CF < 10	0	4	0	0	1	3	0	0	0	2	3	2	5	6	0	0	1	3	1	1	32	2
	CF > 10	8	12	5	9	10	9	3	7	1	5	8	0	7	17	6	1	10	13	12	11	154	8
	cracks	5	1	0	3	2	2	2	0	2	5	1	1	5	6	4	2	0	12	7	10	70	4
	300 FT																						
	BB < 10	3	0	0	1	0	0	0	5	1	0	0	0	1	0	0	0	0	0	0	0	11	1
	BB > 10	8	9	8	11	5	8	13	11	12	10	9	8	5	7	7	8	4	4	13	1	161	8
	CF < 10	3	3	0	1	0	0	0	4	0	7	0	0	1	0	1	2	0	0	0	0	22	1
	CF > 10	7	11	14	13	15	11	13	8	8	1	6	21	13	11	7	5	12	13	6	15	210	11
	cracks	8	8	0	2	2	2	2	3	1	3	9	5	2	3	0	0	2	2	6	1	61	3
	700 FT																						
	BB < 10	1	0	0	1	0	0	0	1	1	0	0	0	2	0	1	1	0	0	1	0	9	0
	BB > 10	6	1	6	3	3	3	0	13	1	0	1	3	0	1	3	1	0	1	2	2	50	3
	CF < 10	10	4	3	1	0	3	1	2	6	1	6	0	2	1	3	0	2	1	2	1	49	2
	CF > 10	4	5	5	1	2	3	0	6	6	5	5	2	8	1	6	2	0	0	1	3	65	3
	cracks	6	7	0	3	0	0	0	2	2	0	6	2	0	3	11	4	3	0	2	1	52	3
	1,000 FT																						
	BB < 10	1	0	0	0	0	0	0	0	0	0	0	0	0	1	0	1	2	0	0	0	5	0
	BB > 10	2	1	0	6	3	0	5	0	0	0	0	0	0	2	0	0	2	0	0	0	21	1
	CF < 10	4	4	1	1	0	2	2	1	0	3	3	1	1	5	2	0	0	2	1	0	33	2
	CF > 10	3	3	0	2	2	1	3	0	2	0	0	1	0	0	0	0	0	1	7	1	26	1
	cracks	1	3	0	3	4	0	2	1	0	0	1	0	2	7	0	1	1	4	1	0	31	2

Note: FT, freeze–thaw; HMW, highly mineralized water; LMW, low mineralized water.

ZAŁĄCZNIK 3

ATTACHMENT 3

Górska M.E., Woronko B., Kossowski T.M., 2023. Factors influencing the development of microtextures on cold-climate aeolian quartz grains revealed by experimental frost action. *Permafrost and Periglacial Processes*, 2023, 1-25. https://doi.org/10.1002/ppp.2179

RESEARCH ARTICLE

WILEY

Factors influencing the development of microtextures on cold-climate aeolian quartz grains revealed by experimental frost action

Martyna E. Górska[1] ⓘ | Barbara Woronko[2] ⓘ | Tomasz M. Kossowski[3] ⓘ

[1]Institute of Geology, Adam Mickiewicz University, Poznań, Poland

[2]Faculty of Geology, University of Warsaw, Warsaw, Poland

[3]Faculty of Human Geography and Planning, Adam Mickiewicz University, Poznań, Poland

Correspondence
Martyna E. Górska, Adam Mickiewicz University, Institute of Geology, Krygowskiego 12, 61-680 Poznań, Poland.
Email: mgorska@amu.edu.pl

Abstract

Aeolian-originated quartz grains of coarse-sand size (0.5–1 mm) were subjected to experimental frost weathering. A total of 1,000 freeze–thaw cycles with temperature ranges from −5 to +10°C were simulated under full water availability conditions. Scanning electron microscope microtextural analysis of grain surfaces conducted after 0, 50, 100, 300, 700, and 1,000 freeze–thaw cycles resulted in different-sized conchoidal fractures and breakage blocks as frost-induced microtextures. The vast majority of these microtextures were encountered on the most convex parts of aeolian grains and their number increased with ongoing freeze–thaw cycles. However, the number of recorded frost-originated microtextures remained relatively small up to 700 freeze–thaw cycles and increased after 1,000 freeze–thaw cycles. Transmission electron microscope microstructural analysis of grains after 0, 100, and 1,000 freeze–thaw cycles showed both primary (e.g., inclusions, grain boundaries) and secondary (e.g., cracks) defects in quartz crystals. The frequency of the latter remained unexpectedly low. The susceptibility of aeolian-originated sand-sized quartz grains to frost-induced modifications is interpreted here to depend mainly on their internal characteristics. These include aeolian-driven development of a subsurface *impact zone* that determines the depth to which frost-originated microtextures develop. The *outer impact zone* consists of a thin layer of surficial crust and a series of more or less parallel ridges arranged into mechanically upturned plates. The *inner impact zone* consists of intact or cracked quartz crystals. The susceptibility of aeolian-originated quartz grains to frost-induced modifications depends therefore on a combination of internal (i.e., original crystallography of quartz grains) and external (i.e., aeolian and frost processes acting upon the grains) factors.

KEYWORDS
frost-exposed skin, micro-frost weathering, outer/inner impact zone, SEM, statistical analysis, TEM

1 | INTRODUCTION

Wind is one of the main agents of physical weathering in the periglacial zone.[1–5] Aeolian sediments are commonly found in the periglacial

zone, in the form of both dunes and cover sands, but also as a part of reworked deposits of other origins, such as glacial, fluvial, fluvioglacial, and slope deposits. The second major factor that affects the physical weathering in periglacial environments is frost weathering operating within the active layer.[2,6–9] Investigations of active-layer deposits of paleo-permafrost have indicated that aeolian sand-sized grains, among others, are one of the most susceptible to frost-weathering modifications.[7] The microtextural effects of frost weathering on their surface include extensive complexes of overlapping small conchoidal fractures arranged in breakage block microtextures.[7,10] According to Górska & Woronko,[11] these microtextures may be considered evidence of an advanced stage of micro-scale frost weathering. The high number and complexity of frost-induced imprints observed on the surface of aeolian-originated quartz grains provide evidence of their high susceptibility to frost action. However, any microtextural studies on quartz grains weathered under natural conditions require consideration of the duration of weathering-process activity, and in the case of frost weathering, the number of freeze–thaw (FT) cycles, which have a major impact on the micro- and macro-scale effects of frost weathering.[11–15] The general question is how many FT cycles are needed to develop such an extensive and complex frost-originated microrelief on the grain surface. Therefore, the assumption of the high susceptibility of aeolian grains to frost-weathering surficial modifications[7] is here called into question. The present study contributes to the verification of this assumption by investigation of frost weathering of aeolian grains simulated under controlled laboratory conditions. The simulation of 1,000 FT cycles provided information on: (a) how FT activity modifies the surface of cold-climate aeolian quartz grains over time, (b) what external (related to processes acting upon the surface of quartz grains) and internal (related to crystallography of quartz grains) factors influence the formation of frost-induced microtextures on their surface, and (c) the impacts of antecedent aeolian activity (i.e., grain-to-grain collisions as the last process that acted upon the grains prior to their deposition) on the susceptibility of quartz grains to frost weathering.

2 | MATERIALS AND METHODS

2.1 | Materials

Sediments of aeolian origin were collected from a Pleistocene inland dune located in the Polish Lowlands (Sławiny site, east Poland; Figure 1). These deposits belong to the European Sand Belt (ESB).[16] Development of cold inland dune forms in this area continued from the Oldest Dryas to Early Holocene[3,4,17–20] under the influence of prevailing westerly winds.[21] It has therefore been assumed that the source material of the studied dune sediments were, among others, fluvial sediments originated from the Vistula River valley located about 100 km to the west (Figure 1).

The sample from the stoss side of a dune was gathered from a depth beyond the range of present-day ground freezing (i.e., ∼3 m) to ensure that these sediments are not disturbed by modern biochemical weathering. The studied quartz grains were classified as showing a different degree of modification of their surfaces by aeolian processes (from nonvisible aeolian-induced modifications, to modifications visible only on the most concave parts of grains, and well-rounded grains with surfaces entirely imprinted by aeolian modifications) which is
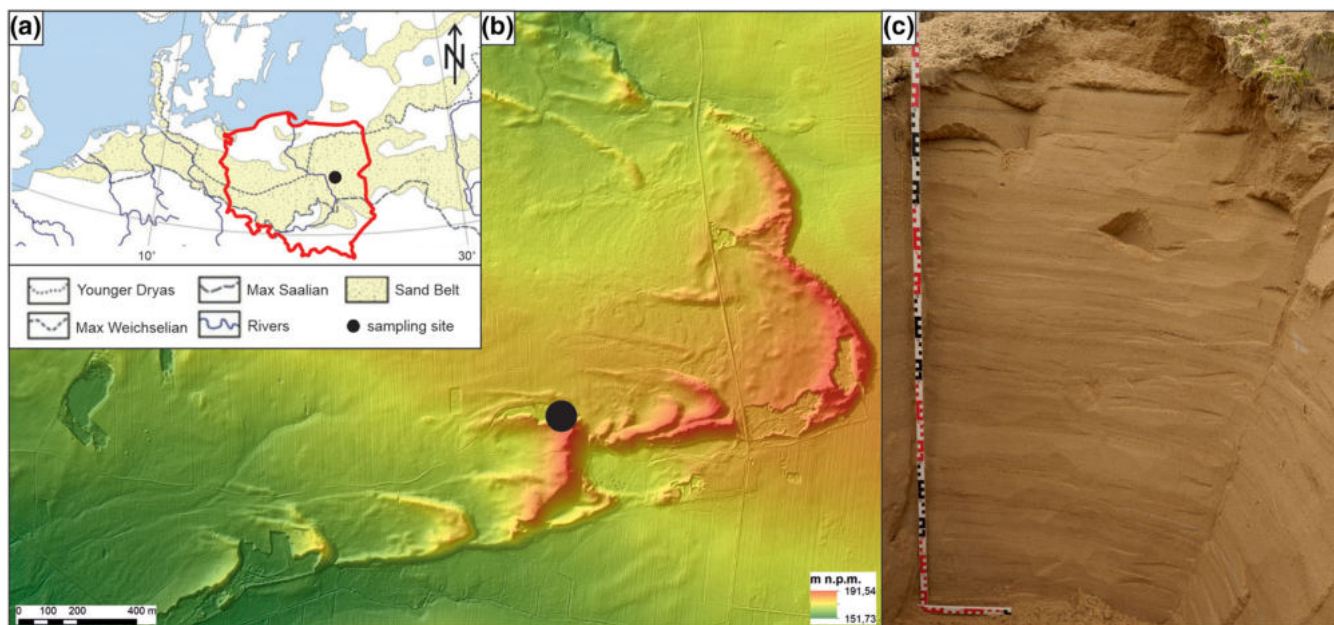

FIGURE 1 Localation of the sampling site. (a)—map of the European Sand Belt with sampling site marked (black dot); (b)—LiDAR image of cold-climate inland dune at the Sławiny site (marked with black dot); (c)—structure of a parabolic dune observed on the stoss side of the studied dune [Colour figure can be viewed at wileyonlinelibrary.com]

indicative of aeolian reworking as the last process acting over the surface of grains prior to burial. Therefore, the imprints of past permafrost-related processes (e.g., Younger Dryas[19,20,22]) have probably undergone aeolian modification.

The grains were sieved to separate the coarse sand fraction (0.5–1 mm) and viewed under a binocular microscope to exclude grains other than quartz from further analysis. Separated coarse sand-sized quartz grains intended for the frost-weathering simulation were divided into equal samples of ∼2 g, stacked on individual Petri dishes, and immersed in water (Table 1).

2.2 | Experimental design

Frost weathering with fixed temperature fluctuations from −5 to +10°C (Figure 2) was simulated using a freeze–thaw device. A commercial upright freezer was equipped with a software program and programmed for automatic and defined temperature changes, permanent condensate drainage, and automatic defrosting. These settings prevented the internal condensation of water vapor and crystallization of ice crystals, respectively. All internal shelves of the device had an individual cooling and heating system, which provided uniform temperature and humidity levels on each shelf.

One complete FT cycle lasted 4 hr and involved freezing (2 hr; temperature decreased to −5°C), constant (1 hr; temperature remained at −5°C) and thawing (1 hr; temperature increased to +10°C) stages. The average freezing rate during the freezing stage

TABLE 1 Detailed characteristic of water

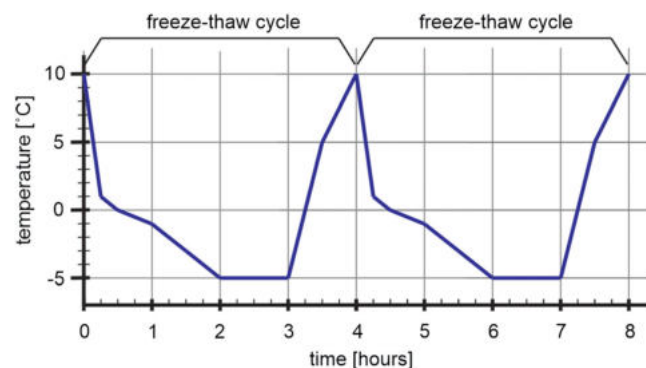| Dissolved solids	Amount (mg/L)
HCO_3^-	121.06
F^-	0.07
Mg^{2+}	5.37
Ca^{2+}	36.39
Na^{2+}	8.29
Sum of dissolved solids (mineralization)	213.09

FIGURE 2 Temperature regime employed in the experimental study [Colour figure can be viewed at wileyonlinelibrary.com]

reached ∼0.06°C/min. The temperature regime used in the study has been adapted to complete freezing and thawing of water and corresponds to that of previous experimental studies.[13,23,24] Details on the experimental design are provided by Górska & Woronko[11] and Górska et al.[14] Water content was controlled macroscopically and water was replenished approximately every 2 days to avoid its complete evaporation. The samples were collected after 50, 100, 300, 700, and 1,000 FT cycles and allowed to dry at room temperature.

2.3 | Laboratory analysis

Aeolian-originated sediments (including both quartz and other grains) were sieved through a sieve column (2–0.063 mm) using a mechanical shaker to determine the grain-size distribution (according to Folk & Ward's classification[25]; using the Gradistat package[26]) and modes of aeolian transport.[27,28]

Microscopic investigation was conducted on sand-sized (0.5–1 mm) quartz grains using a scanning electron microscope (SEM; ZEISS Sigma VP apparatus) at the Scanning Microscope and Microanalysis Laboratory (Faculty of Geology, University of Warsaw). Microtexture analyses followed widely used schemes.[10,29,30] Samples of about 20 randomly selected grains[30,31] from both reference (0 FT cycle) and each frost-weathered sample (subjected to 50, 100, 300, 700, and 1,000 FT cycles) were analyzed. Quartz grains of a given sample were mounted together on a single specimen stub, coated with gold, and placed in the SEM under vacuum. The surface of each quartz grain was scanned at low (∼100–150×) and high (∼1,000×) magnification. Microtextural description included the following grain features: grain edges (sharp/rounded), frequency of fractures (low/high), microrelief diversity (low/medium/high) and presence of surficial microtextures (present vs. absent). The latter refers to both remnants of the original grain microrelief and frost-induced imprints observed on the visible side of the grain. The microtextural features observed on the surfaces of the studied grains include mechanically originated (e.g., conchoidal fracture, breakage blocks, arc-shaped steps, linear step, micro-steps, parallel ridges, subparallel linear fractures, sawtooth fractures, radial fractures) and chemically originated (e.g., dissolution surface, dulled surface, solution crevasses, solution pits) imprints.[10,29,30,32] The percentage frequency of occurrence of the individual microtextures in a given sample (∼20 grains) was estimated. Frost-induced microtextures (i.e., small-[<10 μm] and large-sized [>10 μm] conchoidal fractures and breakage blocks[7,10,15,33]; assigned here as cf, CF, bb, BB, respectively, according to terms introduced by Górska & Woronko[11]; Table 2) and cracks were counted on each grain. Their sum and the average value was estimated for a given sample and analyzed statistically. Furthermore, a location of each frost-induced microtexture (i.e., the microtexture on/within which it occurred) was noted.

The distinction between similar microtextures created by simulated frost action and aeolian processes (that modified the surface of grains prior to sediment deposition) was based on the general appearance of these microtextures. All frost-originated imprints resulting

from the experimental simulation (recognized after each sampling stage, i.e., 50, 100, 300, 700, and 1,000 FT cycles) were sharp-shaped and fresh (bearing no evidence of the amorphous precipitation). The formation of frost-induced mechanical and chemical microtextures occurs simultaneously.[11,14,34] As a consequence, frost-induced mechanical microtextures formed at a given stage of weathering (after a given number of FT cycles) are always fresher than those recognized at the previous stages of weathering or in the reference sample. This distinguishes them from the grain surface and from the crusted surface of similar aeolian-originated microtextures (i.e., cf, CF, bb, BB). The list and definitions of all abbreviations and terms used in the following sections are provided in Table 2.

Based on low-magnification SEM micrographs depicting the whole grain under study, the morphoscopy analysis of Cailleux[35] (with modifications from Goździk[36] and Mycielska-Dowgiałło & Woronko[37]) was performed on all of the studied grains to assess the character of surface and rounding. The share of individual grain types (NU—fresh grain, RM—matt surface of well-rounded grain, EL—shiny well-rounded grain, EM/RM—matt surface on the edges of semirounded grain, EM/EL—shiny semirounded grain, C—cracked grain, others)[37] reflecting different sedimentary environments were determined. Further, the elongation index (here the *En* index) was calculated according to:

$$En = 1 - \frac{width}{length} \qquad (1)$$

with values ranging from 0 for shapes symmetrical in all axes (e.g., circle or square; high sphericity) to 1 for nonsymmetrical, elongated shapes (low sphericity).[38]

Supplementary to SEM examinations, transmission electron microscopy (TEM) analysis was performed at GeoForschungsZentrum Potsdam (GFZ; Germany). Microstructural (TEM) analysis aimed at direct observation of mechanical changes within studied quartz grains, providing an in-depth (micro- up to nanoscale) view of their internal structure. Grains of relatively high roundness were selected from samples after 0, 100, and 1,000 FT cycles during binocular examination. Focused ion-beam (FIB) milling techniques were applied for site-

TABLE 2 List and definitions of all abbreviations and terms used in the text

Abbreviation/term	Description	Text references
cf	Small-sized (<10 μm) conchoidal fractures	Figure 10E
CF	Large-sized (>10 μm) conchoidal fractures	Figure 10F,I Figure 16E
bb	Small-sized (<10 μm) breakage blocks	Figure 10
BB	Large-sized (>10 μm) breakage blocks	Figure 10F,I Figure 16–D,F,I,M
I type cf/ CF (cf$_I$/CF$_I$)	Relatively shallow and flat microforms of seashell shape; their surfaces may be overprinted with, e.g., linear steps, micro-steps, arc-shaped steps; representative of most sedimentary environments	Section 4.2.2. Figure 10G Figure 16B,G,H,N Figure 17A
II type cf/ CF (cf$_{II}$/CF$_{II}$)	Relatively deep microforms with regular shape resembling angular blocks encountered on the surface of quartz grains as cuboid-shaped micro-cavities	Section 4.2.2. Figure 10E,H Figure 16A,E,G,J,K,L,N Figure 17A
Lag time	Time span between the occurrence of the factor that modifies the original microrelief on the grain surfaces (i.e., frost action; 0 FT cycles) and the occurrence of the effects of this process (i.e., frost-induced microrelief; after *n* FT cycles)	Section 4.1.
Abrasion fatigue	Outermost layer of quartz grain that contains the disrupted lattice due to the broken surface structure; it consists of small cracks, dislocations, broken Si–O bonds, projecting vertices, and thus abnormal solubility[50]	Section 4.2.2.
Impact zone	Subsurface part of aeolian quartz grains directly exposed to aeolian-induced stress, and thus showing distinctive internal structure resulting from high-energy grain-to-grain collisions in the cold-climate aeolian environment; it consists of *outer* and *inner* parts	Section 4.2.2. Figure 17
Outer impact zone	Outermost part of the aeolian quartz grain; it forms an amorphous layer consisting of a thin layer of surficial crust and a series of more or less parallel ridges arranged into mechanically upturned plates; it corresponds to *abrasion fatigue*	
Inner impact zone	Inner part of the *impact zone* located below the *outer impact zone*; it consists of a crystalline form of quartz	
Host grain	Innermost part (core) of the aeolian quartz grain consisting of aeolian-unaffected quartz; its internal structure probably corresponds to the processes of quartz formation and does not show any evidence of aeolian activity	Section 4.2.2. Figure 16H Figure 17
Frost-exposed skin (FES)	Outer part of the grain exposed to the greatest stress and modifications due to frequent temperature oscillations across 0°C; it may partially or fully overlap with the *impact zone*	Section 4.2.2. Figure 17

specific sample preparation from the most concave parts of grains. A total of six thin sections (two from each sample) of Pt-coated quartz grains were prepared to study internal inhomogeneities of crystalline quartz grains, including their dislocation and/or deformation structures. This analysis was based on the work of Wenk,[39] which is probably the most comprehensive study on the TEM method to date.

2.4 | Statistical analysis

Several methods were applied for quantitative analysis of microtextures encountered on the surface of the studied quartz grains (Fisher's moments coefficient of skewness, box plot analysis, Hampel filter, Dixon's Q test).

Fisher's moments coefficient of skewness was used to measure the asymmetry of the data distribution (i.e., number of frost-induced microtextures counted for each sample) according to $A = \frac{\mu_3}{\mu_2^{3/2}}$, where μ_i is the ith central moment of the distribution. Sample distributions show positive skewness (asymmetry) for $A > 0$; otherwise the skewness is negative.

The detection of outliers (i.e., grains within one sample, characterized by the numbers of frost-induced microtextures being significantly different from their mean value for the sample) resulted from: (a) analysis of box plots, (b) use of the Hampel filter method, and (c) application of Dixon's Q test. Through approach (a), we identified outliers as those observations whose values are greater than $Q_3 + 1.5 \cdot IQR$ or less than $Q_1 - 1.5 \cdot IQR$, where the Q is the ith quartile of the distribution and IQR is the interquartile range.

The Hampel filter method[40] identifies the outliers in a given distribution without testing the assumption of its normality. Observations falling outside the range: $[M(X) - 4.5 \cdot MAD, M(X) + 4.5 \cdot MAD]$, where $M(X)$ is the median of the set $X = \{X_1, X_2, ..., X_n\}$, MAD is the median absolute deviation, $MAD = M(|X - M(X)|)$, are referred to as outliers.

Dixon's Q test[41] is intended for small ($n < 30$) samples that meet the normality of data distribution, and verifies whether a given observation is an outlier. The formula for this statistic is $Q = \frac{g}{r}$, where g is the absolute value of the difference between the potential outlier and the nearest observation, and $r = max(X) - min(X)$. The null hypothesis that the observation is not an outlier is rejected at the significance level α, if $Q > Q_{\alpha,n}$, where $Q_{\alpha,n}$ is the critical value of Dixon's Q distribution. The normality of distribution was tested using a Shapiro–Wilk test.[42]

3 | RESULTS

The obtained data set includes: (a) the grain-size distribution of aeolian sediment (Figure 3a), (b) microtextural analysis (SEM) of reference (0 FT cycle) and frost-weathered quartz grains (after 50, 100, 300, 700, and 1,000 FT cycles; Figures 4 and 5), (c) microstructural analysis (TEM) of quartz grains (after 0, 100, and 1,000 FT cycles; Figure 6), and (d) statistical analysis (Fisher's moments coefficient of skewness, box plot analysis, Hampel filter, Dixon's Q test; Table 3) of the frost-originated microtextures recorded on the surfaces of weathered quartz grains (Figures 7 and 8).
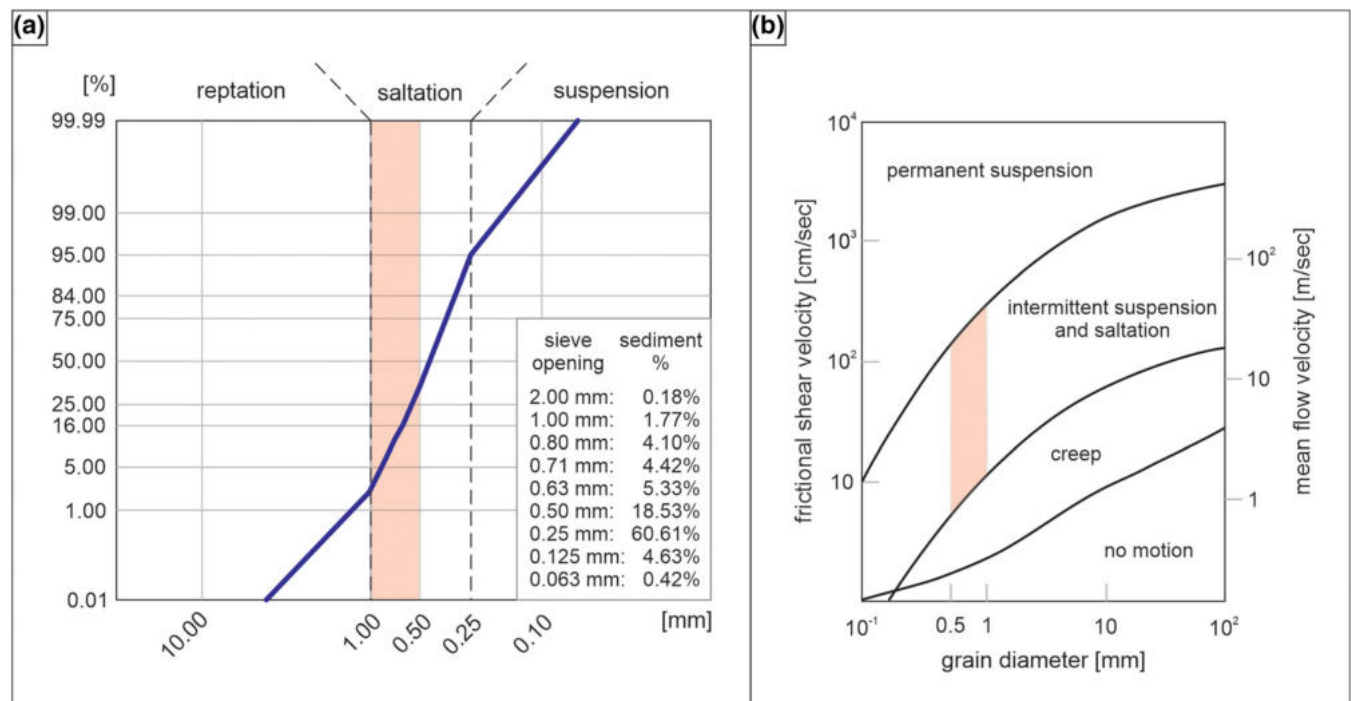

FIGURE 3 Grain-size distribution and sediment transport. (a)—cumulative percentage frequency curve of aeolian sediment under study plotted on a probability scale; (b)—modes of sand transport and fields of transport modes for quartz sand on Earth (modified after Brookfield[52]) [Colour figure can be viewed at wileyonlinelibrary.com]

type of microtexture / FT cycles	0	50	100	300	700	1000
low relief	◑	◑	◑	◑	◑	◑
medium relief	◔	◐	◐	◔	◐	◐
high relief	⊗	⊗	⊗	⊗	⊗	⊗
high frequency fractures	⊗	⊗	⊗	⊗	⊗	◔
low frequency fractures	⊙	⊙	⊙	⊙	⊙	●
edge rounding	⊙	⊙	⊙	⊙	⊙	⊙
sharp features	⊗	⊗	⊗	⊗	⊗	◔
abrasion fatigues	⊗	⊗	⊗	⊗	⊗	⊗
abrasion feature	⊙	⊙	⊙	⊙	⊙	⊙
fresh surface	◔	◔	◑	◐	●	⊙
anastomosis	⊗	⊗	⊗	⊗	⊗	◔
amorphous ppt	⊙	⊙	⊙	⊙	⊙	⊙
dissolution surface	⊗	◔	◔	◔	⊗	◔
dulled surface	◔	◔	◔	◔	⊗	◔
caverns	⊗	◔	◔	⊗	◔	◔
lattice shattering	⊗	⊗	⊗	⊗	⊗	⊗
oriented etch pits	⊗	⊗	⊗	⊗	⊗	⊗
solution crevasses	⊗	◔	◔	⊗	⊗	◔
solution pits	⊗	⊗	⊗	⊗	⊗	◔
arc-shaped steps	⊗	◔	◔	◔	◔	◔
breakage blocks (<0.010mm)	◔	⊗	◔	◔	◔	◑
breakage blocks (>0.010mm)	◔	◔	◔	◔	◐	●
chattermarks	⊗	⊗	⊗	⊗	⊗	⊗
conchoidal fractures (<0.010mm)	◐	◐	◐	◑	◑	●
conchoidal fractures (>0.010mm)	⊗	◔	◔	◐	◑	●
fracture faces	⊗	⊗	⊗	⊗	⊗	◔
linear steps	⊗	◔	◔	⊗	⊗	◔
subparallel linear fractures	⊗	⊗	⊗	◔	◔	⊗
micro-steps	◔	◐	◑	◑	●	●
parallel ridges	◔	◔	◔	◔	◔	◐
radial fractures	⊗	⊗	⊗	⊗	⊗	⊗
sawtooth fractures	⊗	⊗	⊗	◔	⊗	◔
craters	◐	⊗	⊗	⊗	⊗	◔
crescentic gouges	◔	◔	⊗	⊗	◔	◔
V-shaped percussion cracks	⊗	⊗	⊗	⊗	⊗	◔
mechanically upturned plates	⊙	◐	◑	⊙	⊙	●
bulbous edges	⊙	●	⊙	⊙	⊙	⊙
curved grooves	⊗	⊗	◔	⊗	⊗	⊗
deep trough	⊗	◔	◔	◔	◔	◔
straight grooves	◔	⊗	◔	◔	◔	⊗
elongated depressions	◑	◑	◔	◐	◑	◔
scaling	◔	⊗	⊗	⊗	⊗	⊗
adhering particles	⊙	⊙	⊙	⊙	⊙	⊙
cracks	⊗	◔	◔	◔	◔	◑
euhedral silica precipitation	⊗	◔	⊗	◔	◔	⊗
inclusions	⊗	⊗	⊗	⊗	⊗	◔

⊙ 100% ● 76-99% ◑ 51-75% ◐ 26-50% ◔ 1-25% ⊗ 0%

FIGURE 4 Microtextural characteristics of quartz grains for samples under study. Comparison between the reference sample (0 FT cycles) and weathered samples (50, 100, 300, 700, and 1,000 FT cycles) indicates differences in microtextural imprints induced by frost weathering, especially in the frequency of cf, CF, bb, and BB. The abbreviations used (cf, CF, bb, BB) refer to small- (<10 μm) and large-sized conchoidal fractures (>10 μm), and small- (<10 μm) and large-sized breakage blocks (>10 μm), respectively. Detailed descriptions of all the mentioned microtextures may be found in Mahaney[30]

3.1 | Grain-size distribution of aeolian sediment

Aeolian sediments gathered from the Pleistocene inland dune (Sławiny site, Poland; Figure 1) consist largely of medium sand-sized grains of moderately well sorting, symmetrical, and platykurtic distribution.[25] Grains of 0.25–1 mm constitute over 90% of the total.

Fractions of >1 and <0.25 mm represent ∼5 and 2% of the studied sediments (Figure 3a).

3.2 | Microtextural analysis

3.2.1 | Microtextural assemblages of reference grains

The studied sand-sized quartz grains exhibit micro-scale features that are typical of an aeolian origin[27,30] (Figures 4, 9 and 10a–c): low (75%) or medium relief (25%), low frequency of mechanically induced fractures (100%), edge rounding associated with bulbous edges (100%), and mechanically upturned plates (100%; Figure 10a). The last are tightly stacked and cover almost the entire surface of each grain. Numerous small but relatively deep depressions are encountered on their surfaces, making them rough and heterogeneous (Figure 10b). Abrasion features and adhering particles were observed on all of the reference grains (100%). Other microtextures (arc-shaped steps, linear steps, micro-steps, bb, BB, cf, CF) are much less common. The bb microtextures generally occupy the most convex parts of the grains (Figure 10c). Amorphous silica precipitation of a limited spatial range is observed infilling the micro-depressions.

Quartz grains from the reference sample, defined as RM (20%) and EM/RM (80%) types, are characterized by differing degrees of roundness with En index values ranging from 0.1 (grain number 6) to 0.29 (grain number 3; Figure 9).

3.2.2 | Microtextural assemblages of frost-weathered grains

The following description of frost-weathered grains (Figures 10d–i and 11–16) omits the above-mentioned inherited aeolian features (Sect. 3.1.).

Although a low relief is characteristic of all the studied grains regardless of the number of FT cycles, a shift towards the medium relief is noticeable for samples after 50, 100, 700, and 1,000 FT cycles as compared to the reference sample (0 FT cycles; Figure 4). A significantly number of high-relief grains (20%) was noted in the sample after 1,000 FT cycles (Figures 4 and 15). Microfeatures such as edge rounding, bulbous edges, abrasion features, amorphous silica precipitation, and adhering particles are observed on all of the grains (Figures 11–15). Notably, 10% of grains after 1,000 FT cycles exhibited sharp features (Figures 4 and 15).

Frost-originated microtextures (cf, CF, bb, BB) were observed on the surface of all weathered grains (after 50, 100, 300, 700, and 1,000 FT cycles; Figures 10e–i and 16). Their total number increased slightly during the first 700 FT cycles—from 11 up to 98 microtextures observed on the surfaces of grains after 50 and 700 FT cycles, respectively. Further, it increased significantly, up to 358 microtextures recorded after 1,000 FT cycles (Figure 7a). The predominant features encountered on the surface of weathered grains after 1,000 FT cycles are cf and CF (Figures 4 and 7a) which represent 47 and 22% of all
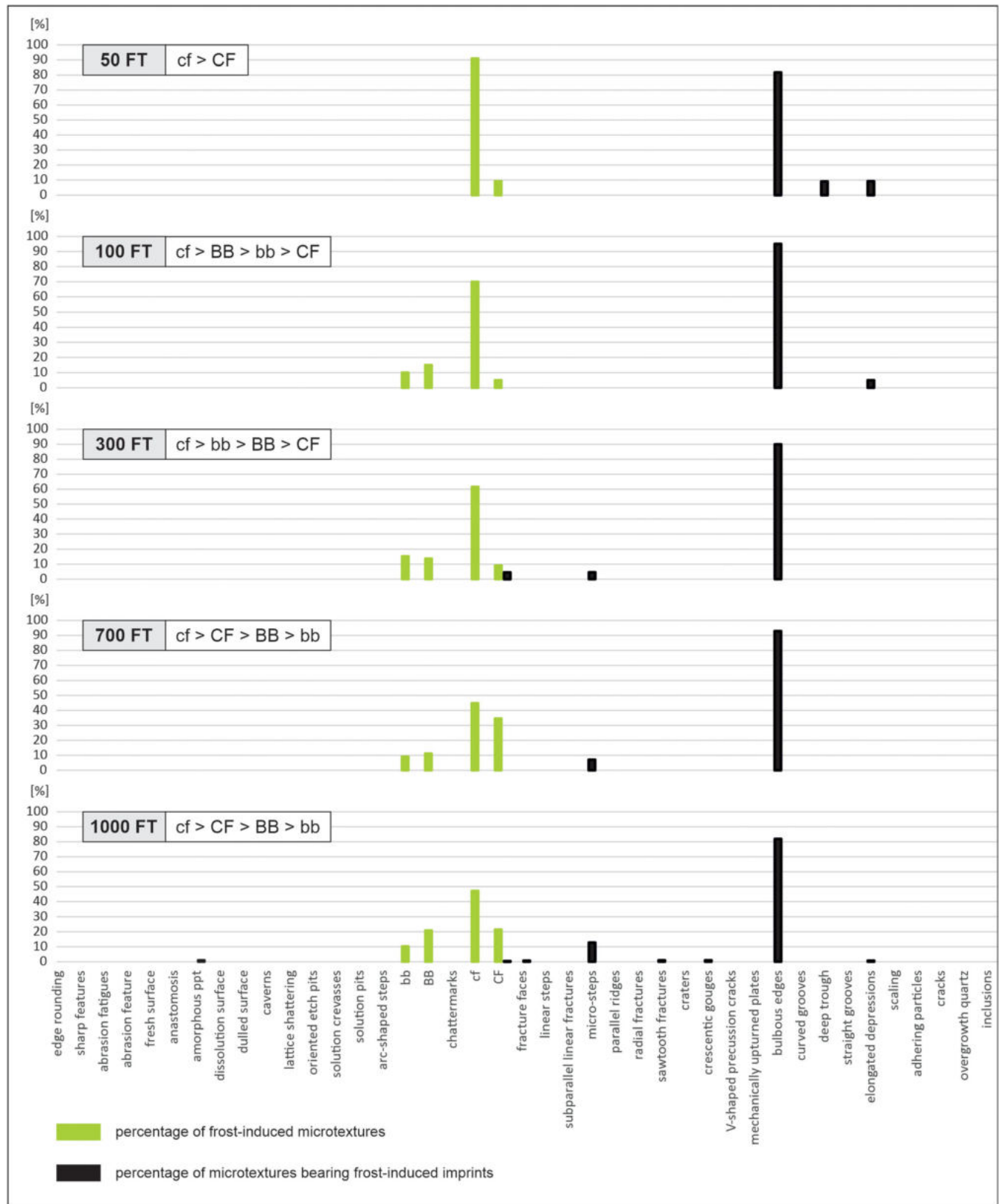
FIGURE 5 Localization of frost-induced microtextures (cf, CF, bb, BB). The percentage values of both the individual frost-induced microtextures and their localization were established in relation to the sum of all those observed within a given sample. The abbreviations used (cf, CF, bb, BB) refer to small- (<10 μm) and large-sized conchoidal fractures (>10 μm), and small- (<10 μm) and large-sized breakage blocks (>10 μm), respectively [Colour figure can be viewed at wileyonlinelibrary.com]
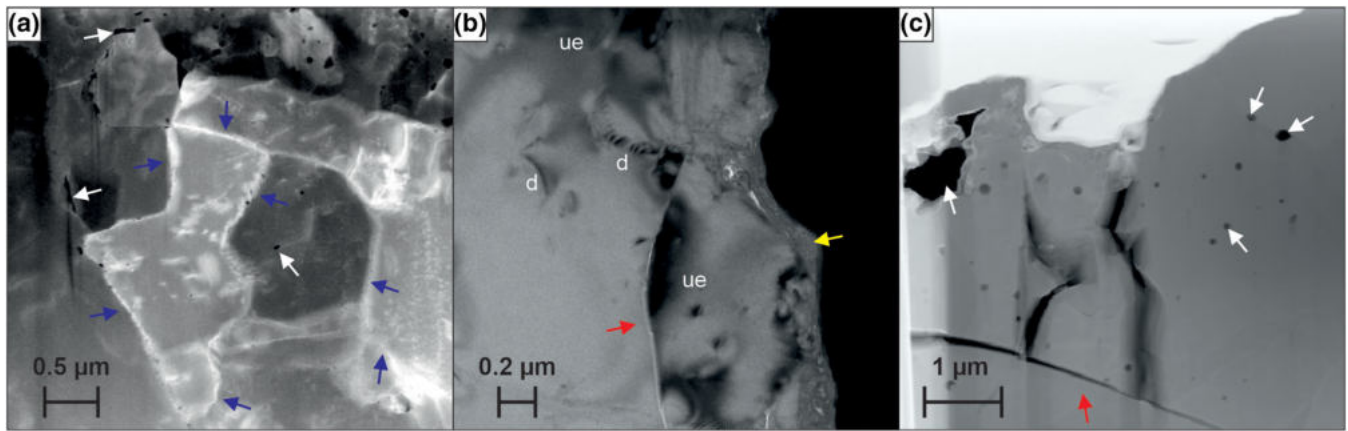
FIGURE 6 TEM micrographs. Microstructural characteristics of quartz grains under study. a—mosaic structure of quartz grain after 100 FT cycles with primary defects: Inclusions/pores (white arrows) and low-angle grain boundaries (blue arrows). No visible frost-induced modifications. b—quartz grain after 1,000 FT cycles with primary defects: undulatory extinction (ue), deformations (d), and secondary defects: aeolian-originated crack (red arrow). The surface of the quartz grain is covered by a surficial crust developed as the *outer impact zone* (yellow arrow). c—quartz grain after 1,000 FT cycles with primary defects: Inclusions/pores (white arrows) and secondary defects: aeolian-originated crack (red arrow) [Colour figure can be viewed at wileyonlinelibrary.com]

TABLE 3 Results of statistical analysis of the samples subjected to 50, 100, 300, 700, and 1,000 FT cycles. A—Fisher's moments coefficient of skewness; B—outlier detection with the number of grain microtextures indicated as outliers from each method; C—Shapiro–Wilk test with indicated W values and *p*-values

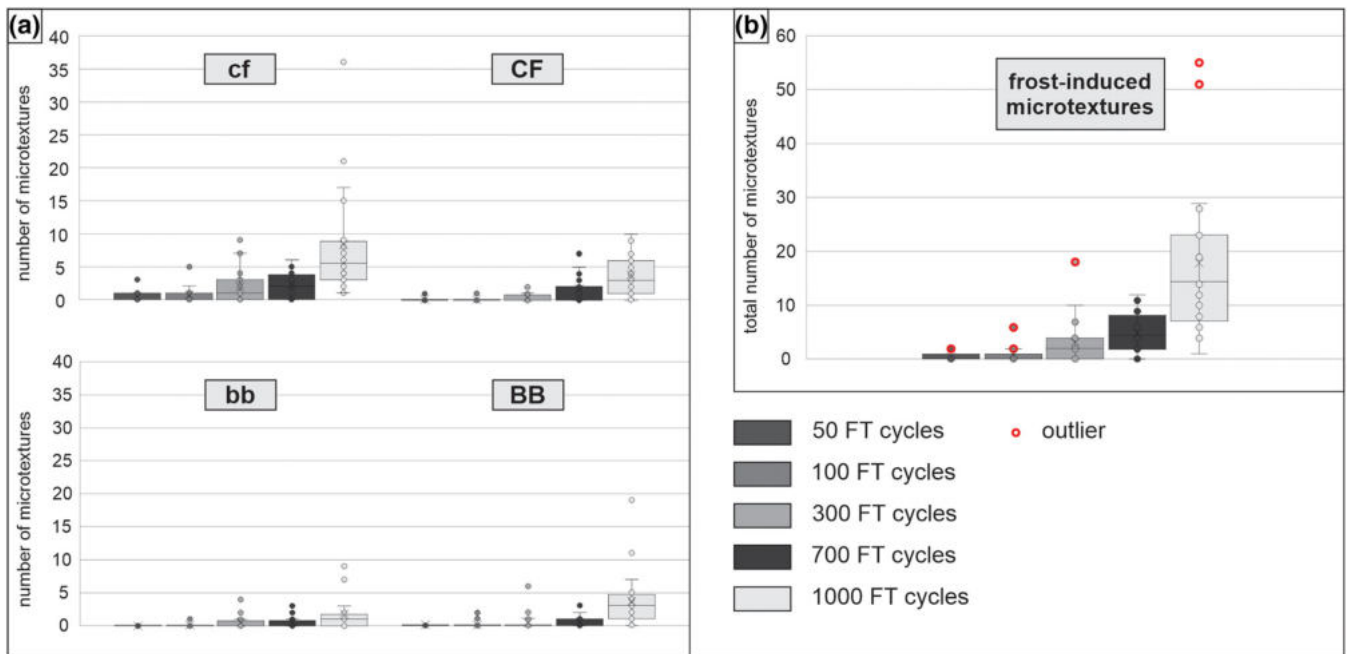| Method/number of cycles			50 FT	100 FT	300 FT	700 FT	1,000 FT
A	Fisher's moments coefficient of skewness	Coefficient values	1.775492	2.227386	2.081607	0.392846	1.404116
B	Outlier detection	Box plots	3	3, 6	18	—	51, 55
		Hampel's filter	1, 3	6	10, 18	—	51, 55
C	Shapiro–Wilk test	W values	0.6243	0.6893	0.7348	0.912	0.84647
		p-values	<0.001	<0.001	< 0.001	**0.0696**	0.005

FIGURE 7 Box plot graphs. (a)—relationship between the number of individual frost-originated microtextures (cf, CF, bb, BB) and the number of FT cycles; (b)—relationship between the total number of frost-originated microtextures (cf, CF, bb, BB) and the number of FT cycles. Statistically detected outliers are marked in red. The abbreviations used (cf, CF, bb, BB) refer to small- (<10 μm) and large-sized conchoidal fractures (>10 μm), and small- (<10 μm) and large-sized breakage blocks (>10 μm), respectively [Colour figure can be viewed at wileyonlinelibrary.com]
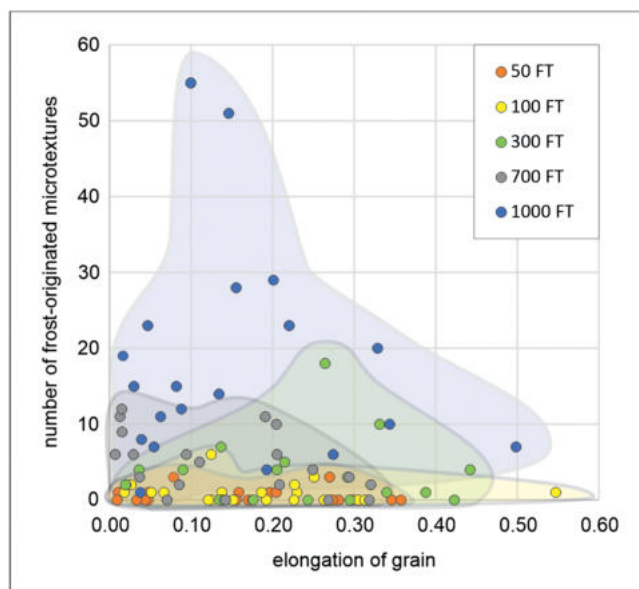
FIGURE 8 Relationship between the total number of frost-originated microtextures (cf, CF, bb, BB) recorded on individual grains and the elongation (*En* index) of grains. The abbreviations used (cf, CF, bb, BB) refer to small- (<10 μm) and large-sized conchoidal fractures (>10 μm), and small- (<10 μm) and large-sized breakage blocks (>10 μm), respectively [Colour figure can be viewed at wileyonlinelibrary.com]

frost-induced microtextures. Minor microtextures are bb (10%) and BB (21%; Figures 4 and, 7a). All the frost-induced microtextures generally occupy the most convex parts of grains (e.g., Figures 5, 10h and 16b,i,o).

Most of the grains from frost-weathered samples were defined as EM/RM (76%) and RM (17%) types, while other types (EM/EL—3%, C/EM/RM—3%, C/EM/EL—1%) represent a minority (Figures 11–15). The *En* index values vary among each sample (50, 100, 300, 700, and 1,000 FT cycles) from 0.1 to 0.55 in general (Figures 11–15). Figure 8 shows a significant increase in the number of frost-originated microtextures recorded on each grain with progressing FT cycles and no evident relationship between the number of frost-induced microtextures recorded on each grain and its *En* index.

3.3 | Microstructural analysis

TEM analysis revealed a mosaic structure of quartz (Figure 6a), indicating that an individual quartz crystal is made up of many smaller ones.[43] Contacts between adjacent crystals are visible as low-angle grain boundaries. Moreover, numerous crystal defects were detected and divided into primary and secondary features. Primary defects originating from crystallization processes include lattice imperfections: crystallographically controlled slip (bending, undulatory extinction), dislocations, and micropores/inclusions (generally <0.5 μm in size; Figure 6) resulting from the displacement or removal of ions from their normal crystallographic position.[43] Secondary crystal defects refer to any mechanical disruptions, that is cracks within quartz grains originating from the

postcrystallization processes such as physical and chemical weathering or an increase of overburden pressure (Figure 6b,c).

3.4 | Statistical analysis

Statistical analysis (Fisher's moments coefficient of skewness, box plot analysis, Hampel filter, Dixon's *Q* test) provided information on microtextural differentiation of grains within individual samples after 50, 100, 300, 700, and 1,000 FT cycles (Table 3).

The results of skew analysis indicate a right-sided asymmetry of the distribution of frost-induced microtextures for all samples. This asymmetry is highest for the sample after 100 FT cycles and is only slightly lower for the sample after 300 FT cycles. The lowest asymmetry value is assigned to samples after 700 FT cycles. The remaining samples (50 and 1,000 FT cycles) are characterized by moderate values (Table 3a).

Box plot analysis with Hampel filtering identified outliers (see Sect. 2.4) in all of the tested samples, except the sample after 700 FT cycles. Detected outliers are assigned to: (a) the largest number of frost-induced microtextures recorded in a given sample; or (b) the two largest numbers of frost-induced microtextures recorded for an individual sample (Figure 7b; Table 3b). The following numbers of frost-induced microtextures were detected as outliers: three for the sample after 50 FT cycles; three and six for the sample after 100 FT cycles; 18 for the sample after 300 FT cycles; and 51 and 55 for the sample after 1,000 FT cycles. The results obtained from both methods (box plots, Hampel filter) are highly consistent (Figure 7b; Table 3b).

The Shapiro–Wilk test was used to verify the null hypothesis on the normality of the distribution of frost-induced microtextures in the samples. In all cases (samples subjected to 50, 100, 300, and 1,000 FT cycles), except the sample after 700 FT cycles, the null hypothesis of the normality of the distribution was rejected at the significance level of 0.05 (Table 3c).

Dixon's *Q* test was run for the sample after 700 FT cycles as it fulfils the assumption of a normal distribution. The null hypothesis was that the largest value in this sample (equal to 12) is not an outlier. The obtained value of Dixon's *Q* test = 0.833 ($p = 0.1886$) leads to its rejection at the significance level of 0.05. The second null hypothesis, stating that the smallest value in the sample (equal to 0) is not an outlier, was also rejected due to the value of Dixon's *Q* test = 0 ($p < 0.001$). It is therefore statistically proven that neither the largest (12) nor the smallest value (0) in the sample is an outlier. This contrasts with the other samples (after 50, 100, 300, and 1,000 FT cycles) where the largest number of frost-induced microtextures was detected as an outlier (Table 3b).

4 | DISCUSSION

Micro-scale frost activity is thought to modify the surface of quartz grains through the formation of surficial cracks[6,12,15] and microtextures.[7,10,33,44–46] The degree of frost-induced resurfacing has previously been assumed to be related to the intensity of weathering action
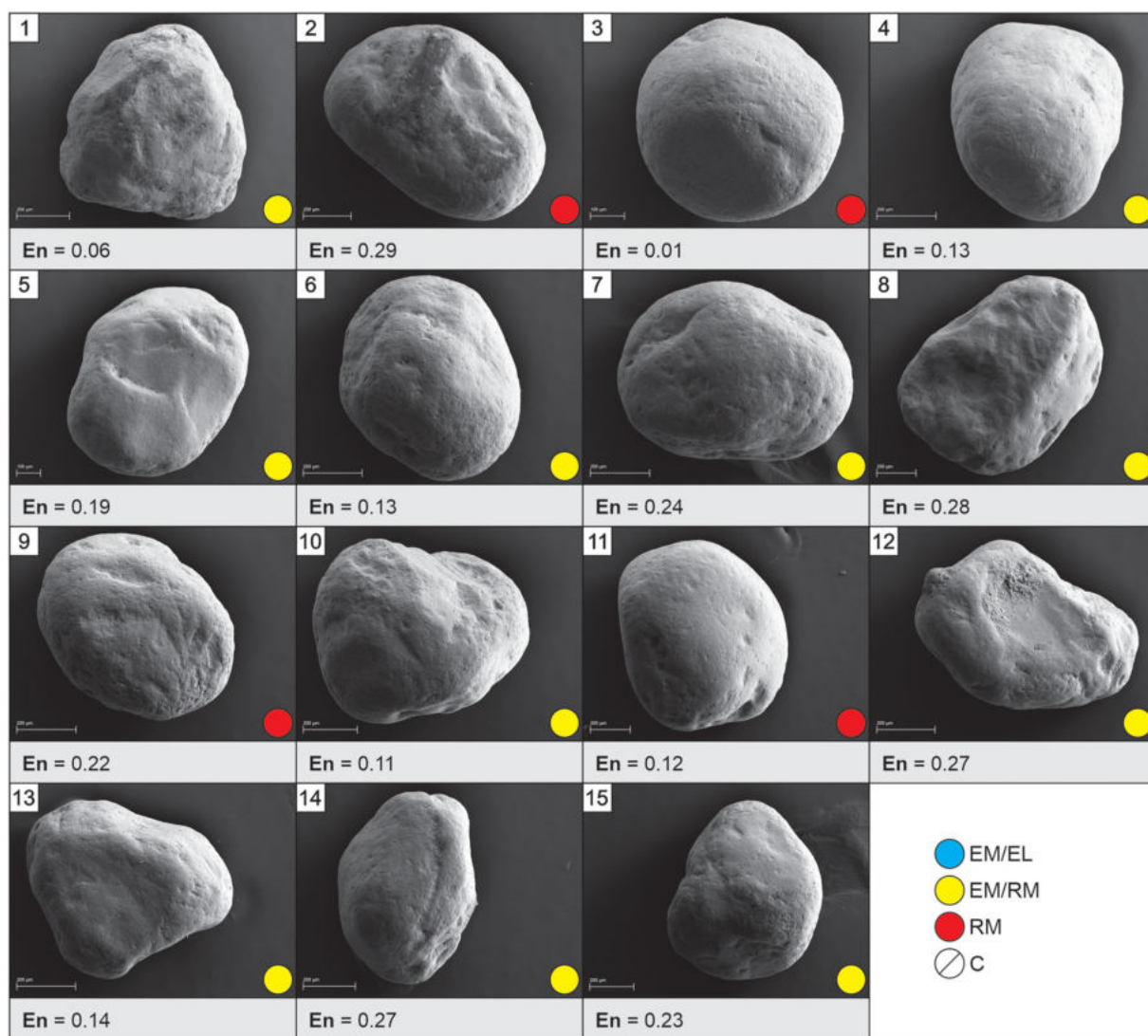
FIGURE 9 Characteristics of quartz grains from the reference sample (0 FT cycle). Differences in grain shape, roundness, elongation, microrelief, and grain classification (NU—resh grain, RM—matt surface of well-rounded grain, EL—shiny well-rounded grain, EM/RM—matt surface on the edges of a semi-rounded grain, EM/EL—shiny semi-rounded grain, C—cracked grain, others)[37] should be noted. The legend also applies to Figures 11–15. [Colour figure can be viewed at wileyonlinelibrary.com]

but only in a qualitative manner (low vs. high), and no recent studies have focused on the quantitative relationships between the number of FT cycles and frost-originated microtextures. Applying these results to the micromorphology of the studied aeolian grains provided a means to investigate some internal characteristics of these quartz grains, and to determine the influence of aeolian-induced modifications of the surface on their frost susceptibility. It is now clear that micro-scale frost weathering of cold-climate aeolian quartz grains is influenced by several factors, the most important of which are discussed below.

4.1 | Influence of FT cycles on the micromorphology of aeolian-originated quartz grains

The results of this experimental study indicate that the number of frost-induced microtextures recorded on the surface of aeolian quartz grains increases with the duration of frost activity (i.e., with an

increase in the number of FT cycles). However, the rate of this increase is unexpectedly low, and in the case of grains exposed to 50–700 FT cycles, it is almost negligible. A significant increase in the number of frost-induced microtextures was recorded after 1,000 FT cycles (Figures 4 and 7). This therefore indicates that the number of FT cycles required to intensify the weathering process to such an extent that its effects are visible on the grain surface is relatively large. This time span between the occurrence of the factor that generates this process (i.e., frost action; 0 FT cycles) and the occurrence of the effects of this process (i.e., frost-induced microrelief; after *n* FT cycles) is defined as the *lag time*. It comprises ~700 FT cycles in the case of the aeolian grains under study, which is at least twice as long as in the case of mechanically crushed (angular with sharp corners and edges) quartz grains subjected to frost weathering where it comprises about 100–300 FT cycles.[14] Such a long *lag time* may be due to the fact that the microrelief of the studied aeolian grains is not conducive to the formation of frost-induced imprints because of: (a) a high degree of
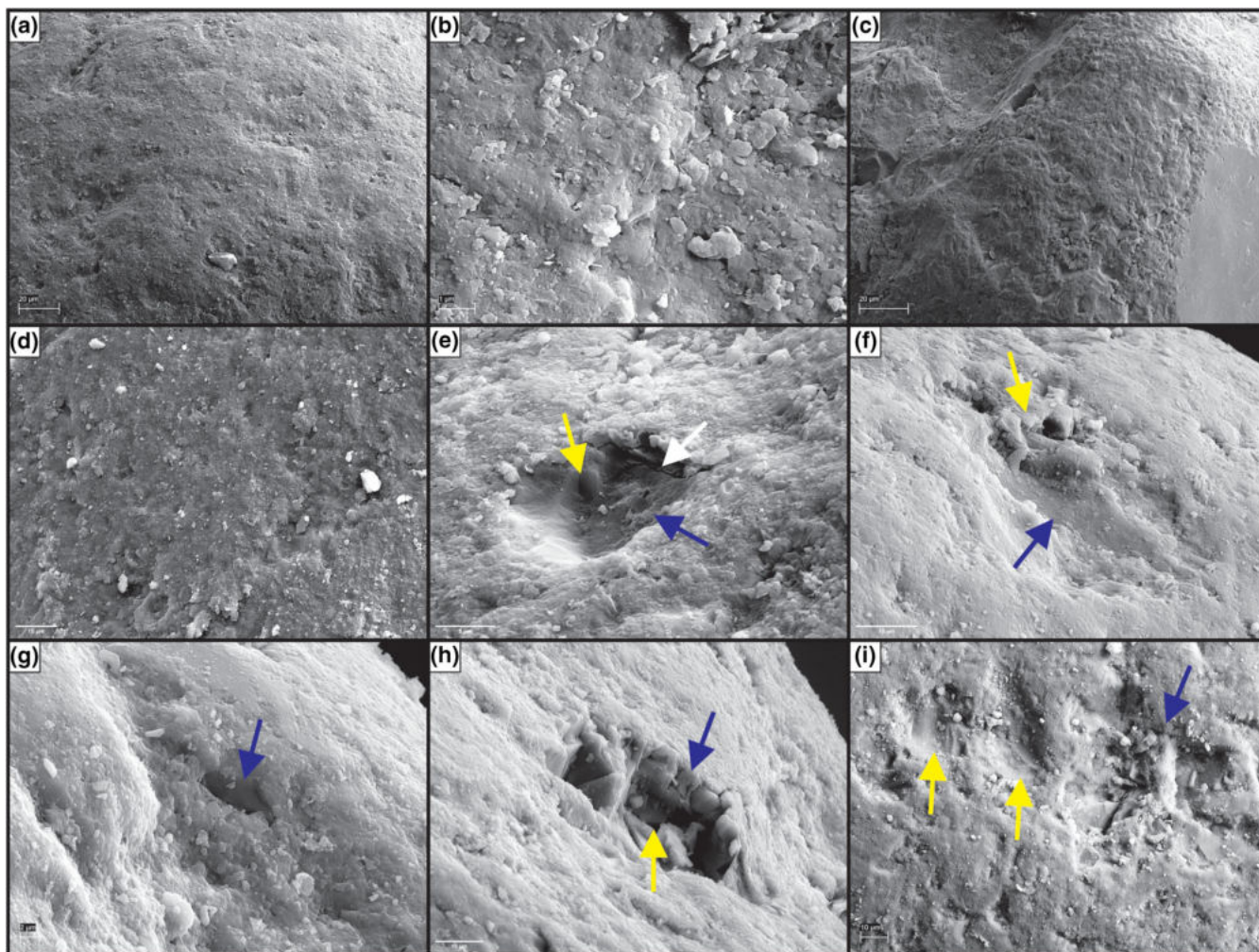
FIGURE 10 SEM micrographs. Microtextural characteristics of studied quartz grains (A–C: 0 FT; D–F: 50 FT; G–I: 100 FT cycles). (a)—fragment of most convex part of grain with mechanically upturned plates; (b)—fragment of crusted surface; (c)—fragment of most convex part of grain with mechanically upturned plated; (d)—fragment of most convex part of grain with mechanically upturned plates, crusted surface, and adhering particles; (e)—fragment of grain surface with mechanically upturned plates, aeolian-originated (crusted) cf (blue arrow), frost-originated cf_{II} (yellow arrow), and associated crack (white arrow); (f)—fragment of grain surface with mechanically upturned plates, aeolian-originated (crusted) CF (blue arrow), and BB (yellow arrow) encountered on the micro-step; (g)—fragment of grain surface covered with surficial crust and mechanically upturned plates, and frost-originated cf_I (arrow) exhibiting fresh surface of host grain; (h)—fragment of most convex part of grain with mechanically upturned plates, crusted surface (*outer impact zone*; blue arrow), and cf_{II} (*inner impact zone*; yellow arrow) which tends to develop into BB associated with cracks; (i)—fragment of grain surface covered with crust, mechanically upturned plates, and adhering particles. Initial form of frost-originated BB (blue arrow) development, encountered on the micro-step and several aeolian-originated CF (yellow arrows) with crusted surfaces. The abbreviations used (cf, CF, bb, BB) refer to small- (<10 μm) and large-sized conchoidal fractures (>10 μm), and small- (<10 μm) and large-sized breakage blocks (>10 μm), respectively. Moreover, cf_I and cf_{II} refer to small- (<10 μm) conchoidal fracture of type I and II, respectively. [Colour figure can be viewed at wileyonlinelibrary.com]

edge rounding (i.e., circularity) and very slightly topographically varied surface (i.e., low relief) of aeolian-originated quartz grains,[32,47,48] which significantly affects the distribution of pressure exerted on the grain surface during frost-induced hydrofracturing; (b) a lack of areas predisposed to the development of frost-induced microtextures, such as micro-steps or other micro-denivelations on the surfaces of grains[7,14]; and (c) the presence of a subsurface thin layer of disrupted lattice (*abrasion fatigue*) within the aeolian-originated quartz grains,[49,50] which can presumably act as a kind of protective layer (Figures 9, 10b and 11–16).

A recorded increase in the number of frost-induced microtextures (cf, CF, bb, BB; Figures 4 and 7) corresponds neither to an increase in their complexity nor to the expansion of their surface area. Regardless of the number of FT cycles, single cf microtextures were predominant on the frost-induced assemblages (grains #1 and 2 on Figure 11; grain #8 on Figure 12; grains #12–14 on Figure 13; grains #14, 17, and20 on Figure 14; grains #1, 14, 17, and 18 on Figure 15). The frequency of bb and BB is significantly lower than that of cf and CF (Figures 11–15). It appears that frost weathering of studied aeolian grains, contrary to mechanically crushed quartz grains,[14] omits an
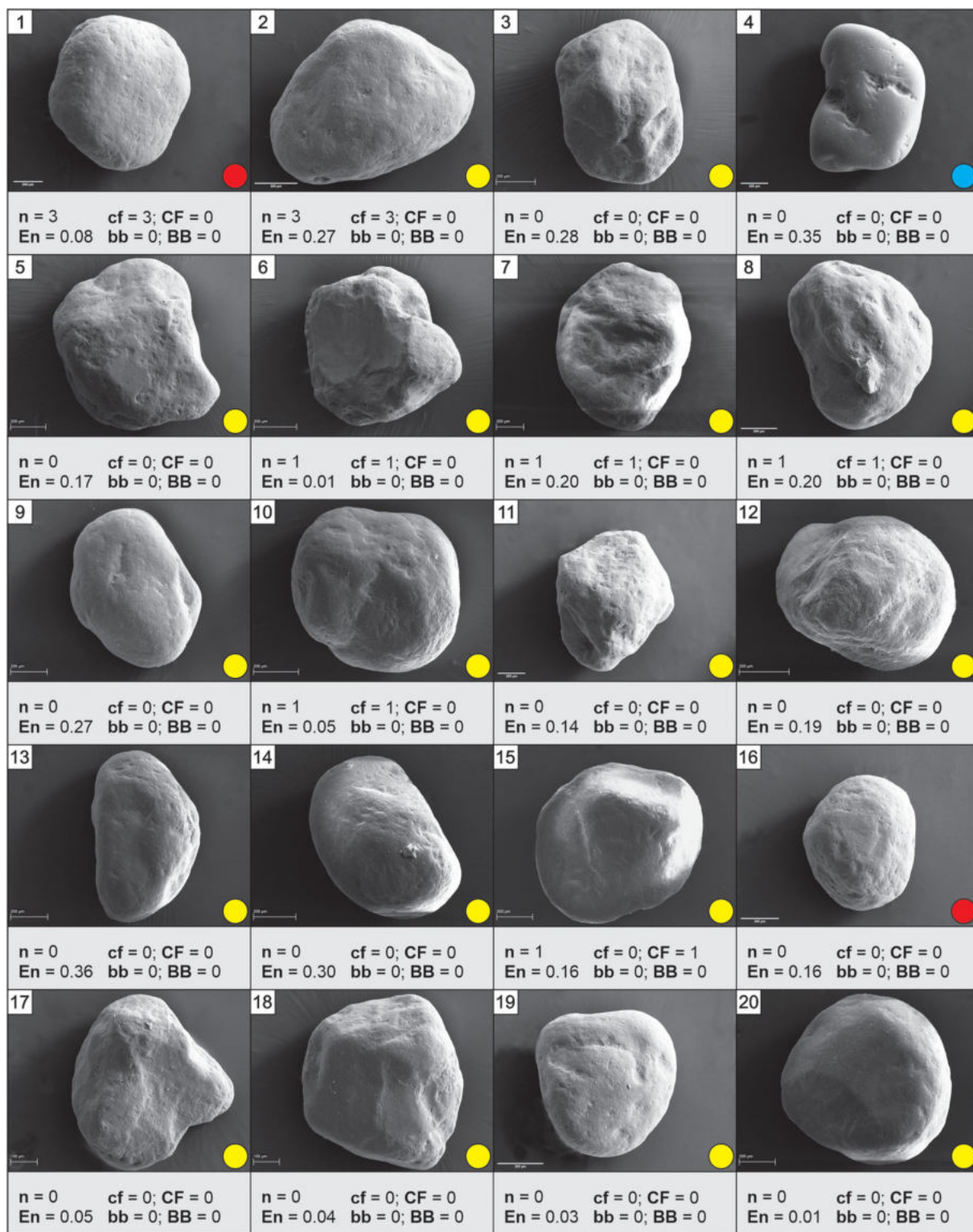
FIGURE 11 Characteristics of quartz grain subjected to 50 FT cycles. Differences in grain shape, roundness, elongations, and number of frost-induced microtextures (cf, CF, bb, BB) should be noted. The abbreviations used (cf, CF, bb, BB) refer to small- (<10 μm) and large-sized conchoidal fractures (>10 μm), and small- (<10 μm) and large-sized breakage blocks (>10 μm), respectively [Colour figure can be viewed at wileyonlinelibrary.com]

initial stage of the process (i.e., the formation of CF), that is thought to initiate the further development of frost-induced microtextures, such as cf and bb imprints on the CF's edges. As a consequence, a small number of cf superimposed on the edges of CF is observed only on the surface of grains exposed to 300 and 1,000 FT cycles. Frost weathering of aeolian quartz grains probably begins with the formation of cf, which may successively evolve into bb and BB (cf → bb → BB).
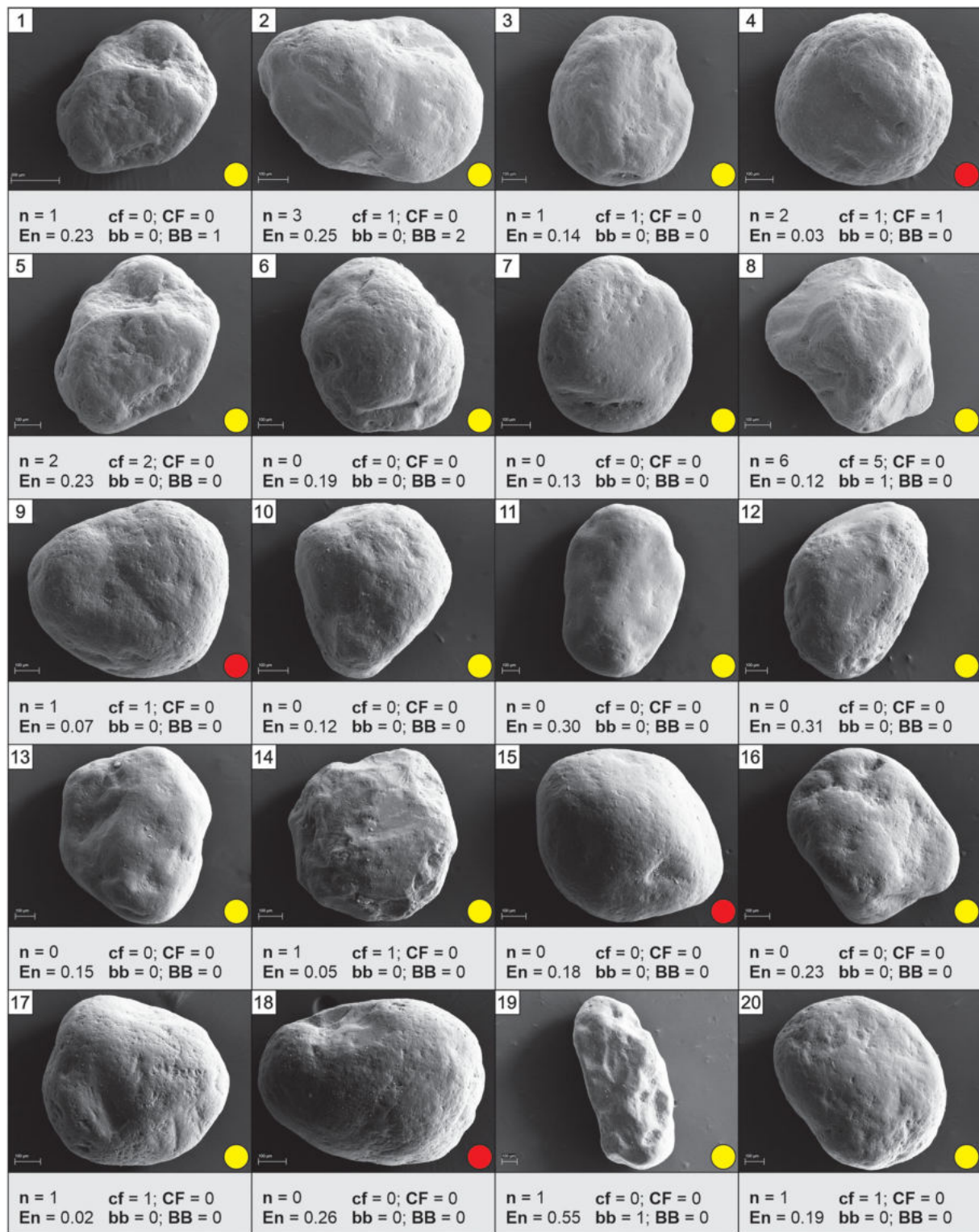
FIGURE 12 Characteristics of quartz grain subjected to 100 FT cycles. Differences in grain shape, roundness, elongation, grain classification, and number of frost-induced microtextures (cf, CF, bb, BB) should be noted. The abbreviations used (cf, CF, bb, BB) refer to small- (<10 μm) and large-sized conchoidal fractures (>10 μm), and small- (<10 μm) and large-sized breakage blocks (>10 μm), respectively. [Colour figure can be viewed at wileyonlinelibrary.com]

The microtextural characteristics of quartz grains subjected to experimental frost weathering (Figures 3, 10d-i, and 11–16) differ significantly from those recorded on grains originating from ancient or present-day active-layer deposits. The latter bear numerous frost-induced microtextures of high complexity and great extent, which seem to indicate very high advancement of the frost weathering
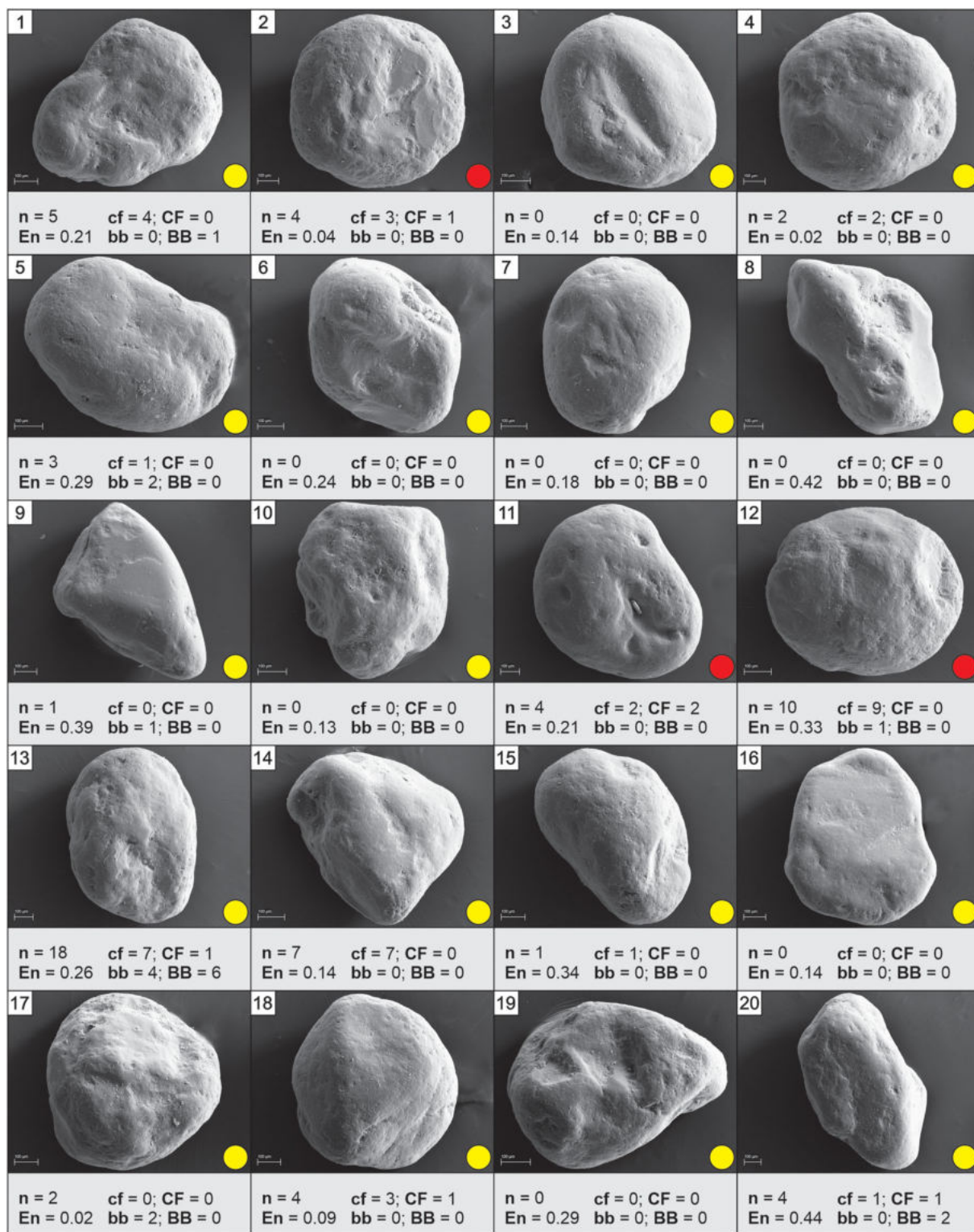
FIGURE 13 Characteristics of quartz grain subjected to 300 FT cycles. Differences in grain shape, roundness, elongation, grain classification, and number of frost-induced microtextures (cf, CF, bb, BB) should be noted. The abbreviations used (cf, CF, bb, BB) refer to small- (<10 μm) and large-sized conchoidal fractures (>10 μm), and small- (<10 μm) and large-sized breakage blocks (>10 μm), respectively. [Colour figure can be viewed at wileyonlinelibrary.com]

process.[7,33] It may be implied from this that the number of FT cycles that affected quartz grains under natural conditions was much higher than employed in the present experimental study. This number, however, is impossible to estimate and therefore the reconstruction of grain weathering history remains unfeasible or remains only qualitative in nature. It also must be considered that there is a much larger number of factors influencing the course and intensity of frost weathering under any natural conditions that are not included in the
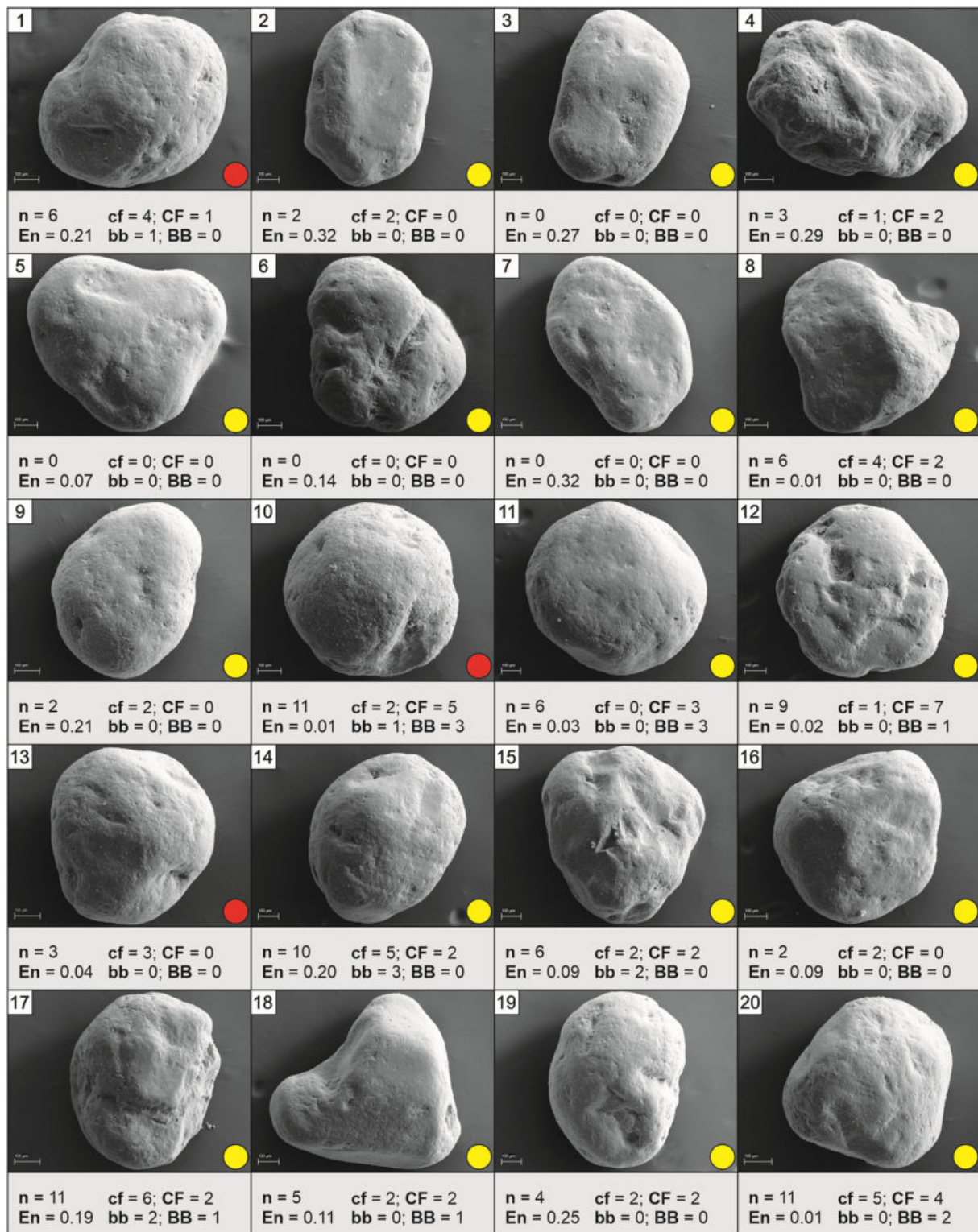
FIGURE 14 Characteristics of quartz grain subjected to 700 FT cycles. Differences in grain shape, roundness, elongation, grain classification, and number of frost-induced microtextures (cf, CF, bb, BB) should be noted. The abbreviations used (cf, CF, bb, BB) refer to small- (<10 μm) and large-sized conchoidal fractures (>10 μm), and small- (<10 μm) and large-sized breakage blocks (>10 μm), respectively. [Colour figure can be viewed at wileyonlinelibrary.com]

experimental study, for example the grain-size distribution, presence of clay minerals, and distribution of water pressure in the sediment during freezing and thawing.[51–53] Their combined action may cause the course, intensity, and/or effects of frost-driven weathering of quartz grains in the natural environment to be different from those observed in this experimental study.
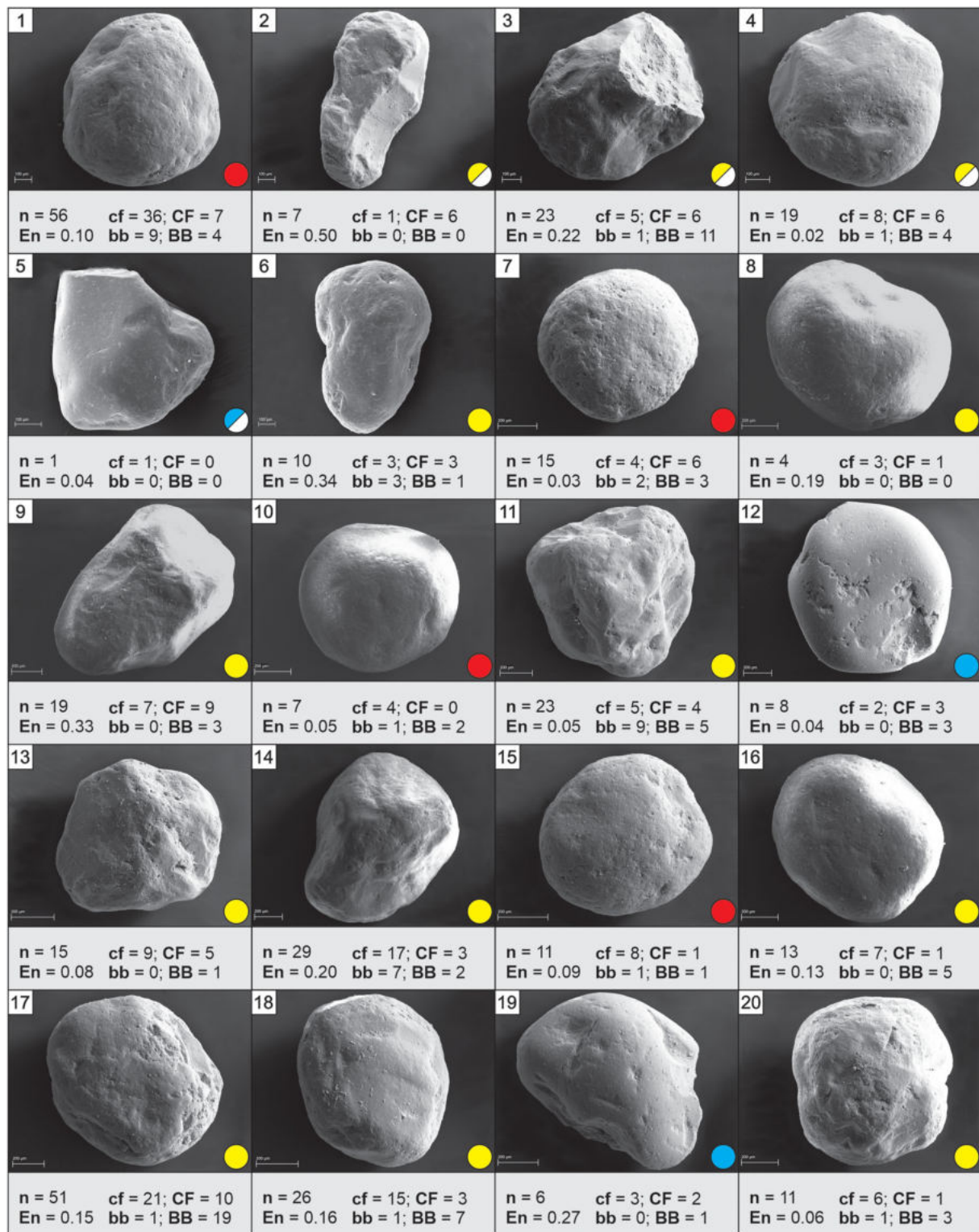
FIGURE 15 Characteristics of quartz grain subjected to 1,000 FT cycles. Differences in grain shape, roundness, elongation, grain classification, and number of frost-induced microtextures (cf, CF, bb, BB) should be noted. The abbreviations used (cf, CF, bb, BB) refer to small-(<10 μm) and large-sized conchoidal fractures (>10 μm), and small- (<10 μm) and large-sized breakage blocks (>10 μm), respectively. [Colour figure can be viewed at wileyonlinelibrary.com]
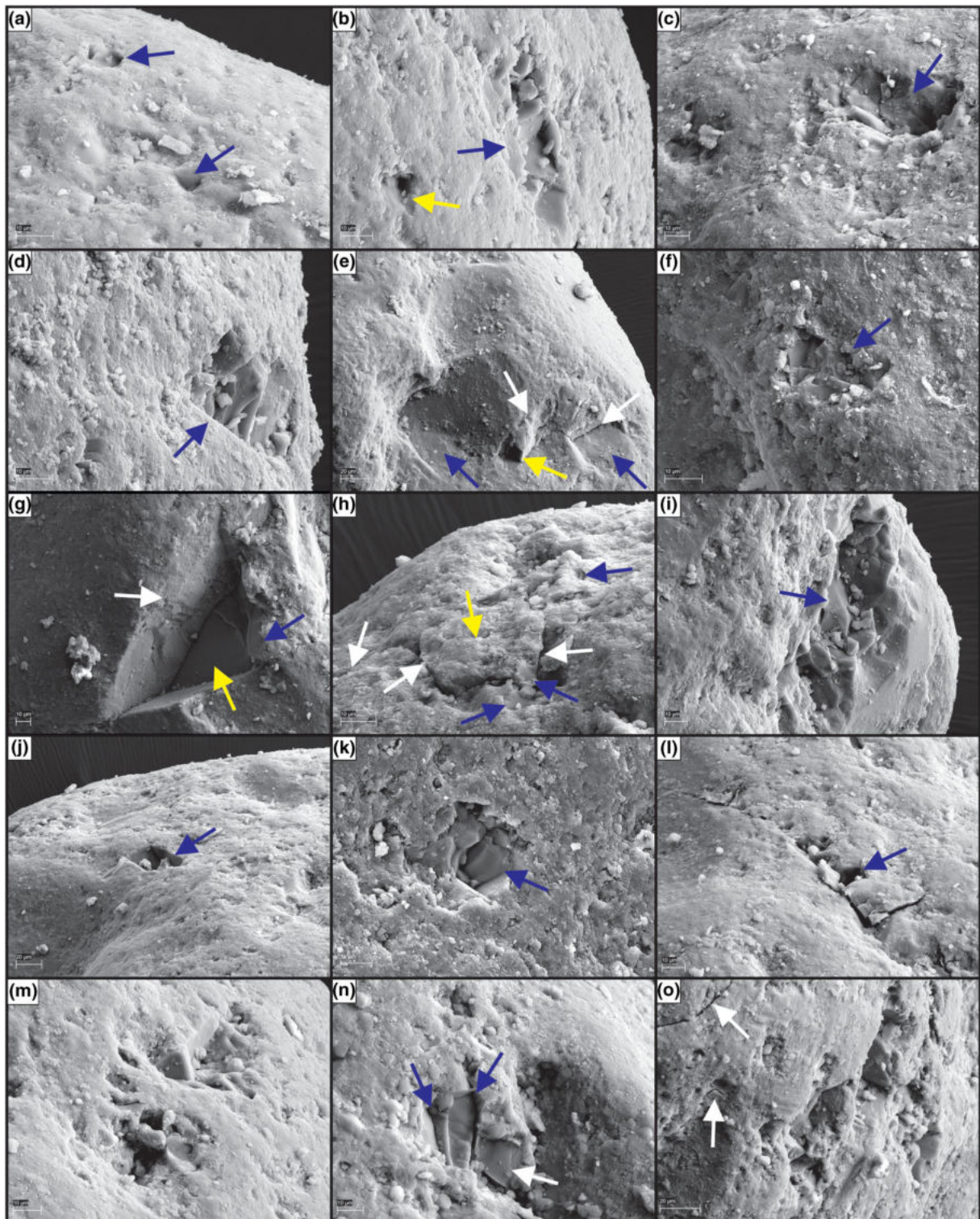
FIGURE 16 Legend on next page.

FIGURE 16 Microtextural characteristics of studied quartz grains (A–C: 300 FT; D–I: 700 FT; J–O: 1000 FT). a—fragment of grain surface with mechanically upturned plates, adhering particles, and frost-originated cf_{II} microtextures (arrows); b—fragment of grain surface with mechanically upturned plates, frost-originated cf_I (yellow arrow), and BB microtexture (blue arrow); c, d—fragment of most convex part of grain with mechanically upturned plates and frost-originated BB microtexture (arrow); e—fragment of most convex part of grain with mechanically upturned plates, aeolian-originated CF microtextures (blue arrows), frost-originated CF_{II} imprinted on micro-step (yellow arrow), and associated cracks (white arrows); f—fragment of most convex part of grain with mechanically upturned plates, adhering particles, and frost-originated BB microtexture (arrow); g—fragment of grain surface with mechanically upturned plates, adhering particles, and frost-induced CF_I (blue arrow) and CF_{II} (yellow arrow) microtextures development of which was crystallographically determined, as evidenced by the etched crystal face (white arrow); h, fragment of most convex part of grain with mechanically upturned plates, frost-originated cf_I microtextures (blue arrows), and associated cracks (white arrows). A fragment of grain seems to be already detached from the host grain (yellow arrow) and it may spall off revealing frost-originated cf_{II} microtexture. iI—fragment of most convex part of grain with mechanically upturned plates and frost-originated BB complex; j—fragment of most convex part of grain with mechanically upturned plates and frost-originated CF_{II} microtexture (arrow); k—fragment of grain surface with mechanically upturned plates, adhering particles, and fresh, frost-originated cf_{II} microtexture (arrow); l—fragment of most convex part of grain with mechanically upturned plates, frost-originated cf_{II} microtexture (arrow), and associated cracks development of which was crystalographically determined; m—fragment of most convex part of grain with mechanically upturned plates and frost-originated BB complex; n—fragment of grain surface with mechanically upturned plates and frost-originated cf_I (white arrow) and cf_{II} (blue arrows) microtextures; o—fragment of most convex part of grain with mechanically upturned plates, frost-originated BB complex, and cracks (arrows). The abbreviations used (cf, CF, BB) refer to small- (<10 μm) and large-sized conchoidal fractures (>10 μm), and large-sized breakage blocks (>10 μm), respectively. Furthermore, cf_I and cf_{II} refer to small- (<10 μm) conchoidal fracture of type I and II, respectively [Colour figure can be viewed at wileyonlinelibrary.com]

4.2 | The influence of active aeolian processes on the micro-scale modification of quartz grains

4.2.1 | Duration of active aeolian processes

The presence of spherical grains with a matt surface (observed with magnifying binocular lenses) in aeolian deposits is considered evidence of long-term wind activity in a given area.[5,54,55] The relationship between the width and length of a grain was useful for estimating the length of aeolian processes as the final shape of grains subjected to grain-to-grain collisions should be a sphere.[56] However, if quartz grains are already spherical when entering aeolian transport, any estimation of the duration of aeolian processes is impossible. On the other hand, grains of low sphericity and high degree of roundness, characterized by high values of the *En* index, are indicators of short-term aeolian activity.[56] Their microrelief results from aeolian-driven processes, while their shape remains inherited from previous, nonaeolian, sedimentary environment(s). Modification of grain microrelief in aeolian environments has been experimentally proven to occur rapidly, as opposed to any changes in the grain shape.[57,58] Therefore, it can be concluded that the studied quartz grains were subjected to relatively short aeolian transport (Figures 9 and 11–15), but accurate estimation of the duration of aeolian transport to which the grains were subjected is not feasible.

Bearing in mind that the most convex parts of grains (Figure 5) are particularly predisposed to the development of frost-induced imprints, the question arises whether there is any relationship between the duration of aeolian abrasion, which leads to the effective rounding of its most convex fragments, and the susceptibility of the grain to frost weathering.

The results of grain-size analysis of the aeolian deposits under study (Figure 3a) indicates saltation as a main transport mode (>90%) affecting grains from the 0.25–1.00-mm fraction. The mean flow velocity required to transport grains of the studied size fraction (0.5–1 mm) reaches at least 5–10 m/s,[1,27,28,59] which is consistent with the aeolian transport modes estimated for quartz sand (Figure 3b). However, it is widely acknowledged that under cold-climate conditions, aeolian transport is influenced by: (a) elevated sand-transport rates that may even be 70% greater than for an equal wind speed in a hot desert,[1,60] and (b) lower threshold wind velocities required to entrain grains into the movement.[61] In particular, the latter has been demonstrated throughout a series of experimental studies conducted in Antarctica.[62] It can therefore be reasonably assumed that the grains under study were transported at speeds greater than those resulting from the generally accepted values (Figure 3b).

At the time of grain-to-grain collisions, the kinetic energy of each quartz grain is at least partly converted to elastic energy in the grain.[50] It is therefore advisable also to make reference to the character of the bed over which the transport takes place. In the case of cold-climate aeolian environments, grains transported in saltation may jump over partially or completely frozen ground. The elasticity of grain impacts on cold beds has been shown to be increased since the decreased tension of water adsorbed onto particle surfaces at low temperatures is postulated to reduce interparticle cohesion.[60] Besides grains involved in active aeolian transport (i.e., moving in reptation, saltation, and suspension), some grains may be attached to the bed due to the freezing process and only their protruding parts remain exposed to abrasion. Their release and incorporation into the aeolian sand flux occur as a result of further abrasion and sublimation. This means that sand flux may be actively supplied with grains of different origin and degree of roundness (e.g., EM/EL and EL type of grains; Figures 9 and 11–15), and thus different susceptibility to surface-modifying frost weathering. This is clearly evidenced by the large variation in the numbers of frost-induced microtextures recorded on individual grains under study (Figure 7a) and statistically detected outliers (Figure 7b; Table 3b).
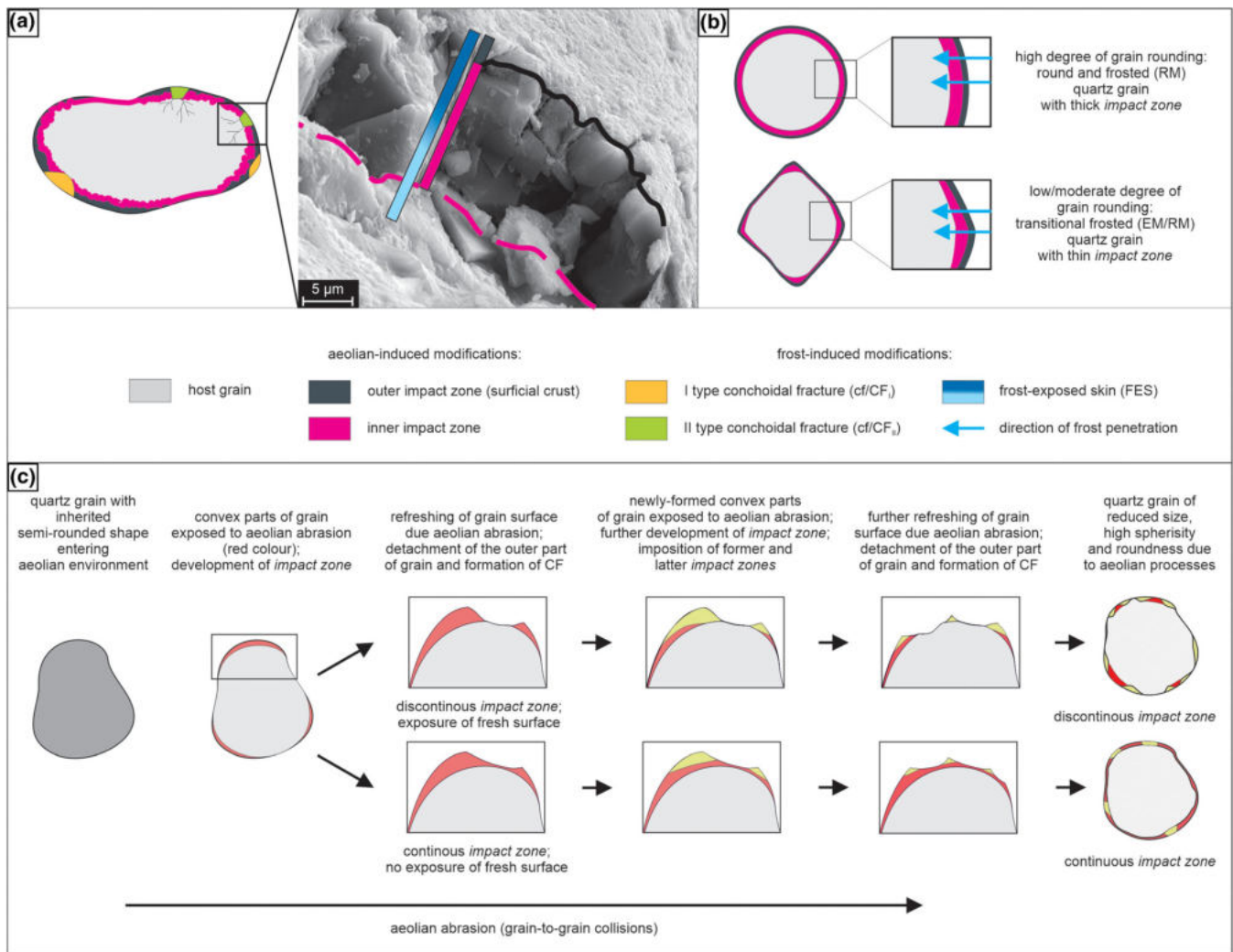
FIGURE 17 Theoretical scheme of the *impact zone* within aeolian-originated quartz grains. a—cross-section through an aeolian-originated quartz grain subjected to frost action. Aeolian-induced modifications resulted in the formation of the *impact zone*. b—arrangement of the *impact zone* across quartz grains of different degrees of rounding. c—development of a continuous and discontinuous *impact zone* over time due to active aeolian processes [Colour figure can be viewed at wileyonlinelibrary.com]

4.2.2 | Impact zone in aeolian quartz grains

Frost-induced microtextures observed on the surface of the studied quartz grains were encountered mainly on their most convex parts. These protrusions bear microtextural assemblages that are diagnostic of aeolian processes/environments, namely mechanically upturned plates[27,30,58,63–65] (Figures 4, 10e,h, and 16b,d,i,m,o). None of the frost-induced microtextures were recorded on the surface of concave parts of microrelief developed mainly as equidimensional and elongated depressions. Their surfaces are generally smoothed-over, with no traces of mechanically upturned plates. These micro-depressions on the surface of aeolian grains may be: (a) inherited from surface-modifying processes that operated in previous sedimentary environment(s),[49] and/or (b) a remnant of CF developed due to grain-to-grain collisions in an aeolian environment.[27,64]

Numerous studies of the microtextural peculiarities of aeolian quartz grains have shown that the modification of grain surfaces due to high-energy grain-to-grain collisions is manifested by a thin layer of disrupted crystal lattice of quartz grains, referred to as *abrasion fatigue*.[30,50] This is manifested on the surface of studied grains by aeolian-originated surficial features, including mechanically upturned plates, amorphous precipitated crust, few CF microtextures, and cf microtextures being in a minority (Figures 9 and 10a–c). This surface assemblage became overprinted by frost-induced diagnostic microtextures (cf, CF, bb, BB)[7,10,15,33] as a result of experimental FT simulation. Our attention was drawn to frost-induced cf/CF microtextures because of their specific shape, which was used here as the basis for distinguishing two types of this microtexture: (a) type I cf/CF—relatively shallow and flat (relatively high width-to-depth ratio) microforms, representative of most sedimentary environments[30] (referred

as cf$_I$/CF$_I$; Figure 10g), and defined by Mahaney[30] as "a smooth curved fracture, with a ribbed appearance, similar to the curve of a conch or seashell (…)"; and (b) type II cf/CF—relatively deep (relatively low width-to-depth ratio) microforms with regular shape resembling angular blocks (referred as cf$_{II}$/CF$_{II}$) encountered on the surface of quartz grains as cuboid-shaped micro-cavities (Figure 10h). The latter constitute the majority (∼95%) of those frost-induced cf/CF microtextures observed on the surface of the studied aeolian grains. These microtextures were not observed on the surface of mechanically crushed quartz grains subjected to experimental frost activity, nor on quartz grains originated from any natural environment, including glacial sediments.[11,30,44,66] The shape of cf$_{II}$ clearly distinguishes them from the well-known cf$_I$ microtextures. We believe this may be treated as an incentive to introduce a new term for these microforms. However, for the purposes of this work, these features (cf$_{II}$) were assigned to the general group of cf microtextures. The coexistence of cf$_I$ and cf$_{II}$ on the surface of the studied frost-subjected aeolian quartz grains indicated that, apart from general factors conditioning micro-scale frost weathering (i.e., number of FT cycles, water content, micro-relief), there is an additional factor which determines the shape of these microforms (cf$_I$, cf$_{II}$). We believe it is directly related to the depth to which these microforms penetrate the quartz grains. It seems this depth does not exceed ∼10 μm on the most convex parts of the grains, as revealed by TEM analysis (Figure 6b,c). We conclude that this depth corresponds to the thickness of the outer layer of quartz grains which were entirely exposed to high-energy grain-to-grain collisions in the cold-climate aeolian environment, that is directly exposed to aeolian-induced stress, and thus receiving the greatest amount of the energy released during the collisions. SEM and TEM analysis indicated that the internal structure (resulting from aeolian processes) of aeolian-originated quartz grains is not uniform (Figures 6 and 17a) and differs between its outer and inner parts. Therefore, we introduce the concept of an aeolian-originated *impact zone* and aeolian-unaffected *host grain* to distinguish between these portions of each grain.

The outermost part of the aeolian quartz grain, termed here the *outer impact zone* (Figure 17a), consists of a thin layer of surficial crust and a series of more or less parallel ridges arranged into mechanically upturned plates (Figure 17a). We refer to this layer as *abrasion fatigue*[67] described by Krinsley and McCoy[50] in their important but neglected paper. They characterized this outermost layer of the quartz grain as containing the disrupted lattice due to the broken surface structure, and provided a further description of it—"This layer contains small cracks, dislocations, broken Si–O bonds, projecting vertices, and thus abnormal solubility (…)" and "The layer of disrupted lattice material generally increases in crystallinity towards the center of the grain, but if the particle is small and perhaps has spalled off a sand sized grain, it may consists of disrupted lattice quartz almost completely (…)". This surficial crust, referred to here as the *outer impact zone*, usually covers the entire surface of the studied grains, regardless of the degree of their roundness. Based on our analysis, we believe that its thickness may reach a maximum of a few micrometers, ranging from maximum values on the concave parts of grains to minimum values on their convex parts (Figure 17b). TEM analysis showed

the *outer impact zone* on the concave part of grain reaching a thickness of ∼0.1–0.2 μm (Figure 6b).

The *impact zone*, below its amorphous *outer* part, consists of a crystalline form of quartz (Figure 17a). Due to its distinct forms (amorphous vs. crystalline), we therefore recommend identifying this layer in the structure of a quartz grain as the *inner impact zone*. We believe it may reach about 10 μm in thickness (Figures 6 and 17a,b) and consist of: (a) fragments of undisturbed quartz crystals that do not bear any mechanical damage, (b) fragments of slightly cracked quartz crystals, or (c) fragments of both disturbed or undisturbed quartz crystals, the terminations of which are arranged into breakage block microtextures. The last correspond to the "blocky areas" observed by Wellendorf and Krinsley[64] on quartz grains subjected to experimental aeolian processes operating at winds speed of 8 m/s for 3 hr. A local superimposition of mechanically upturned plates on the blocky terrain was interpreted as evidence of the aeolian origin of the latter.[64] Therefore, we also associate these breakage blocks, and thus the *inner impact zone*, with high-energy grain-to-grain collisions that acted in the former aeolian environment.

Kaldi et al[57] reported rapid growth of upturned plates superimposed on "microblocks" encountered on the surface of quartz grains from fluvial environments subjected to experimental aeolian action. It can therefore be concluded that the *inner impact zone* may be formed within grains subjected to saltation in both aeolian and fluvial (channel) environments.[68] The commonly known differences in the surface micromorphology of quartz grains originating from these environments stem from the presence of surficial crusts (i.e., *abrasion fatigue* developed as an *outer impact zone*) encountered on the aeolian-transported grains[50] and its absence on the fluvially transported grains.[48,68] It is logical that amorphous silica dissolved from the grain surface due to grain-to-grain collisions in water is also subjected to water transport and becomes dispersed in the transporting fluid.

We therefore conclude that the formation of an aeolian-induced *impact zone* and its spatial extent are limited to those parts of quartz grains that have been directly exposed to abrasion, and thus depend mainly on the shape of quartz grain. In the case of subrounded and low-sphericity aeolian quartz grains, it is limited to their most convex parts and declines with distance from the protrusion, whereas it may develop around the entire surface of well-rounded and high-sphericity aeolian quartz grains (Figure 17b). In line with the above-mentioned statement by Krinsley and McCoy[50] that the thickness of the *abrasion fatigue* layer (here termed the *outer impact zone*) depends on the grain size, it can be assumed that the same relationship probably applies to the thickness of the *inner impact zone*.

Further towards the center of the grain, below the *inner impact zone*, there is an intact *host grain* (Figure 17a) that has not been exposed to destructive aeolian abrasion. It appears that a large amount of energy released during aeolian grain-to-grain collisions is accommodated mainly in the outermost part of quartz grains that includes the surficial layer of *abrasion fatigue* (i.e., *outer impact zone*) and underlying *inner impact zone*. This aeolian-induced energy can pass through the crystal, which was only briefly mentioned by Kaldi et al[57] in a supplement to their work. We are convinced that this

issue, although not addressed so far, is of key importance in the context of the formation of microtextures on the surface of quartz grains. Despite the fact that frost-induced modifications affect mostly surface and subsurface parts of quartz grains, their host grains may also experience the destructive action of frost weathering due to the presence of defects in the quartz crystal lattice[14] (e.g., inclusions; Figure 6a,c).

The internal structure of the outer part of aeolian quartz grains presented above is thought to have a profound effect on the development of any further mechanically induced damage inflicted on its surface. We postulate that the *outer impact zone* (= *abrasion fatigue*; Figure 11a,b,d) inhibits the formation of frost-induced microtextural peculiarities. This is reinforced by the fact that the *outer impact zone* generally lacks any surficial cracks, and even if they are present, they are relatively sparse and small (Figures 10 and 16). It appears that the only way the *inner impact zone* may be affected by frost weathering is through destruction of the *outer impact zone*, which allows frost action to penetrate into the grain. We consider that when a single cf (especially cf$_{II}$) is formed within the *inner impact zone,* its further destruction becomes more effective, that is development of frost-induced imprints is facilitated.

Frost-induced microtextures (cf, CF, bb, BB) recognized on the surface of the studied grains occupy their most convex parts (Figure 5), where the *inner impact zone* probably reaches its greatest thickness, in contrast to the *outer impact zone* which is presumably thinnest there (Figure 17b). The development of frost-induced imprints within the *inner impact zone* is certainly facilitated by the presence of bb/BB with microtexturally diversified relief and single cracks. Moreover, the susceptibility of the *inner impact zone* to frost weathering may be enhanced due to repeated freezing and thawing of water, as the freezing front exerts great pressure on the grain-surrounding unfrozen water film, and further on the surface of the quartz grain. This outer part of the grain exposed to the greatest stress and modifications due to frequent temperature oscillations across 0°C was referred as the *frost-exposed skin* (FES) and estimated for sand-sized vein-quartz grains at ∼10–15 μm by Górska & Woronko.[11] As a consequence, the aeolian-originated *impact zone* and frost-originated FES layer overlap, since both involve the outermost parts of quartz grains (Figure 17a,b). Their joint influence on the formation of frost-induced microfeatures on aeolian-originated quartz grains seems to be of great importance and results in specific microtextural characteristics.

4.2.3 | Refreshment of the aeolian-originated quartz grains

Aeolian-driven abrasion leads to a gradual smoothing of the grain surface along with an increase in the degree of their roundness.[27,54,55,69,70] This fact, coupled with the observation of single, shallow and extensive CF microtextures (strongly modified by aeolian processes and therefore classified as depressions[27]) imprinted on the surface of aeolian quartz grains (e.g., Figures 10f,i and 16e), clearly

indicates that the abraded surface of a grain undergoes the process of refreshment. Depending on the depth of detachment, the formation of aeolian-induced CF reveals a new (i.e., previously covered) grain surface. We consider that it may affect the entire *impact zone* or a significant part of it and generally does not penetrate into the underlying *host grain* (Figure 17c). Further aeolian abrasion therefore acts on the surface of a different degree of freshness, and thus different susceptibility to the formation of surficial imprints, both aeolian- or frost-induced imprints. As a consequence, the *impact zone* re-develops (Figure 17c). Depending on grain shape, the extent of this new *impact zone* may move deeper into the grain. We think the development of *outer* and *inner impact zones* is simultaneous, as has been already suggested by Wellendorf and Krinsley.[64] More experimental research is needed to confirm this hypothesis.

Assuming that these simultaneous processes of aeolian abrasion (with development of an *impact zone*) and surface refreshment last until the final termination of wind-blown action in a given area (Figure 17c), it is difficult to determine the stage of *impact zone* development within individual quartz grains from a population concerned. This is one of the reasons why the number of frost-induced microtextures recorded on individual grains from one sample varies more than might be expected (Figures 7 and 8), as evidenced by the detected outliers (Table 3b). It is especially clear in the case of the sample exposed to 300 and 1,000 FT cycles where ranges of frost-originated imprints vary from 0 to 18 (grains #3 and 13 on Figure 13) and 1 to 55 (grains #7 and 1 on Figure 15), respectively. Moreover, it should be noted that some of the grains subjected to frost weathering do not bear any surficial microtextures originating from this process. We interpret these as: (a) grains whose surficial crust (i.e., *outer inner zone*) is thick enough to prevent their development; (b) grains subjected to frost weathering, the efficiency of which was insufficient (due to its short duration and/or low intensity) to destroy the *outer impact zone* and modify the surface; (c) grains whose *inner impact zone* was not fully developed, that is the duration of aeolian processes was too short to affect internal structure of grain; or (4) grains whose surface was refreshed during aeolian processes.

We suppose that after the termination of wind-blown processes, the *inner impact zone* becomes inactive (i.e., it does not develop further). Studies on cold-climate aeolian deposits evidenced a predominance of extensive frost-induced BB complexes on the surface of quartz grains subjected to frost action under natural environmental conditions.[7] It may be implied from these studies that the formation of extensive BB microtextures is favored as frost action exploits already existing aeolian-originated BB (here introduced as the *inner impact zone*) for the development of extensive frost-derived BB microtextures on the surface of aeolian quartz grains. Aeolian-originated BB are therefore reactivated and their microtexturally diversified relief enhances the destructive effects of frost weathering.

Refreshment of the grain surface may also be a postsedimentary process in relation to the aeolian processes affecting the grain. It is then associated with the exposure of grains to frost action and resulting hydrofracturing process,[2,6,33,71] which also leads to the formation

of frost-induced CF, revealing fresh grain surfaces. It is thought that their development is confined to the *frost-exposed skin* (FES), which may partially or fully overlap with the *inner impact zone* (Figure 17). The refreshment of quartz grains, whether as a result of aeolian- or frost-driven processes, exposes their fresh surfaces which may be both more resistant (if intact quartz crystals are revealed) or more susceptible (if topographically varied surfaces are revealed) to frost weathering and any mechanical damage.

4.3 | Influence of crystal structure on the micromorphology of aeolian-originated quartz grains

Frost-induced microtextures recognized on the surface of the studied quartz grains include individual cf, CF, bb, and BB (Figures 4 and 7), which generally occupy grain protrusions (Figure 5). However, the distribution of cf sometimes seems to be locally arranged as they are organized along a line (Figure 16l) or grouped into larger clusters (Figure 16m,o). It appears that this orderly manner of their distribution is linked to quartz crystallography and refers to cleavage in quartz crystals that follows along the r, z, m, c, a, s, and x planes.[72] Wellendorf and Krinsley[64] conducted a detailed study on crystallography of quartz and its relationship to surface microtextures. They stated that a system of fractures follows the c axis of the grain; upturned plates or cleavage plates follow the r(1011) or z(0111) cleavages; and blocky areas represent traces parallel to m(1010) cleavage in quartz. The formation of extensive BB complexes, commonly observed on the surface of aeolian quartz grains[7,64] is therefore thought to depend on a particular crystallographic direction combined with their exposure to aeolian abrasion processes. Otherwise, when a nonsusceptible crystallographic direction is exposed to aeolian- or frost-driven processes (or other surface-modifying processes), the development of any surficial microtextures may cease or require a longer *lag time*.[14]

Both primary and secondary crystal defects revealed through TEM analysis (Figure 6) are interpreted here to exert a profound influence on the development of any surficial imprints. Primary defects referred to lattice imperfections may include crystallographically controlled slip, dislocations, and micropores/inclusions. If located near the grain surface, these defects may be affected by frost weathering and contribute to any mechanical damage or modifications of grains. Secondary crystal defects include cracks which may be of both aeolian and/or periglacial (frost) origin (Figure 6b,c). A distinction between them is difficult due to the surprisingly small number of cracks recorded within quartz grains from both reference (0 FT cycles) and frost-weathered (after 100 and 1,000 FT cycles) samples in this experiment. For that reason, the distribution of stress acting upon a grain surface during specific processes (wind vs. frost action) should be considered while interpreting the origin of individual cracks. Differences lie in the grain surface exposed to the process. Aeolian activity exerts pressure on a limited surface of a grain affected by a direct grain-to-grain collision. As a consequence, aeolian-induced cracks are generally small, discontinuous,

located inside the grain, and do not reach its surface (Figure 6b,c). On the other hand, simulated frost action affected the entire surface of each grain (all grains contain a thin layer which can be easily be penetrated by negative temperature from all sides; see Sect. 2.2.), and therefore frost-induced cracks are thought to be continuous (i.e., cracks extend from the inside of the grain to its surface). TEM analysis revealed some internal features of the studied quartz grains that are thought to exert a profound influence on the development of any surficial imprints. However, due to the complexity of the method (specialized equipment, FIB-cut preparation, time-consuming analysis) and its resolution (small area of TEM view; nano- up to micro-scale), the conducted investigations remain very local. Further detailed studies are required to define the relationship between quartz crystallography and the formation of surficial microtextures.

5 | CONCLUSIONS

Experimental simulation on micro-scale frost weathering of cold-climate aeolian quartz grains revealed some internal features of quartz that are interpreted to exert a profound influence on the formation of any surficial microtextures. The data obtained from this experimental simulation of 0–1,000 FT cycles show that:

1. Frost weathering is an effective agent that modifies the surface of aeolian-originated quartz grains. It results in the formation of different-sized conchoidal fractures (cf, CF), breakage blocks (bb, BB), and cracks. The predominant fractures are cf divided into cf_I and cf_{II}. The number of frost-induced microtextures observed on the grain surfaces increases with ongoing frost activity. However, it remains relatively small up to 700 FT cycles and increases after 1,000 FT cycles.
2. The susceptibility of aeolian-originated quartz grains to frost-induced modifications depends on their internal characteristics resulting from aeolian processes. Aeolian abrasion contributes to modification of quartz grain structure and development of a subsurface *impact zone* which consists of *outer* and *inner* parts.
3. Development of the *impact zone*, especially its *inner* part, within aeolian quartz grains originating from cold-climate environments depends on: (a) grain shape and roundness, (b) the duration of aeolian process and exposure of the grain to abrasion, and (c) refreshment of grain surfaces due to aeolian abrasion. All these factors differentiate and modify the grains, and influence the subsequent formation of frost-induced microtextures. The vast majority of them are encountered on the most convex parts of aeolian grains.
4. Microstructural characteristics involving both primary (e.g., inclusions, grain boundaries) and secondary (e.g., cracks) defects in quartz crystals have an effect on the development of both aeolian- and frost-induced microtextures on the surfaces of quartz grains.

CONFLICT OF INTEREST

The authors declare that they have no known competing financial interests or personal relationships that could have appeared to influence the work reported in this paper.

DATA AVAILABILITY STATEMENT

The data that support the findings of this study are available from the corresponding author upon reasonable request.

ORCID

Martyna E. Górska https://orcid.org/0000-0002-8460-2812
Barbara Woronko https://orcid.org/0000-0002-2763-5650
Tomasz M. Kossowski https://orcid.org/0000-0002-9976-4398

REFERENCES

1. Seppala M. *Wind as a geomorphic agent in cold climates*. Cambridge: Cambridge University Press; 2004. 358pp.
2. French H. *The periglacial environment*. Wiley-Blackwell, 544 pp; 2017. doi:10.1002/9781119132820.
3. Kasse C. Sandy aeolian deposits and environments and their relation to climate during the last glacial maximum and Lateglacial in northwest and Central Europe. *Progr Phys Geogr: Earth Environ*. 2002;26(4):507-532. doi:10.1191/0309133302pp350ra.
4. Isarin RFB, Renssen H. Reconstructing and modelling late Weichselian climates: the younger Dryas in Europe as a case study. *Earth Sci Rev*. 1999;48(1-2):1-38. doi:10.1016/S0012-8252(99)00047-1.
5. Woronko B, Bujak Ł. Quaternary aeolian activity of Eastern Europe (a Poland case study). *Quat Int*. 2018;478:75-96. doi:10.1016/j.quaint.2017.03.058
6. Matsuoka N, Murton J. Frost weathering: recent advances and future directions. *Permafr Periglac Process*. 2008;19(2):195-210. doi:10.1002/ppp.620
7. Woronko B, Pisarska-Jamroży M. Micro-scale frost weathering of sand-sized quartz grains: micro-scale frost weathering of quartz grains. *Permafr Periglac Process*. 2016;27(1):109-122. doi:10.1002/ppp.1855
8. Ballantyne CK. *Periglacial geomorphology*. Wiley-Blackwell; 2018. 472 pp.
9. Maji V, Murton JB. Experimental observations that simulated active-layer deepening drives deeper rock fracture. *Permafr Periglac Process*. 2020;31(2):296-310. doi:10.1002/ppp.2041
10. Woronko B. Micromorphology of quartz grains as a tool in the reconstruction of periglacial environment. *Contemp Issues Polish Geogr*. 2012;111:131.
11. Górska ME, Woronko B. Multi-stage evolution of frost-induced microtextures on the surface of quartz grains – an experimental study. *Permafr Periglac Process*. 2022;33(4):470-489. doi:10.1002/ppp.2164

12. Matsuoka N. Microgelivation versus macrogelivation: towards bridging the gap between laboratory and field frost weathering. *Permafr Periglac Process*. 2001;12(3):299-313. doi:10.1002/ppp.393
13. Wright JS. The spalling of overgrowths during experimental freeze–thaw of a quartz sandstone as a mechanism of quartz silt production. *Micron*. 2000;31(6):631-638. doi:10.1016/S0968-4328(99)00074-8
14. Górska ME, Woronko B, Kossowski TM, Pisarska-Jamroży M. Micro-scale frost-weathering simulation – changes in grain-size composition and influencing factors. *Catena*. 2022;212:106106. doi:10.1016/j.catena.2022.106106
15. Schwamborn G, Schirrmeister L, Frütsch F, Diekmann B. Quartz weathering in freeze–thaw cycles: experiment and application to the el'gygytgyn crater lake record for tracing siberian permafrost history. *Geogr Ann Ser B*. 2012;94(4):481-499. doi:10.1111/j.1468-0459.2012.00472.x
16. Zeeberg J. The European sand belt in eastern Europe - and comparison of late glacial dune orientation with GCM simulation results. *Boreas*. 1998;27(2):127-139. doi:10.1111/j.1502-3885.1998.tb00873.x
17. Hilgers A. *The chronology of late glacial and Holocene dune development in the northern central European lowland reconstructed by optically stimulated luminescence (OSL) dating*PhD thesis,. University of Cologne; 2007.
18. Zieliński P, Sokołowski RJ, Woronko B, Fedorowicz S, Jankowski M, Standzikowski K. Sandy deposition in a small dry valley in the periglacial zone of the last glacial maximum: a case study from the Józefów site, SE Poland. *Quat Int*. 2016;399:58-71. doi:10.1016/j.quaint.2015.08.089
19. Moska P, Jary Z, Sokołowski RJ, et al. Chronostratigraphy of late glacial aeolian activity in SW Poland – a case study from the Niemodlin plateau. *Geochronometria*. 2020;47(1):124-137. doi:10.2478/geochr-2020-0015
20. Moska P, Sokołowski RJ, Jary Z, et al. Stratigraphy of the late glacial and Holocene aeolian series in different sedimentary zones related to the last glacial maximum in Poland. *Quat Int*. 2021;630:65-83.
21. Renssen H, Lautenschlager M, Schuurmans CJE. The atmospheric winter circulation during the younger Dryas stadial in the Atlantic/-European sector. *Climate Dynam*. 1996;12(12):813-824. doi:10.1007/s003820050145
22. Dzieduszyńska D, Petera-Zganiacz J, Roman M. Vistulian periglacial and glacial environments in Central Poland: an overview. *Geol Quarterly*. 2020;64:54-73. doi:10.7306/gq.1510
23. Lautridou JP, Ozouf JC. Experimental frost shattering: 15 years of research at the Centre de Géomorphologie du CNRS. *Prog Phys Geogr: Earth Environ*. 1982;6(2):215-232. doi:10.1177/030913338200600202
24. Murton JB, Coutard JP, Lautridou JP, et al. Experimental design for a pilot study on bedrock weathering near the permafrost table. *Earth Surf Proc Land*. 2000;25(12):1281-1294. doi:10.1002/1096-9837(200011)25:123.0.CO;2-U
25. Folk RL, Ward WC. Brazos River Bar: a study in the significance of grain size parameters. *J Sediment Petrol*. 1957;27(1):3-26. doi:10.1306/74D70646-2B21-11D7-8648000102C1865D
26. Blott SJ, Pye K. GRADISTAT: a grain size distribution and statistics package for the analysis of unconsolidated sediments. *Earth Surf Process Landforms*. 2001;26(11):1237-1248. doi:10.1002/esp.261
27. Pye K, Tsoar H. *Aeolian sand and sand dunes*. Berlin Heidelberg: Springer; 2009. doi:10.1007/978-3-540-85910-9
28. Brookfield ME. Aeolian processes and features in cool climates. *Geol Soc Lond Spec Publ*. 2011;354(1):241-258. doi:10.1144/SP354.16
29. Helland PE, Holmes MA. Surface textural analysis of quartz sand Grains from ODP site 918 off the southeast coast of Greenland suggests glaciation of southern Greenland at 11 ma. *Palaeogeography Palaeoclimatology Palaeoecology*. 1997;135(1-4):109-121. doi:10.1016/S0031-0182(97)00025-4

30. Mahaney WC. *Atlas of sand grain surface textures and applications*. Oxford University Press; 2002. 237pp.

31. Culver SJ, Bull PA, Campbell S, Shakesby RA, Whalley WB. Environmental discrimination based on quartz grain surface textures: a statistical investigation. *Sedimentology*. 1983;30(1):129-136. doi:10.1111/j.1365-3091.1983.tb00655.x

32. Vos K, Vandenberghe N, Elsen J. Surface textural analysis of quartz grains by scanning electron microscopy (SEM): from sample preparation to environmental interpretation. *Earth-Science Reviews*. 2014; 128:93-104. doi:10.1016/j.earscirev.2013.10.013

33. Woronko B, Hoch M. The development of frost-weathering microstructures on sand-sized quartz grains: examples from Poland and Mongolia: development of frost-weathering microstructures on sand quartz grains. *Permafr Periglac Process*. 2011;22(3):214-227. doi:10.1002/ppp.725

34. Dietzel M. Impact of cyclic freezing on precipitation of silica in me–SiO2–H2O systems and geochemical implications for cryosoils and sediments. *Chem Geol*. 2005;216(1-2):79-88. doi:10.1016/j.chemgeo.2004.11.003

35. Cailleux A. Les actions éoliennes périglaciaires en Europe. *Bull Soc Géol France*. 1942;41:1-176.

36. Goździk J. Zastosowanie morfometrii i graniformametrii do badań osadów w kopalni węgla brunatnego Bełchatów [usage of morphometry and graniformametry in the investigations of the sediments in the brown coal mine in Bełchatów]. *Studia Regionale PWN*. 1980;4: 101-114. [in polish].

37. Mycielska-Dowgiałło E, Woronko B. Analiza obtoczenia i zmatowienia powierzchni ziarn kwarcowych frakcji piaszczystej i jej wartość interpretacyjna [analysis of roundness and matt surface of the quartz grains and its interpretive value]. *Przegląd Geol*. 1998;46:7 [in polish].

38. Malvern Instruments Ltd., 2008. Morphologi G3 user manual, UK.

39. Wenk HR. *Electron microscopy in mineralogy*. Berlin Heidelberg, 573pp: Springer; 1976. doi:10.1007/978-3-642-66196-9

40. Hampel FR. A general qualitative definition of robustness. *Ann Math Stat*. 1971;42(6):1887-1896. doi:10.1214/aoms/1177693054

41. Dixon WJ. Analysis of extreme values. *Annals of Mathematical Statistics*. 1950;21(4):488-506. doi:10.1214/aoms/1177729747

42. Shapiro SS, Wilk MB. An analysis of variance test for normality (complete samples). *Biometrika*. 1965;52(3-4):591-561. doi:10.1093/biomet/52.3-4.591

43. Frederickson AF. Mosaic structure in quartz. *J Mineral Soc Am*. 1955; 40:1-9.

44. Woronko B. Frost weathering versus glacial grinding in the micromorphology of quartz sand grains: processes and geological implications. *Sediment Geol*. 2016;335:103-119. doi:10.1016/j.sedgeo.2016.01.021

45. Kowalkowski A. Holocene rusty and rusty brown soils in the tundra and taiga of middle Sveden. *Soil Sci Annual XLIX*. 1988;29-44.

46. Schwamborn G, Mayer H, Fedorov G, Schirrmeister L, Hubberten H. Ground ice and slope sediments archiving late Quaternary paleoenvironment and paleoclimate signals at the margins of El'gygytgyn impact crater, NE Siberia. *Quatern Res*. 2006;66(2):259-277. doi:10.1016/j.yqres.2006.06.007

47. Szerakowska S, Woronko B, Sulewska MJ, Oczeretko E. Spectral method as a tool to examine microtextures of quartz sand-sized grains. *Micron*. 2018;110:36-45. doi:10.1016/j.micron.2018.04.008

48. Lindé K, Mycielska-Dowgiałło E. Some experimentally produced microtextures on grain surfaces of quartz sand. Geografiska Annaler. *Ser a, Phys Geogr*. 1980;62:171-184.

49. Klatkowa H. Ślady środowiska eolicznego w rzeźbie powierzchni ziarn kwarcowych, wyniki analiz w elektronowym mikroskopie skaningowym [tracks of aeolian conditions on the relief surface of the quartz-sand grains – results of the electron microscope study]. *Acta Geogr Lodzensia*. 1976;37:93-108. [in polish].

50. Krinsley DH, McCoy F. Aeolian quartz sand and silt. In: *Scanning electron microscopy in the study of sediments*; 1978:249-260.

51. Hall K. Freeze-thaw activity at a Nivation site in northern Norway. *Arctic Alpine Res*. 1980;12(2):183-194. doi:10.2307/1550515

52. Hallet B, Walder JS, Stubbs CW. Weathering by segregation ice growth in microcracks at sustained subzero temperatures - werification from an experimental study using acoustic emissions. *Permafr Periglac Process*. 1991;2(4):283-300. doi:10.1002/ppp.3430020404

53. Matsuoka N. Rock weathering processes and landform development in the Sør Rondane Mountains, Antarctica. *Geomorphology*. 1995; 12(4):323-339. doi:10.1016/0169-555X(95)00013-U

54. Mycielska-Dowgiałło E. Estimates of late glacial and Holocene aeolian activity in Belgium, Poland and Sweden. *Boreas*. 1993;22:165-170.

55. Mycielska-Dowgiałło E. *Eolizacja osadów jako wskaźnik startygraficzny czwartorzędu [the record of aeolian processes on sediments as an indicator of the quaternary stratigraphy]*. University of Warsaw; 2001. 141pp. [in polish].

56. Chmielowska D, Woronko B, Dorocki S. Applicability of automatic image analysis in quartz-grain shape discrimination for sedimentary setting reconstruction. *Catena*. 2021;207:105602. doi:10.1016/j.catena.2021.105602

57. Kaldi J, Krinsley DH, Lawson D. Experimentally produced aeolian surface textures on quartz sand grains from various environments, 261–274. In: Whalley WB, ed. *[in] scanning electron microscopy in the study of sediments*. Norwich, England; 1978.

58. Costa PJM, Andrade C, Mahaney WC, et al. Aeolian microtextures in silica spheres induced in a wind tunnel experiment. *Geomorphology*. 2013;180-181:120-129.

59. Pernarowski L. Oprocesie sortowania piasków eolicznych na przykładzie wydm okolic Rzędzowa [on aeolian sorting of sand: example from dunes of Rzędzew region]. *Czasopismo Geograficzne*. 1959;30: 33-60. [in polish].

60. Neuman CM. Effects of temperature and humidity upon the transport of sedimentary particles by wind. *Sedimentology*. 2004;51(1):1-17. doi:10.1046/j.1365-3091.2003.00604.x

61. Ayling BF, McGowan HA. Niveo-eolian sediment deposits in coastal South Victoria land, Antarctica: indicators of regional variability in weather and climate. *Arctic, Antarctic, and Alpine Research*. 2006; 38(3):313-324. doi:10.1657/1523-0430(2006)38[313:NSDICS]2.0.CO;2

62. Lancaster N. Flux of Eolian sediment in the McMurdo dry valleys, Antarctica: a preliminary assessment. *Arctic, Antarctic, and Alpine Research*. 2002;34(3):318-323. doi:10.1080/15230430.2002.12003500

63. Krinsley DH, Doornkamp J. *Atlas of quartz sand surface textures*. Cambridge University Press; 1973. p. 37.

64. Wellendorf W, Krinsley D. The relation between the crystallography of quartz, and upturned aeolian cleavage plates. *Sedimentology*. 1980; 27(4):447-453. doi:10.1111/j.1365-3091.1980.tb01193.x

65. Marshall JR, Bull PA, Morgan RM. Energy regimes for aeolian sand grain surface textures. *Sediment Geol*. 2012;253-254:17-24.

66. Mahaney WC. Pleistocene and Holocene glacier thicknesses, transport histories and dynamics inferred from SEM microtextures on quartz particles. *Boreas*. 1995;24(4):293-304. doi:10.1111/j.1502-3885.1995.tb00781.x

67. Pascoe KJ. *An introduction to the properties of engineering materials*. Netherlands, 439pp: Springer; 1978. doi:10.1007/978-94-011-7068-0

68. Woronko B, Giriat D, Łosiak A. *Micromorphology of quartz grains as a tool to recognise fluvial deposits on an examples of field and experimental study. 10th international conference on fluvial sedimentology*. University of Leeds; 2013. UK 14–19 July 2013.

69. Margolis SV, Krinsley DH. Submicroscopic frosting on Eolian and subaqueous quartz sand grains. *Geol Soc America Bull*. 1971;82(12):

3395-3406. doi:10.1130/0016-7606(1971)82[3395:SFOEAS]2.0.CO;2

70. Woronko B, Zieliński P, Sokołowski RJ. Climate evolution during the Pleniglacial and late glacial as recorded in quartz grain morphoscopy of fluvial to aeolian successions of the European Sand Belt. *Geologos*. 2015;21(2):89-103. doi:10.1515/logos-2015-0005

71. Walder J, Hallet B. A theoretical model of the fracture of rock during freezing. *Geol Soc Am Bull*. 1985;96(3):336-346. doi:10.1130/0016-7606(1985)962.0.CO;2.

72. Bloss FD, Gibbs GV. Cleavage in quartz. *Am Mineral*. 1963;48:821-838.